NAS7-100

ROCKET RESEARCH
CORPORATION

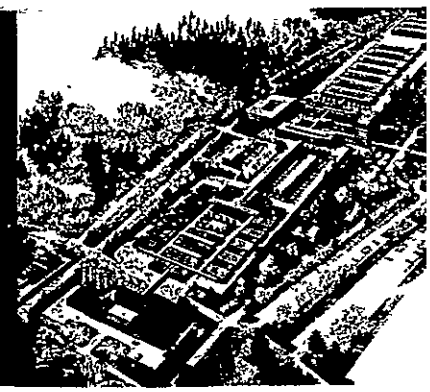

REDMOND, WASHINGTON

FINAL REPORT AND ADDENDUM

ROCKET RESEARCH CORPORATION
York Center
Redmond, Washington 98052

MARINER JUPITER/SATURN LCSSE THRUSTER/VALVE ASSEMBLY AND INJECTION PROPULSION UNIT ROCKET ENGINE ASSEMBLIES

0.2-lbf T/VA Development and Margin Limit Test Report

Contract No.: 954108

Submitted To:

California Institute of Technology
Jet Propulsion Laboratory
4800 Oak Grove Drive
Pasadena, California 91103

This document has been prepared in accordance with the Contract Data Requirements List (CDRL), Data Requirement Description (DRD) Number TE 001, DRL Line Item Number 003

RRC Document No.: RRC-76-R-499

Date: December 12, 1975

Prepared By: E. C. Clark
E. C. Clark
Development Engineer

Contributing Authors:
V. Terkun
Structural Analysis

Chuck Cunningham
C. R. Cunningham
Thermal Analysis

Approved By: Walter W. Wilson
W. W. Wilson
Program Manager

This work was performed for the Jet Propulsion Laboratory, California Institute of Technology, sponsored by the National Aeronautics and Space Administration under Contract NAS7-100.

TABLE OF CONTENTS

LIST OF FIGURES

LIST OF FIGURES (Continued)

LIST OF FIGURES (Continued)

LIST OF FIGURES (Concluded)

LIST OF TABLES

1.0 SCOPE

This report documents the tests conducted during the LCSSE/MJS 0.2-lbf T/VA (Rocket Research Corporation P/N 26970) development test program. Two thrusters were tested during this test program in accordance with the requirements of Jet Propulsion Laboratory Specification ES 509778. A general description of the test methods and equipment is included. Explicit test procedures listing the equipment used and detailed step-by-step procedures can be found in the documents referenced in Section 3.0 of this report. The results of this test program are presented in detail along with the individual T/VA disassembly results and data reduction techniques used to reduce the raw test data. The computerized performance model generated as a result of this test program is compared with the actual test results. A description of the construction of the performance model is not contained in this report, but is published in RRC Report 76-R-498.

2.0 SUMMARY OF RESULTS

2.1 INTRODUCTION

Two RRC 0.2-lbf thruster valve assemblies (T/VA's) were subjected to the development test program for the combined JPL Low-Cost Standardized Spacecraft Equipment (LCSSE) and Mariner Jupiter/Saturn '77 spacecraft (MJS) programs. The T/VA's allocated to the test program are identified as JPL P/N 10065398 (RRC P/N 26970-303-11), S/N's D01 and D02. The development test program commenced on February 28, 1975, with the start of acceptance testing and continued until the completion of teardown inspection of T/VA D01 on October 15, 1975.

The development test program was designed to achieve the following program goals:

1. Demonstrate T/VA design compliance with JPL Specification ES509778
2. To conduct a complete performance C_f map of the T/VA over the full operating range of environment
3. Demonstrate T/VA life capability and characteristics of life margin for steady-state limit cycle and momentum wheel desaturation duty cycles
4. Verification of structural design capability
5. Generate a computerized performance model capable of predicting T/VA operation over pressures ranging from 420 to 70 psia, propellant temperatures ranging from 140°F to 40°F, pulse widths of 0.008 to steady-state operation with unlimited duty cycle capability, and finally predict the transient performance associated with reactor heatup during any given duty cycle, start temperature, feed pressure, and propellant temperature conditions.

The results of the development testing indicate successful demonstration of the above goals except as noted herein. C_f mapping tests were completed measuring impulse bits with pulse widths of 8 milliseconds over the entire feed pressure range. The correlation resulting from the C_f tests is complete and can be used for all future testing for MJS and future LCSSE users. The structural and thermal design was fully demonstrated to meet the requirement of ES 509778. The T/VA demonstrated its capability to sustain operation for long-duration firing ($\geq$6 hours) and accumulate a total of 60 hours (20 hours' margin over the requirement of 40 hours). In addition to the 60 hours of steady state, an accumulation of over 300,000 pulses was demonstrated on the same T/VA. The generation of the performance model was successfully completed with the incorporation of both steady-state and transient data over the entire matrix of duty cycle, feed pressure, and propellant temperature ranges. The preliminary model (to be updated after TA testing) is capable of predicting any combination of duty cycles with pulse widths of 8 milliseconds to steady state over the entire operating, feed pressure, and temperature range. The momentum wheel desaturation margin test was not successfully demonstrated because of an operator failure; but all duty cycles were tested at a feed pressure of 420 psia, and the T/VA design compliance is predicted for this mode of

operation. The ability of the T/VA to meet the performance requirements of ES 509778 was demonstrated with the exception of steady-state roughness and steady-state response. This noncompliance was previously identified at the 0.2-lbf T/VA CDR in May 1975, based on the results of the development and breadboard T/VA acceptance tests. The values recommended are summarized in Section 8.0 of this report.

This section presents a summary of the problems encountered during the test program along with the test synopsis. Also included is a description of the hardware tested and a summary of the differences between the development configuration and the design changes made for the qualification and flight T/VA configurations.

2.2 TEST SYNOPSIS

The development T/VA S/N D01 was subjected to the test series shown in Figure 2-1. Essentially the test program was completely successful and progressed smoothly until Appendix N, the performance mapping test was reached. At the onstart of the performance mapping test, the first duty cycle tested was a 0.008-second pulse width. It was noted that the fuel consumption was abnormally large for this size pulse, and further investigation yielded problems with the valve driver circuitry. The test setup resulted in a 1-volt clipping at the valve close signal, and therefore the actual closure was 10 to 20 milliseconds longer than desired. The problem was corrected and the performance mapping test repeated. At this point in time, it was realized that the small pulse widths measured during the C_f mapping tests were also affected by this test setup problem. Therefore, the C_f mapping tests were reinstituted as shown in Figure 2-1 after the performance mapping tests. Another problem occurred during the performance mapping test when the T/VA failed to produce chamber pressure at the lowest tested feed pressure of 70 psia, the smallest pulse width of 0.008 second, and a propellant temperature of 40°F. The problem corrected itself by changing to the 1% duty cycle. In addition, the problem did not exist at the 70°F propellant temperature. The failure was directly attributed to the aniline in the Amendment 1 hydrazine used for this test series which had been previously identified during a separate test series involving large numbers of accumulated limit cycle operations. The corrective action for this test failure is the use of purified hydrazine, which has been done for the MJS '77 program.

A problem with the T/VA seat design was also identified during the performance mapping tests. The valve seat design did not allow adequate clearance for thermal expansion of the seat material, nor did it allow for venting of the back side of the seat. This problem was corrected by redesign of the T/VA valve seat and will be incorproated on the qualification and flight T/VA's. The problem was noticed when the peak chamber pressure and chamber pressure integral would decay drastically during the performance mapping tests. There was no indication of propellant flow rate through the engine. Additionally, during the performance mapping tests at the small pulse widths, specific impulse measurements below the JPL requirement of 100 lbf-sec/lbm were recorded. Recent testing at JPL indicates that substantial impulse is available in the tailoff portion of the pulse from 600 milliseconds to 6 seconds after pulse termination. During the JPL test series, specific impulse values were never measured below the 100 lbf-sec/lbm values. As a corrective action for the qualification test series, a low range chamber pressure transducer will be incorporated so that this tailoff impulse can be measured.

0.2-lbf STANDARDIZED THRUSTER/VALVE ASSEMBLY DEVELOPMENT TEST FLOW PLAN, T/VA S/N D01

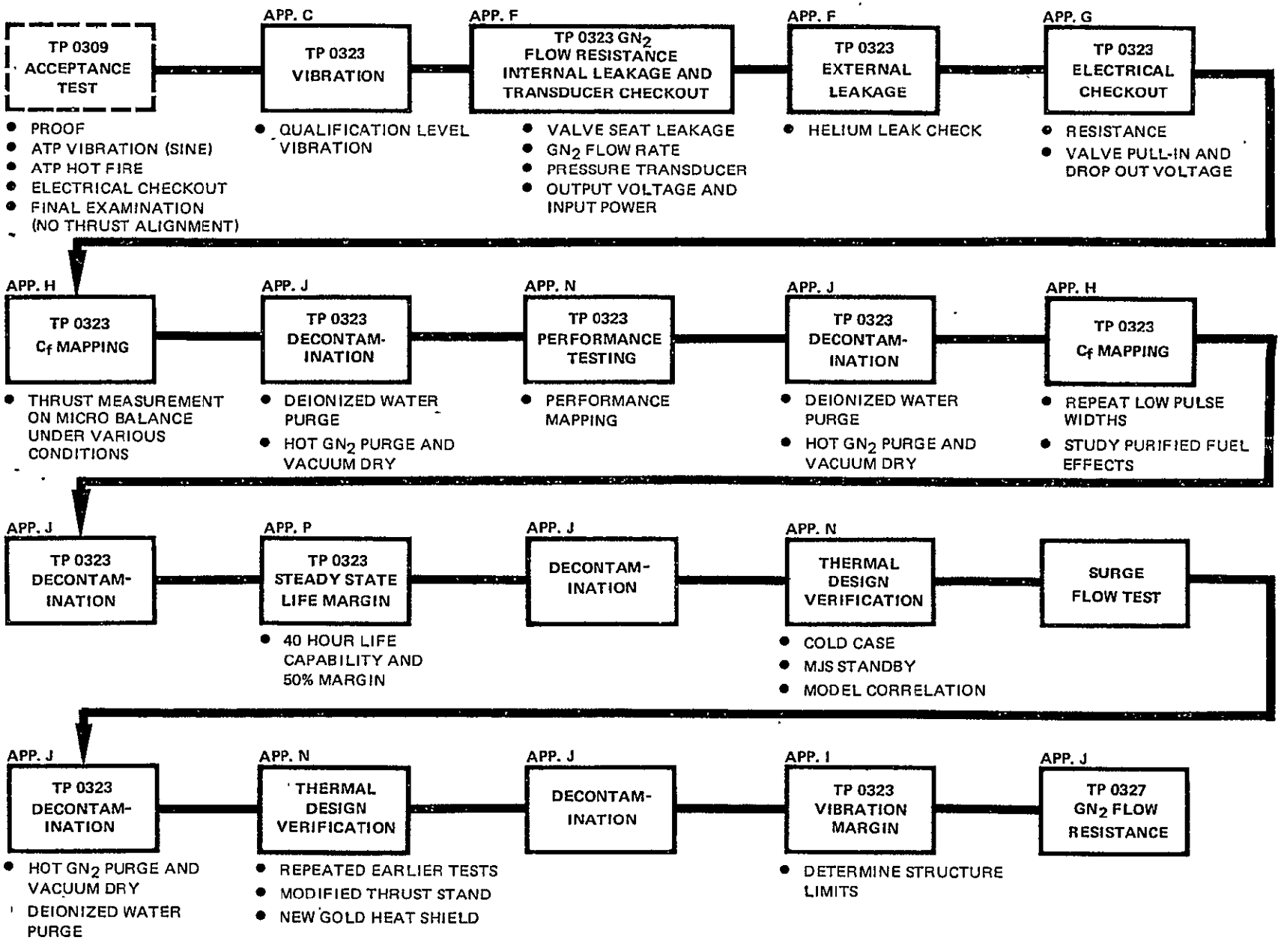

Figure 2-1

As stated earlier, the Cf mapping tests were repeated at the low pulse widths of 0.008, 0.020, and 0.040 seconds. This was a result of the test setup anomaly involving the suppression of the valve circuitry mentioned above. In addition, tests were conducted using purified hydrazine. The results indicated that only a very slight change in Cf value was noticed, and this change was within the data scatter. The results then of the Cf mapping tests using Amendment 1 hydrazine will then be used exclusively for all future data reduction for the remainder the LCSSE/MJS program and for future programs.

Originally it was planned to conduct the thermal design verification tests immediately after the performance mapping tests. However, to study the worst-case possible condition, it was decided to insert the steady-state life margin tests ahead of the thermal design tests. This was done as shown in Figure 2-1. After the steady-state life margin test, observations made with the hardware were that the gold-plated heat shields were very badly degraded. However, the thermal design verification tests were conducted with the degraded heat shield. The results of this test indicate that the catalyst bed temperature could not be maintained above the design minimum of 250°F with the degraded heat shield. Additionally, the test data indicated that the original conservative thermal model presented the best correlations with the measured test data. The T/VA successfully completed operational startup in the MJS standby mode using 0.010-second pulse widths with no propellant freezing. However, an anomaly had occurred in the standby mode when a 10-second steady-state test was fired. Propellant freezing did occur in this particular case; the data analysis resulted in the observation that the propellant inlet tube was not conditioned properly, allowing freezing in this area. Before removing the engine from the test setup, a surge flow test was conducted. This test was conducted to simulate the flight bleed-in procedure to be used for the MJS mission. Propellant was evacuated from the T/VA up to the propellant tank enable valve. A vacuum was then drawn in this portion of the line and the propellant pressurized to 405 psig upstream of the enable valve. The enable valve was then opened and the propellant allowed to surge into the evacuated T/VA feed line.

The T/VA was then removed from the test cell and decontaminated and then returned into thermal design verification test. In this test, the cell is modified to center the T/VA within the environmental test shroud. Also, a new gold-plated aft heat shield was assembled on to the T/VA. The test series as conducted earlier were repeated, and the results indicated successful design verification of the T/VA. The propellant inlet tube was conditioned properly for this test series, and the 10-second steady-state test repeated successfully in the standby mode.

The T/VA was then subjected to vibration margin testing. It was during this test series that the predicted failure of the pressure transducer mounting bracket welds occurred. The T/VA was then subjected to a complete disassembly and inspection.

The second development T/VA, S/N D02, was subjected to the test series shown in Figure 2-2. As shown in addition to the qualification level vibration test, the T/VA was subjected to the pyrotechnic shock environment. The results of this environmental testing indicated that the T/VA design is capable of meeting the requirements of Specification ES509778. This development thruster was then subjected to a life test consisting of duty cycles which typify a momentum wheel

0.2-lbf STANDARDIZED THRUSTER/VALVE ASSEMBLY DEVELOPMENT TEST FLOW PLAN T/VA S/N D02

Figure 2-2

desaturation mode. The duty cycle used was defined by mission sequence 2 in Specification ES509778. Approximately 42% of the life test was completed, and a total of 46 cold starts with the catalyst bed conditioned to 40°F were accumulated. The test series was not completed as a result of a test operator error which caused a significant damage to the catalyst bed. This test was operated in an automated mode with only periodic surveillance. This allowed continuous operation over a 24-hour period. The operator error occurred on Friday, July 11, 1975. Test data was gathered at the beginning of sequence 34 (reference Section 6.0), and the T/VA set up for automated operation for the weekend following. However, the sightglass valve was inadvertently left open and the tank valve closed. This allowed depletion of propellant in the feed system and approximately 2,000, 1.0-second on, 10-second off pulses were accumulated with a mixture of gaseous nitrogen and hydrazine. Concurrently, with the above failure, a catalyst particle was passed through the bedplate and lodged in the nozzle throat. This particle was removed from the throat, and the T/VA was returned to testing. Results of subsequent testing indicated that significant damage to the catalyst bed had occurred and that the pressure drop of the T/VA was increasing, causing a decrease in impulse bit and thrust level. A second failure occurred on July 28, 1975, when excessive roughness and increased valve pressure drop caused the operation of the T/VA to terminate without commanding the valve closed. A flow check was made after the thruster chamber pressure had dropped to 0, and no flow was measured. Results of the failure analysis indicated that the operation of the T/VA with GN_2 initiated a void in the catalyst bed and that further operation of the T/VA after this initial failure increased the void and caused blockage in the bedplate due to rough operation. The excessive roughness during the last test sequence caused backflow through the valve and subsequently caused the valve seat to expand thermally, resulting in flow blockage. The test series was terminated, and the T/VA was completely disassembled and inspected.

A complete discussion of the test results of the two development thrusters and a description of their disassembly are presented in Sections 6.0 and 7.0 herein.

2.3 HARDWARE DESCRIPTION

The development T/VA's were built to the LCSSE/MJS breadboard configuration, P/N 26970-303-11. Figure 2-3 presents an isometric of this configuration and describes some of the basic piece parts, along with their locations, that are referred to in this report. Referencing the T/VA preliminary design review, three basic changes were incorporated into the development and breadboard configurations. These changes consist of the addition of the saddleblock and cabled tie (used to secure the temperature sensor and thruster heater leadwire transition tubes), the revisions to the mounting structure to open up the slot for the valve temperature sensor/valve heater leadwires, and the revision of the propellant inlet adapter.

During the course of the development testing, several other design changes were incorporated based on analysis and early development test results. These changes were incorporated prior to the T/VA critical design review. Figures 2-4 and 2-5 summarize these changes along with the three changes which were incorporated as stated above on the development and breadboard configurations. As shown in Figure 2-4, the following changes were incorporated in the T/VA design:

LCSSE/MJS 0.2-lbf T/VA
DEVELOPMENT/BREADBOARD CONFIGURATION
P/N 26920-303-11

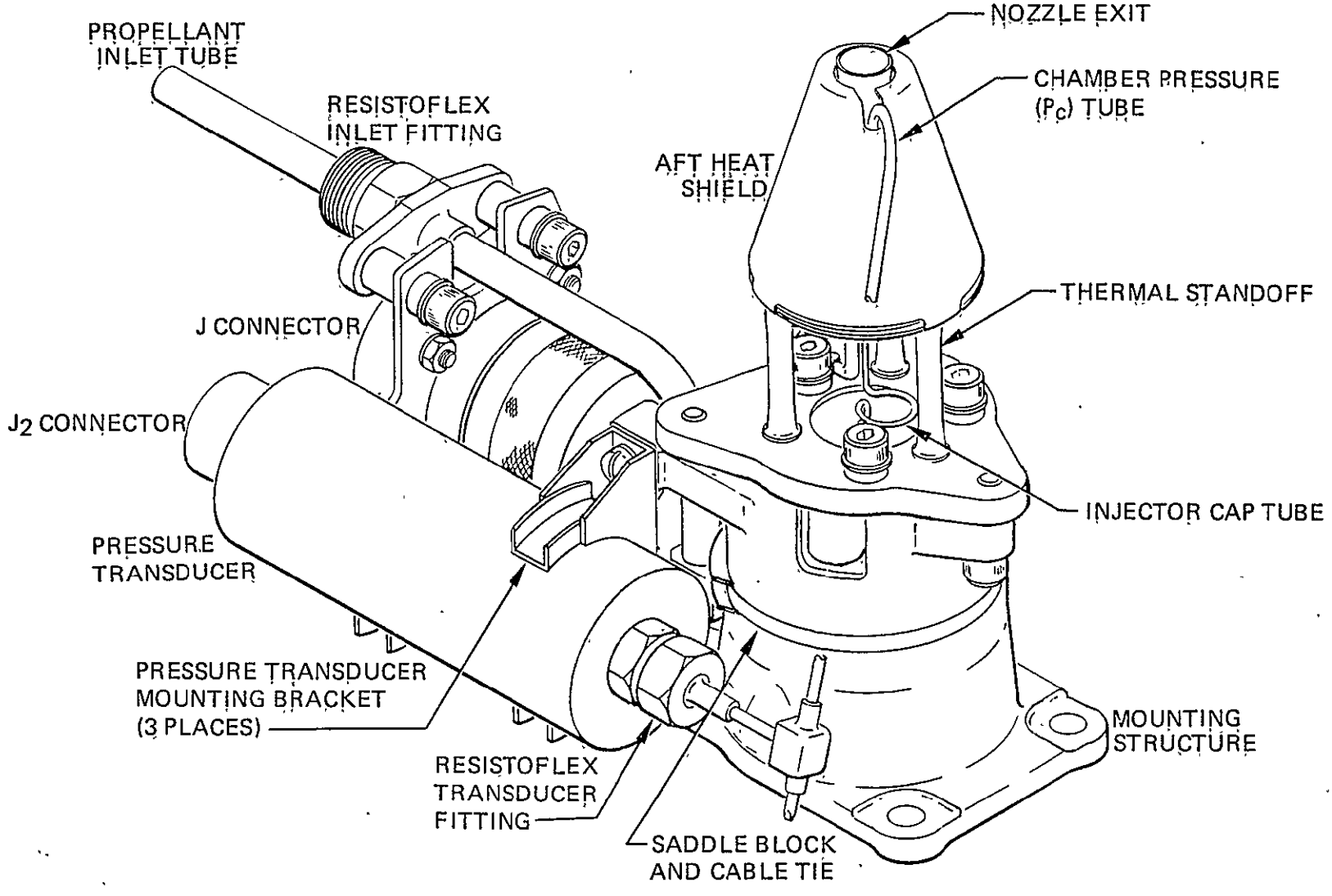

Figure 2.

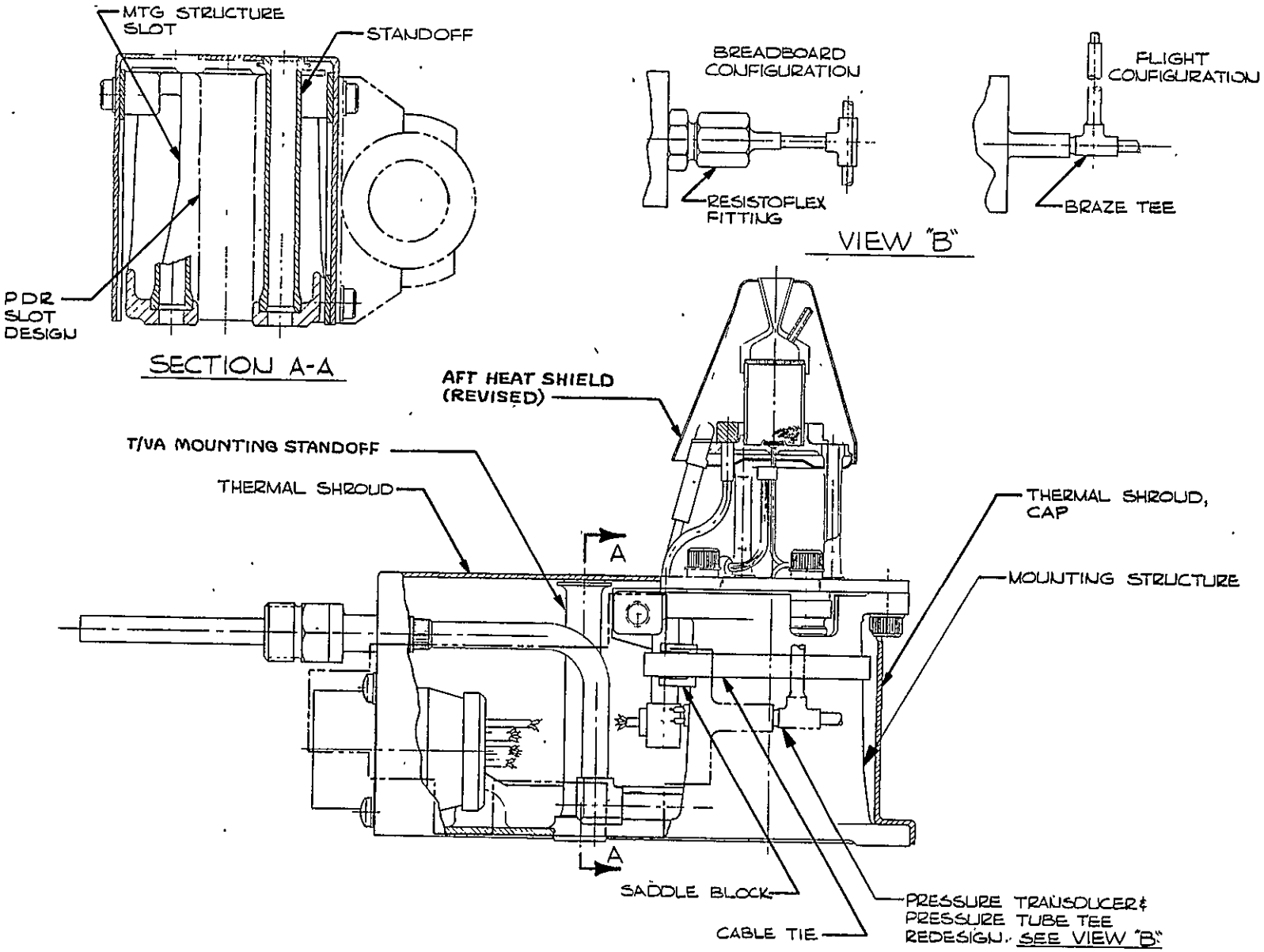

Figure 2-4

THRUSTER / VALVE SUB-ASSEMBLY

POST PDR CHANGES

Figure 2-5

1. A thermal shroud was added.
2. The pressure transducer inlet fitting was changed to delete the resistoflex fitting and incorporate a brazed unit.
3. The pressure transducer tube tee was redesigned.
4. The T/VA mounting standoffs were added.
5. The mounting structure was revised to add two extra mounting bosses for the thermal shroud and to incorporate the T/VA mounting standoffs.
6. The aft heat shield design was revised to provide additional room for the temperature sensor and thruster heater.

The design changes incorporated on the T/VA subassembly are shown in Figure 2-5 and described as follows:

1. The nozzle P_C tube joint was modified to incorporate an EB braze joint, and also the wall thickness of the P_C tube was reduced to 0.010 inch.
2. The bedplate was modified as shown to incorporate narrower slots, keeping the flow area the same. This was done as a part of the corrective action to eliminate the possibility of plugging the nozzle throat with a catalyst particle.
3. The catalyst bed pack was revised to increase the amount of overpack. This also was done as a part of corrective action to reduce the roughness level of the T/VA during steady-state operation.
4. The injector screen tabs were revised to reduce the manufacturing costs. Shown on the left-hand side of the sketch, in the upper right-hand corner, is the original tab configuration which was narrower at the top to facilitate bending for screen retention. The modification consisted of removing this narrowed section and leaving the tab thickness constant throughout its length. This did not alter the bending capability of the tab.
5. The valve/injector interface was modified as shown to incorporate the epoxy shim. This was done in an effort to ensure that the minimum holdup volume from the propellant outlet to injector inlet is maintained.
6. The valve heater, thruster heaters, and temperature sensor envelopes were revised to incorporate the leadwires protruding 90 degrees to the thrust axis. This was incorporated to ease the routing of the wires to the J-1 connector.

As a result of the design changes mentioned above, it became necessary to modify T/VA S/N D01 prior to the thermal design verification tests to incorporate the thermal shroud and the mounting standoffs. Also, it was necessary to tape the pressure transducer with the Scheldahl thermal control tape. In order to achieve this, a new mounting structure with all the revisions mentioned above was incorporated. This revision was done immediately following the steady-state life margin test, prior to the repeat of the thermal design verification test as outlined above in paragraph 2.2. Also, the old development aft heat shield was removed and a new flight-type gold-plated heat shield was assembled on the T/VA.

In addition to the above changes, the following changes were incorproated for the qualification and flight T/VA designs after the completion of the T/VA ciritical design review. They are:

1. The thermal standoff material was changed from Haynes 25 to Hastelloy B.
2. The valve seat was redesigned to eliminate the seat thermal expansion and venting problem.
3. The Scheldahl thermal control tape adhesive was changed from GE SR-585 to 3-M Y966.
4. The thruster heater manufacturing process was changed to incorporate an argon backfill.
5. The T/VA configurations were changed as follows:
   a. Type I – Removed the temperature sensor and valve heaters
   b. Type II – Removed the valve heater.

3.0 APPLICABLE SPECIFICATIONS AND REPORTS

This section presents the applicable specifications for the LCSSE/MJS development test program.

1. Jet Propulsion Laboratory (JPL) Equipment Specification ES 509778 entitled, "0.9-N (0.2-lbf) Standardized Hydrazine Attitude Control Propulsion Thruster/Valve Assembly, Flight Equipment Detail Specification For."

2. Acceptance Test Plan, TP-0309

3. Development Test Plan, TP-0323

Appendix A	Development Flow Plan T/VA No. 1
Appendix B	Development Flow Plan T/VA No. 2
Appendix C	Vibration
Appendix D	Pyrotechnic Shock
Appendix E	Internal Leak, GN_2 Flow Resistance and Transducer Calibration
Appendix F	External Leak
Appendix G	Electrical Checkout
Appendix H	C_f Mapping Test Procedure
Appendix J	Decontamination
Appendix K	GN_2 Flow Resistance
Appendix L	Vibration Margin
Appendix M	Momentum Wheel Desaturation Life and Life Margin
Appendix N	Performance Mapping and Thermal Design Verification
Appendix P	Steady-State Life Margin

4. LCSSE/MJS 0.2-lbf T/VA Performance Analysis Report, 76-R-498.

5. LCSSE/MJS 0.2-lbf T/VA Thermal Analysis Report, 74-R-448.

6. LCSSE/MJS 0.2-lbf T/VA Structural Analysis Report, 74-R-450.

4.0 TEST EQUIPMENT AND METHODS

This section presents a general description of the test facilities, equipment, and methods employed during the LCSSE/MJS 0.2-lbf T/VA development test program. For detailed step-by-step procedures, the reader is referred to documents referenced in Section 3.0.

4.1 PERFORMANCE MAPPING AND THERMAL DESIGN TESTING

The performance mapping and thermal design verification tests were completed in RRC test chamber No. 1. This chamber is 9 feet in diameter and has a volume of 612 cubic feet. Vacuum pumping is accomplished by use of a high capacity Stokes mechanical vacuum pump along with a CDC diffusion pump to give a maximum altitude capability of 460,000 feet. The CDC diffusion pumps were used only for the thermal design test. A schematic of the test setup for the performance mapping tests is presented in Figure 4-1. The propellant tank, control valves, and gaseous nitrogen pressurization system shown in the left-hand side of the schematic, are housed within the enclosed propellant cart. The sightglasses were mounted on the exterior walls of the cart, and were employed to measure both steady-state and pulse-mode propellant consumption. Each individual sightglass was calibrated prior to the installation to establish the sightglass volume, and hence fuel volume as a function of height. Volumetric fuel flow was then determined from the change in fuel level and the sightglass calibration. (Refer to Section 5.0 for a complete definition of this calculation.) The closed-circuit television system shown in Figure 4-2 was used to read fuel levels against a calibrated metric scale located next to each sight glass. The camera is mounted on a transversing system with both horizontal and vertical movement capability. The readings were taken directly in the data center during the test using the TV monitor screen. The thermal conditioning systems shown in Figure 4-1 were employed to control the thermal environment during the performance mapping testing. As shown, the fuel heat exchangers and T/VA mount bracket were connected to a common conditioning system. The T/VA was completely enclosed by a shroud and target which was controlled by a separate conditioning system to a constant temperature of 70°F throughout the performance mapping test. The instrumentation list for performance mapping is presented in Table 4-1. Notice that the sole measurement of chamber pressure was provided by the flight transducer. The Statham test cell transducer, which was formerly planned to be used, was deleted to decrease the internal volume or holdup volume associated with the additional transducer and provide better pulse shapes during the performance mapping tests.

For the thermal design verification test, the test setup was changed slightly from that shown in Figure 4-1. The T/VA shroud and target was controlled directly using liquid nitrogen to obtain the -250°F external environment. Conditioning system 1 was then used to control the fuel heat exchanger temperature, and the T/VA mount bracket was separated and controlled separately by conditioning system No. 2. This allowed independent control of both the fuel temperature and T/VA mount temperature to meet the necessary requirements of the thermal design test. Figure 4-3 presents the thermcouple locations monitored during the thermal test. Table 4-2 presents the additional instrumentation list used over and above the performance mapping test and describes the

PERFORMANCE MAPPING TEST SETUP

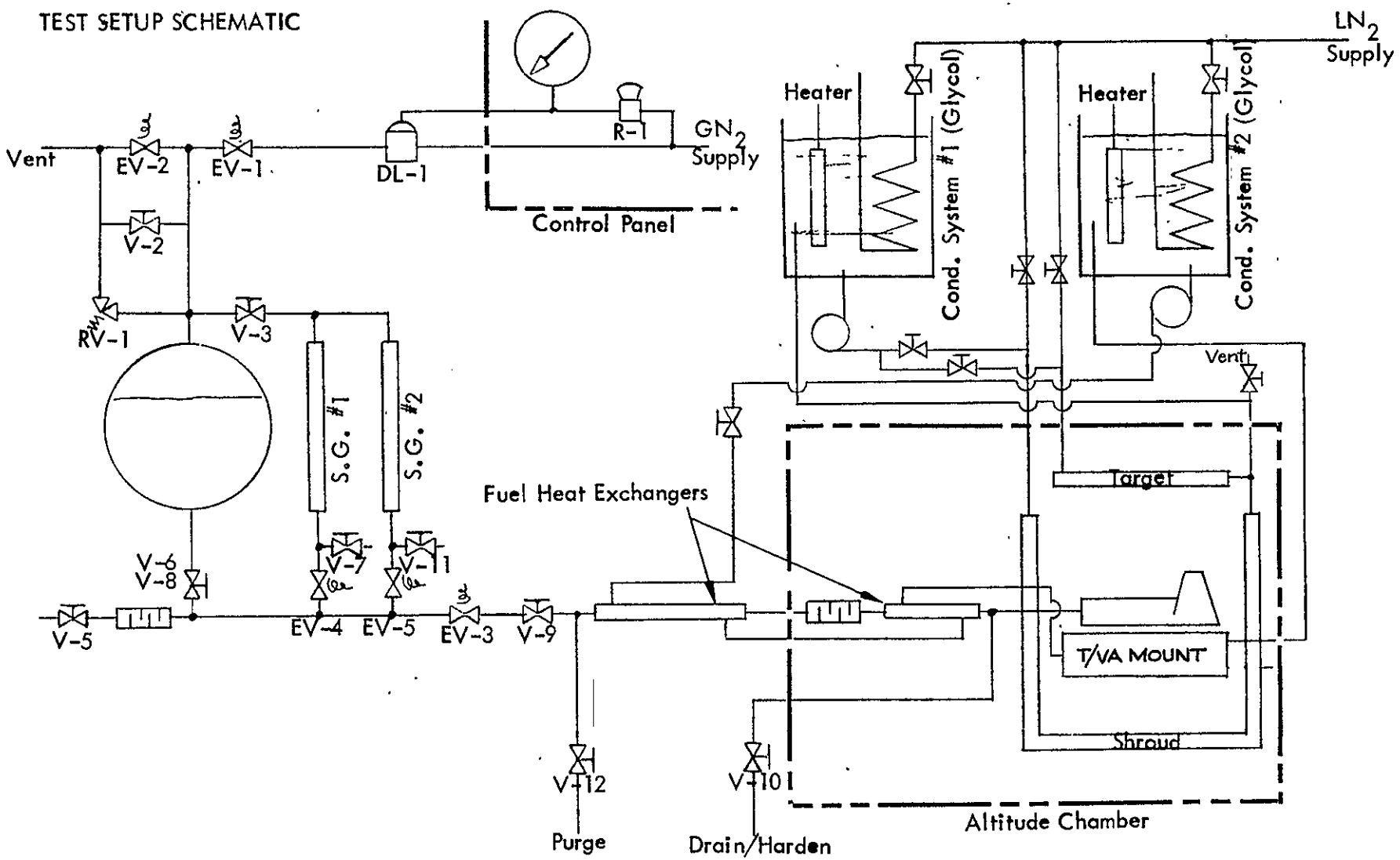

Figure 4-1

CLOSED CIRCUIT TELEVISION SYSTEM USED FOR SIGHTGLASS READING

1633-2

SIGHTGLASS READER

1633-3

TEST CONTROL BAY MONITOR

Table 4-1
PERFORMANCE MAPPING -- INSTRUMENTATION LIST

Parameter	Symbol	Type	Range	Recording			
				SCR	OSC	DDS	MAN
Fuel inlet pressure	P_f	Statham 288	0–50 psig	X	X	X	
Altitude chamber pressure	P_a	Statham	0–1 psia	X			
T/VA chamber pressure	P_{cfl}	Flight	0–350 psia	X	X	X	
Fuel tank pressure	–	Heise	0–600 psig				X
Altitude chamber pressure	–	Bendix	1μ to amb				X
Fuel inlet temperature	T_{fi}	T/C	0–5 mv	X		X	
Sightglass temperature No. 1	T_{sg1}	T/C	0–5 mv	X			
Sightglass temperature No. 2	T_{sg2}	T/C	0–5 mv	X			
Target temperature	T_{10}	T/C	0–10 mv	X			
Engine mount temperature	T_{15}	T/C	0–5 mv	X		X	
Shroud temperature	T_{11}	T/C	0–5 mv	X		X	
Chamber temperature	R_{+1}	Flight	0–1 v	X		X	
Propellant valve temperature	T_1	T/C	0–5 mv	X		X	
Reactor wall A temp. (T_{c1})	T_{2A}	T/C	0–50 mv	X		X	
Reactor wall B temp. (T_{c2})	T_{2B}	T/C	0–50 mv				
Valve mount flange temperature	T_3	T/C	0–50 mv	X			
Injector flange temperature	T_7	T/C	0–50 mv	X		X	
Reactor heat shield temperature	T_6	T/C	0–50 mv	X		X	
Nozzle throat temperature	T_{16}	T/C	0–50 mv	X		X	
Bed heater voltage	B_h	N/A	0–50 vdc	X			
Bed heater current	I_h	N/A	0–50 ma	X			
TCV voltage	V_v	N/A	0–50 vdc		X	X	
TCV current	I_v	N/A	0–100 ma		X		
Reference frequency	H_z		0–100 Hz		X		
Event marker	E	N/A	N/A	All	X		
P_c integrator*	P_{cIn}	Mark	N/A		X		
Sightglass No. 1 level (TV)	H_{sg1}	1	N/A				X
Sightglass No. 2 level (TV)	H_{sg2}		N/A				X

*Use only if DDS is inoperative

THERMAL DESIGN TEST
T/C LOCATIONS

DECIMAL TOLERANCE
.XX ± .03 , .XXX ± .010
√ , ∠ ± °

Figure 4-3

Table 4-2
THERMAL MARGIN TEST – INSTRUMENTATION LIST

Parameter	Symbol	Type	Range	Recording			
				SCR	OSC	DDS	MAN
Forward heat shield temperature	T_4	T/C	0–50 mv	X			
Standoff temperature	T_5	T/C	0–50 mv	X			
Aft heat shield temperature	T_6	T/C	0–50 mv	X			
Propellant supply interface temp.	T_{14}	T/C	0–10 mv	X			
Thermal shunt temperature	T_{17A}	T/C	0–50 mv	X			
Mount bracket temp. (valve section)	T_{19}	T/C	-2 to +8 mv	X			
Mount bracket temp. (propellant line section)	T_{21}	T/C	-2 to +8 mv	X			
Propellant line temperature	T_{24}	T/C	-2 to +8 mv	X			
Pressure transducer temperature	T_{25}	T/C	-3 to +7 mv	X			
Temperature sensor sheath temperature	T_{26}	T/C	0–50 mv	X			
Heater sheath temperature	T_{27}	T/C	0–50 mv	X			
Cocoon (propellant line section) temperature	T_{29}	T/C	-8 to +12 mv	X			
Cocoon (valve section) temperature	T_{30}	T/C	-8 to +12 mv	X			
Temperature sensor transition temperature	T_{31}	T/C	0–20 mv	X			
Heater transition temperature	T_{32}	T/C	0–20 mv	X			

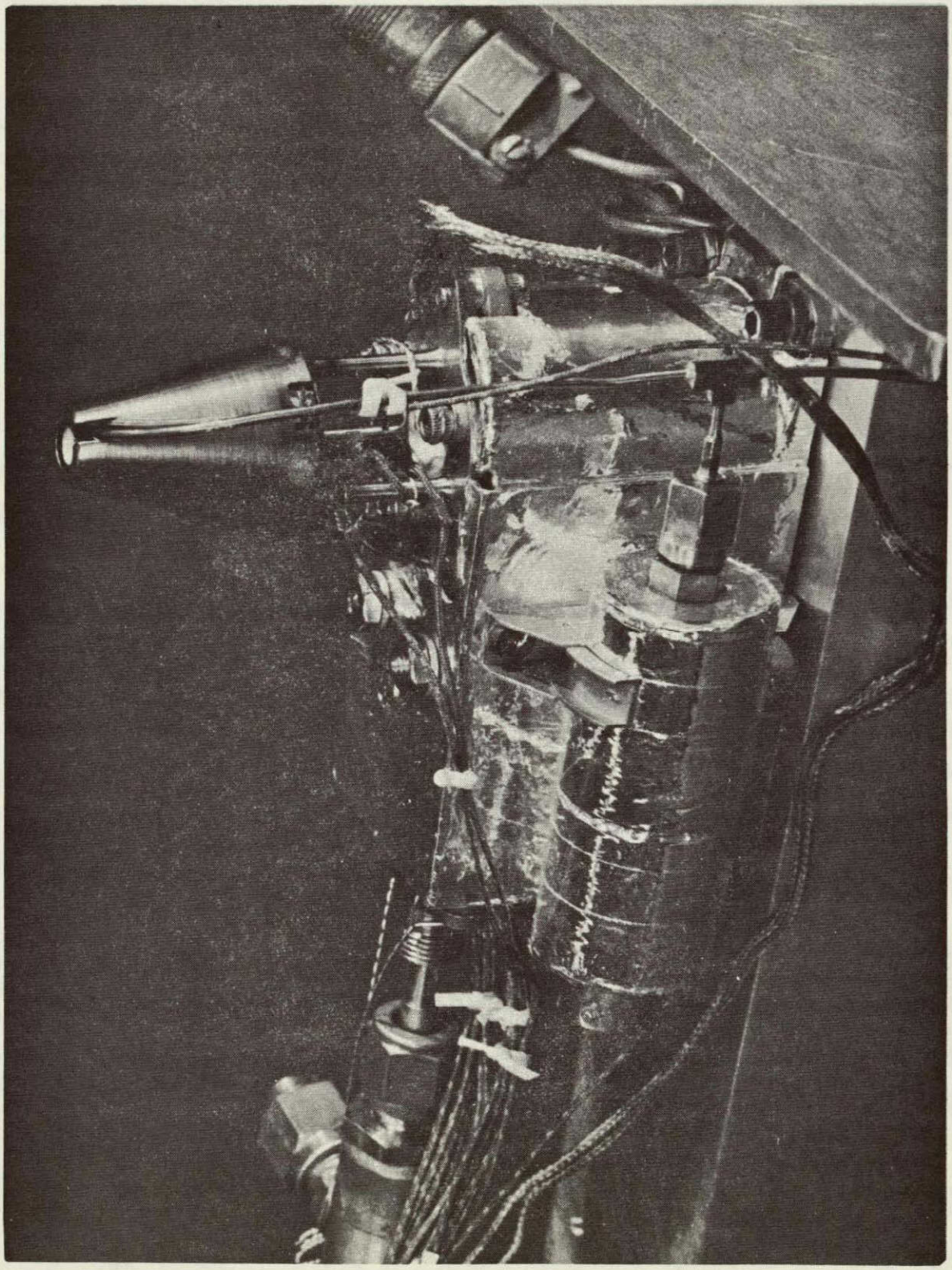

LCSSE/MJS T/VA D01 THERMAL DESIGN TEST

Figure 4-4

locations of the thermocouples. Notice that the numerical system used for the temperature locations corresponds to the nodes employed in the LCSSE/MJS thermal model. Figures 4-4 and 4-5 present two views of the T/VA S/N D01 used for the thermal design test. Also shown are the REA mount brackets and the heat exchanger used to condition the propellant inlet temperature to the T/VA. After the electrical cabling was connected to the J-1 and J-2 connectors, the wiring was routed next to the heat exchanger; copper wire was then wrapped around the heat exchanger and electrical wiring, and then mylar insulation wrapped around it to provide a constant temperature junction at the T/VA. This simulated the actual in-flight spacecraft design which will limit the heat losses through the electrical wiring. Figure 4-6 shows the T/VA insulation and the thermal shroud. The T/VA is not visible, however, the mount bracket and a portion of the T/VA pressure transducer can be seen. All of the propellant and conditioning lines were insulated using the mylar cloth. Also, the T/VA instrumentation wiring lines were insulated so that radiation losses would be negligible.

The test sequences were controlled using a micropulser. This device has thumbwheel switches which enable the operator to select the pulse on and off times and also the number of pulses. The general procedure used to conduct the performance mapping test duty cycles was to set the micropulser to the desired test duty cycle, check all instrumentation ΔC's, check the condition or readiness of the digital acquisition system, and to determine if all T/VA temperatures were at the desired pre-sequence test condition. The reader here is referred to Section 5.0 for a complete description of the test duty cycles employed. The test data was recorded during the initial startup transient and after approximately 100 to 150 pulses (during the middle portion of the transient) and finally at the thermal equilibrium conditions for each test duty cycle.

The procedure used during the thermal design test was to closely monitor all the T/VA temperatures as well as the shroud and mount condition temperatures. During the nonfiring conditions, the test sequence was considered at thermal equilibrium when there was no change in any temperature greater than $2^{o}F$ per hour.

The propellant used for both performance mapping and thermal design testing was MIL-P-26536C, Amendment I hydrazine. Figure 4-7 presents the analysis sheet and the acceptance levels necessary to meet the Amendment I hydrazine requirements. Rocket Research Corporation has a further stipulation on the propellant requirements shown for silicon content to be no greater than 0.05 ppm. This was arrived at from other programs and is necessary to eliminate silicon buildup in the injector during long-duration firing, producing thrust degradation. The propellant particulate contamination level was also checked and verified that it met the requirements of RRC Level GC per PS-0025. Particulate count samples were required to be taken within 3 manufacturing days of the T/VA installation prior to connection of the fuel inlet line to the T/VA. In addition, if a component in the fuel feed system was replaced after the system certification, a sample was drawn through the appropriate bleed valve and analyzed for particulate contamination. The nitrogen purge system was also certified for particulate contamination to Level GC per PS-0025. This was required to be completed within 8 days prior to the installation of the T/VA.

LCSSE/MJS T/VA D01 THERMAL DESIGN TEST

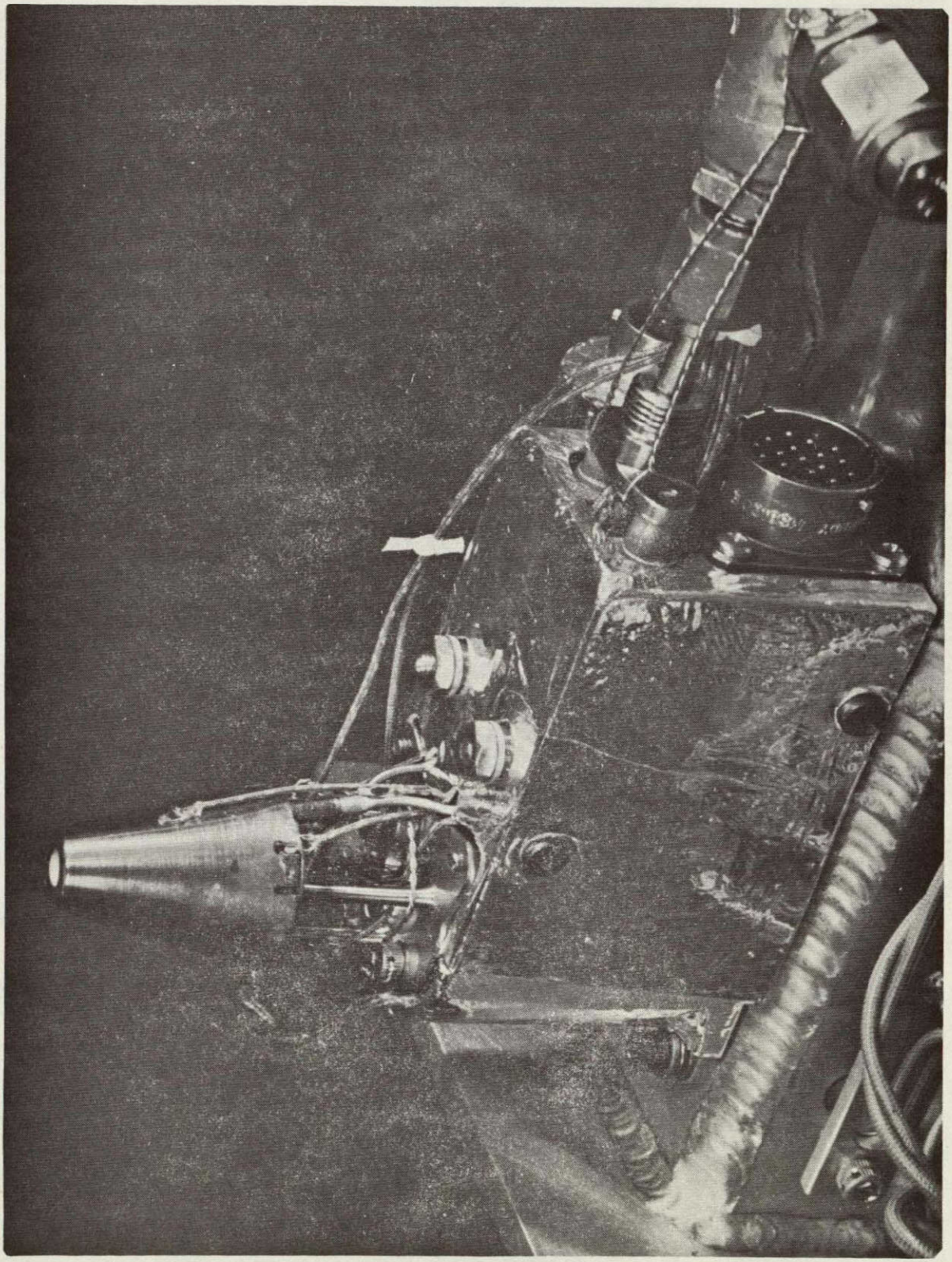

Figure 4-5

LCSSE/MJS T/VA D01 THERMAL DESIGN TEST SETUP

Figure 4-6

PROPELLANT ANALYSIS SHEET

ROCKET RESEARCH CORPORATION
HYDRAZINE ANALYTICAL FORM
FOR HYDRAZINE MEETING MIL-P-26536, AMENDMENT 1

Date Sampled: _____ Originator: _____ Approval: _____

Date Due: _____ Sample ID: _____

Date Received: _____ Charge No.: _____ Control No.: _____

DISPOSITION OF SAMPLE:

Analyses Requested: Check Box for All ☐	Check for Partial	Acceptable Level
a. N_2H_4, % by weight per RRC-M&P-0015, Para. 4.2.2.1 or Para. 4.2.2.2	☐	98.50% min.
b. NH_3, % by weight per RRC-M&P-0015, Para. 4.2.2.2	☐	0.40% max.
c. H_2O, % by weight, per RRC-M&P-0015, Para. 4.2.2.2	☐	1.00% max.
d. Trace organics, per TP-0294, Rev. "A", Para. 3.3	☐	200 ppm max.
e. Aniline, % by weight, per Para. 4.2.3 of RRC-M&P-0015	☐	0.50% max.
f. Total nonvolatiles, % by weight, per RRC-M&P-0015, Para. 4.2.4	☐	20.0 ppm max.
g. Particulate, per RRC-M&P-0015, Para. 4.2.5	☐	1.0 mg/l max.
h. Corrosivity, per RRC-M&P-0015, Para. 4.2.6	☐	25 ppm Fe max.
i. Chloride, per TP-0295	☐	5 ppm max.
j. Iron, per TP-0294, Rev. "A", Para. 3.9	☐	20 ppm max.
k. CO_2, per TP-0331	☐	200 ppm max.
l. Silicon, per TP-0294, Rev. "A", Para. 3.6 and 3.9 (optional—not required)	☐	0.05 ppm max.

(RESULTS ON PAGE 2 ATTACHED)

4.2 MOMENTUM WHEEL DESATURATION TESTING

The momentum wheel desaturation test was set up in RRC altitude chamber 4. This chamber is 4-1/2 feet in diameter and has a total volume of 96 cubic feet. The altitude capability is a maximum of 250,000 feet. High capacity Stokes mechanical vacuum pumps are used, and there are no diffusion pumps for this particular test cell. Figure 4-8 presents the schematic of the test setup used. Figures 4-9 and 4-10 show the installation of the T/VA into the test cell. The conditioning coils shown in close proximity of the T/VA were conditioned to 35 to 40°F and enabled quicker cooldown times associated with the momentum wheel desaturation type test duty cycles. It also allowed institution of cold starts where the bed temperature of the T/VA was allowed to reach a temperature of 40°F prior to starting of the test duty cycle. This test was an automated test and incorporated the RRC Mark III micropulser system. The micropulser was used to control the test duty cycle for on and off time and the total number of pulses for a given pulse train. The starting temperature of each pulse train was then controlled using the chamber wall temperature monitored on a strip chart using a limit switch. Tests were then initiated using the desired start temperature. After the total pulses required for the pulse train were fired, the T/VA operation was terminated automatically by the micropulser. When the T/VA cooled down to its desired start temperature, the pulse train would then again be initiated. The instrumentation recorded was similar to the performance mapping test program on T/VA D01. Amendment I hydrazine was used throughout the test program. Contamination samples of both the hydrazine and gaseous nitrogen supply were conducted identically as stated in paragraph 4.1.

4.3 C_f MAPPING TESTS

The C_f mapping tests were conducted in test chamber 1, the same test cell used for performance and thermal design testing. Figure 4-11 presents a picture of the RRC microthrust balance used to measure steady-state and pulse-mode C_f. For a complete description of the fundamentals of the thrust balance, the reader is referred to Section 5.0 in this report. Figure 4-12 presents a schematic of the propellant feed system, which was completely contained on the upper platform of the microthrust balance. As shown, tank 1 was used as the propellant supply tank, with tanks 2 and 3 used for the nitrogen pressurization. Tank 2 was pressurized to the same pressure as the propellant tank, and tank 3 was charged to 1,500 psi at the beginning of the test series while the test cell was at sea-level conditions. This enabled repressurization of tanks 1 and 2 during the test sequencing without having to open the test chamber and returned to sea-level conditions.

Presented in Figure 4-13 are the various calibration weights that were used along with their moment arms during the C_f mapping tests. The locations of these calibration weights are shown in Figure 4-13, and they were controlled using an electric motor which raised and lowered the platform they rested on. The equivalent thrust levels were then calculated by summing the moments imparted by the different calibration weights to the balance.

4.4 ENVIRONMENTAL TESTING

The development vibration testing using the qualification test levels was conducted in the RRC environmental test laboratories. The test equipment consisted of a Ling-Model 300B vibration shaker driven by a Ling 35-power amplifier rated at 35 Kva. The shaker has a rating of 8,000 lbf in

MOMENTUM WHEEL DESATURATION TESTING SETUP

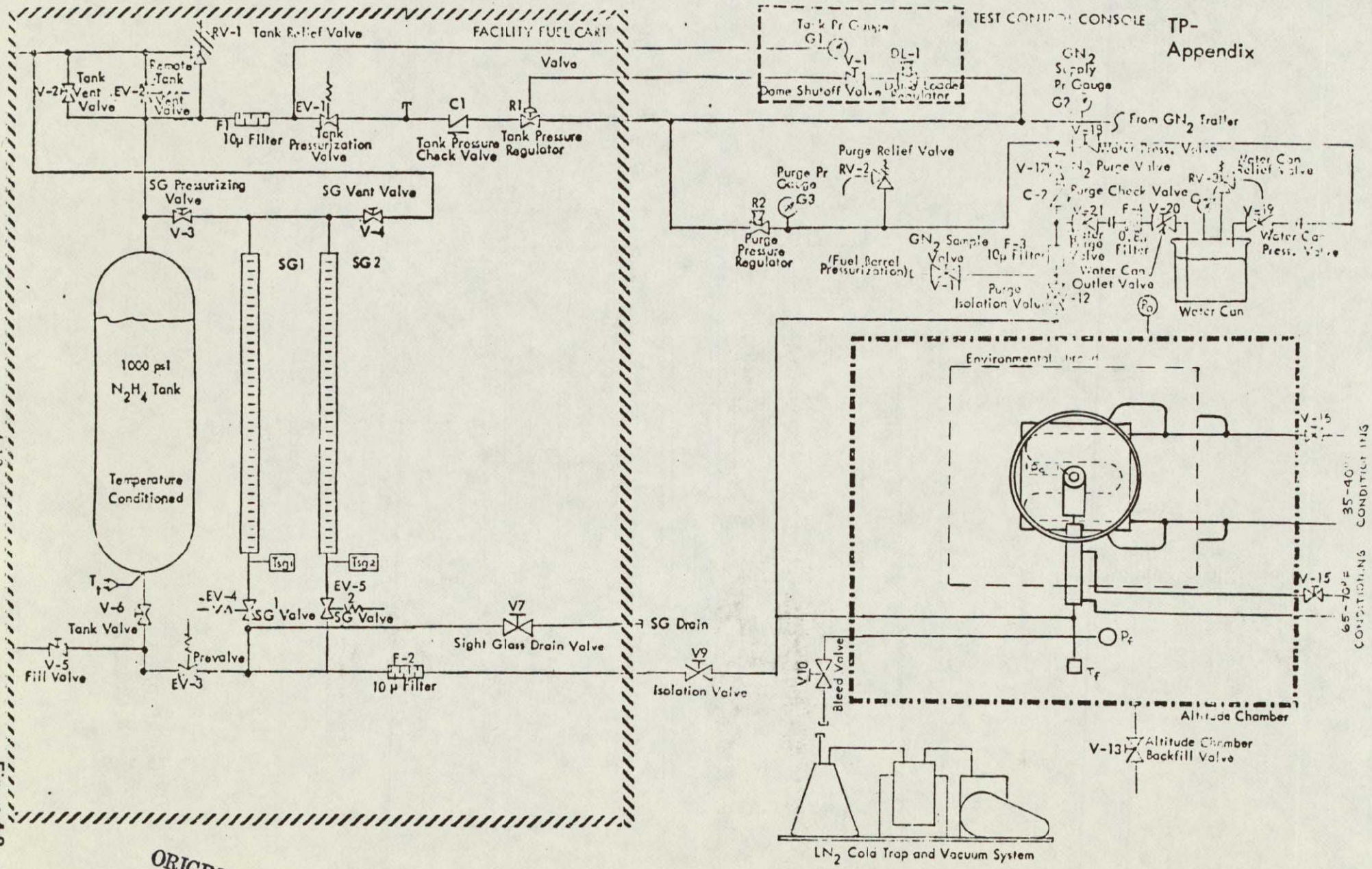

TP-Appendix

Figure 4-8

Figure 4-9

T/VA D02 TEST INSTALLATION

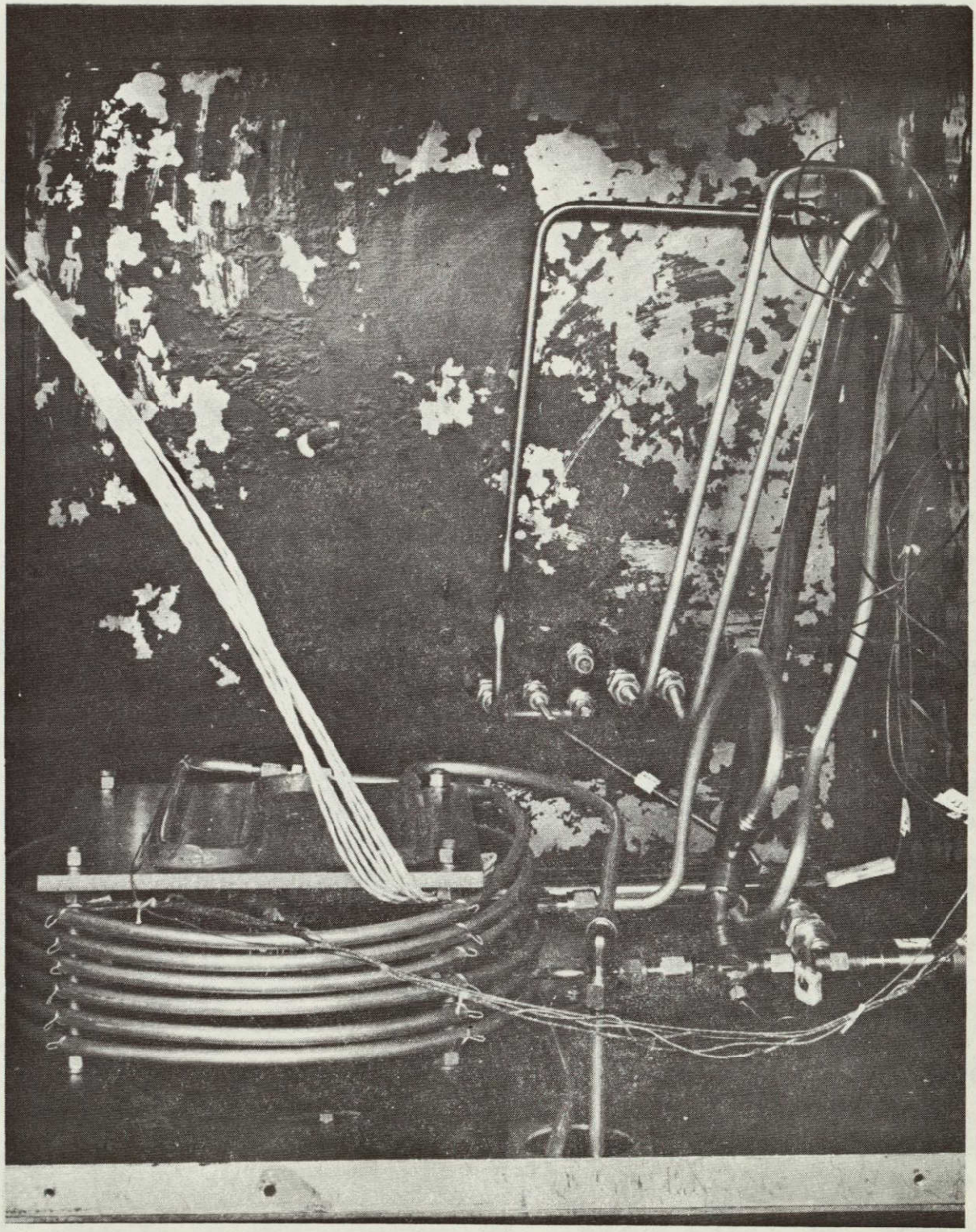

Figure 4-10

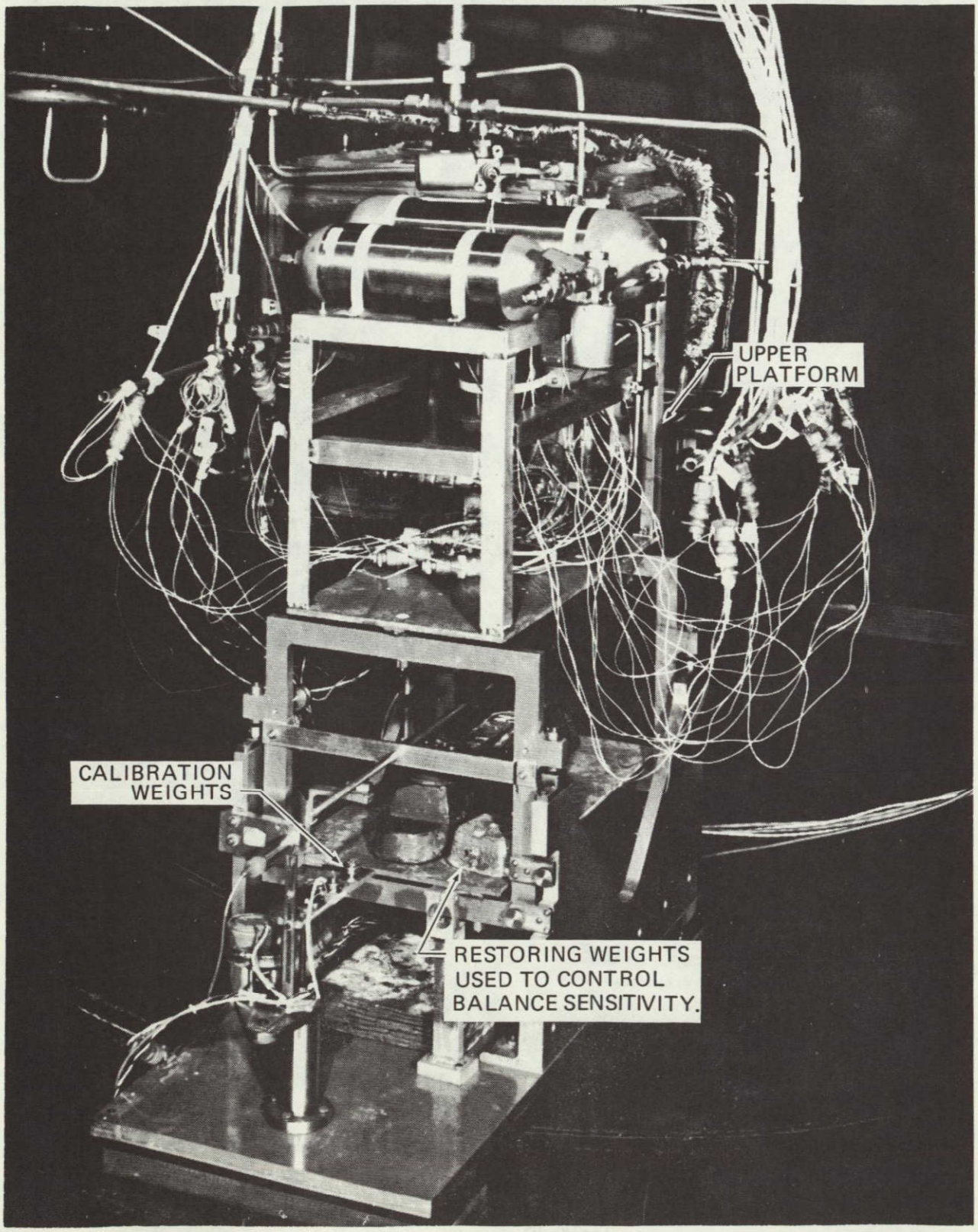
UPPER
PLATFORM
CALIBRATION
WEIGHTS
RESTORING WEIGHTS
USED TO CONTROL
BALANCE SENSITIVITY.

Figure 4-11

SCHEMATIC OF THE PROPELLANT FEED SYSTEM
CONTAINED ENTIRELY ON THE RRC MICROTHRUST
BALANCE UPPER PLATFORM

DECIMAL TOLERANCE
.XX ± .03 , .XXX ± .010
√ , ∠ ± °

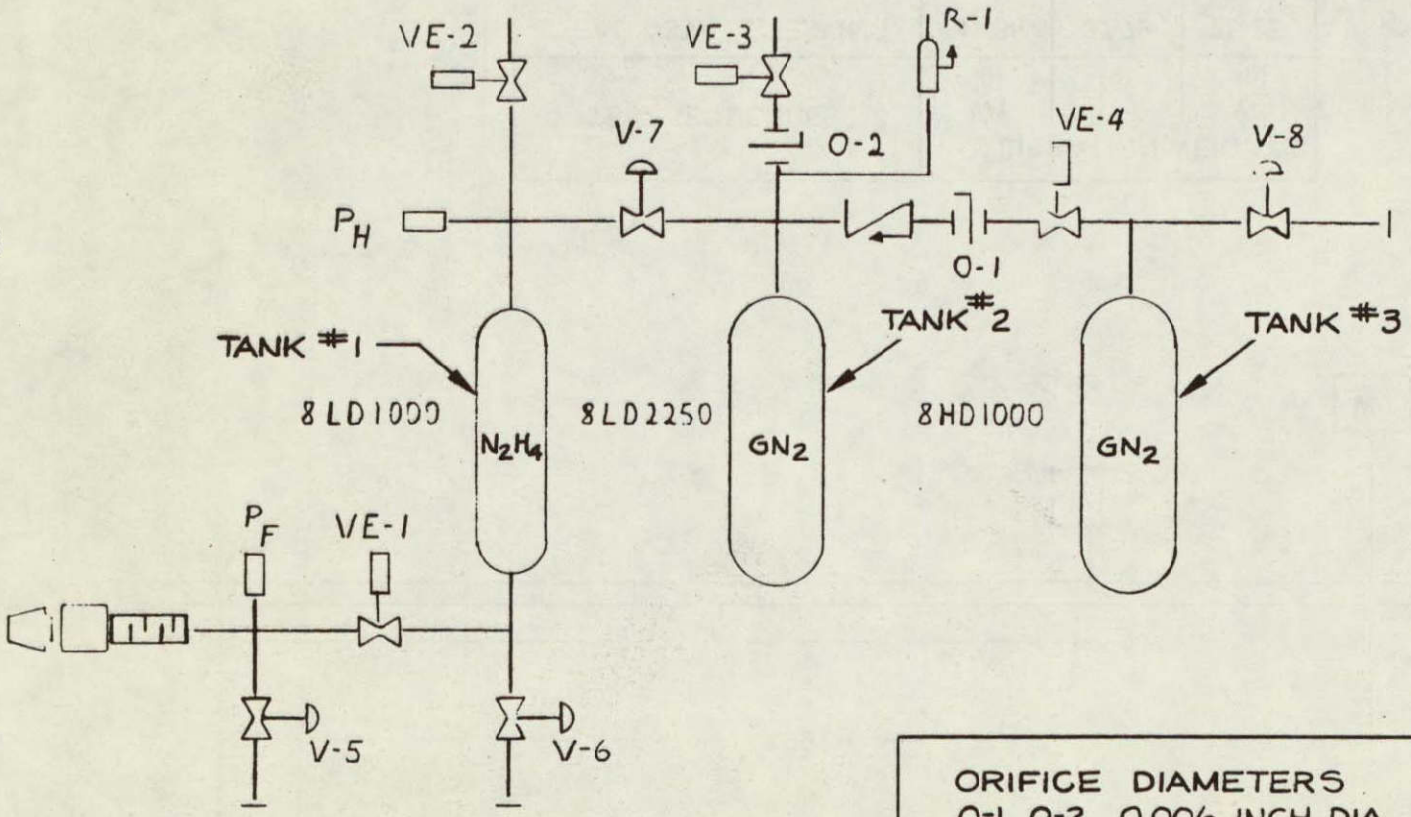

ORIFICE DIAMETERS O-1, O-2, 0.006 INCH DIA.
RELIEF VALVE PRESSURE R-1 500 PSI

Figure 4-12

11097-69

MICROTHRUST CALIBRATION WEIGHTS AND MOMENTUM ARMS

MOMENTUM ARMS OF THE THREE CALIBRATION WEIGHTS

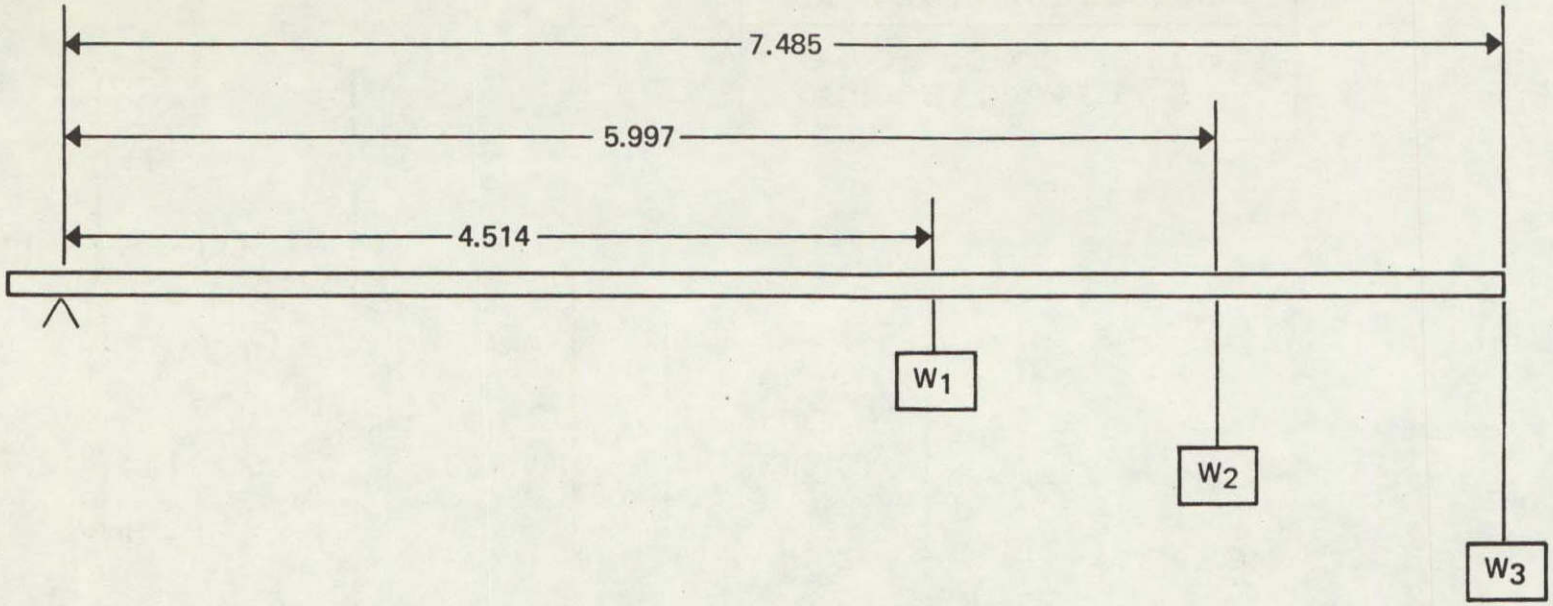

TEST SEQUENCES	CALIBRATION WEIGHTS		
	W_1 (g)	W_2 (g)	W_3 (g)
STEADY-STATE TESTING	41.86	37.79	25.25
LARGE PULSE WIDTH	14.95	11.25	9.00
SMALL PULSE WIDTHS	2.99	2.25	1.80

Figure 4-13

the sinusoidal mode and 6,000 lbf in the random mode. The vibration frequency range is from 10 to 2,050 Hz with a 45-channel spectrum equalization and spectrum analysis capability. Figure 4-14 presents an illustration of the vibration test setup. Both development thruster D01 and D02 were vibrated at the same time in the nozzle-up orientation. In addition, a nitrogen pressurization source regulated to 10 ± 2 psig was attached to each T/VA inlet tube. Each T/VA nozzle was then covered with plater's tape, and two inverted graduated cylinders were attached using Tygon tubing to the Pc test port fitting. This setup then enabled the measurement of valve seat leakage during vibration.

The pyro shock test was conducted on T/VA D02 at a Boeing environmental test facility. Figures 4-15 through 4-17 present pictures of the test setup, and Figures 4-18 through 4-21 present pictures of the equipment used for this test. The detailed description of the results of these tests is contained in paragraph 6.1 of this report.

ILLUSTRATION OF THE VIBRATION TEST SETUP

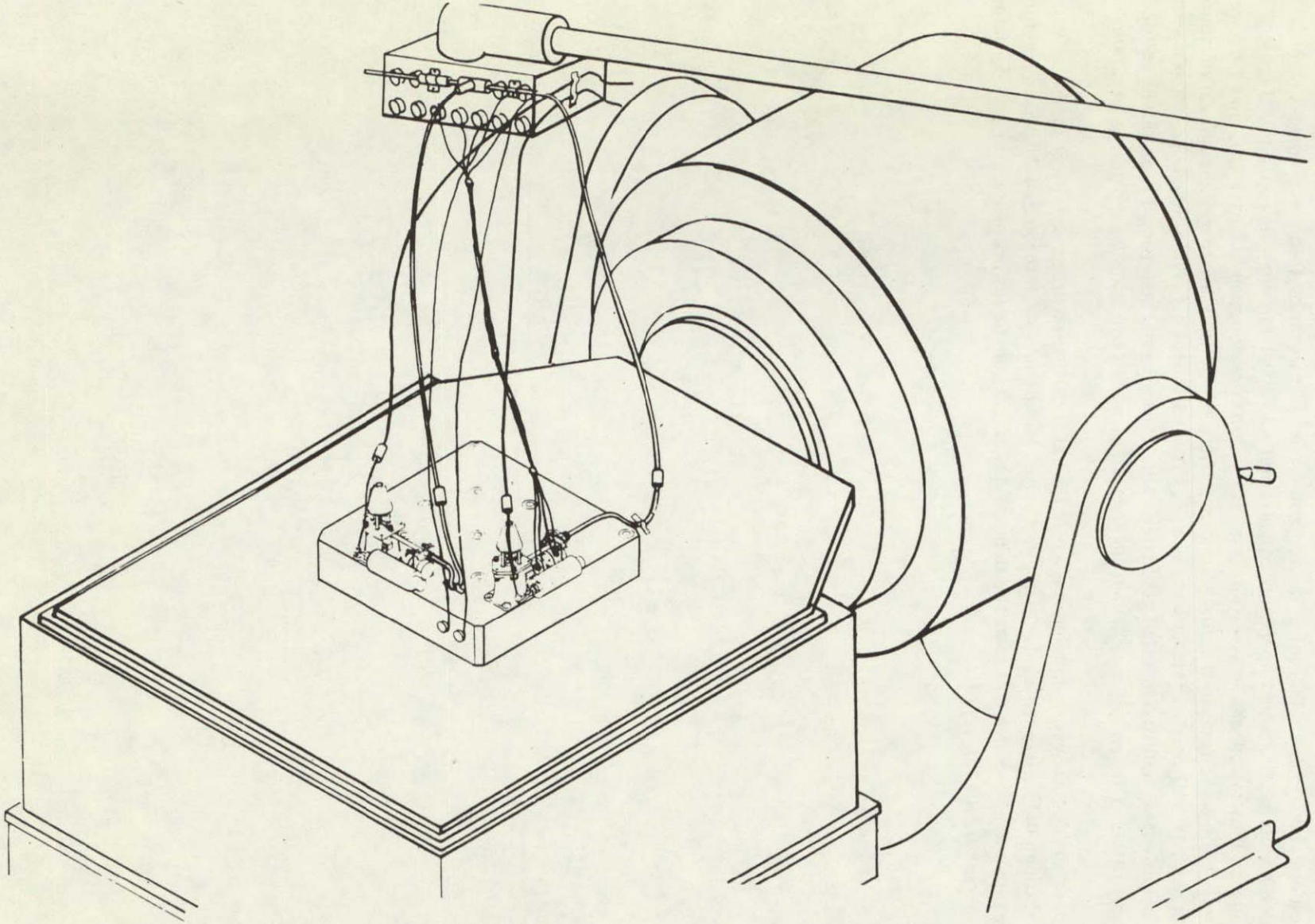

Figure 4-14

LCSSE/MJS THRUSTER VALVE PYRO SHOCK TEST X AXIS

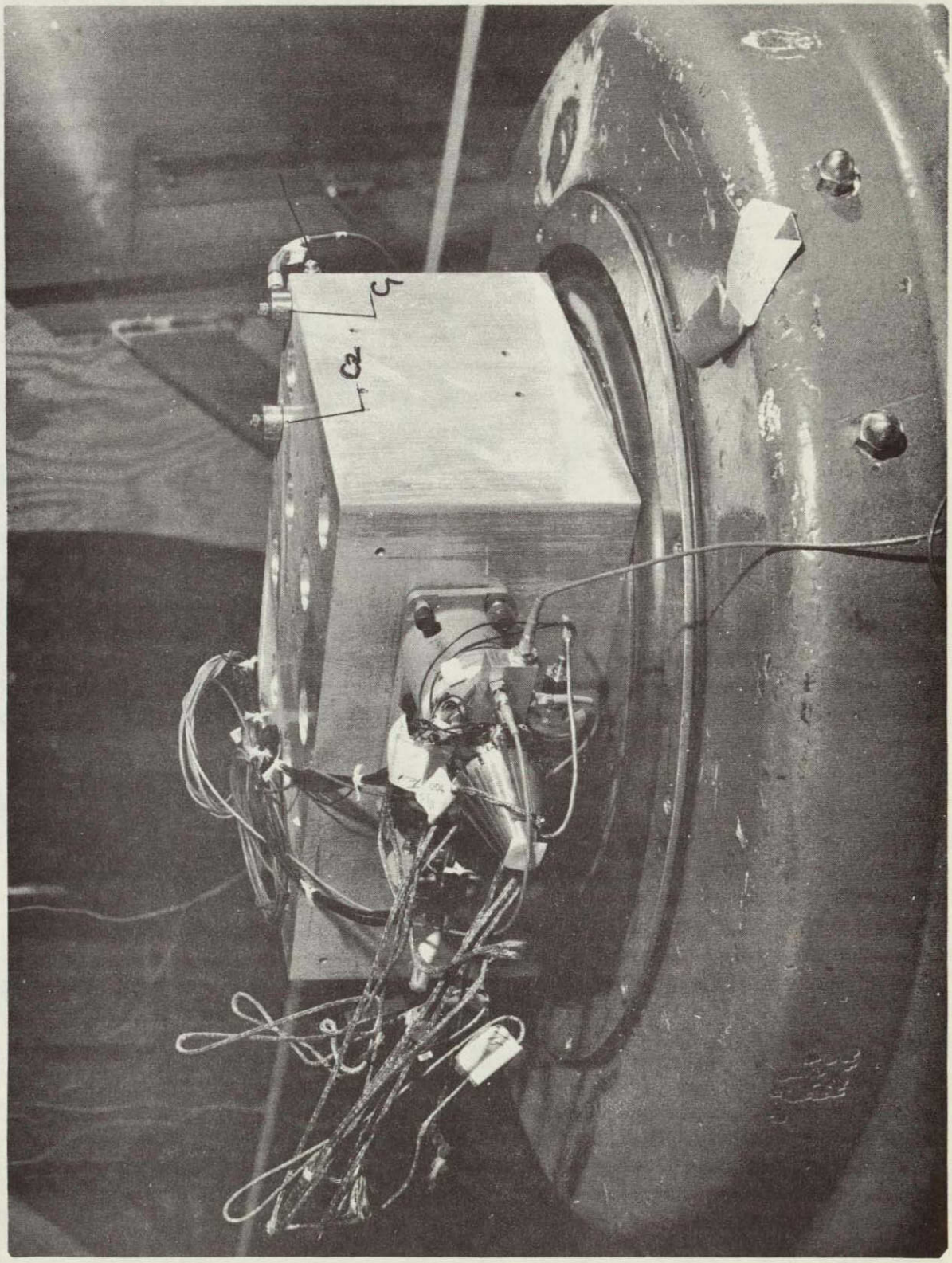

Figure 4-15

LCSSE/MJS THRUSTER/VALVE PYRO SHOCK TEST Y AXIS

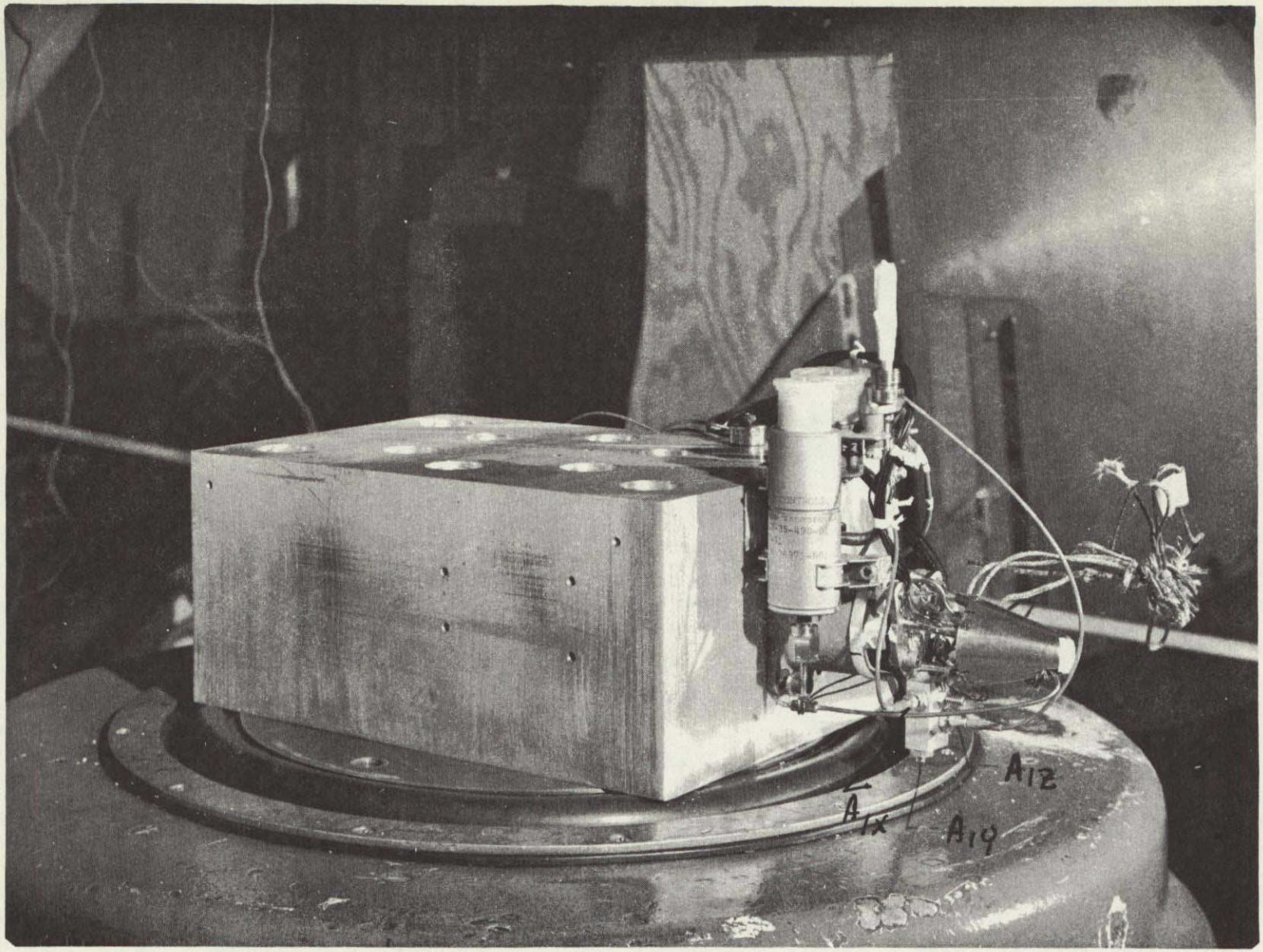

Figure 4-16

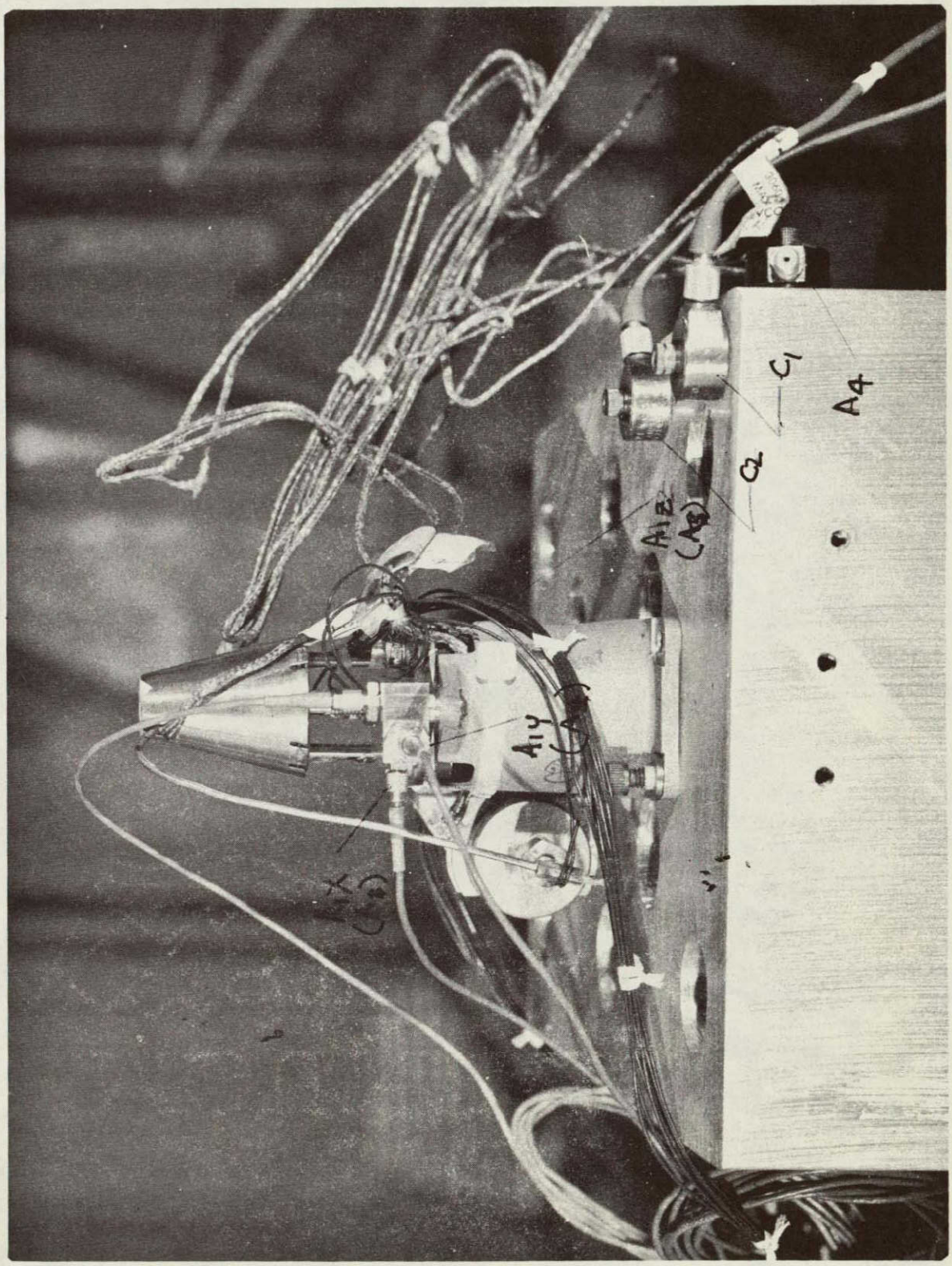

LCSSE/MJS THRUSTER/VALVE PYRO SHOCK TEST Z AXIS

ORIGINAL PAGE IS
OF POOR QUALITY

LCSSE/MJS THRUSTER/VALVE PYRO SHOCK TEST CONTROL CONSOLE

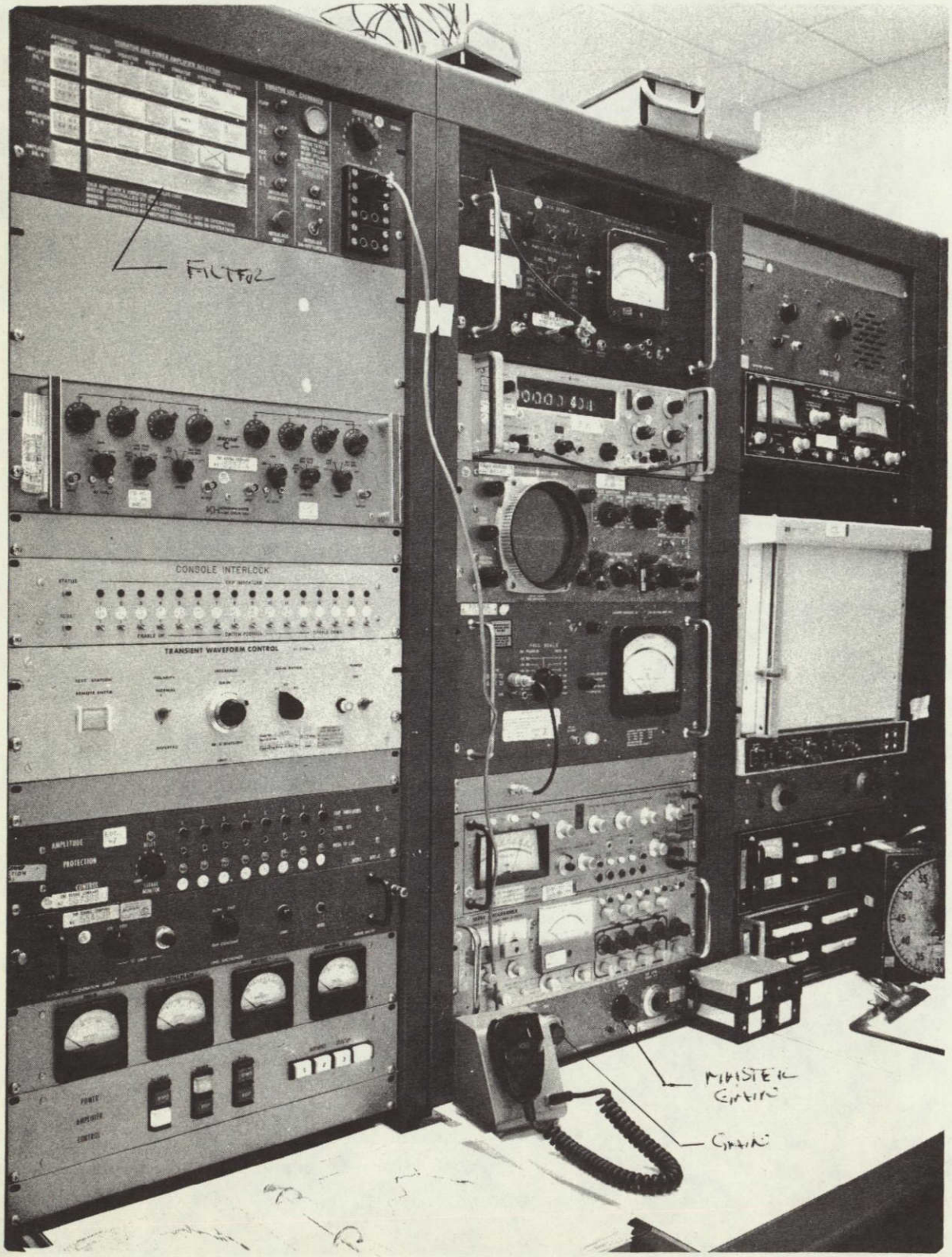

LCSSE/MJS THRUSTER/VALVE PYRO SHOCK TEST PATCH PANEL CONTROL CONSOLE

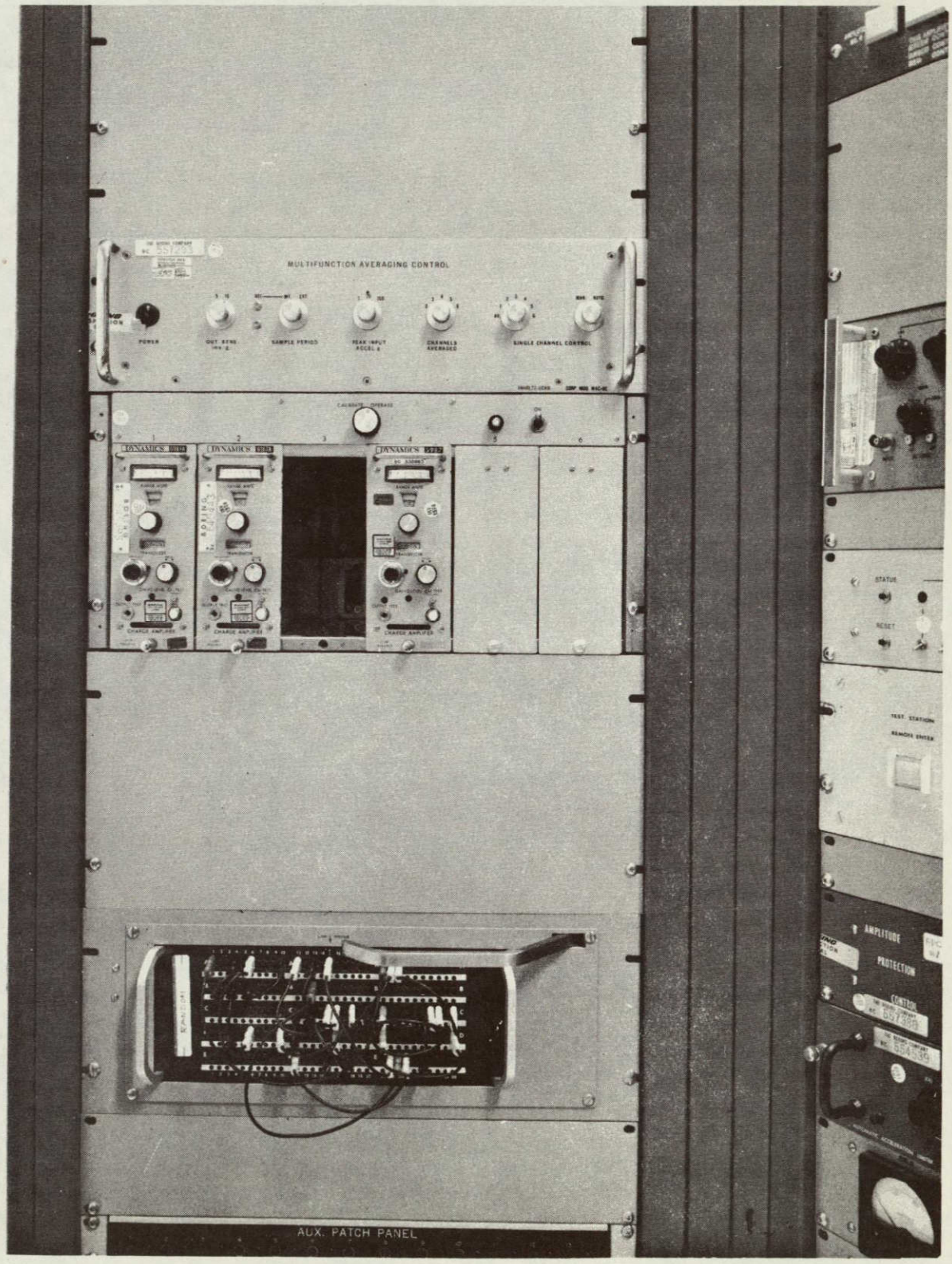

LCSSE/MJS THRUSTER/VALVE PYRO SHOCK TEST SHOCK SYNTHESIZER AND GEN.

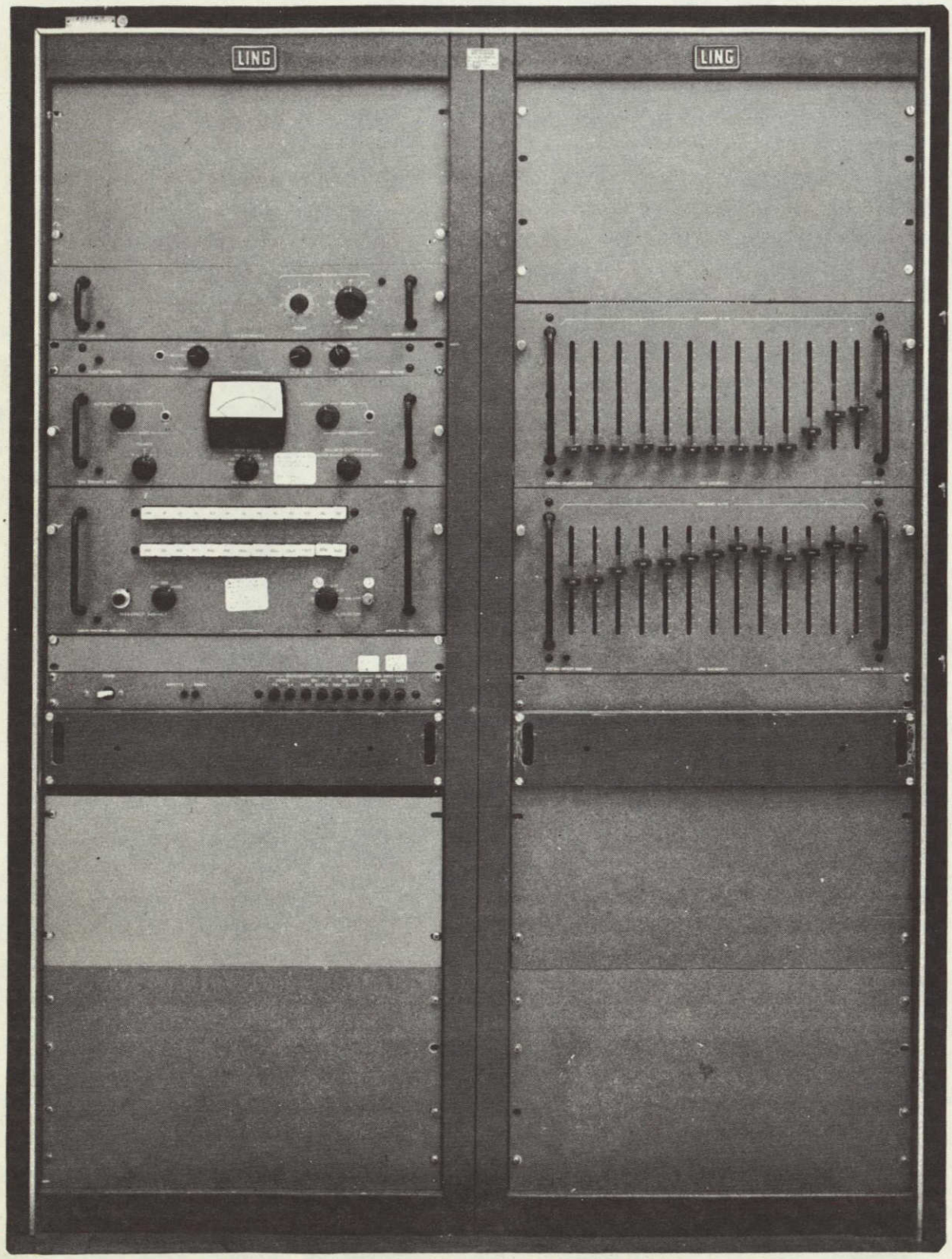

LCSSE/MJS THRUSTER/VALVE PYRO SHOCK TEST INSTRUMENTATION RACK

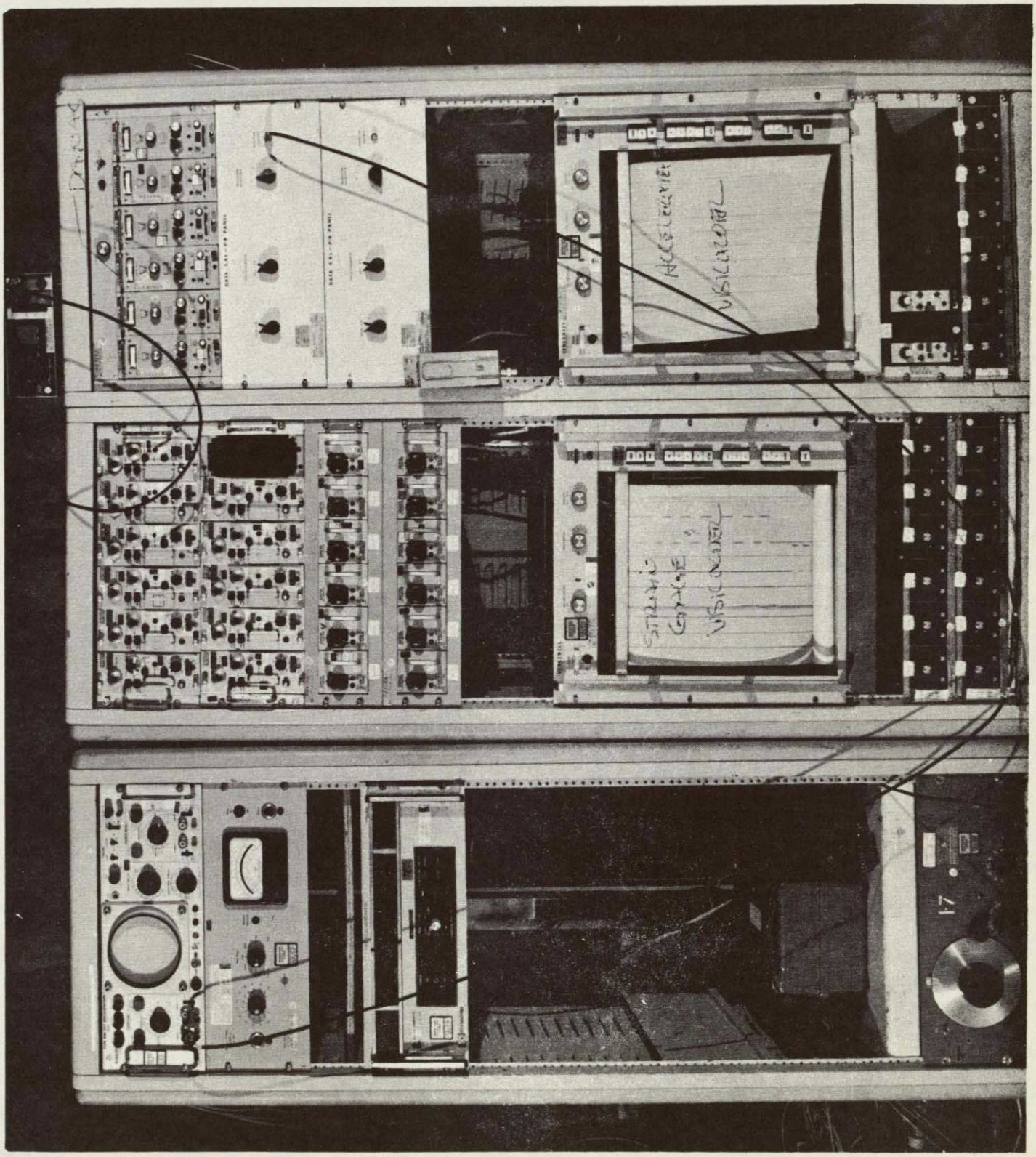

Figure 4-21

5.0 DATA REDUCTION TECHNIQUES

This section presents the data reduction techniques applied to the raw data generated during the development test program and is subdivided to describe steady state, pulse mode, and C_f data reduction. The methods discussed below apply to both digital and manual data reduction. The digital system was the primary method used (manual reduction used as a backup for performance mapping). However, manual data reduction was exclusively used for C_f mapping and steady-state life margin tests.

5.1 STEADY-STATE DATA

The first parameter discussed will be the measurement of thrust. Steady-state thrust was measured during the C_f-mapping test series. Data reduction for this test series is discussed in paragraph 5.3. For the performance mapping and steady-state life margin tests thrust was calculated using a 250 millisecond data averaging interval occurring at the end of the steady-state test, and the C_f data as follows:

$$F_{cal} = P_c C_f A_{t\ hot} \tag{1}$$

where

P_c = Measured chamber pressure using the Statham facility test transducer.
NOTE: The Standard Controls flight transducer was used for performance mapping.

C_f = Derived from the C_f versus P_c curve generated as a part of C_f mapping tests.

$A_{t\ hot} = 0.9986\ A_{t\ cold}\ [1 + 2\alpha\Delta T]$ where

$\alpha = 8.24 \times 10^{-6}$

$\Delta T = T_{throat} - 70^{o}F$

The performance parameters specific impulse (I_{sp}) and characteristic velocity (c*) were derived as follows:

$$I_{sp} = \frac{F_{cal}}{\dot{W}} \tag{2}$$

and

$$c^* = \frac{P_c\ A_{t\ hot}\ 32.17}{\dot{W}} \tag{3}$$

where

$\dot{\bar{w}}$ = The average propellant flowrate measured during the last 10 to 20 seconds of the steady-state test.

Propellant flowrate was measured using a sightglass and the value calculated as follows:

$$\dot{\bar{w}} = \frac{\Delta H \cdot K_{sg} \cdot 2.6417 \times 10^{-4} \cdot \rho_p}{\Delta t} \quad (4)$$

where

ΔH = Sightglass deflection, cm

K_{sg} = Sightglass constant, cm^3/cm

ρ_p = Propellant density, lbm/gal (at measured propellant temperature)

Δt = The time of sightglass operation

Two calculations were made to determine the T/VA roughness level. The period used for determination was 5.0 seconds minimum, and or the data interval whichever was larger. The two methods employed were as follows:

a. $$\frac{P_c \max - P_c \min}{2\bar{P}_c} X100\ (\pm\%) \quad (5)$$

b. Standard deviation in $P_c = \frac{\sigma}{\bar{P}_c} X100 \quad (6)$

where $\sigma = \sqrt{\frac{\sum_{i=1}^{i=n} (P_{ci} - \bar{P}_c)^2}{n-1}}$

The steady-state response time were calculated based on the percent of chamber pressure reached at 500 milliseconds. The definitions employed were based on the requirements of ES 509778:

a. Ignition rise time (TI) = the time from valve signal on to 10 percent P_c (at 500 milliseconds)

b. Rise response (TR) = the time from valve signal on to 90 percent P_c (at 500 milliseconds)

c. The decay response (TD) = the time to 10 percent P_c based on the average P_c over the last 250 milliseconds.

5.2 PULSE MODE PERFORMANCE

The pulse mode impulse bit was calculated from the chamber pressure integral using the C_f correlation generated as a part of this development program.

$$I_{bit} = \int_{t_{on}}^{t_{off} + 0.9} P_c \, dt \cdot C_f \cdot A_{t\,hot} \tag{7}$$

As shown, the integration period was equal to the electrical pulse width commanded plus 0.900 seconds. The definition for hot throat area is the same as shown above under the steady state discussion, except that T_{nozzle} was calculated using a correlation between the flight temperature sensor and T_{nozzle}.

The centroid time was calculated as the time from valve command signal ON to 1/2 the total integral of chamber pressure as described above for impulse bit.

The centroid bit and impulse bit repeatability values were calculated as follows:

$$\frac{\text{Max} - \text{Min}}{\text{Max} + \text{Min}} \times 100 = \pm\%$$

This method checks within 0.5 percent of the 3σ statistical value and greatly reduces the cost of data reduction.

The rotational efficiency was calculated from the integral of P_c for the spin rate stipulated by the respective duty cycle. Rotation efficiency is defined as:

$$\%\,\text{Eff} = 100\,X \quad \int_{Rot} P_c dt \Big/ \int P_c dt \tag{8}$$

where

$$\int_{Rot} P_c dt = \left[\left(\int P_c - \cos \Omega t \right)^2 + \left(\int P_c - \sin \Omega t \right)^2 \right]^{1/2} \tag{9}$$

$$\Omega = \text{Spin rate} = \frac{2\pi}{\text{Pulse ON time} + \text{OFF time}} \tag{10}$$

Pulse mode response times are calculated in a similar manner as steady-state response, except that the chamber pressure level used to define 100 percent P_c is more complex. The response times to 10 percent rise (TR), 10 percent decay (TD), and 90 percent rise (TR) are based on peak chamber pressure, where peak chamber pressure is defined as:

a. Maximum measured P_c for pulse widths $<$60 milliseconds.

b. Average P_c for the last 20 milliseconds of the pulse for pulse widths $\geq$60 milliseconds.

The pulse mode specific impulse was calculated as follows:

$$\text{P.M. } I_{sp} = \frac{I_{bit}}{w_p}$$

where

I_{bit} = Impulse bit defined above

$$\overline{w}_p = \frac{\Delta H \cdot K_{sg} \cdot 2.6417 \times 10^{-4} \cdot \rho_p}{N} \qquad (11)$$

where

ΔH = Sightglass deflection, cm

K_{sg} = Sightglass constant, cm^7/cm

ρ_p = Propellant density, lbm/gal (at measured propellant temperature)

N = Number of pulses taken during the sightglass measurement.

5.3 C_f DATA REDUCTION

As a part of the 0.2-lbf T/VA development program, C_f data for both steady state and pulse mode operation was generated. The RRC microthrust, or compound pendulum, balance was used to measure thrust and impulse bit. This section describes the balance fundamentals and the methods employed for data reduction.

The basic principle of the compound pendulum balance is that of a freely suspended pendulum. When acted upon by a steady-state force, the pendulum is displaced an amount proportional to the amplitude of the force. Thus, a steady-state thrust is measured by allowing the pendulum balance to reach an equilibrium position with the applied thrust and observing the balance displacement. When acted upon by an impulsive force, the pendulum, being initially at rest, instantly reaches a maximum velocity and therefore, a maximum kinetic energy which is directly proporational to the impulse delivered. When the pendulum reaches its maximum swing, all the kinetic energy imparted is stored as potential energy, which is directly proportional to the square of displacement of the pendulum. Total impulse is therefore measured by allowing the balance to receive the entire impulse and observing the maximum displacement of the pendulum.

5.3.1 Steady-State Thrust Measurement

In order to most easily visualize the relationship between the steady-state forces acting on the balance, the compound pendulum is represented as a single pivot arm of length 2L rotating about a point as shown in Figure 5-1. A detailed analysis of the complete balance proves this representation to be correct. The thrust acts horizontally at the upper end of the pivot arm. The weights on the top and bottom platforms, W_T and W_B, respectively, are considered to be concentrated at the ends of the pivot arm. When the balance is displaced an amount X by a steady-state thrust F, a summation of moments about the pivot axis yields the equation:

$$(W_B - W_T)\, X = F(L^2 - X^2)^{1/2} \qquad (12)$$

Since X is maintained extremely small compared to L, this equation can be written:

$$(W_B - W_T)\, X = FL \qquad (13)$$

COMPOUND PENDULUM BALANCE
FORCE BALANCE DIAGRAM

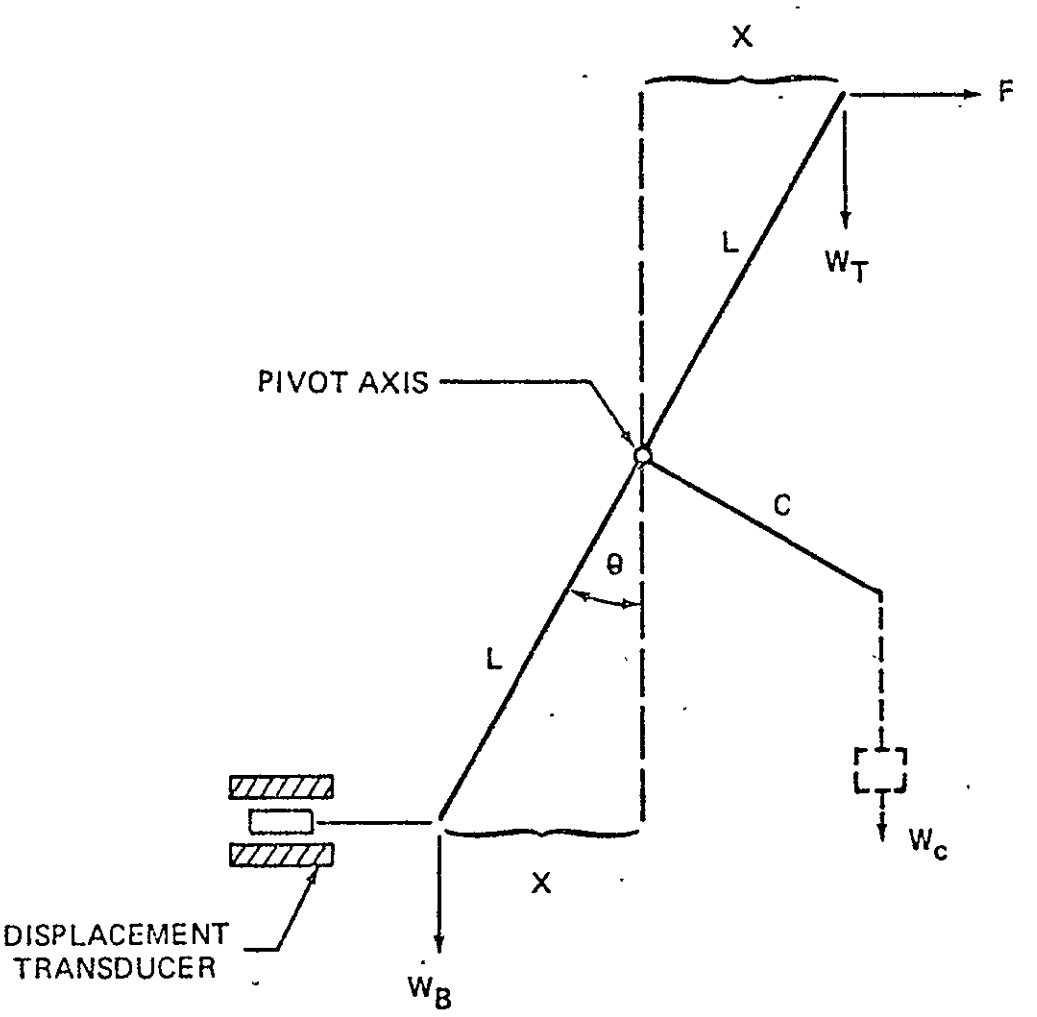

NOTE: THE DISPLACEMENT X HAS BEEN GREATLY EXAGGERATED IN PROPORTION TO L FOR CLARITY.

Prior to a test, the balance is displaced by a calibration weight, W_C, suspended from the cantilever beam at a horizontal distance c from the pivot axis. Again, summing the moments about the pivot axis, the following relationship is obtained:

$$(W_B - W_T) X = W_C C \tag{14}$$

By comparing displacement transducer outputs obtained from the calibration steps with that obtained with a steady-state thrust applied, the magnitude of the thrust can be determined by linear interpolation using equivalent thrust values for the calibration steps. Therefore, if X_C is the displacement of the calibration weight(s) then:

$$F = \frac{W_C}{X_C} \cdot \frac{C}{L} \cdot X \tag{15}$$

Since the calibration weights and momentum arms are constant for a given test setup it follows that

$$F = \frac{F_{cal}}{X_C} X \text{ where } F_{cal} = \frac{W_C \cdot C}{L} \tag{16}$$

5.3.2 Pulse Mode Impulse Measurement

During pulse-mode operation, the balance can again be considered to be the simple pendulum shown in Figure 5-1. If the balance is at rest in the vertical position, an impulsive force F will accelerate the pendulum nearly instantaneously to a maximum velocity according to the impulse-momentum equation:

$$\int_0^t F dt = MV \tag{17}$$

where:

F	=	Thrust
t	=	Pulse duration
M	=	Balance mass
	=	$W_T + W_B$
V	=	Maximum velocity at end of pendulum arm

The pendulum now has a velocity and therefore a kinetic energy:

$$K.E. = 1/2\, MV^2 \tag{18}$$

This kinetic energy is completely stored as potential energy when the pendulum reaches its maximum displacement. Now, rewriting equation (13) as:

$$F = \frac{(W_B - W_T)}{L} X \tag{19}$$

it is evident that the pendulum is essentially a linear spring with an effective "spring constant" given by:

$$K = \frac{W_B - W_T}{L} \tag{20}$$

At its maximum displacement, a linear spring has a potential energy:

$$P.E. = 1/2\ KX^2 \tag{21}$$

and the storage of the pendulum's kinetic energy as potential energy is described by the equation:

$$1/2\ MV^2 = 1/2\ KX^2 \tag{22}$$

Solving for momentum:

$$MV = (MK)^{1/2} X \tag{23}$$

The impulse delivered to the balance is, therefore, directly proportional to the maximum balance displacement.

It is not practical to calculate impulse by measuring the actual balance mass, restoring force, and displacement. It is necessary, therefore, to develop a means whereby values for delivered impulse can be determined using only the observed response of the balance. After receiving the delivered impulse, the pendulum oscillates at its natural frequency which, with no damping present, is equal to:

$$w = \left[\frac{K}{M}\right]^{1/2} \tag{24}$$

where:

w = Natural frequency, radians/second.

Solving for M yields:

$$M = \frac{K}{w^2} \tag{25}$$

Substituting (25) into (23) yields:

$$MV = \frac{K}{w} X \tag{26}$$

If a known force F is impressed on the balance, a displacement X results such that:

$$F = KX \tag{27}$$

where K is defined by equation (20), and equation (26) can be written:

$$MV = \frac{F}{w} \tag{28}$$

Since the natural frequency can be defined as:

$$w = \frac{2\pi}{T} \tag{29}$$

where T equals the period (in seconds), equation (28) becomes:

$$MV = \int_0^t F dt = \frac{F_{SS}\, T}{2\pi} \tag{30}$$

Therefore, by observing the balance deflection on a recorder which is calibrated from a known force (W_C) and measuring the total period, one can calculate the equivalent momentum required to produce the same deflection. The equivalent steady-state thrust F_{SS} in equation (30) is found by the same linear interpolation as described above for steady-state thrust calibration.

The above analysis assumes that the impulse is delivered to the pendulum in an infinitely small time interval, such that no change in potential energy occurs while the thrust is applied. However, pulse mode operation requires a finite pulse width. For the LCSSE/MJS 0.2-lbf T/VA these pulse widths ranged from 0.008 to 0.500 seconds. In addition, characteristic thruster tailoff times indicate impulse is delivered at very low levels for at least 2.0 to 5.0 seconds. Therefore, the data reduction technique described below was applied to account for these items.

Figure 5-2 illustrates a typical pulse-mode trace for the 0.2-lbf T/VA. Practical limitations with restoring force and displacement transducer resolution limited the maximum period to approximately 8.0 seconds. As a result, thruster impulse being delivered past the point of maximum balance deflection (T_2) altered the effective balance natural frequency. That is, the effect of impulse being supplied past the time T_2 has the effect of slowing down the balance and, therefore, the theoretical balance period is not $T_4 - T_1$ as would be expected. Thus, the actual thrust integration or impulse measurement stops at the point of maximum balance deflection T_2. Therefore, the actual integration time is $T_2 - T_1$ and

$$MV_{measured} = \int_{T_1}^{T_2} F dt \tag{31}$$

PULSE MODE BALANCE THRUST MEASUREMENT

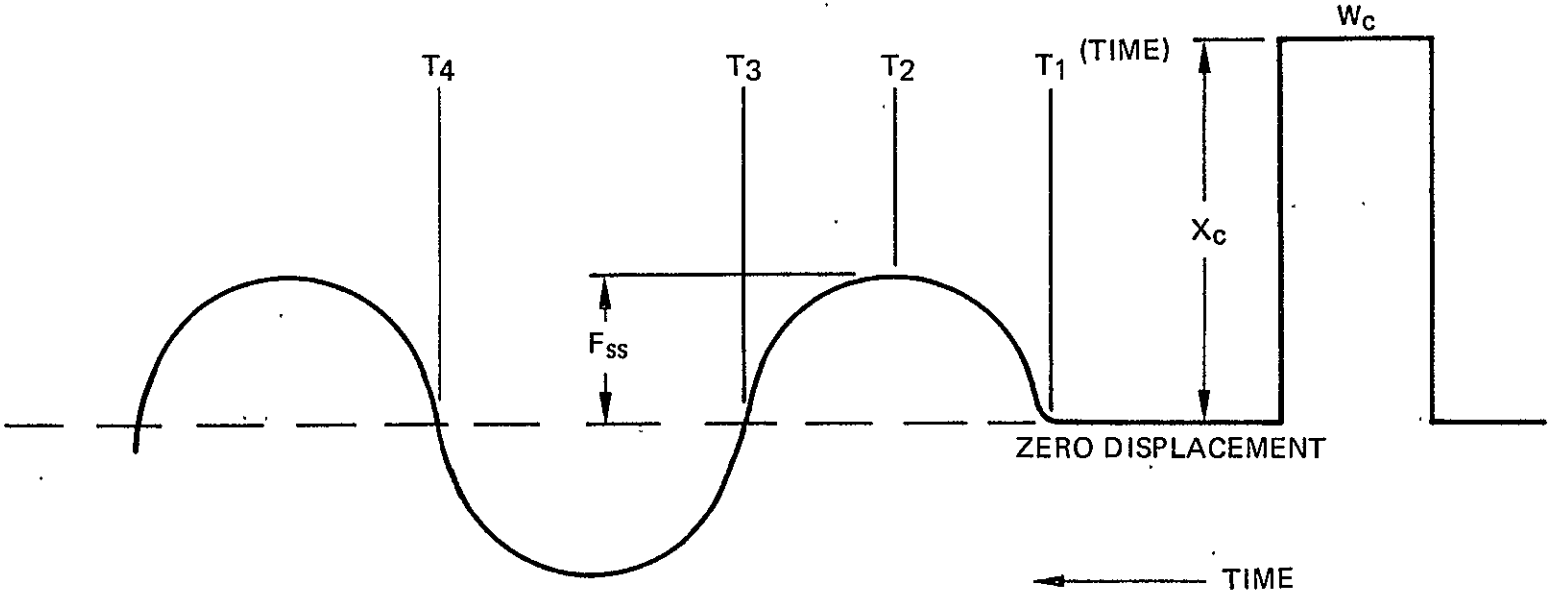

T = TOTAL PERIOD = $T_4 - T_1$

Figure 5-2

If the assumption is made that no impulse is supplied past the time T_2, then the period would equal

$$T = 4\,(T_2 - T_1) \tag{32}$$

and

$$\int_{T_1}^{T_2} F\,dt = \frac{2\,F_{ss}\,(T_2 - T_1)}{\pi} \tag{33}$$

Equation (33) represents the total impulse that can be measured with the 0.2-lbf thruster applied over the time increment $T_2 - T_1$.

The definition of pulse mode thrust coefficient is:

$$C_f = \frac{\int_o^t F\,dt}{\int_o^t P_c\,dt \cdot A_{t\,hot}} \tag{34}$$

Therefore, it is necessary to calculate the integral of chamber pressure during the same time increment the impulse is measured. As a result,

$$C_f = \frac{\int_{T_1}^{T_2} F\,dt}{\int_{T_1}^{T_2} P_c\,dt \cdot A_{t\,hot}} \tag{35}$$

In order to obtain the pressure integral, the time period $T_2 - T_1$ was measured from the thrust trace, and then the chamber pressure trace was hand integrated using a planimeter.

As stated earlier, the maximum balance period achieved was 8.0 seconds. In order to increase resolution at smaller pulse width the calibration weights were changed and the displacement transducer output amplified. As a result of the increased balance sensitivity, damping of the balance to obtain zero deflection prior to pulsing was not possible. The total amplitude of this deflection was calculated to be in the range of 0.001 to 0.003 inch. Creation of a mechanical system to damp this was impractical from both a schedule and cost standpoint. In addition, zero shift of the balance would be a constant problem with such a device. It was, therefore, decided to account for this zero deflection by estimating the increase or decrease in total momentum caused by the initial motion of the balance.

Figure 5-3 presents a sketch of a typical pulse-mode balance displacement measurement, where the initial movement of the balance is large with respect to the momentum transferred by the pulse. In order to define the instantaneous momentum, the sine wave was converted to polar coordinates using the 0-degree reference shown in Figure 5-3. This notational reference was used exclusively for all reduced data. It follows that, instantaneous momentum supplied initially by the balance is:

$$I_{i1} = M|X_{i\,max}|\, w \cos\theta \tag{36}$$

where

$\|X_{i\,max}\|$	=	The absolute value of the maximum initially displacement (reference Figure 5-3)
$\dot{w}$	=	The balance natural frequency
θ	=	Angular referenced as shown in Figure 5-3
M	=	Balance mass

Also the instantaneous momentum resulting from the combination of the initial momentum and the momentum imparted by the pulse is

$$I_{i2} = M|X_{max}|\, w \cos\theta \tag{37}$$

where:

$\|X_{max}\|$	=	The absolute value of the maximum displacement after the pulse (reference Figure 5-3)

It should be noted that the natural frequency, w, is assumed to be equal before and after the pulse since it is proportional to the propellant consumed (weight loss in the top platform (W_T), which is very small for pulse operation).

At the instant the pulse is fired the principle of conservatism of momentum yields:

$$M|X_{i\,max}|\, w \cos\theta_1 + I_p = M|X_{max}|\, w \cos\theta_2 \tag{38}$$

where

$M\|X_{i\,max}\|\, w \cos\theta_1$	=	The initial momentum of the balance at $\theta = \theta_1$
I_p	=	The impulse supplied by the pulse
$M\|X_{max}\|\, w \cos t\, \theta_2$	=	The resultant momentum after the pulse at $\theta = \theta_2$.

Solving for the momentum supplied by the pulse yields

$$I_p = M_w\,[\,|X_{max}|\cos\theta_2 - |X_{i\,max}|\cos\theta_1\,] \tag{39}$$

TYPICAL PULSE MODE BALANCE DISPLACEMENT TRACE WITH AN INITIAL MOVEMENT OF THE BALANCE

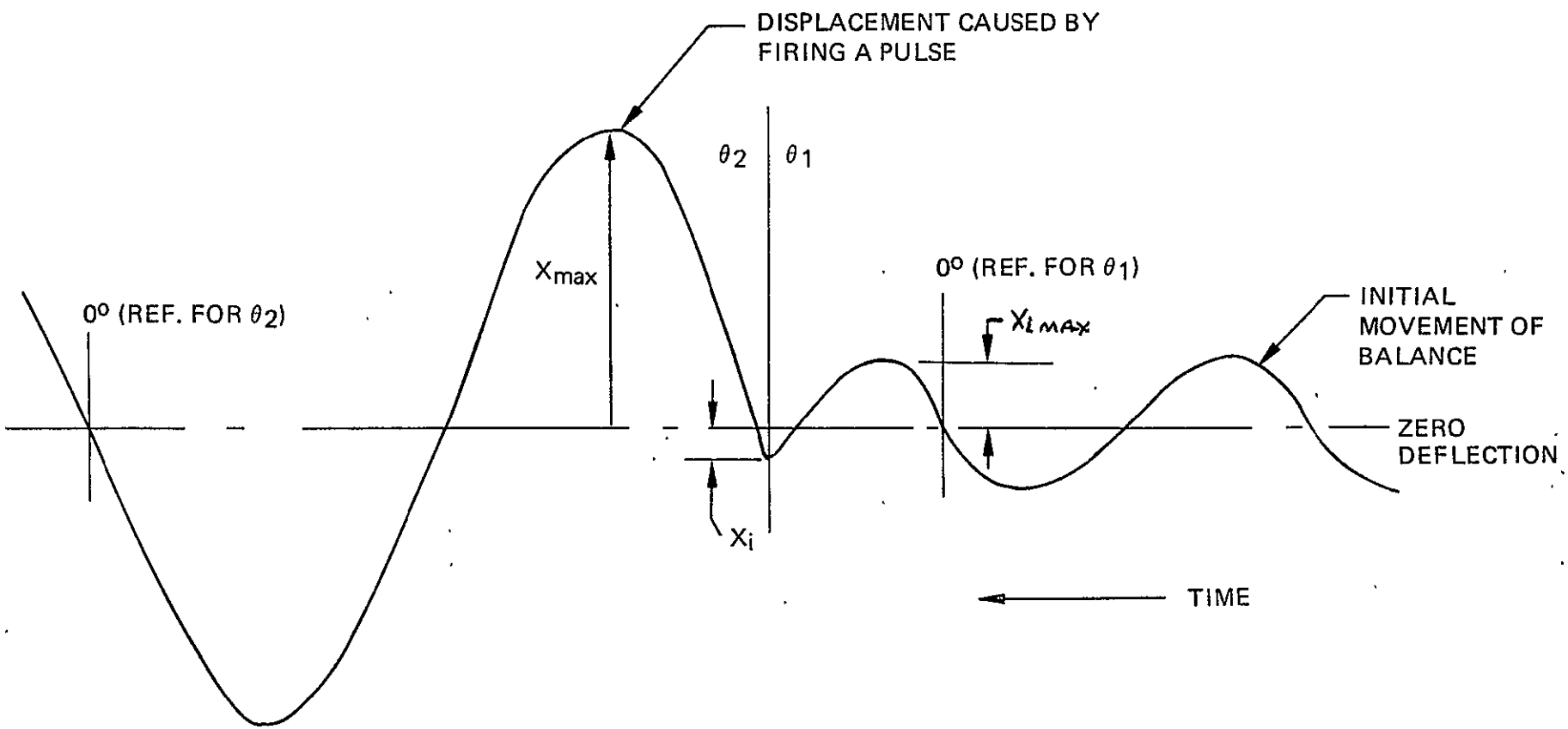

Figure 5-3

Using the linear interpolation for equivalent steady-state thrust as described above by equation (27):

$$F_i = |X_{i\,max}|\,K = \text{Initial equivalent steady-state value of thrust} \tag{40}$$

$$F_{max} = |X_{max}|\,K = \text{Final value of the equivalent steady-state thrust} \tag{41}$$

Substituting this linear interpolation into equation (39):

$$I_p = M_W K\,[F_{max}\cos\theta_2 - F_i\cos\theta_1] \tag{42}$$

Since,

$$w2 = \frac{K}{M} \tag{43}$$

Therefore, it follows that

$$I_p = \frac{1}{w}\,(F_{max}\cos\theta_2 - F_i\cos\theta_1) \tag{44}$$

or

$$I_p = \frac{T}{2\pi}\,(F_{max}\cos\theta_2 - F_i\cos\theta_1) \tag{45}$$

The value of the impulse imparted by the pulse is, therefore, calculated by measuring the values of F_{max}, $F_{i\,max}$ θ_1 and θ_2 respectively. This procedure was used for the 0.008-second pulse widths (and some low pressure 0.02-second pulse), where the values of F_{max} and $F_{i\,max}$ were nearly the same in magnitude.

For pulse widths of 0.02 second and larger, the initial balance displacement was proportionally smaller than the impulse imparted by the pulse. As a result it was observed that greater accuracy could be obtained by substituting the vector equivalent for cos θ_2 rather than measuring θ_2 (the greater accuracy was achieved because the larger deflections caused greater difficulty in measuring θ_2). Figure 5-4 presents plots of displacement versus angular position (θ) for the two cases where the pulse is fired with the balance moving inline and against the thrust axis. Notice that the relationship between the measured X_{max}, $X_{i\,max}$, and the resultant displacement can be described by

$$X_p = |X_{max}|\cos\theta_2 - |X_{i\,max}|\cos\theta_1 \tag{46}$$

which represents the displacement shown in equation (39). The vectorial value of X_p is shown in both cases in the positive direction along the 0 degree axis, due to the fact that the thruster is fired

LINEAR DISPLACEMENT VERSUS BALANCE ANGULAR POSITION, θ

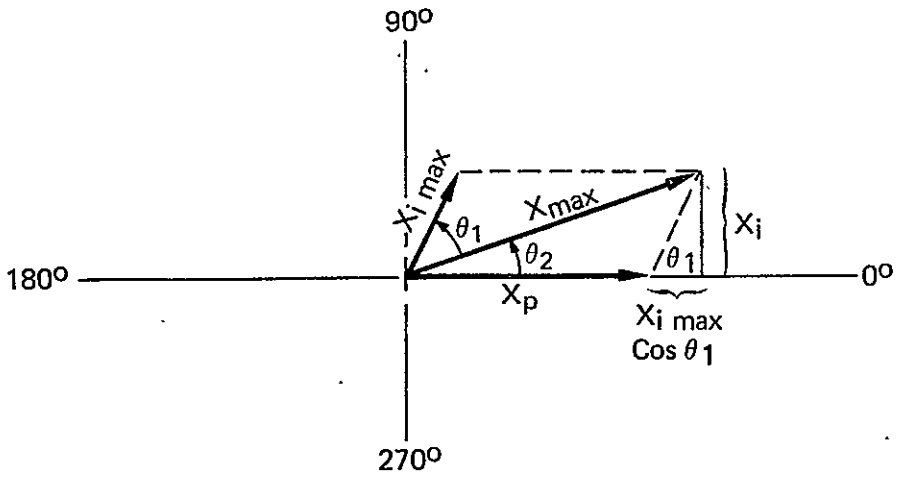

CASE A: $X_{max} > X_p$ (PULSE FIRED WITH BALANCE TRAVELING IN SAME DIRECTION)

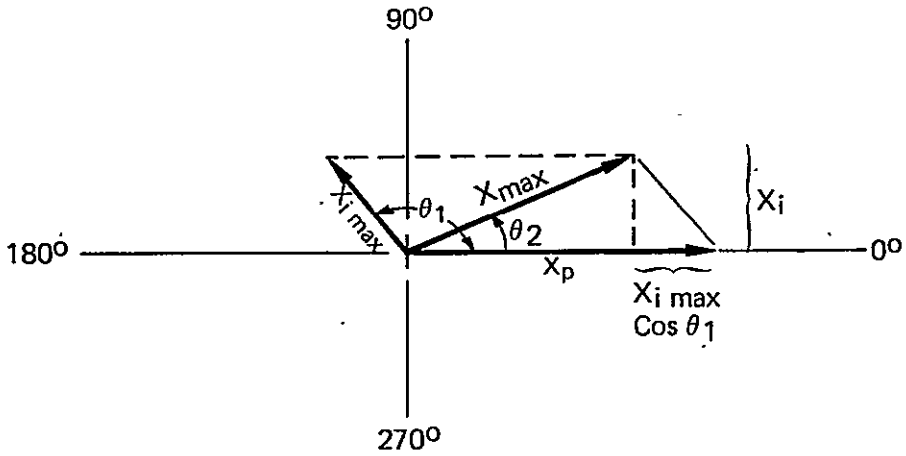

CASE B: $X_{max} < X_p$ (PULSE FIRED WITH BALANCE TRAVELING IN OPPOSITE DIRECTION)

in a fixed position, with respect to the balance movement. Using the Pythagorean theorm it follows that

$$X_{max}^2 = (|X_p| + |X_{i\,max}| \cos\theta)^2 + (X_i)^2 \tag{47}$$

$$X_p = \sqrt{X_{max}^2 - X_i^2} - |X_{i\,max}| \cos\theta \tag{48}$$

Using the linear spring assumption (F = KX), and substituting into equation (45) yields

$$I_p = \frac{T}{2\pi}\left(\sqrt{F_{max}^2 - F_i^2} - F_{i\,max} \cos\theta_1\right) \tag{49}$$

From Figure 5-4 it can be observed that the following relationship exists which equates equations (45) and (49)

$$F_{max} \cos\theta_2 = \sqrt{F_{max}^2 - F_i^2} \tag{50}$$

In summary, equation (33) was used to calculate the pulse mode impulse bit when initial balance deflections were zero or very small compared to the impulse bits. Generally, this applied to the 0.200- to 0.500-second pulse widths. For pulse widths with initial balance movements, equations (45) and (49) were used depending on the proportionate amount of initial deflection compared to the deflection caused by the pulse.

6.0 TEST RESULTS

6.1 VIBRATION AND VIBRATION MARGIN TESTING

The MJS 0.2-lbf T/VA (D01) was subjected to 1) vibration, 2) simulated pyrotechnic shock, and 3) margin vibration testing. Low level sinusoidal vibration, qualification level (T.A.). sinusoidal vibration, acceptance level (F.A.) random vibration, and qualification level (T.A.) random vibration testing were conducted at RRC vibration facilities between April 14 and 23, 1975. The simulated pyro shock environment testing was performed at The Boeing Company, Kent Space Center. The test was started on May 7, 1975, and completed on May 21, 1975. Margin vibration test was done at RRC on September 30, 1975.

For all vibration and shock tests, the T/VA was instrumented with strain gauges and accelerometers. Test data was recorded on oscillograph paper and magnetic tape.

6.1.1 Vibration Testing

The primary objectives of the vibration test were 1) determine whether a tracking filter should be used for all sine tests and 2) show that the MJS 0.1-lbf T/VA Type I design was structurally sound. To accomplish these goals, the T/VA was instrumented with eight strain gauges and six response accelerometers at locations shown in Figure 6-1. Sinusoidal and random excitations were applied along the T/VA's three orthogonal axes. In addition to low level (2 g) sine testing, the T/VA was subjected to F.A. (random) and T.A. (sine and random) levels given in JPL Specification ES 509778, Revision A, and presented in Table 6-1. Measurable GN_2 leakage was obtained from both T/VA propellant valves during this test, results were:

Axis	T/VA S/N D01	T/VA S/N D02
Z	1,440 scch	360 scch
Y	25.2 scch	24 scch
X	0	193 scch

The first sequence of tests were 2 g sine sweeps at 2 octaves/minute from 5 to 2,000 cps. To reduce test time and because no resonances were observed below 200 cps, the low level sine test starting frequency was changed from 5 to 200 cps. For each axis, the sine test was run with and without a tracking filter. Strain data were recorded on oscillograph paper and were used as the criteria whether the tracking filter was to be utilized during sine testing or not. A high level (F.A.) sine test was conducted along the x axis with the tracking filter and then without. This test was performed to verify that higher excitation produced the same conclusion about the tracking filter as the low level testing. Following tracking filter evaluation testings, the T/VA was subjected to qualification level (T.A.) sine excitation, acceptance level (F.A.) random vibration, and qualification level (T.A.) random vibration. A summary of all test runs is presented in Table 6-2.

MJS 0.2-LBF T/VA
(D01)

VIBRATION INSTRUMENTATION

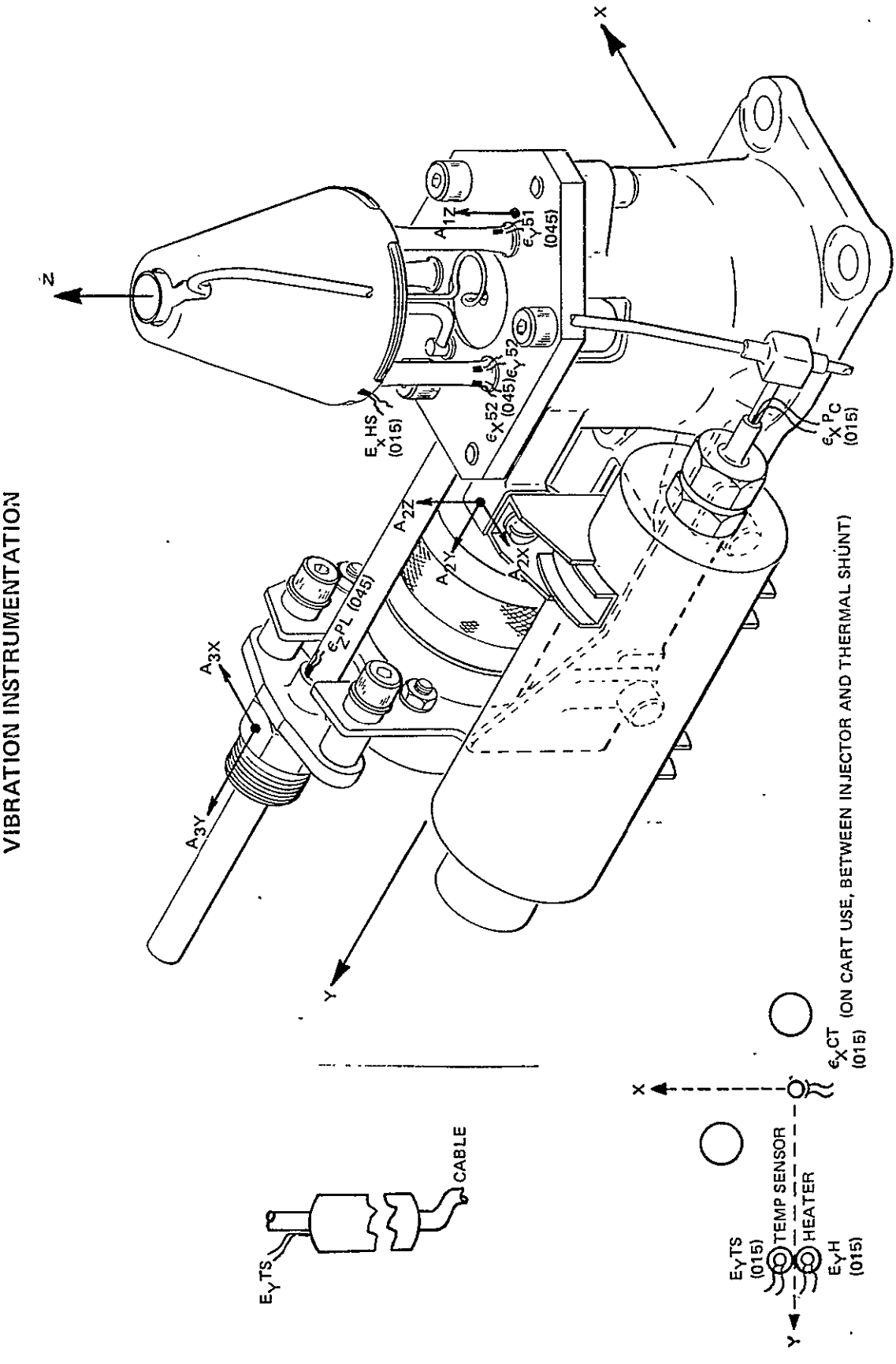

Figure 6-1

Table 6-1
MJS 0.2-lbf T/VA
VIBRATION TEST ENVIRONMENTS

A. Sine

Frequency (cps)	Amplitude	Rate
5 – 27.1	0.8 in. D.A.	2 oct/min
27.1 – 80	30 g	
80 – 150	20 g	
150 – 2,000	10 g	

B. Random

Frequency (cps)	Amplitude		Rate
	F.A. (17.25 g rms)	T.A. (29 g rms)	
25 – 40	–	–	+12 db/oct
40 – 600	0.355 g^2/cps	1.0 g^2/cps	Flat
600 – 200	–	–	-9 db/oct
	(3 min/axis)	(5 min/axis)	

It was found from low level sine vibration and x axis F.A. level sine vibration that including the tracking filter during sinusoidal vibration had negligible effect on the dynamic response of the T/VA structure. Therefore, to simplify testing, RRC recommended, and JPL approved, that the tracking filter be eliminated during sinusoidal vibration at the T/VA.

High level vibration strain gauge data are presented in Table 6-3 for the more critical strain locations. Heat shield tab stress was found to be very low (<3 ksi) during sine vibration and as a result, strain gauge ϵXHS was not monitored for subsequent runs. Strain data for ϵYTS and ϵYH are not presented in Table 6-3 since strains were below yield, and they do not represent critical structural member. The highest stresses (strains) developed in the T/VA during vibration occurred for y axis random vibration (T.A. level). The propellant line and the P_C tube had strains of 2.90 and 2.10 in./in., respectively. It should be noted that P_C tube stress would have been even higher without the constraint imposed on the P_C tube fitting. The tube that joined the T-junction of the P_C tube (near pressure transducer) had a heavy fitting at the end which is not a flight item. This fitting was bonded to the vibration fixture with dental cement. Analysis showed that the P_C tube

Table 6-2
MJS 0.2-lbf T/VA D01
VIBRATION TESTS SCHEDULE
(4-14-75 to 4-23-75)

Run No.	Axis	Vibration Type	Vibration Level	Rate (Time)	Comment
1	Y	Sine	2.0	2 oct/min	5 to 2,000 cps
2	Y	Sine			100 to 2,000 cps
3	X	Sine			5 to 2,000 cps
4	Z	Sine			5 to 2,000 cps
5	Z	Sine			5 to 2,000 cps (with tracking filter)
6	Y	Sine			200 to 2,000 cps (with tracking filter)
7	X	Sine			200 to 2,000 cps (with tracking filter)
8	X	Sine	F.A.		200 to 2,000 cps (with tracking filter)
9	X	Sine			200 to 2,000 cps (no tracking filter)
10	Z	Sine	T.A.		5 to 2,000 to 5 cps
11	Y	Sine			5 to 2,000 to 5 cps
12	X	Sine			5 to 2,000 to 5 cps
13	Z	Random	F.A.	3 min	17.6 g rms
14	Y	Random			17.3 g rms
15	Z	Random			17.1 g rms
16	Z	Random	T.A.	5 min	28.5 g rms
17	Y	Random			28.8 g rms
18	X	Random	T.A.	5 min	29.0 g rms

Table 6-3
MJS 0.2-lbf T/VA STRAIN GAUGE DATA

Run No.	Axis	Vibration Type	Frequency (Time)	Strain – 10^3 in./in.						Offset
				ϵYS1	ϵYS2	ϵXS2	ϵXCT	ϵZPL	ϵXP_C	10^{-3} in./in.
10	Z	Sine	450	–	–	–	0.10	0.26	0.17	ϵXCT = 0.35
		(T.A.)	800	0.18	0.20	0.08	0.10	–	0.25	ϵXP_C = 0.02
			1,300	0.14	0.15	0.09	0.40	0.12	0.45	
			1,600	–	–	–	0.28	–	0.35	
			1,900	–	–	–	0.40	0.12	–	
11	Y	Sine	470	–	–	–	–	0.31	–	
		(T.A.)	620	0.16	0.10	0.32	0.16	–	0.25	
			800	0.33	0.35	–	0.16	–	0.38	
			900	–	0.20	0.13	0.15	–	0.40	
			1,300	–	–	–	0.20	–	–	
			1,500	–	–	–	–	–	0.22	
			1,900	–	–	–	0.15	–	–	
12	X	Sine	410	0.15	0.12	0.13	0.15	0.20	0.23	
		(T.A.)	610	0.21	–	0.24	0.12	–	0.31	
			780	0.13	0.14	–	0.08	–	0.18	
			1,130	–	–	0.12	0.13	–	0.14	
			1,500	–	–	–	–	–	0.18	
			1,800	–	–	–	0.12	–	0.10	
13	Z	Random (F.A.)	(3 min)	0.40	0.40	0.24	0.52	1.10	0.75	
14	Y	Random (F.A.)	(3 min)	0.55	0.58	0.53	0.43	1.15	1.10	
15	X	Random (F.A.)	(3 min)	0.37	0.32	0.57	0.43	0.42	1.05	ϵYS1 = 0.03
16	Z	Random (T.A.)	(5 min)	0.65	0.45	0.43	0.93	2.55	1.25	ϵZPL = 0.40
17	Y	Random (T.A.)	(5 min)	0.95	1.00	1.15	0.73	2.90	2.10	ϵZPL = 0.10
18	X	Random (T.A.)	(5 min)	0.73	0.80	0.93	1.10	0.70	2.00	ϵYS2 = 0.13 ϵXCT = 0.23 ϵXP_C = 0.55

configuration shown in Figure 6-1 would have stresses above yield. As a result, the P_C line was redesigned for the predicted P_C tube stresses which were low. The propellant tube stress, although high, was below yield, as shown by the strain offset in Table 6-3. Other stresses were low with zero or small amounts of permanent offset; 0.002 in./in. offset is defined at yield.

Accelerometer data was reduced on x-y plots, and a summary is presented in Table 6-4. As for the strain data, only high level vibration data are given. The acceleration data by itself does not tell sometimes which resonances are caused by what structural deformation. However, combined with strain data, a clearer picture is obtained about various structural modes. For example, the lowest T/VA frequency (410 to 470 cps) is characterized by mounting bracket deformation, i.e., bending and twisting of channel section of bracket. The second mode at about 620 cps is due to lateral deformation of conical portions of the mounting bracket. Modes due to REA deformation are also obtained by cross-checking strain and acceleration data.

6.1.2 Shock Test

The pyrotechnic shock environment represented by Figure 5 of JPL specification ES 509778, Revision A, was synthesized on an electrodynamic shaker at The Boeing Company, Kent Space Center. Strain and acceleration data were recorded on magnetic tape and on oscillograph paper for quick-look option. In addition to the strain gauges (7) and response accelerometers (3) on the T/VA (Figure 6-2), four accelerometers were attached to the shock fixture at locations shown in Figures 4-15 through 4-17 of Section 4.0. These accelerometers were used for control, monitor, and to record crosstalk.

Prior to exposure of the T/VA to shock excitation, the best-fit shock spectrum was synthesized and shock spectrum plotted. Figure 6-3 shows a typical response spectrum generated for shock with a bare fixture or with the T/VA on. The test data in Figure 6-3 follows the required curve between 200 and 2,000 cps. However, below and above this range the test response spectrum was off considerably. Nevertheless, the shock was found to be acceptable since T/VA critical resonances were above 200 cps and below 2,000 cps.

To safeguard the T/VA against shock overtest, a low level (half level) shock was initially applied along each test axis prior to three full level shock exposures. The primary purpose of this lower excitation was to determine shock transmissibility and verify calibrations for response data recording. If shock transmissibility (Q) was below 20, then the full level test was to proceed. However, for test axis with Q above 20, the shock was to be resynthesized until Q was 20 or less. After it was determined that the response spectrum was acceptable, that transmissibilities were low and that strains were valid, the full level shock was then applied to the T/VA.

Half-level shock testing along the three test axes showed that acceleration transmissibilities were below Q = 20, as shown in Figures 6-4 through 6-11. In addition, half-level shock strain data on oscillograph plots showed strain offsets to be below yield.

Table 6-4
MJS 0.2-lbf T/VA D01
VIBRATION TEST ACCELERATION DATA

Run No.	Vibration Type	Frequency (cps)	Acceleration, g rms					
			A1Z	A2X	A2Y	A2Z	A3X	A3Y
10Z	Sine (T.A.)	450	–	28.0	–	–	16.0	18.0
		810	–	–	17.0	15.0	10.0	23.0
		1,200	16.5	31.0	–	–	–	–
		1,330	16.5	–	60.0	52.0	–	38.0
		1,620	26.0	40.0	56.0	23.0	11.0	–
		1,800	25.2	–	–	–	–	–
11Y	Sine (T.A.)	470	Acceleration on fixture	11.0	–	–	19.0	30.0
		620		31.0	20.0	–	–	14.0
		810		7.0	36.0	17.0	25.0	15.0
		960		–	20.0	13.0	27.0	45.0
		1,120		17.0	9.6	12.0	33.0	34.0
		1,300		–	–	7.0	–	15.0
		1,500		10.0	11.6	–	–	–
		1,600		10.0	11.5	6.4	–	24.0
		1,800		10.0	–	–	3.2	–
12X	Sine (T.A.)	410		91.0	8.5	4.8	71.0	19.0
		610		27.0	8.1	1.6	9.0	15.0
		770		–	11.2	5.9	–	–
		860		–	–	–	17.0	–
		1,120		37.0	15.0	8.0	2.8	10.0
		1,500		12.0	9.5	5.3	4.0	20.0
		1,800		10.0	3.6	5.7	5.9	–
13Z	Random (F.A.)	–	23.0	–	27.0	46.0	20.0	38.0
14Y	Random (F.A.)	–	7.5	15.5	29.5	19.5	35.0	52.0*
15X	Random (F.A.)	–	8.0 (A2Z)	62.0*	13.0	9.5	44.0	22.0
16Z	Random (T.A.)	–	35.0	23.0	(A2Y) Off	37.0	28.0	66.0
17Y	Random (T.A.)	–	14.0	20.0	(A2Y) Off	10.0	31.0	69.0
18X	Random (T.A.)	–	15.0	70.0	(A2Y) Off	9.5	70.0	21.0

*Signal clipped

MJS 0.2-LBF T/VA
(D01)

PYRO SHOCK INSTRUMENTATION

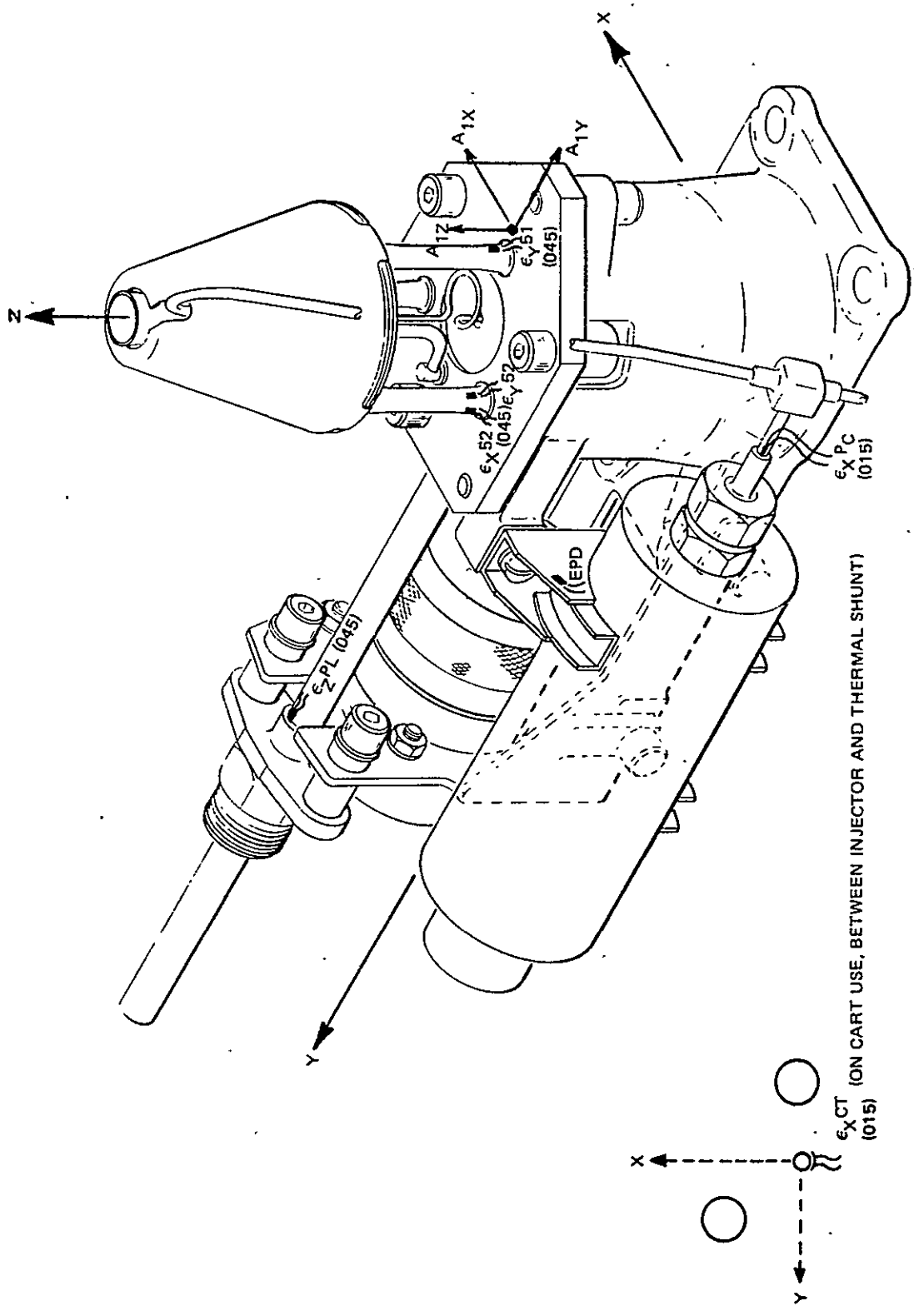

Figure 6-2

ORIGINAL PAGE IS
OF POOR QUALITY

TYPICAL RESPONSE SPECTRUM

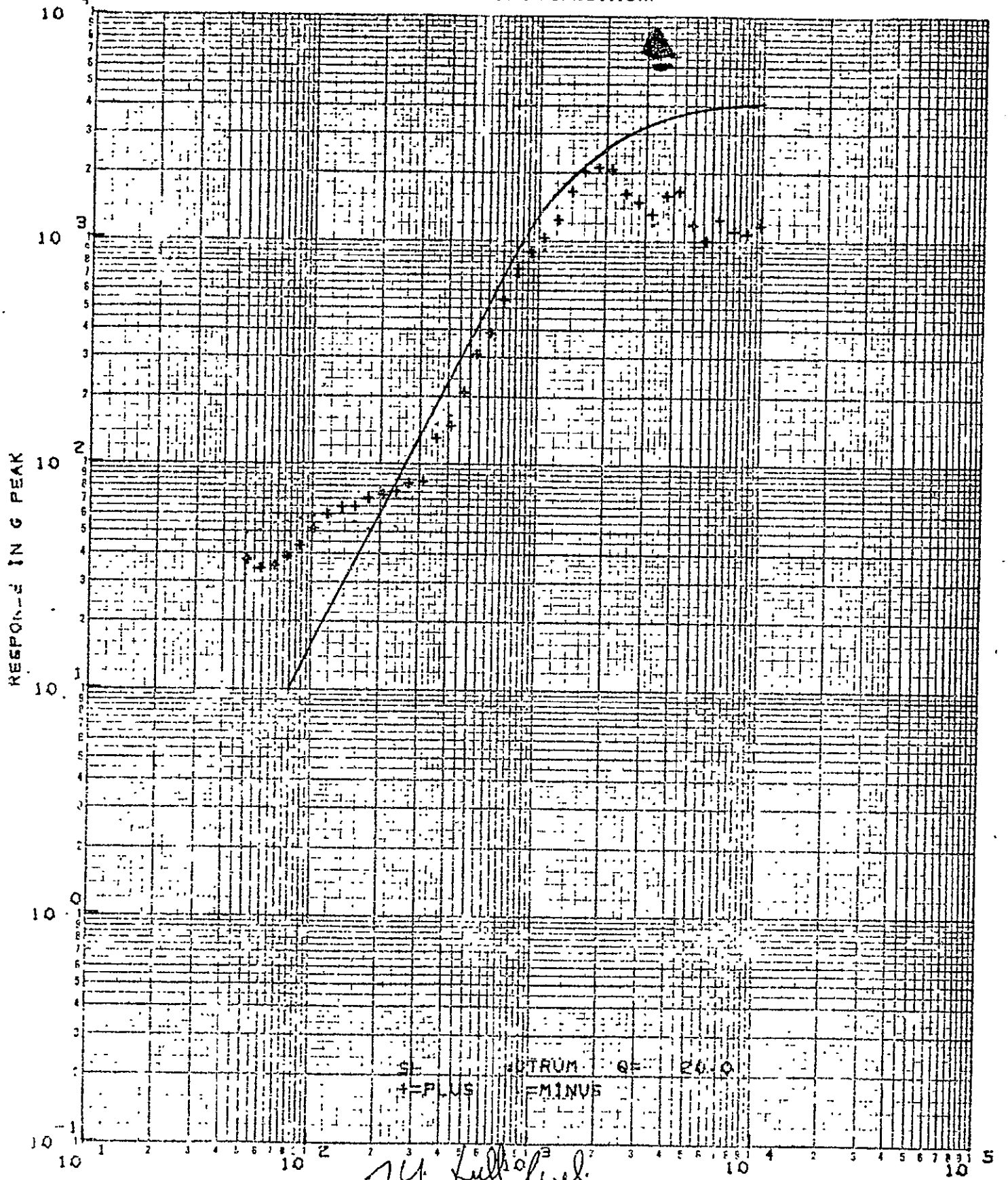

PULSE 7Y

Figure 6-3

CALC	DLF 5/20/75			
CHECK				
APPD				
APPD				

2-36137500-145

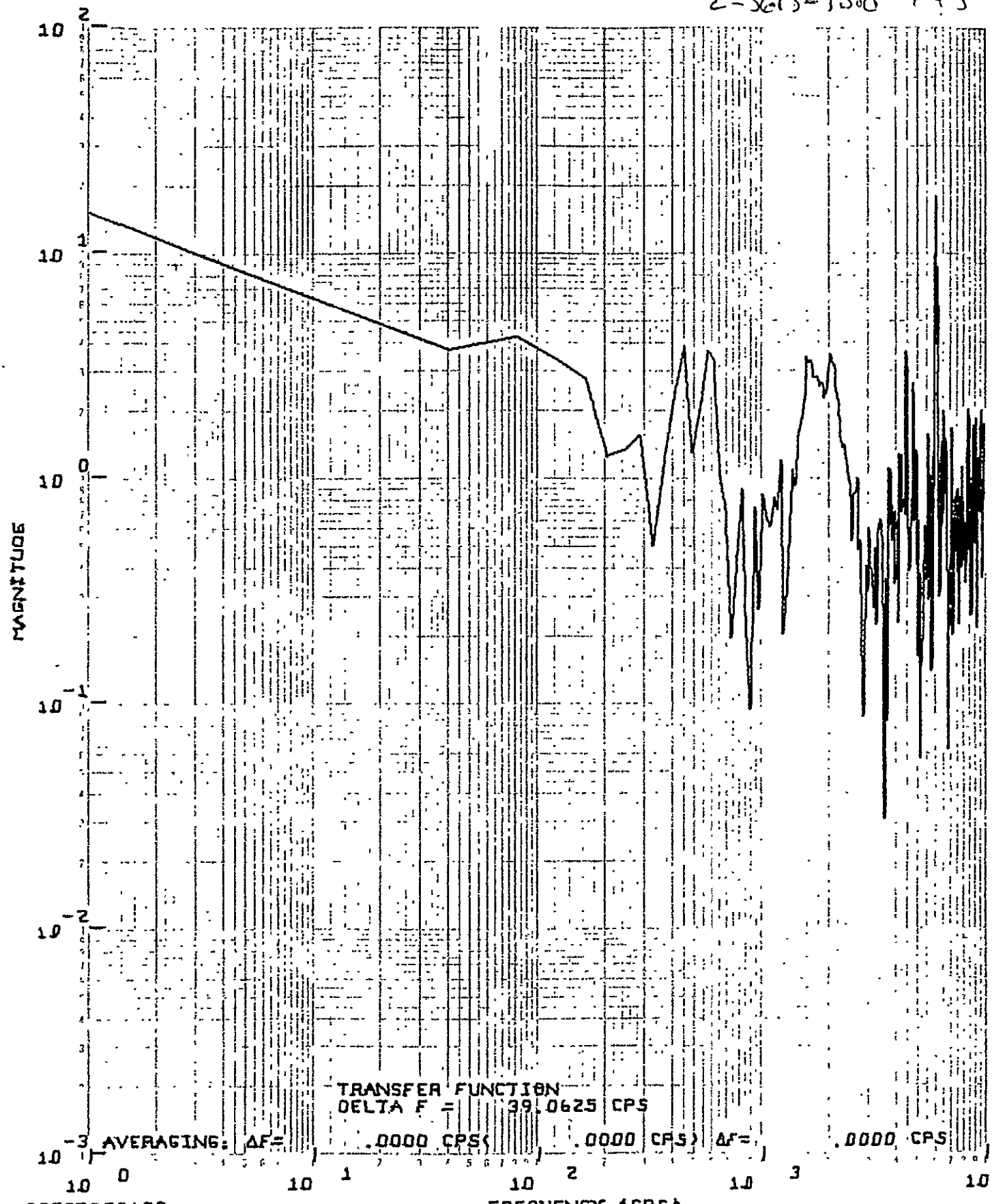

	OWE 05/19/75	ROCKET RESEARCH THRUSTER VALVE ASSEMBLY SHOCK TEST ½ Level — X	A1X 49

Figure 6-4

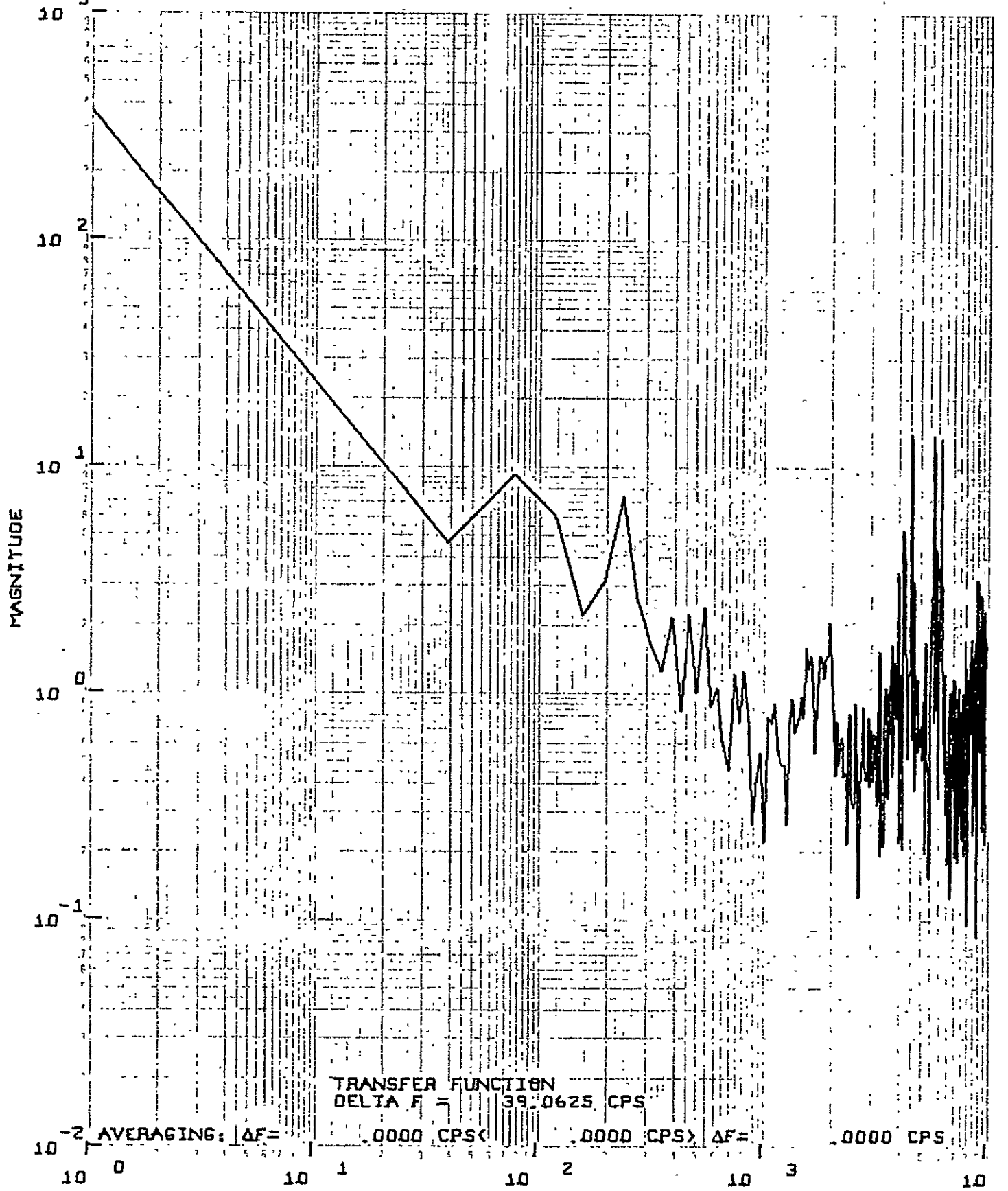

Figure 6-5

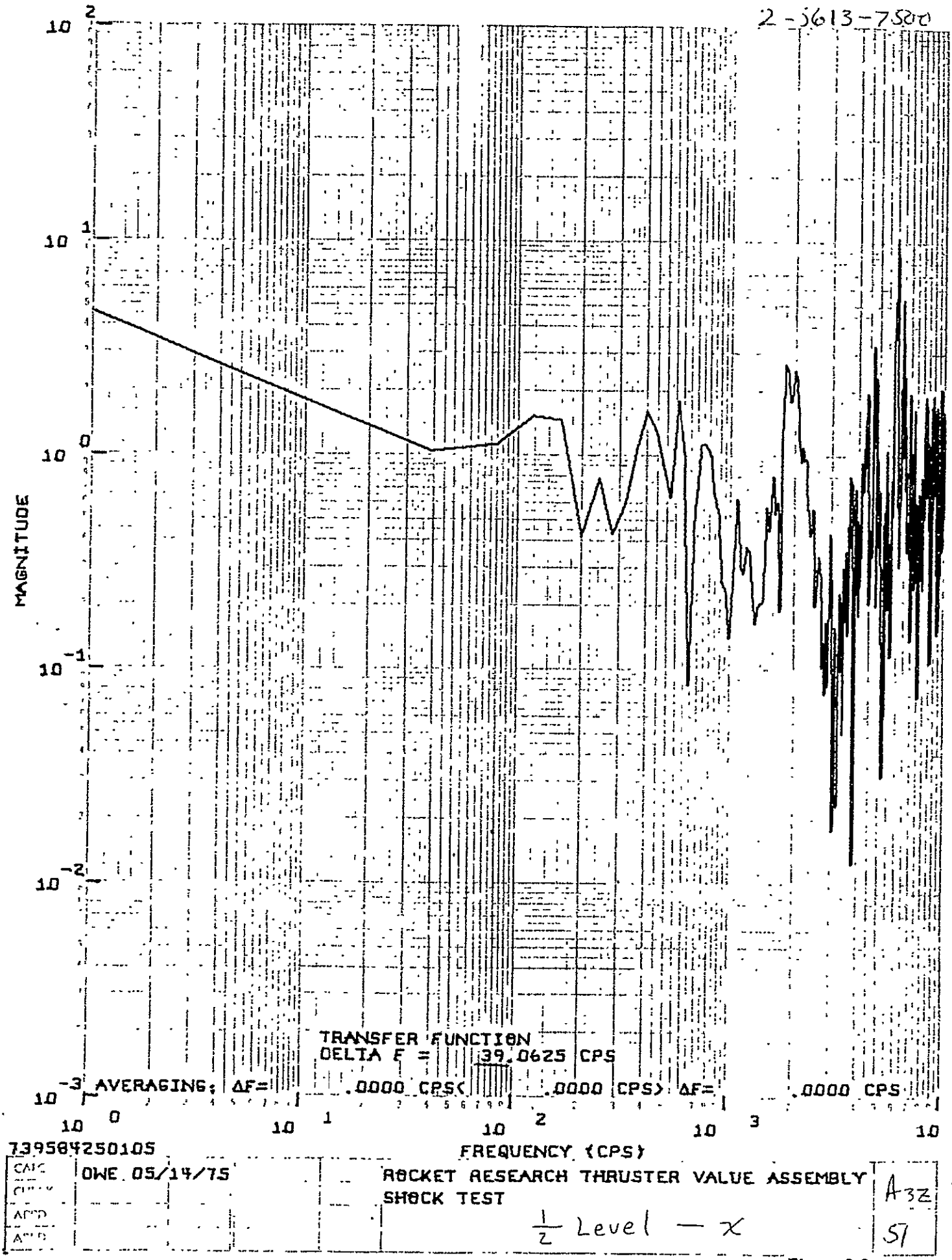
2-5613-7500
MAGNITUDE
FREQUENCY (CPS)
TRANSFER FUNCTION
DELTA F = 39.0625 CPS
AVERAGING: ΔF= .0000 CPS< .0000 CPS> ΔF= .0000 CPS
739584250105
DWE 05/14/75
ROCKET RESEARCH THRUSTER VALVE ASSEMBLY
SHOCK TEST
1/2 Level — X
A-32
57

Figure 6-6

2-5613-7500-14

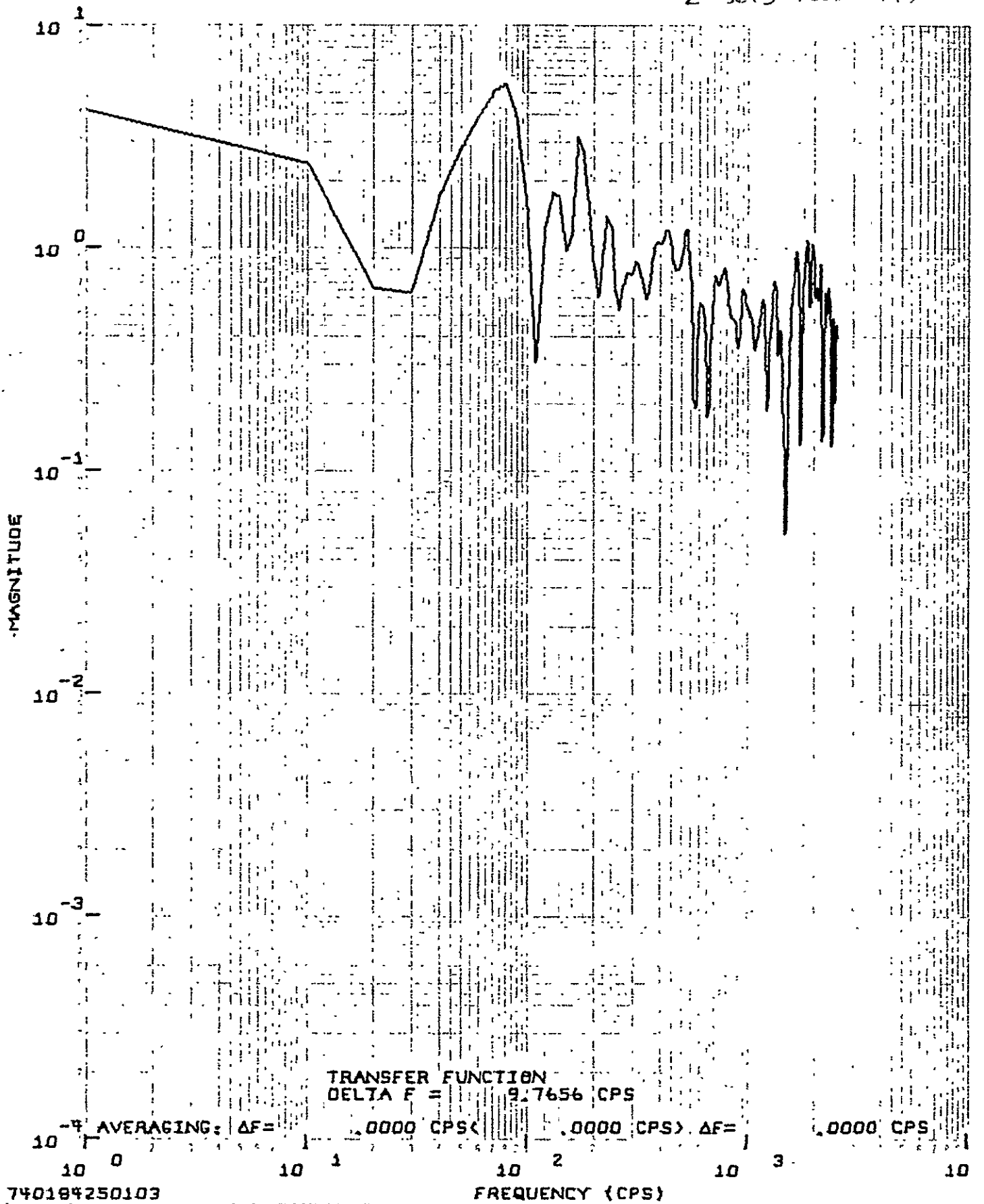

7401845250103

DLF 5/21/75

ROCKET RESEARCH THRUSTER VALVE ASSEMBLY
SHOCK TEST

1/2 Level — Y

RUN 6Y

A1X

87

Res 5/27/75

Figure 6-7

2-5613-7580 -145

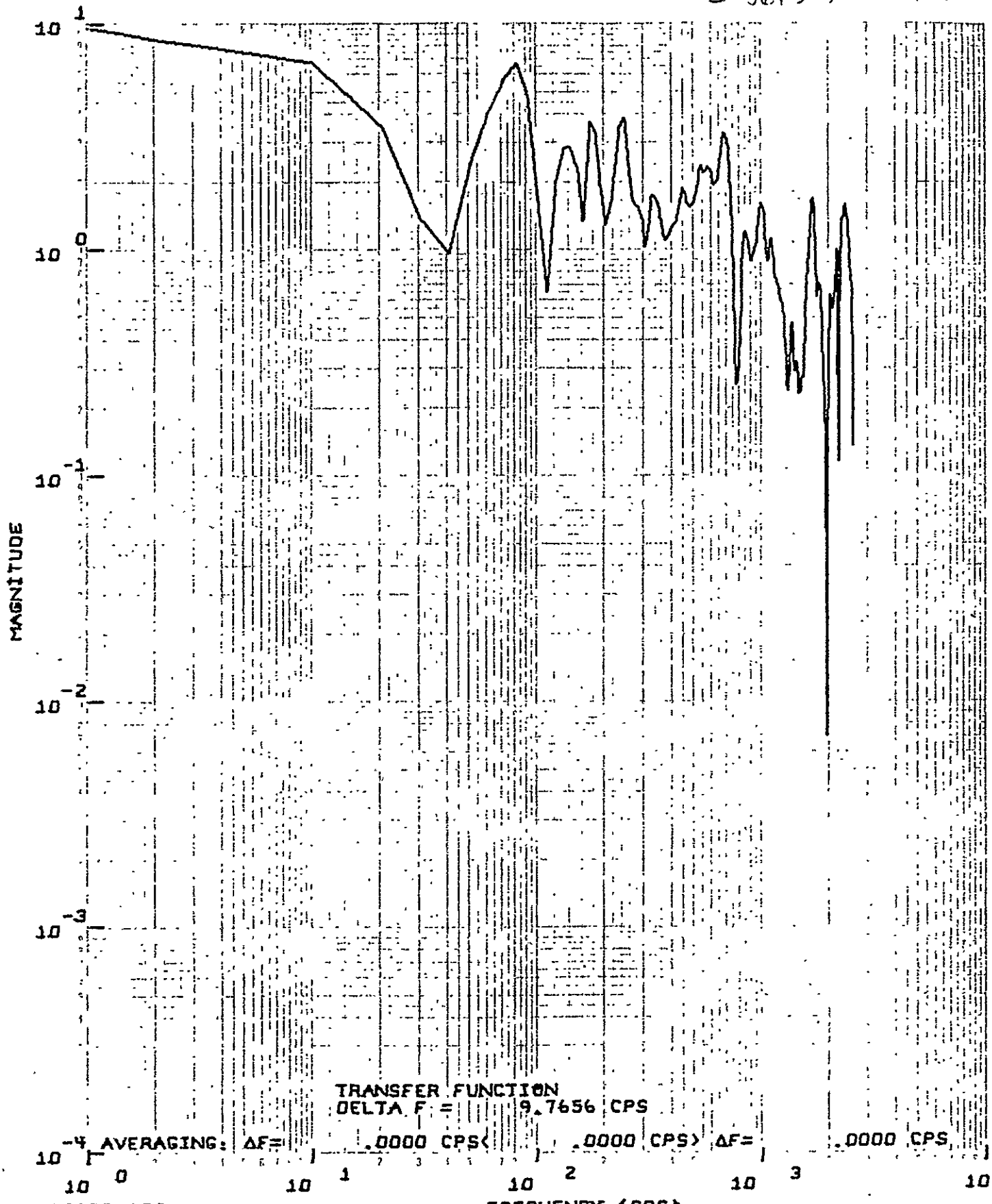

7401842501O4

	OLF 5/21/75	ROCKET RESEARCH THRUSTER VALVE ASSEMBLY SHOCK TEST	Az Y
	RCS 5/27/5	RUN 6Y ½ Level — Y	88

Figure 6-8

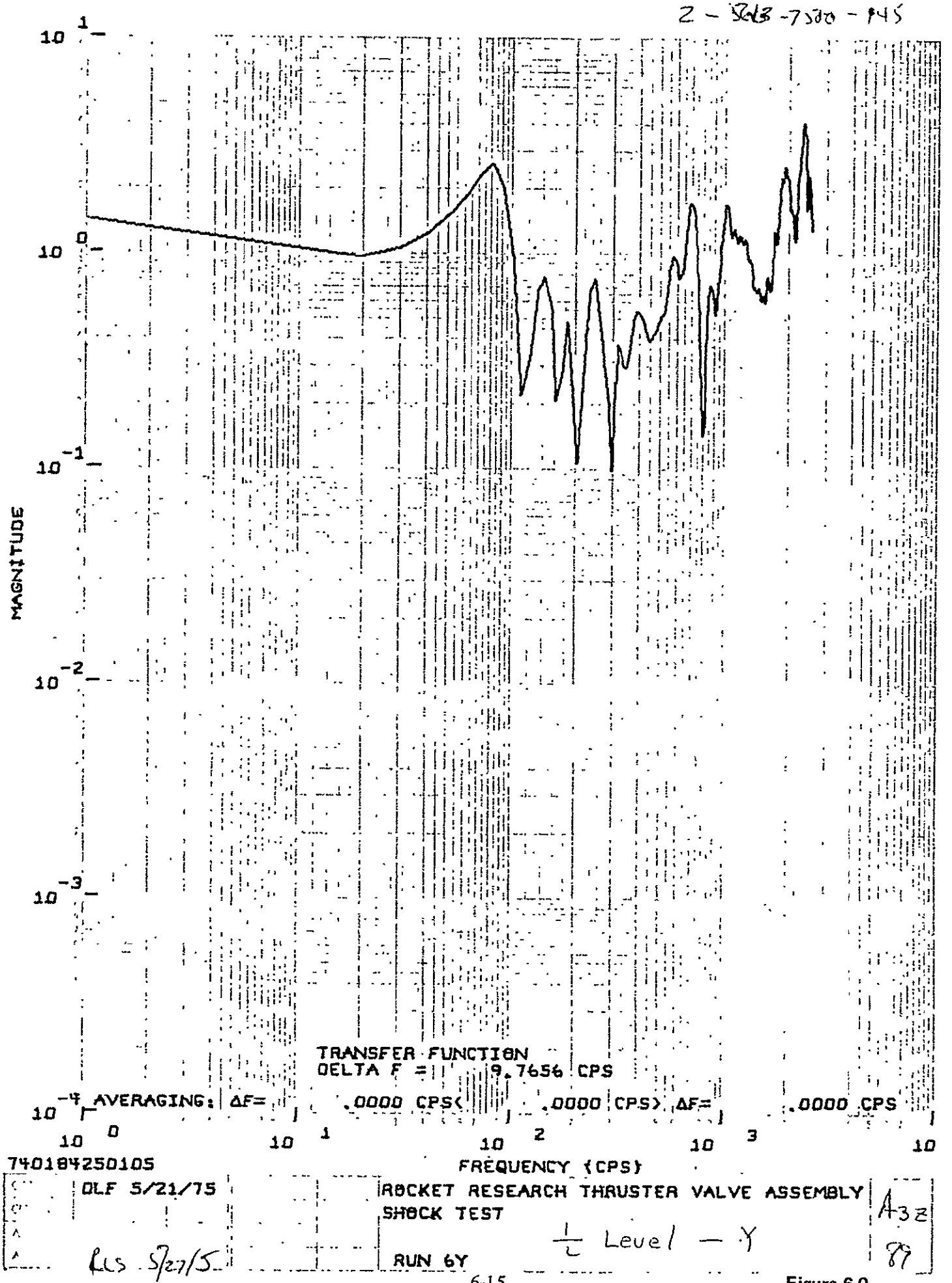
2 - SGB-7500 - 145
MAGNITUDE
TRANSFER FUNCTION
DELTA F = 9.7656 CPS
AVERAGING: ΔF= .0000 CPS(.0000 CPS) ΔF= .0000 CPS
FREQUENCY (CPS)
74018425010S
DLF 5/21/75
ROCKET RESEARCH THRUSTER VALVE ASSEMBLY
SHOCK TEST
RUN 6Y
1/2 Level — Y
A3z
89
RLS 5/27/75

Figure 6-9

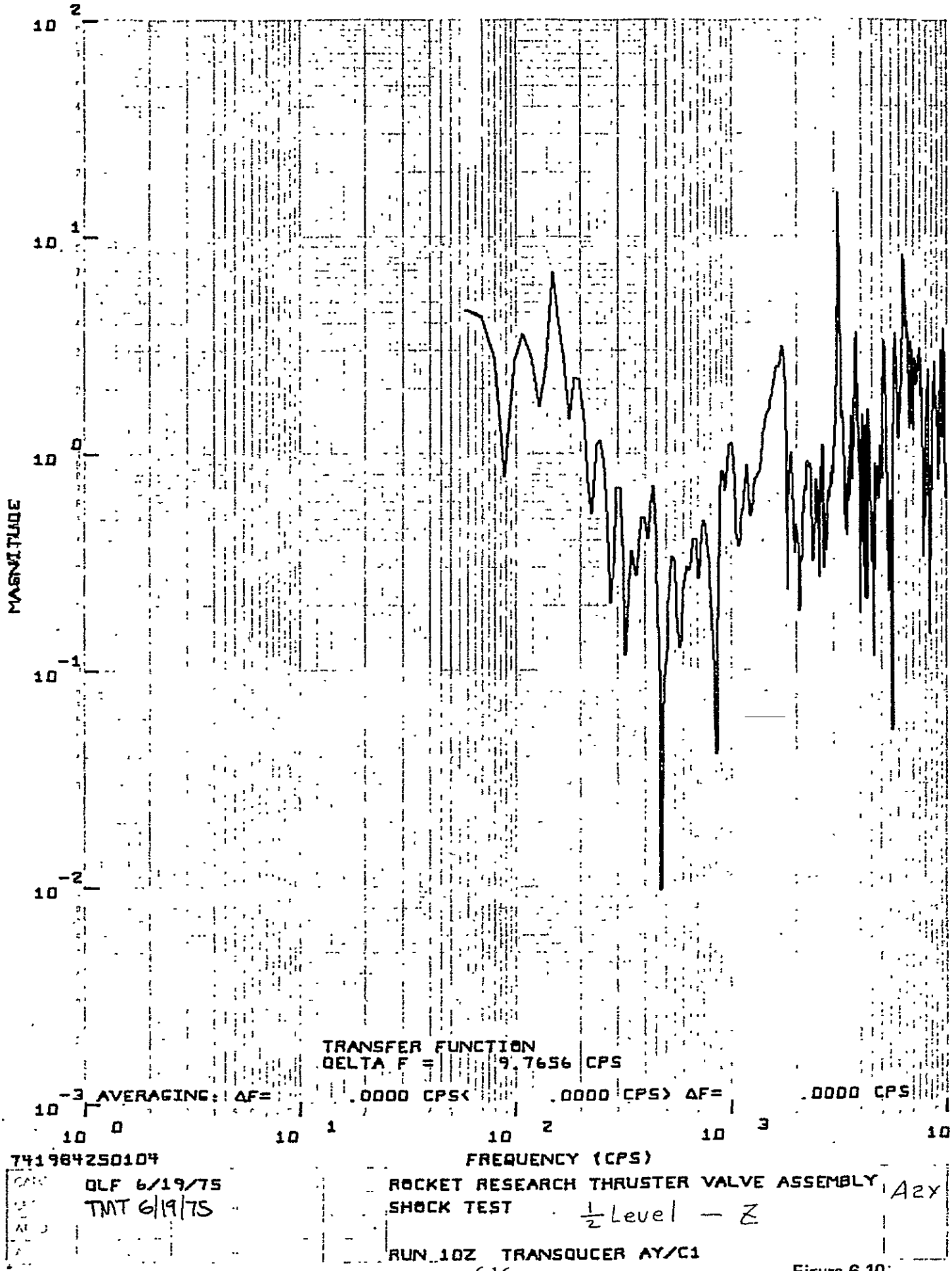
MAGNITUDE
10 2
10 1
10 0
10 -1
10 -2
10 -3
TRANSFER FUNCTION
DELTA F = 9.7656 CPS
AVERAGING: ΔF= .0000 CPS< .0000 CPS> ΔF= .0000 CPS
10 0
10 1
10 2
10 3
FREQUENCY (CPS)
7419842501O4
OLF 6/19/75
TMT 6/19/75
ROCKET RESEARCH THRUSTER VALVE ASSEMBLY
SHOCK TEST
1/2 Level — Z
A2X
RUN 10Z TRANSDUCER AY/C1

Figure 6-10

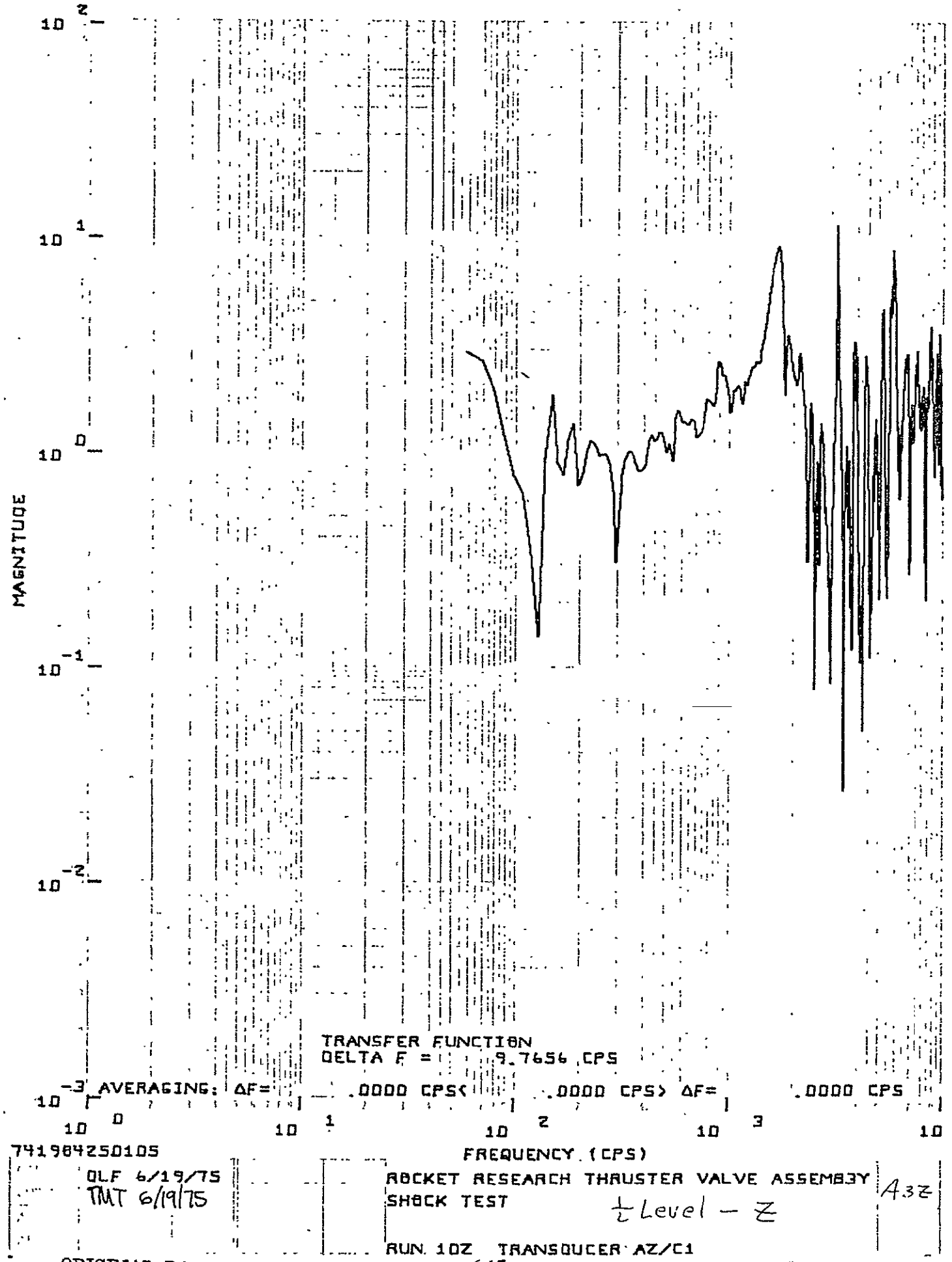

ORIGINAL PAGE IS
OF POOR QUALITY

Figure 6-11

Full-level pyro shock testing along the x and y axes produced large strain offset in the P_C tube, as shown in Table 6-5. The total offset, produced by combining strain offset for each x and y shock, exceeded yield. However, this was expected, and that is why the P_C tube was redesigned for flight. What was unexpected was the large strain offset recorded by the capillary tube strain gauge. Large stresses were predicted (CDR presentation) for all critical structural members of T/VA under pyrotechnic shock loading. However, the state of the art for calculating pyro shock induced stresses is such that seldom low stresses (positive margins of safety) are predicted. Therefore, when high strains (Figures 6-12 through 6-15) and large offsets were obtained for z axis shock, a full review of analysis, test instrumentation, shock excitation, and strain data was conducted.

Table 6-5
MJS 0.2-lbf T/VA
PYRO-SHOCK STRAIN GAUGE DATA

Shock No.	Level	Strain – 10^{-3} in./in.							Offset* in./in.
		ϵYS1	ϵYS2	ϵXS2	ϵXCT	ϵXPL	ϵXP_C	ϵPD	
3X	Full	–	–	–	–	0.26	3.50	3.30	$\epsilon XP_C = 0.0008$
5X	Full	2.75	2.45	4.80	2.28	0.45	3.25	3.55	
7Y	Full	–	–	–	–	0.70	5.50	3.28	$\epsilon XP_C = 0.0010$
9Y	Full	2.90	2.18	4.60	2.30	0.79	4.85	3.90	$\epsilon XP_C = 0.0002$
10Z	1/2	–	–	–	4.17	–	1.95	–	ϵXCT = 0.00067
11Z	Full	1.53	1.23	2.18	10.10	1.62	2.10	0.49	ϵXCT = 0.00127
12Z	Full	–	–	–	9.60	–	–	–	ϵXCT = 0.00025
13Z	Full	1.85	1.20	2.20	8.50	1.46	1.90	0.95	ϵXCT = 0.00010

*0.002 in/in offset is yielding

First, it was verified that the strain plots were accurate by comparing offsets recorded on oscillograph and magnetic tape. Next, transmissibility plots were made for two full level shocks (tests 12 and 13). However, it was found that for frequencies below 2,000 cps, Q was less than 20 for response along the two critical axes, as shown in Figures 6-16 through 6-19. It was deduced that at frequencies where Q exceeded 20 (Figures 6-16, 6-17, and 6-18), the structural response was negligible. This is shown to be true when capillary tube strain time-history data has peak strain occurring at a frequency of about 1,600 cps, as shown in Figures 6-12 through 6-15. The excitation time-history (Figure 6-20) also has a dominant frequency component of approximately 1,600 cps in the time domain when peak strains are induced in the capillary tube. Figures 6-21 and 6-22 show that T/VA response accelerations are high ($\approx$2,000 g) at a frequency of about 1,600 cps. Furthermore, sine vibration strain and acceleration data (Tables 6-3 and 6-4) show a significant

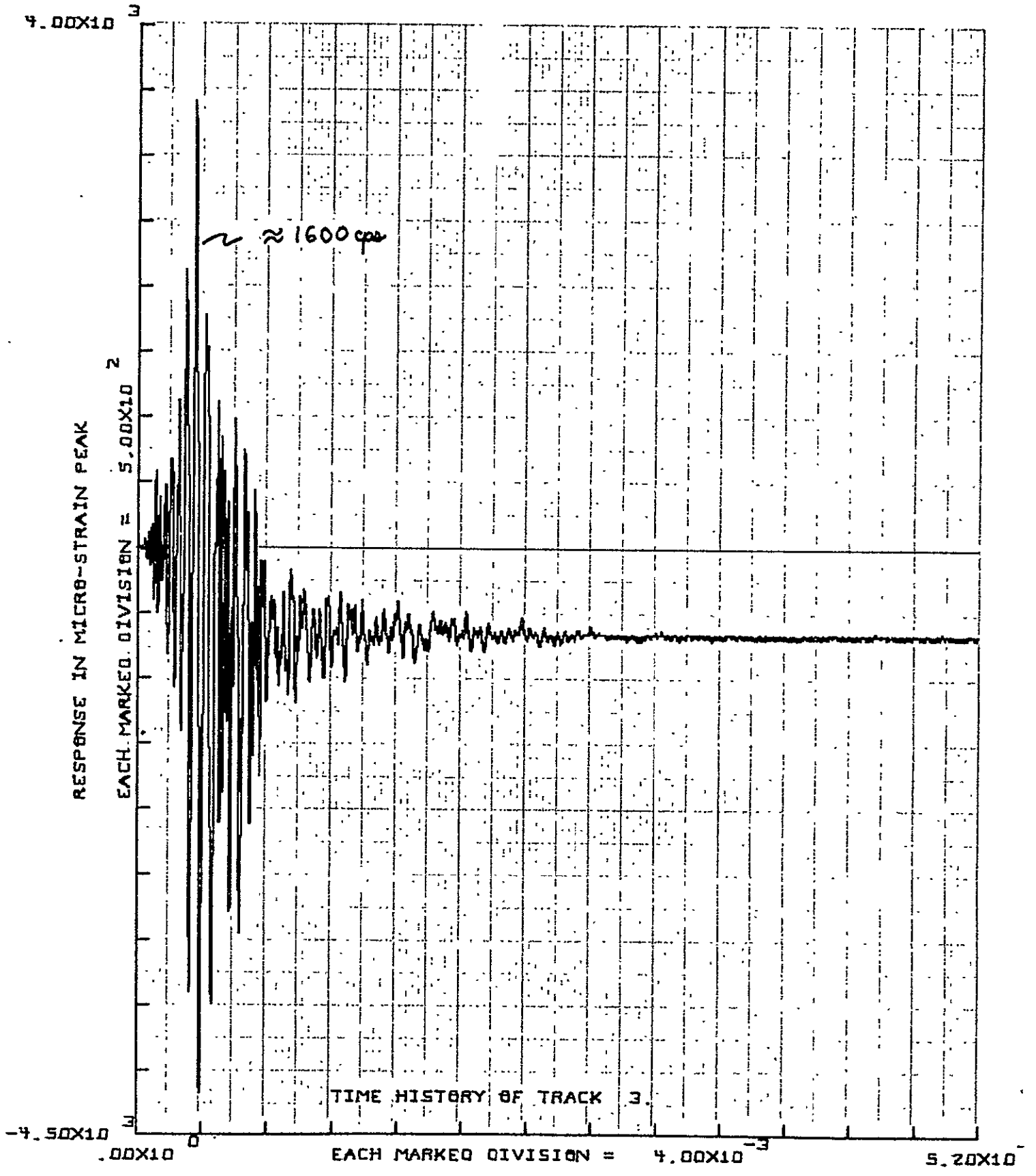
4.00X10 3
≈ 1600 cps
RESPONSE IN MICRO-STRAIN PEAK
EACH MARKED DIVISION = 5.00X10 2
-4.50X10 3
TIME HISTORY OF TRACK 3.
.00X10 0
EACH MARKED DIVISION = 4.00X10 -3
5.20X10 -3
7419842603
TIME IN SECONDS
CHKD OLF 6/19/75
CHK'D TMT 6/19/75
APP'D
APP'D
ROCKET RESEARCH THRUSTER VALVE ASSEMBLY
SHOCK TEST
RUN 10Z TRANSDUCER 53 (½ LEVEL)
EXCT

Figure 6-12

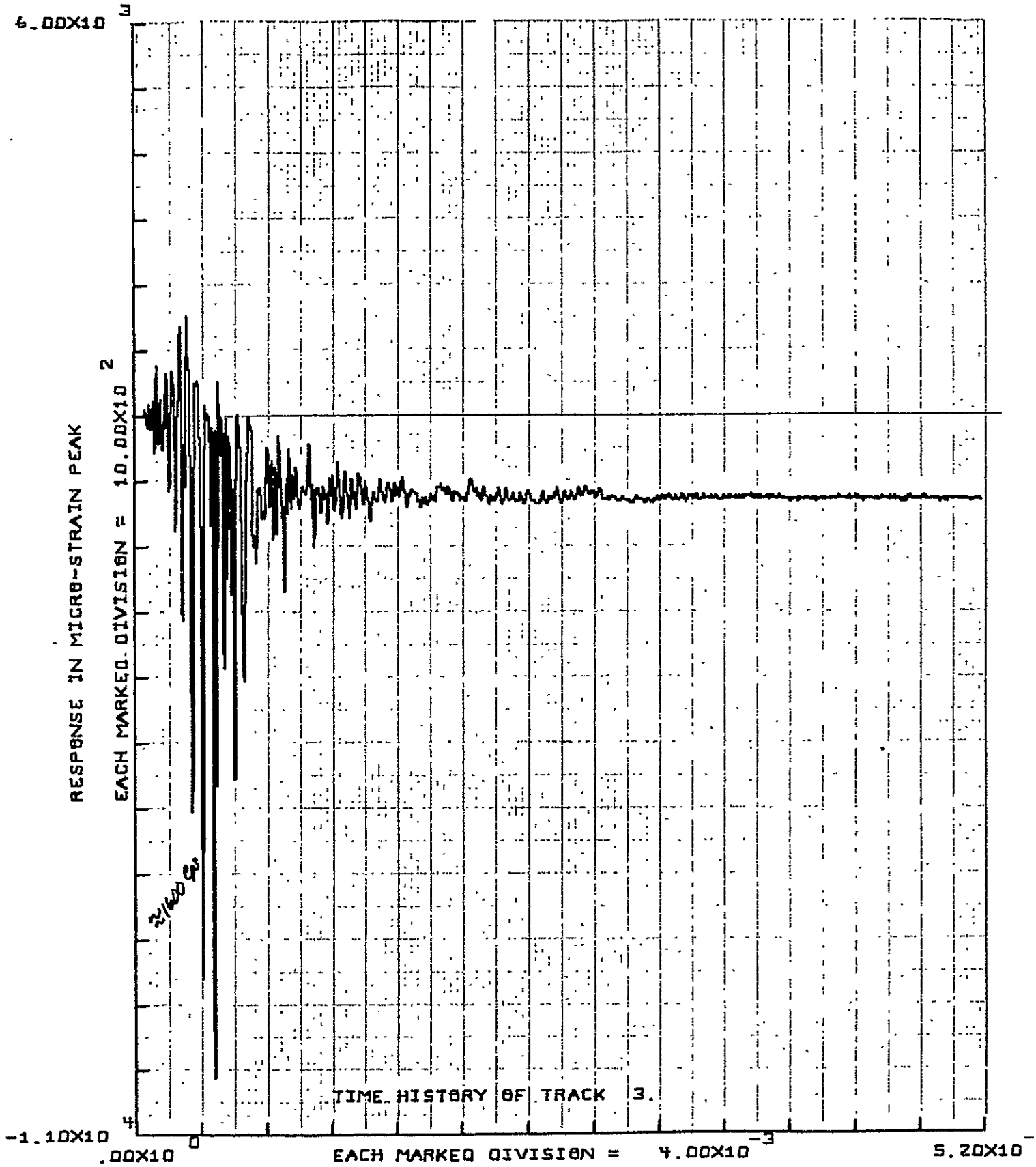
6.00X10 3
2
4
RESPONSE IN MICRO-STRAIN PEAK
EACH MARKED DIVISION = 10.00X10
-1.10X10
TIME HISTORY OF TRACK 3.
.00X10
0
EACH MARKED DIVISION = 4.00X10 -3
5.20X10
7419842603
TIME IN SECONDS
CALC DLF 6/19/75
CHK TMT 6/19/75
APPD
APPD
ROCKET RESEARCH THRUSTER VALVE ASSEMBLY
SHOCK TEST
RUN 11Z TRANSDUCER S3

Figure 6-13

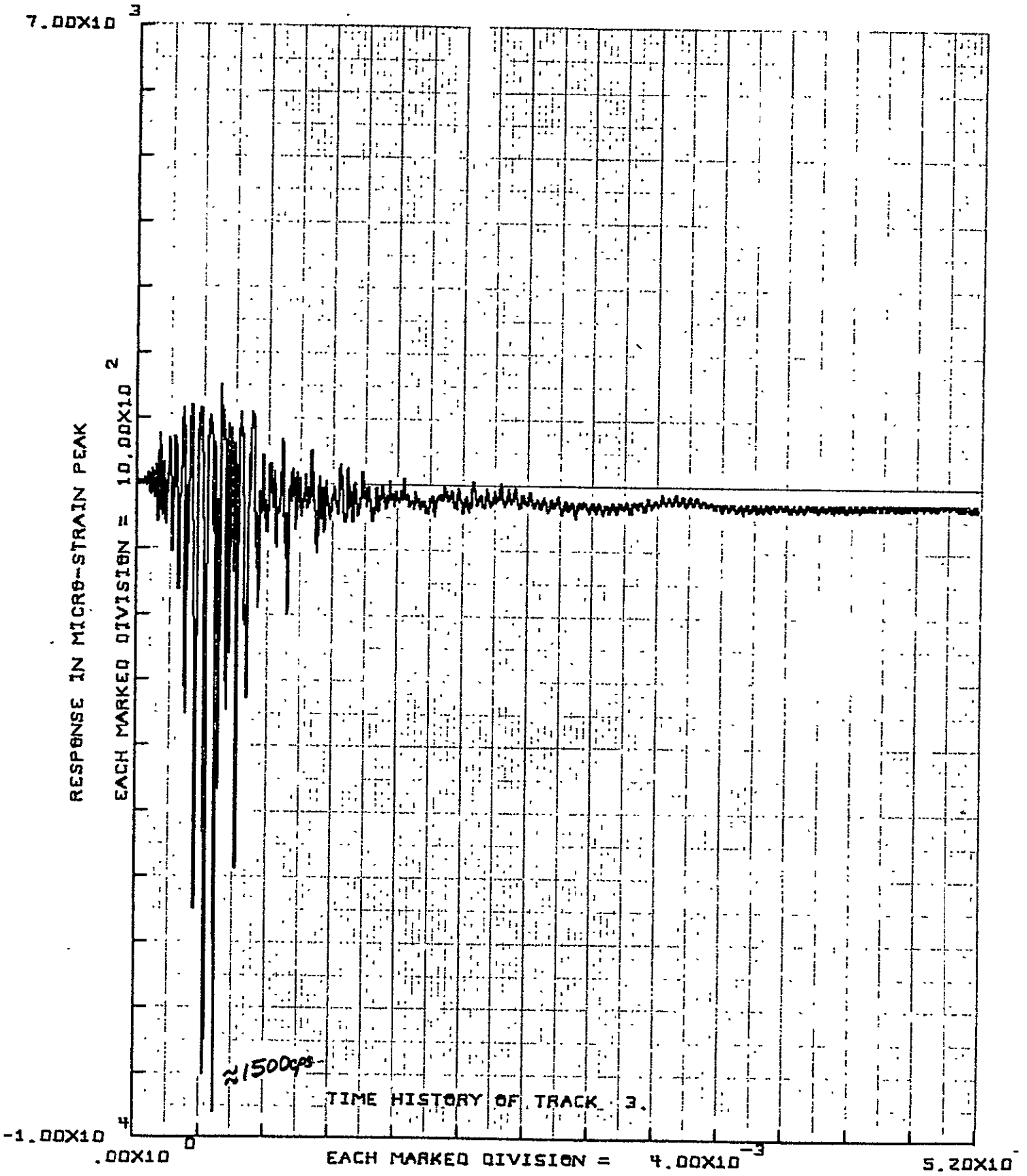

7419842603

CALC	DLF 6/19/75		ROCKET RESEARCH THRUSTER VALVE ASSEMBLY SHOCK TEST	ϵ_{XCT}
CHK'D	TMT 6/19/75			
APP'D			RUN 122 TRANSDUCER S3	
APP'D				

Figure 6-14

2-5613-7528-145

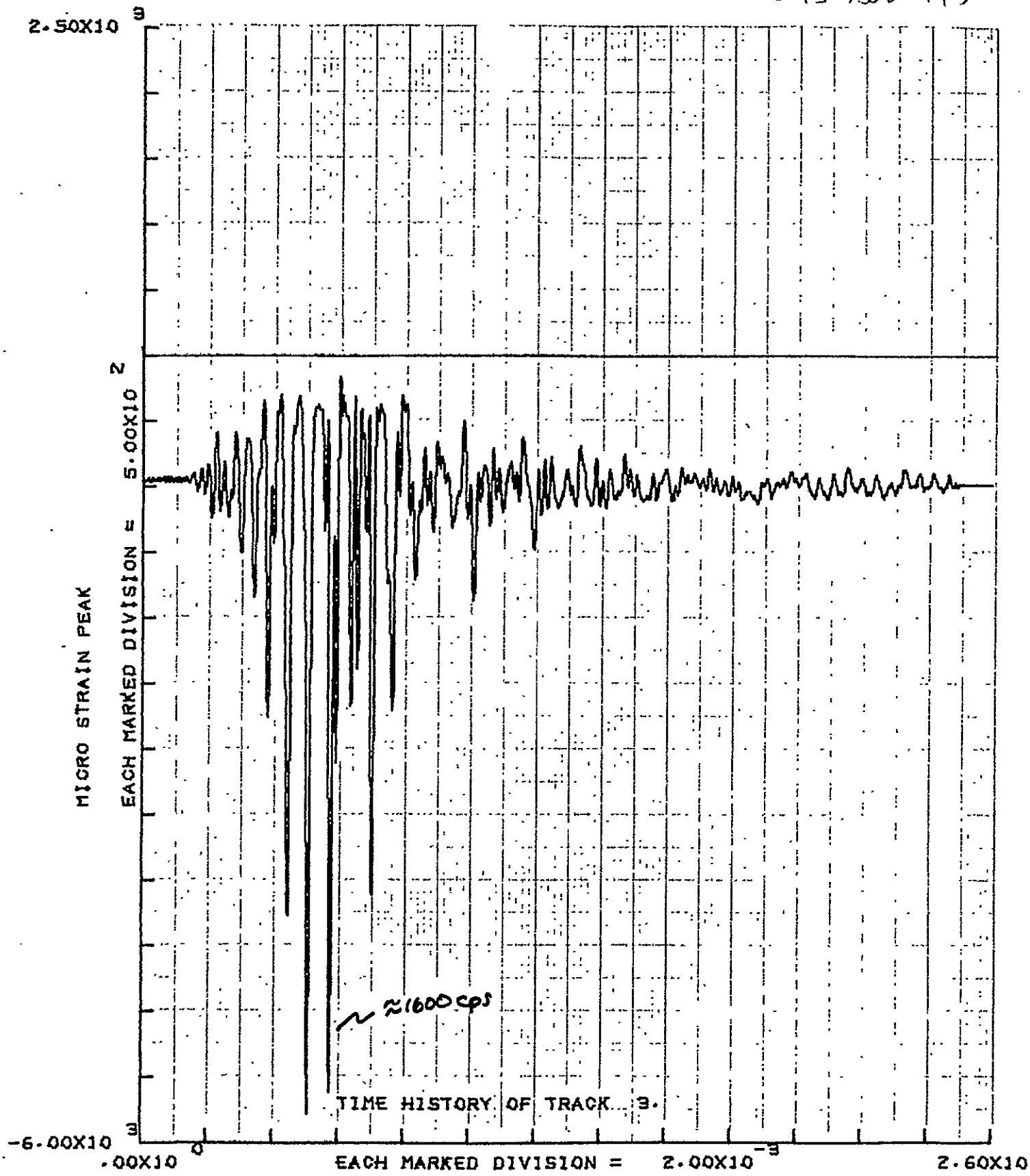

7404842609

CALC	DWE 5/21/75			ROCKET RESEARCH THRUSTER VALVE ASSEMBLY SHOCK TEST	EXCT
CHK	GS 5-22-5				
APPD	TMT 5-27-5			RUN 19Z	124
APPD	[illegible] 5/27				

Figure 6-15

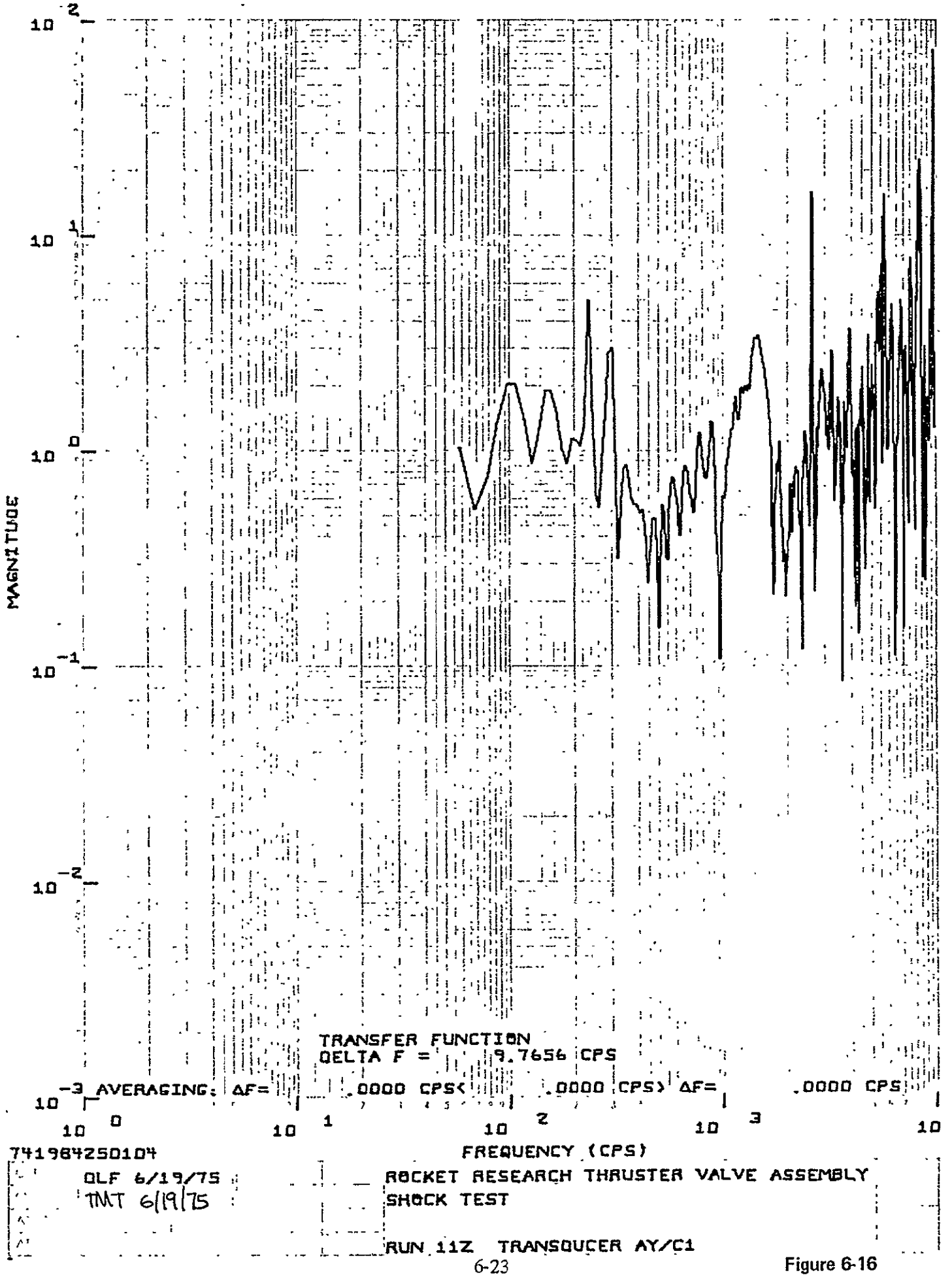
MAGNITUDE
FREQUENCY (CPS)
TRANSFER FUNCTION
DELTA F = 9.7656 CPS
AVERAGING: ΔF= .0000 CPS< .0000 CPS> ΔF= .0000 CPS
74198425010A
OLF 6/19/75
TMT 6/19/75
ROCKET RESEARCH THRUSTER VALVE ASSEMBLY
SHOCK TEST
RUN 11Z TRANSDUCER AY/C1

Figure 6-16

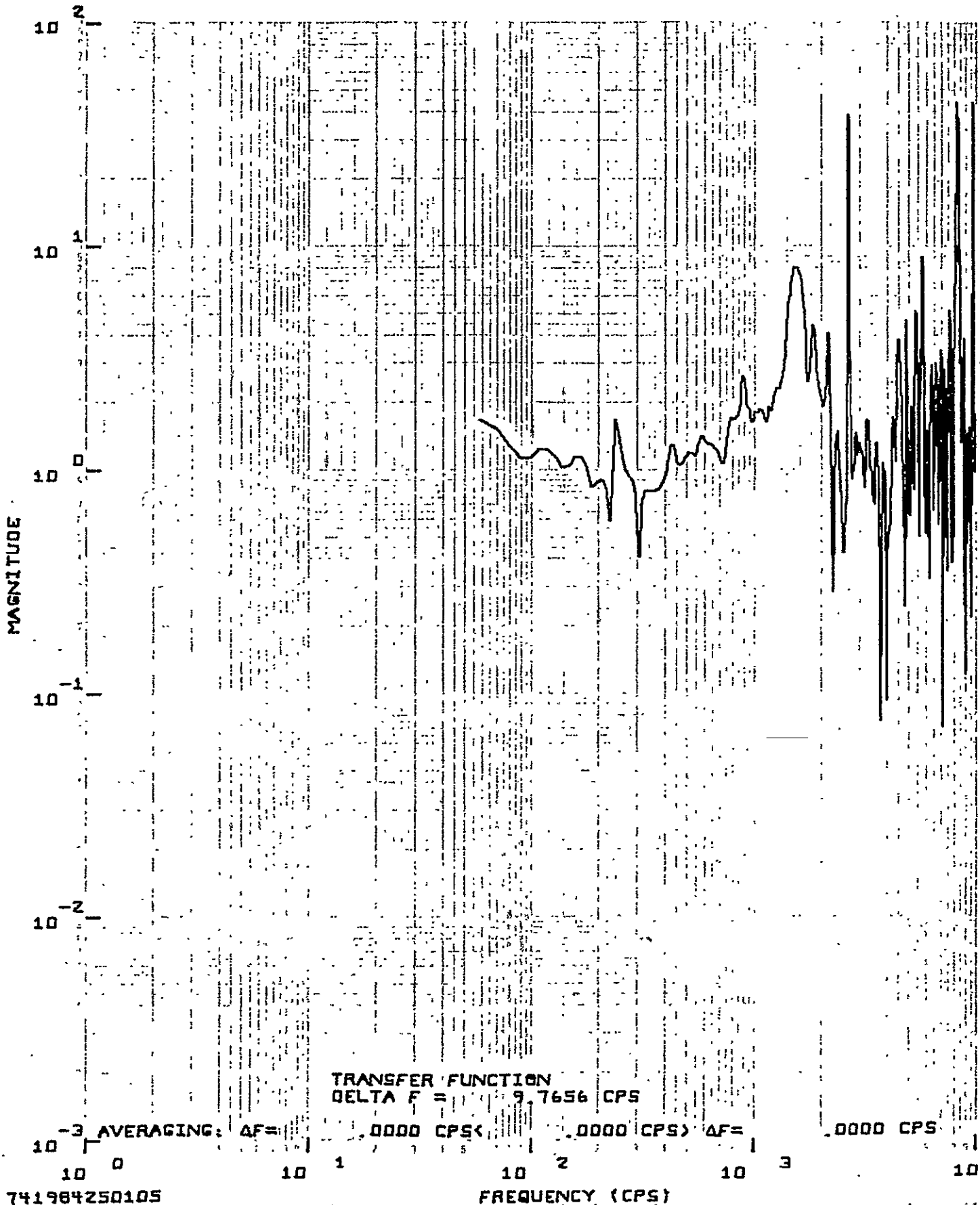

7419842501OS

DLF 6/19/75	ROCKET RESEARCH THRUSTER VALVE ASSEMBLY
TMT 6/19/75	SHOCK TEST
	RUN 11Z TRANSDUCER AZ/C1

Figure 6-17

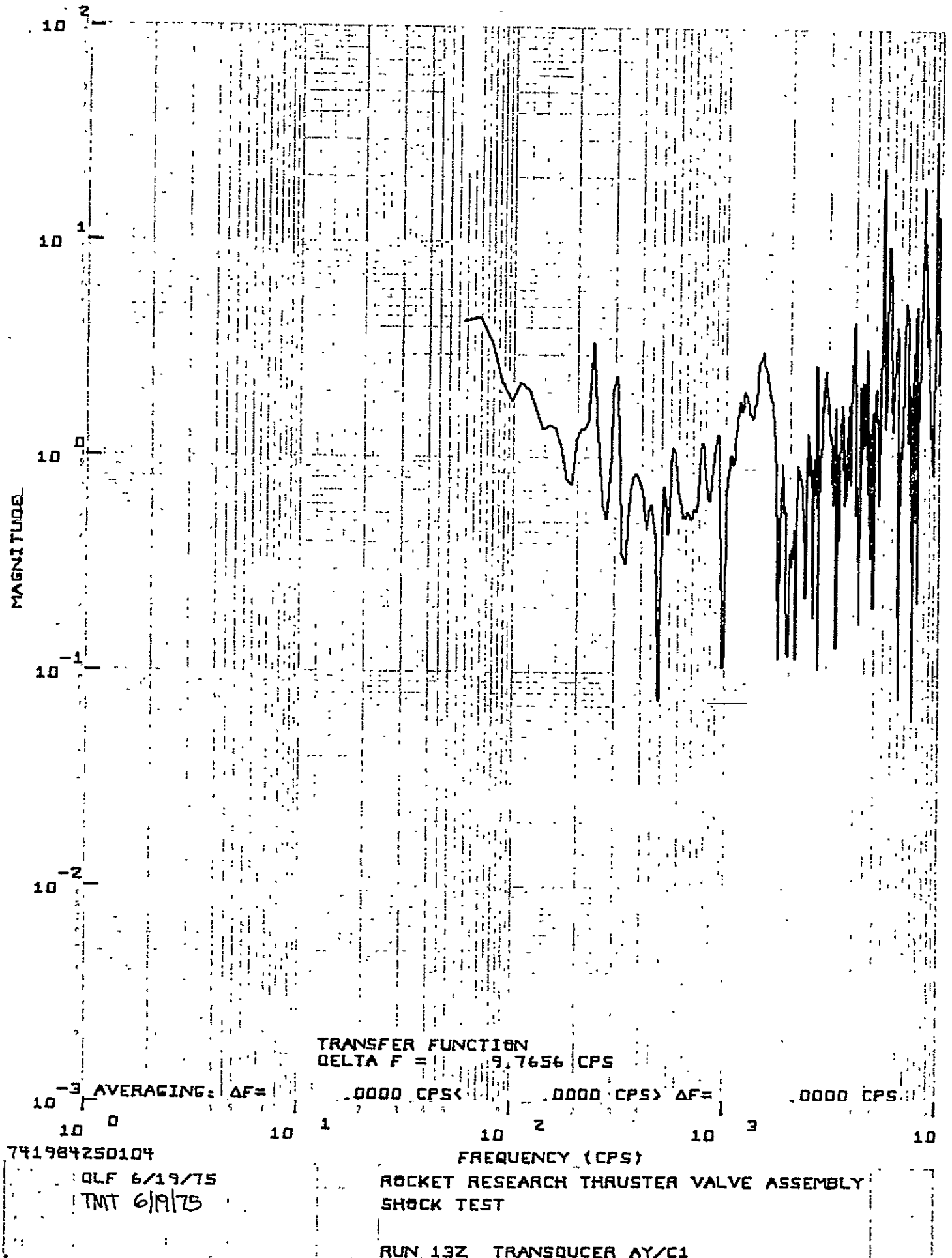
MAGNITUDE
FREQUENCY (CPS)
TRANSFER FUNCTION
DELTA F = 9.7656 CPS
AVERAGING: ΔF= .0000 CPS< .0000 CPS> ΔF= .0000 CPS
7419842S0104
QLF 6/19/75
TNT 6/19/75
ROCKET RESEARCH THRUSTER VALVE ASSEMBLY
SHOCK TEST
RUN 13Z TRANSDUCER AY/C1

Figure 6-18

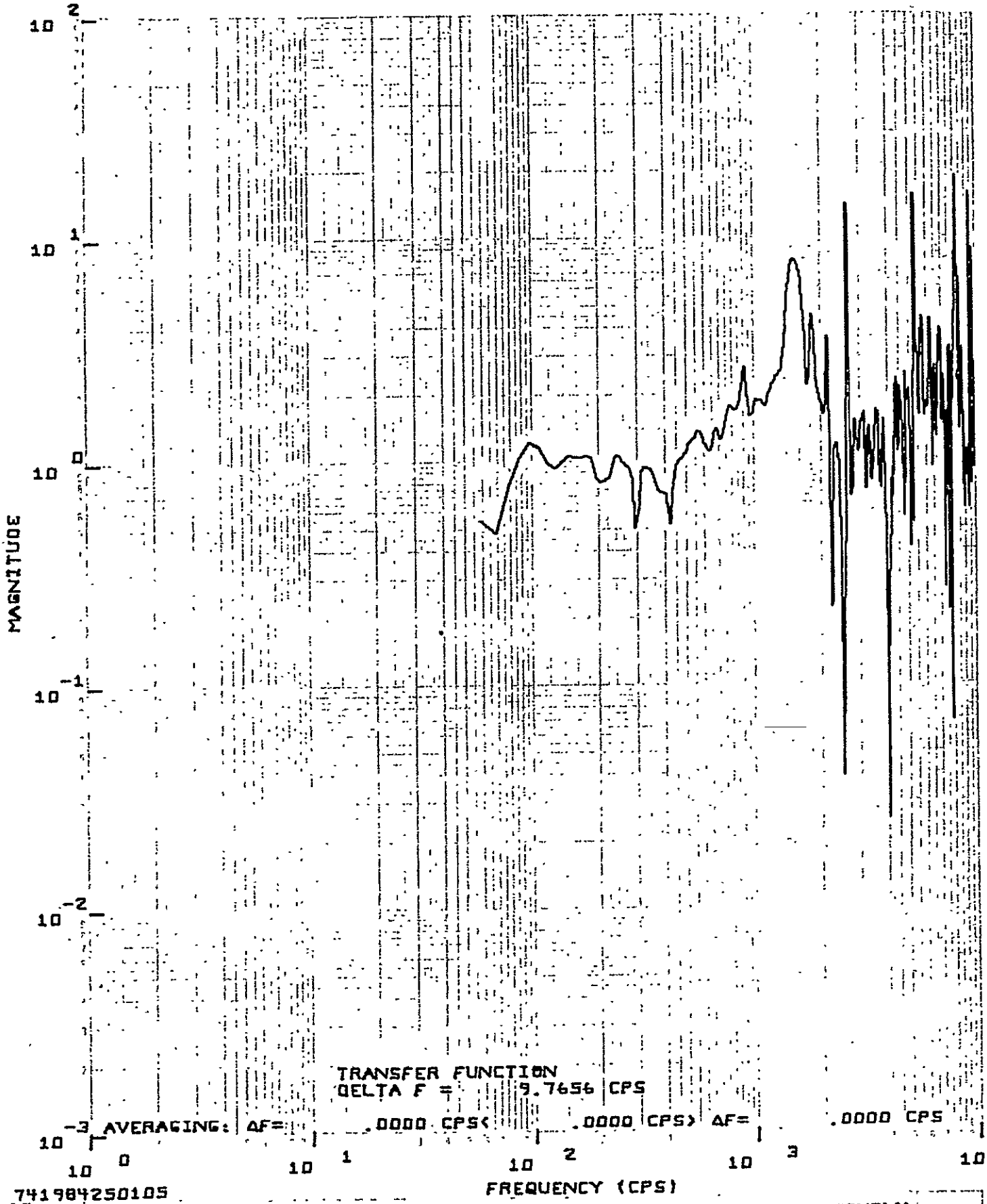
MAGNITUDE
FREQUENCY (CPS)
TRANSFER FUNCTION
DELTA F = 9.7656 CPS
AVERAGING: ΔF= .0000 CPS< .0000 CPS> ΔF= .0000 CPS
7419842501O5
OLF 6/19/75
TMT 6/19/75
ROCKET RESEARCH THRUSTER VALVE ASSEMBLY
SHOCK TEST
RUN 13Z TRANSDUCER AZ/C1

Figure 6-19

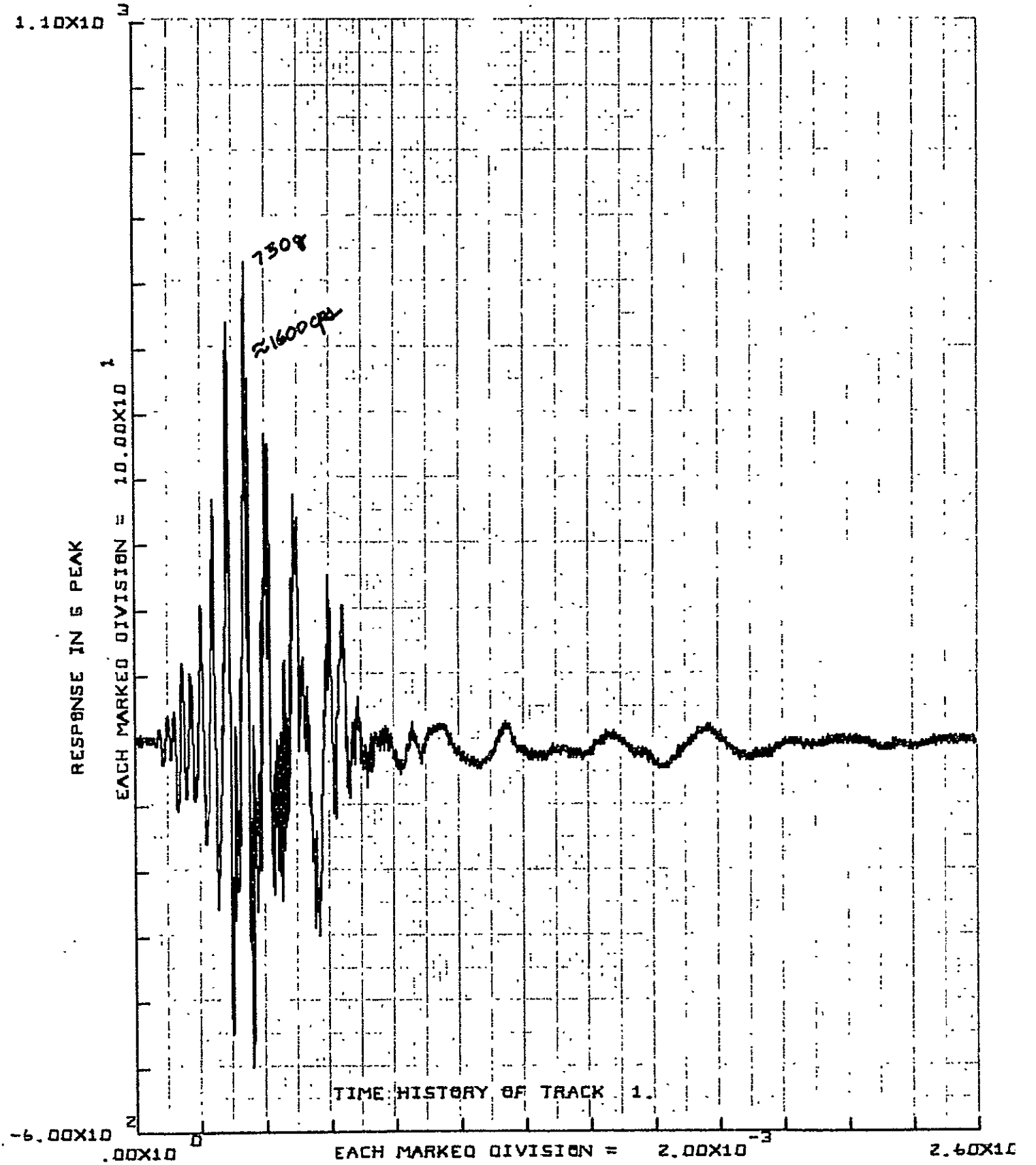
1.10X10 3
7308
≈1600 ps
RESPONSE IN G PEAK
EACH MARKED DIVISION = 10.00X10 1
-6.00X10 2
TIME HISTORY OF TRACK 1.
.00X10 0
EACH MARKED DIVISION = 2.00X10 -3
2.60X10
7419842501
TIME IN SECONDS
CALC QLF 6/18/75
CHK'D TMT 6/19/75
ROCKET RESEARCH THRUSTER VALVE ASSEMBLY
SHOCK TEST
RUN 12Z TRANSDUCER C1

Figure 6-20

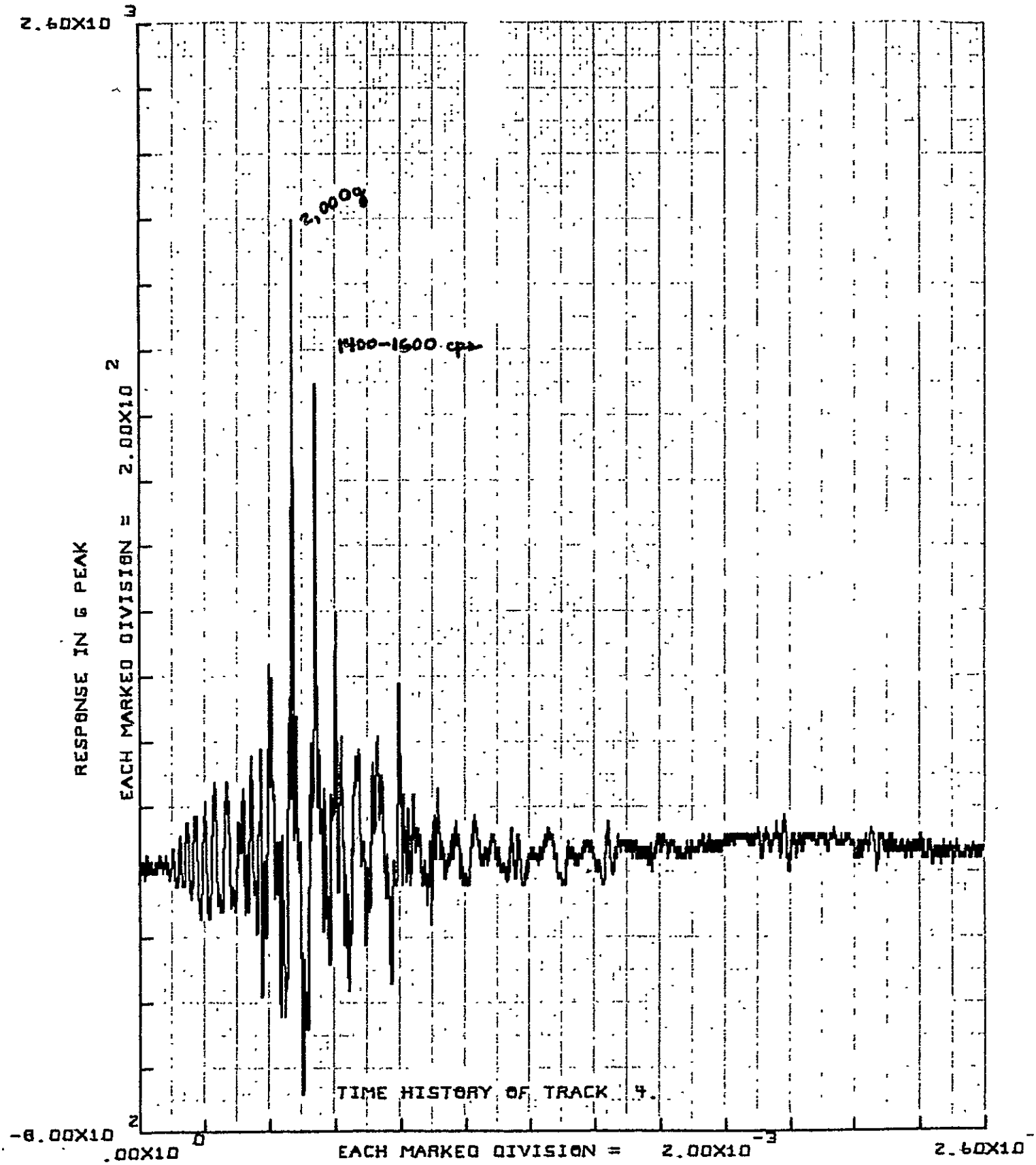

7419842504

DRN	DLF 6/18/75		ROCKET RESEARCH THRUSTER VALVE ASSEMBLY SHOCK TEST
CHK	TMT 6/19/75		
APP			RUN 12Z TRANSDUCER AY
APP			

Figure 6-21

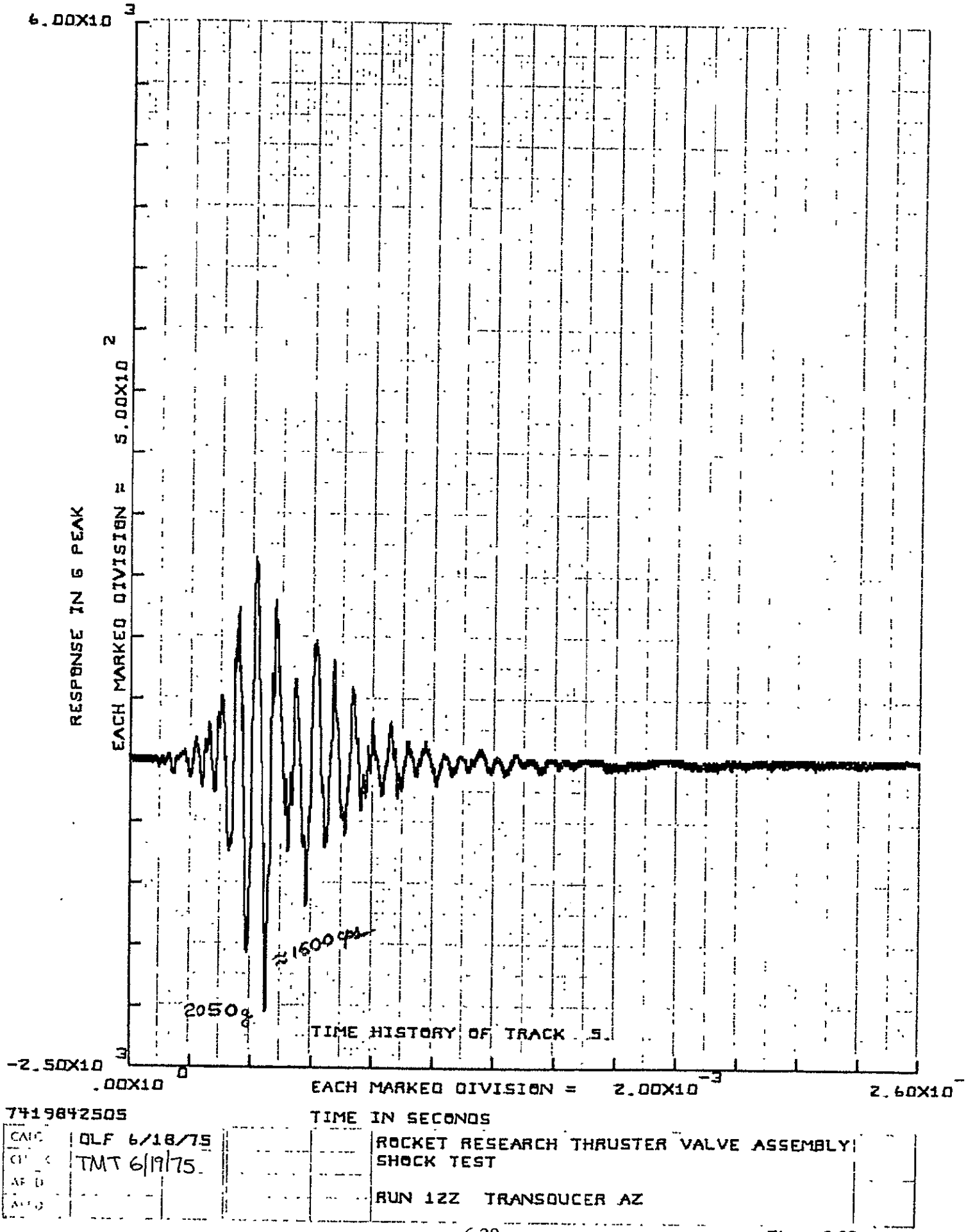
6.00X10 3
5.00X10 2
RESPONSE IN G PEAK
EACH MARKED DIVISION =
-2.50X10 3
.00X10 0
EACH MARKED DIVISION = 2.00X10 -3
2.60X10 -3
TIME IN SECONDS
2050g
1600 cps
TIME HISTORY OF TRACK 5.
7419842505
CALC OLF 6/18/75
CHK TMT 6/19/75
APD
APD
ROCKET RESEARCH THRUSTER VALVE ASSEMBLY
SHOCK TEST
RUN 12Z TRANSDUCER AZ

Figure 6-22

T/VA resonance at 1,600 cps which can induce high capillary tube stresses. Therefore, all the proper combinations of input and T/VA resonance were present during z axis shock excitation to produce high strain. The last item investigated was how valid were the capillary tube strains. The strain gauge (EA-06-015CK-120), with a grid of 0.020 inch wide and 0.015 inch long, was bonded to a 0.026-inch diameter tube. This gauge had to be attached to an almost inaccessible portion of the capillary tube between the injector and the thermal shunt lug; tube length less than 0.10 inch. The only way this gauge could be bonded was by making an epoxy platform for which the strain gauge was attached. Because of this arrangement, the possibility exists that the capillary tube strain gauge was recording strain due to combined tube and epoxy deformation. Furthermore, what the strain gauge was seeing was more due to epoxy yielding and not the capillary tube. It is obvious that capillary tube strain was high even to half-level shock (Figure 6-12); but, the change in strain characteristic from almost symmetrical strain pattern about the zero strain axis for half-level shock (Figure 6-12) to those obtained for full-level shock (Figures 6-13 through 6-15) indicated that the strains observed were not all tube strains. Therefore, it is very probable that high strains were developed in the capillary tube during z axis shock, but the strains did not produce the strain offset given in Table 6-5. An attempt will be made to verify this during pyro shock testing of qualification /VA. Also, the T/VA disassembly (Section 7.0) indicated no significant increase in capillary tube pressure drop, indicating no significant damage occurred.

6.1.3 Margin Vibration Test

A thermal shroud was added to the MJS 0.2-lbf T/VA D01 unit for margin vibration testing. This required that the mounting bracket also be changed to the flight-type since the breadboard configuration had no provisions for attaching the thermal shroud. Another change in this test unit from the previously vibrated D01 structure was the tie-down bolts. Two standoff-type bolts were used through the inside holes for attaching the T/VA to the vibration fixture.

The instrumentation used for margin vibration testing was similar to that utilized during previous vibration and shock testing of the D01. The strain gauges and accelerometer locations given in Table 6-6 are the same as shown in Figures 6-1 and 6-2. Seven strain gauges and five accelerometers were utilized. Strains were recorded on oscillograph paper and acceleration on magnetic tape.

The test plan called for subjecting the T/VA to qualification (T.A.) level sinusoidal and random vibrations.

The T/VA went through almost 50 percent of qualification level vibration exposure when the test was suspended due to pressure transducer structural failure. The test was stopped at about 4.3 minutes of random vibration along the y axis. This was also after the T/VA had been subjected to sine and random vibration in the z direction. The pressure transducer failure occurred in the ball welds that join the pressure transducer legs to the cylindrical body. Prior to the weld failure, the bolts attaching the pressure transducer to the T/VA mounting bracket were found to be loose at the conclusion of z axis random vibration.

Table 6-6
MJS 0.2-lbf T/VA D01
MARGIN VIBRATION TEST DATA

A. Strain Data

Run No.	Vibration Type	Frequency cps	Strain – 10^{-3} in./in.						
			ϵYS1	ϵYS2	ϵXS2	ϵXCT	ϵZPL	ϵXP_C	ϵPD
2Z	Sine (T.A.)	450	0.12	0.06	–	–	0.70	–	–
		750	0.16	–	0.13	0.11	–	0.23	0.08
		900	–	–	–	0.09	0.15	–	–
		1,100	0.11	0.14	0.11	0.15	–	0.68	–
		1,600	0.20	–	–	1.30	–	0.16	–
4Z	Random (T.A.)	t < 3.7 min	0.66	Out	0.66	1.50 (1,600)	3.15 (450)	1.90 (1,100)	0.24
		t ⩾ 3.7 min	1.20	Out	1.40	2.00		2.00	1.00
6Y	Random (T.A.)	t < 2 min	0.80 (830)	Out	0.64	0.60 (1,600)	Out	2.00 (1,100)	0.20 (450)
		t > 3.2 min	0.80 (750)	Out	2.00 (750)	0.75 (1,600)	Out	2.25	0.50

(XXX) Dominant frequency in cps

B. Acceleration Data

Run No.	Vibration Type	Frequency cps	Acceleration – g*				
			A1X	A1Y	A1Z	A3X	A3Z
2Z	Sine (T.A.)	450	–	–	–	68.0	160.0
		750	10.0	15.0	15.0	–	6.0
		900	–	–	–	5.3	–
		1,000	–	–	–	–	18.0
		1,100	18.0	4.0	–	–	–
		1,300	–	6.5	18.0	–	29.0
		1,600	9.5	–	30.0	–	–
		1,700	–	–	–	21.0	31.0
		2,000	75.0	45.0	50.0	–	–
4Z	Random (T.A.)	–	14.5	12.5	30.0	42.0	90.0

*g rms for random vibration

Review of the strain data (oscillograph trace) showed that bolt looseness occurred about 80 seconds before the end of a 5-minute random vibration test in z direction. There was an abrupt increase in strain of about 100 percent at that time. Test was not stopped then since this was a test to determine what margin the T/VA had for vibration above qualification requirements.

There were two possible reasons why the pressure transducer bolts became loose. This was the first mounting structure with the Rosan Slimset locked-in inserts. It was later found that an improper installation method was used for putting the inserts into the T/VA mounting bracket. The other possibility was that the pressure transducer attachment bolts' torque was probably below minimum. The pressure transducer bolts were removed with the thermal shroud in order to bond a strain gauge to the propellant tube. When the shroud and pressure transducer were put back on, an ordinary screwdriver was used to torque the bolts, since a special tool for torquing the flat pan head both with a "hi-torque" recess was unavailable.

Before y axis vibration, the loose bolts were retorqued. The y axis random vibration strain data did not show anything unusual happening until about 2 minutes into the run. At that point, the standoff (ϵXS2) and P_C tube (ϵXP_C) strains started increasing to one side and the zero strain also shifting. This shift continued until the test was stopped at approximately 4.3 minutes when it became apparent that something was loose on the T/VA. Inspection of the T/VA revealed that the pressure transducer body was no longer attached to the legs by way of ball welds; five welds on the double legs and three welds on the single leg.

It is difficult to predict whether or not the pressure transducer welds failed because of the loose bolts. However, since ball weld failure was predicted, the request was made during PDR to increase the number of welds. The flight pressure transducer units did incorporate this change from the breadboard/development configuration. Therefore, no weld failure is expected in the flight-type pressure transducer hardware.

6.1.4 Test Versus Analysis

In comparing test data with predicted results, the objectives of analysis and testing should be kept in mind. Analysis is performed to ensure that structural integrity is maintained during exposure to various dynamic loading conditions. This is accomplished by assuming worst-case conditions which yield conservative results. The objective of testing is to qualify the design by test and to verify that predicted results were conservative. Therefore, the criteria utilized when evaluating test and analytical results is dependent on many factors. These and other factors will be discussed in the following paragraph in relation to the various test results when compared with analysis.

Comparison of test and predicted resonant frequencies shows good correlation at higher frequencies. However, the analytical fundamental frequency is much higher (608 cps versus 410 to 470 cps) than test values. The primary reason for this large difference (29 to 48 percent) is the mounting bracket's mathematical model. The T/VA's lower natural frequencies are dependent on the bracket's stiffness characteristics. This requires the use of a large number of plate elements to simulate the mounting bracket; but because of computer limitations and also computer cost, the

bracket was modeled with these constraints in mind. The first mode has a significant effect on the propellant tube and pressure transducer stresses only. Therefore, it was assumed that other parameters (damping) would tend to offset this discrepancy in frequency, and the resulting dynamic response (stress) would be conservative. This was verified by test data which showed below yield stresses at the propellant tube and pressure transducer legs at peak stress locations. Above yield stress was predicted for the pressure transducer leg (M = -0.17) and slightly below yield (MS = 0.05) was obtained for the propellant line when the T/VA was subjected to random vibration. For pyro shock environment, the predicted stresses for propellant tube and pressure transducer were more than twice the yield stress. However, during shock testing, no yielding was noted at either stress location.

Several factors need to be considered before discussing the comparison between test and analytical stress data. First, analysis is based on a linear model which assumes a linear stress-strain relationship. However, material properties above the proportional limit are nonlinear and, unless predicted and test stresses are low, it is difficult to compare the two. Second, test data consist of strain measurements which have to be converted to stress values for stress comparison. Since dynamic stress-strain curves are not available for most materials used in the T/VA, this is difficult to do. Third, test results presented in Tables 6-3 and 6-6 are maximum strains for all locations. Statistical analysis of test data, using Rayleigh distribution of peaks, shows that most of these strains are 4-sigma values whereas analysis is based on 3-sigma stress results. Finally, the dynamic analysis of the MJS 0.2-lbf T/VA was based on worst-case assumptions and predicted results yield conservative values. Therefore, when one considers these problems, the most meaningful interpretation of test and analysis data for measured or predicted high-stress or strain levels is their relation to yield stress or strain.

To illustrate what was discussed in the preceeding paragraph, predicted stresses were converted to strains and maximum amplitudes compared for random vibration environment in Table 6-7. (It would have been better to compare stresses since the T/VA was designed using stress criteria. However, true dynamic stress-strain curves are unavailable to convert measured strains to stresses.) One notes how close the predicted strains are to test strains for the thermal standoff and capillary tube. However, if one considers the fact that test strains are very likely 4-sigma level, the correlation is not as good. Nevertheless, it should be kept in mind that the MJS 0.2-lbf T/VA was designed for worst-case dynamic conditions, and the object of the test was to show that predicted levels were conservative. Therefore, standoff and capillary tube stress (strain) satisfies this condition. However, just the opposite appears for random vibration strain developed in the propellant tube. The test strain is more than two times the predicted strain (0.0029 versus 0.00128 in./in.). In this case, one should look at the yield stress for predicted stress and strain offset for test strain. The predicted stress margin of safety is 0.05. This means that yielding of the tube does occur but is just below 0.002 in./in. offset (yield by definition). The total strain offset measured in propellant tube was about 0.0005 in./in. Therefore, it is deduced from this that predicted stress was conservative. How conservative is it can only be obtained from a true dynamic stress-strain curve for propellant tube material.

Table 6-7
VIBRATION AND PYRO SHOCK STRAINS (10^{-3} in./in.)
TEST VS. ANALYSIS*

Structural Component	Random Vibration		Pyro Shock	
	Test	Analysis	Test	Analysis
1. Thermal standoff	1.15	1.43	4.80	4.86
2. Capillary tube	1.10	1.16	10.10	4.99
3. Propellant tube	2.90	1.28	1.62	3.21
4. Pressure transducer leg	–	–	3.90	3.26

*Predicted strain = (Predicted stress)/(Young's Modulus)

Table 6-7 also presents a comparison between test and analysis for pyrotechnic shock environment. The interpretation applied to these results is somewhat different from that used for comparing vibration stresses (strains). For one thing, the material behaves differently under high g, high frequency impact loading than under cyclic or static load. Also, predicted stresses for all four structural members given in Table 6-7 were 2 to 4 times above yield stress (CDR report). Yet, past experience shows that seldom yielding occurs in members with predicted stresses 2 to 3 times yield for pyro shock conditions. Although some pyro shock test and predicted strains in Table 6-7 are close, this may be coincidental or that these members were undergoing linear deformation (below proportional limit). The important fact is that the T/VA structure did not yield during application of three full-level shocks along each axis (in addition to half-level shocks) although yielding was predicted analytically but not expected.

Due to structural failure of the T/VA during early phase of margin vibration testing, insufficient test data is available for extensive comparison with analysis or even previous test results. However, the data obtained shows certain definite changes from previous tests. The fundamental frequency was still 450 cps but some of the intermediate resonances were lowered (see Tables 6-3, 6-4, and 6-5). The most prevalent factor is that during sine vibration at 450 cps, the propellant tube strain was 3 times that recorded during previous vibration test. The acceleration at location A3X also tripled. Analysis showed no such increase occurring as a result of incorporating thermal shroud and standoff tie-down bolts. Only two structural members show a significant increase in predicted stress for random vibration along the z axis. The thermal standoffs and capillary tube have stresses 28 and 22 percent higher, respectively. However, these stresses are still below the material yield allowable. Test strain data in Table 6-6 shows a slight increase in standoff stress and about a 61 percent increase in capillary tube strain. However, the increase in strain is only 23 percent in the propellant tube strain in the first 3.7 minutes of testing, i.e., before the bolt became completely loose. Because of the uncertainty of the effect of the pressure transducer tie-down bolts, it is difficult to say what their

influence was on the test results. Analysis indicated some changes in the dynamic response of the flight configuration T/VA from the breadboard development type. However, this change should not be as prominent as was observed during partial margin vibration testing. To verify this, a flight-type T/VA will be instrumented with strain gauges and accelerometers during qualification level vibration testing. The same unit will also be subjected to pyro shock testing, and strains will be measured as well.

6.2 THERMAL DESIGN VERIFICATION TESTING

This section presents the results from the LCSSE/MJS 0.2-lbf T/VA thermal design development testing. The goals of this test series were to determine the catalyst bed heater power required to maintain adequate prefiring, bed temperatures, correlate the thermal model with test results, determine the T/VA capability to fire when stabilized at the MJS standby mode with no heater power, and to determine the gold plated heat shield emittance degradation due to the 1,100°F predicted maximum temperatures during operation. This test series was conducted after the performance, C_f mapping, and steady-state life margin tests had been completed. Table 6-8 presents a summary of the test sequences conducted.

6.2.1 Catalyst Bed Heater Power

The original development testing to determine catalyst bed heater power requirements (Reference Table 6-8) was repeated because the original heat shield emittance ranged from 0.07 to 0.13 and above.

For the repeated testing, the aft shield was replaced by an unfired shield with a 0.04 value of emittance. The forward shield was cleaned on the outside; however, it had an emittance which was probably at least 0.13. Thus, the average emittance for all gold shielding of the reactor was not less than 0.05, which was assumed in the thermal model.

Predevelopment test measurements of the thermal standoffs showed that they were of minimum resistance very close to the minimum values assumed in the thermal model. Thus, the test results can be considered pessimistic since standoff resistance and heat shield emittance are the primary factors affecting catalyst bed heater power.

Figures 6-23, 6-24, and 6-25 give test results and compare thermal model predictions for catalyst bed heater powers of 1.4, 1.55, and 3.11 watts. The analytical results are in parentheses. Thermal model details will be discussed in the next section.

Figure 6-23 shows that the catalyst bed does not exceed 250°F with a 1.4-watt heater as had been expected based on the "REALISTIC" thermal model of reference 74-R-448. Figure 6-24 shows that a 250°F catalyst bed can be achieved with 1.55 watts and agrees with the "CONSERVATIVE" thermal model which predicts 249 to 255°F compared with a measured value of 250°F. The small differences here between predicted and measured values are probably due to degraded rhodium plating resulting from the extensive testing that preceded the thermal vacuum test. The 249°F is the analytical prediction based upon no rhodium on the nozzle.

Table 6-8
THERMAL DESIGN VERIFICATION
COLD CASE THERMAL CYCLES

Sequence Number	Fuel T-14 Inlet °F	T/VA T-15 Mount °F	Shroud & T-11 Target °F T-10	Transducer Power	Thruster Heater Power (watts)
1 V1 V2 V3	40	40	<-250	ON	1.40 2.00 2.50
2 V1 V2 V3	40	85	<-250	ON	1.40 2.00 2.50
3	40	50	<-250	ON	1.40
5*	40	50	<-250	OFF	OFF
6	Using Sequence 5 temperature conditions fire a 10 second steady-state test at a feed pressure of 70 psia.				
7	40	42 to 46	<-250	OFF	OFF
7-1	40	50	-250	OFF	OFF
8	Using Sequence 7-1 temperature condition, fire 3 10 msec pulses in the limit cycle mode, then fire a duty cycle of 10 msec ON, 1.0 second OFF for the thermal equilibrium				
1A	40	40	<-250	ON	1.550
1b	40	40	<-250	ON	3.106

*Note Sequence 4 was deleted.

Figure 6-25 shows that the same degree of thermal model correlation with test exists at higher bed powers essentially double that of Figure 6-24. Note that boundary condition temperatures simulating deep space, spacecraft mount, and spacecraft propellant line interface were essentially held constant throughout the testing depicted in Figures 6-23, 6-24, and 6-25.

Figure 6-26 presents the effects of spacecraft mount temperature variation on catalyst bed temperature. A 3-degree increase in mount temperature results in a 1-degree increase in catalyst bed temperatures. This value agrees with the first development tests which were accomplished with the degraded heat shields.

ORIGINAL PAGE IS
OF POOR QUALITY

MJS 0.2-lbf T/VA DEVELOPMENT TEST RESULTS
RETEST WITH NEW AFT HEAT SHIELD
1.40-WATT BED HEATER

*ANALYTICAL VALUES IN PARENTHESES

1. PROPELLANT VALVE
2. REACTOR WALL
3. VALVE MOUNT FLG
4. FWD HEAT SHIELD
5. REACTOR STANDOFFS
6. AFT HEAT SHIELD
7. INJECTOR FLANGE
8. NOZZLE DIVERGENT
9. REACTOR HEATER
10. DEEP SPACE B.C.
11. VALVE SEAT
12. CATALYST BED
13. VALVE HEATER
14. PROP SUPPLY B.C.
15. SPACECRAFT B.C.
16. NOZ CONVERGENT
17. CAP. TUBE/SHUNT
18. MECHANICAL INTERFACE
19. MT BKT (VALVE SECT)
20. SHIELDS/INJECTOR JCT
21. MT BKT (PROP LINE SECT)
22. ELECTRICAL CONNECTOR
23. PROPELLANT LINE ENTRANCE
24. PROPELLANT LINE FITTING
25. PRESSURE TRANSDUCER
26. TEMP SENSOR SHEATH
27. HEATER SHEATH
28. P-DCR LINE
29. SHROUD (PROP LINE SECT)
30. SHROUD (VALVE SECT)
31. TEMP SENSOR TRANSITION
32. HEATER TRANSITION
33. PROPELLANT LINE EXIT
34. PROP LINE/VALVE INTF

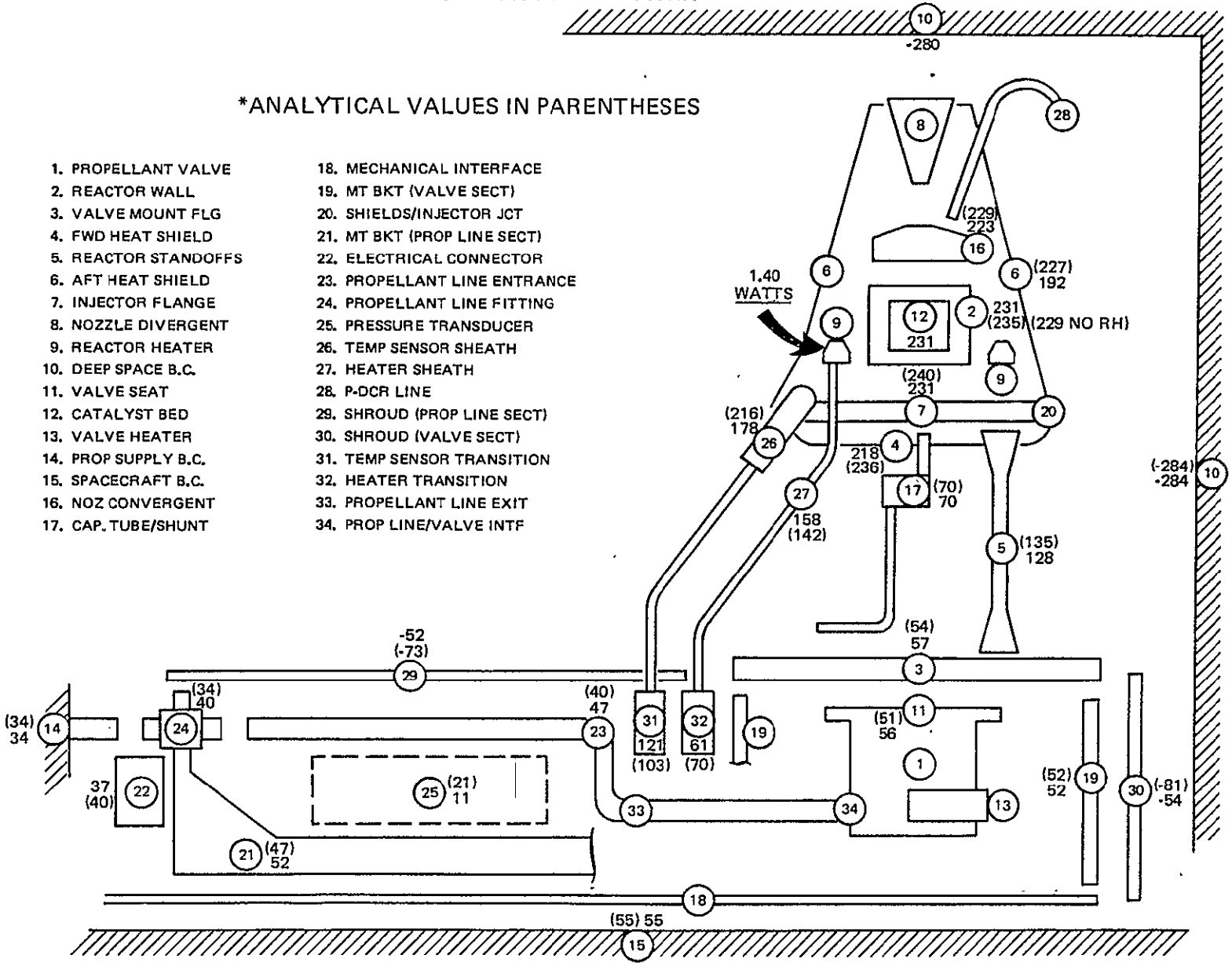

Figure 6-23

MJS.0.2-lbf T/VA DEVELOPMENT TEST RESULTS
RETEST WITH NEW AFT HEAT SHIELD
1.55-WATT BED HEATER

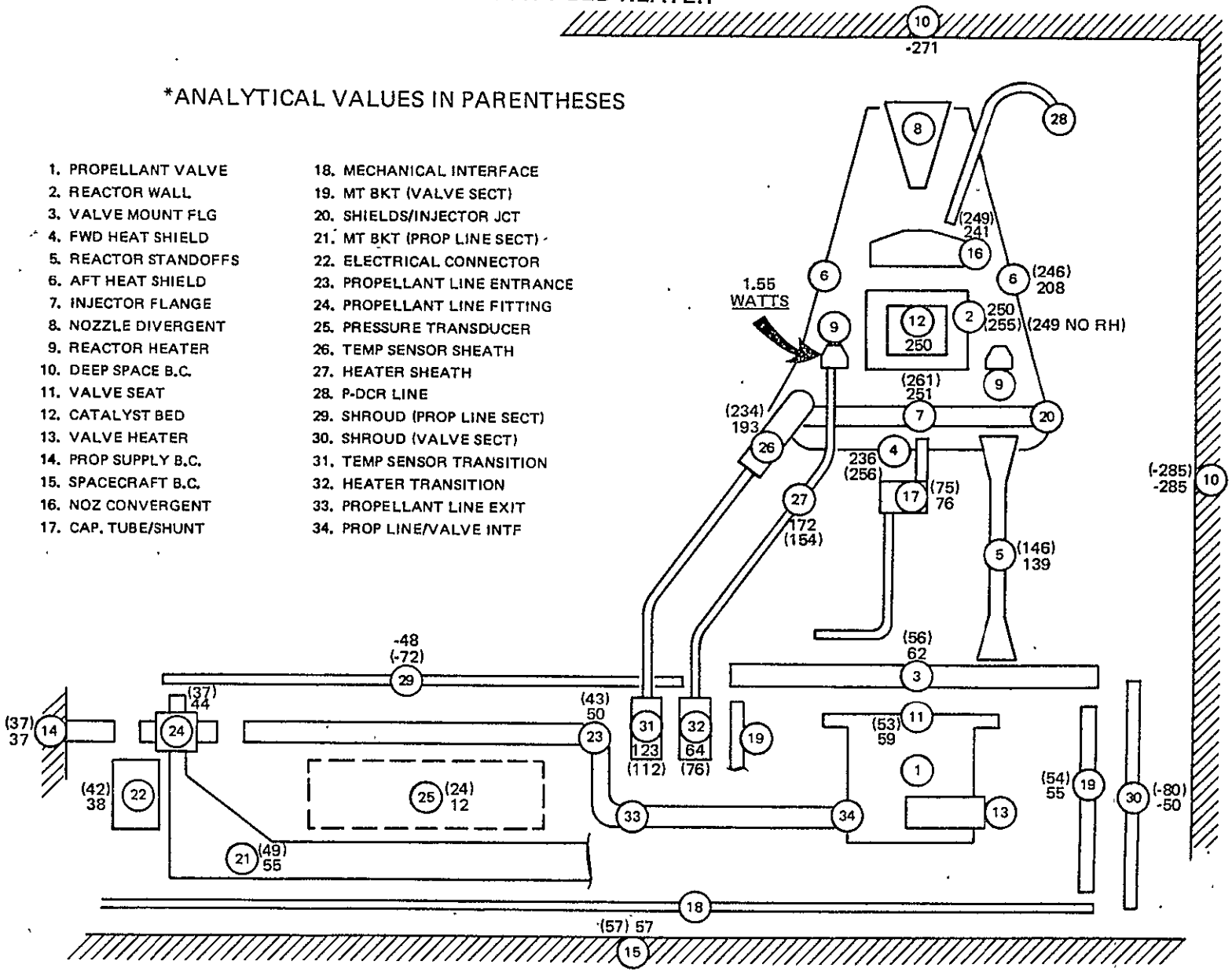

Figure 6-24

ORIGINAL PAGE IS
OF POOR QUALITY

MJS 0.2-lbf T/VA DEVELOPMENT TEST RESULTS
RETEST WITH NEW AFT HEAT SHIELD
3.11-WATT BED HEATER

*ANALYTICAL VALUES IN PARENTHESES

1. PROPELLANT VALVE
2. REACTOR WALL
3. VALVE MOUNT FLG
4. FWD HEAT SHIELD
5. REACTOR STANDOFFS
6. AFT HEAT SHIELD
7. INJECTOR FLANGE
8. NOZZLE DIVERGENT
9. REACTOR HEATER
10. DEEP SPACE B.C.
11. VALVE SEAT
12. CATALYST BED
13. VALVE HEATER
14. PROP SUPPLY B.C.
15. SPACECRAFT B.C.
16. NOZ CONVERGENT
17. CAP. TUBE/SHUNT
18. MECHANICAL INTERFACE
19. MT BKT (VALVE SECT)
20. SHIELDS/INJECTOR JCT
21. MT BKT (PROP LINE SECT)
22. ELECTRICAL CONNECTOR
23. PROPELLANT LINE ENTRANCE
24. PROPELLANT LINE FITTING
25. PRESSURE TRANSDUCER
26. TEMP SENSOR SHEATH
27. HEATER SHEATH
28. P-DCR LINE
29. SHROUD (PROP LINE SECT)
30. SHROUD (VALVE SECT)
31. TEMP SENSOR TRANSITION
32. HEATER TRANSITION
33. PROPELLANT LINE EXIT
34. PROP LINE/VALVE INTF

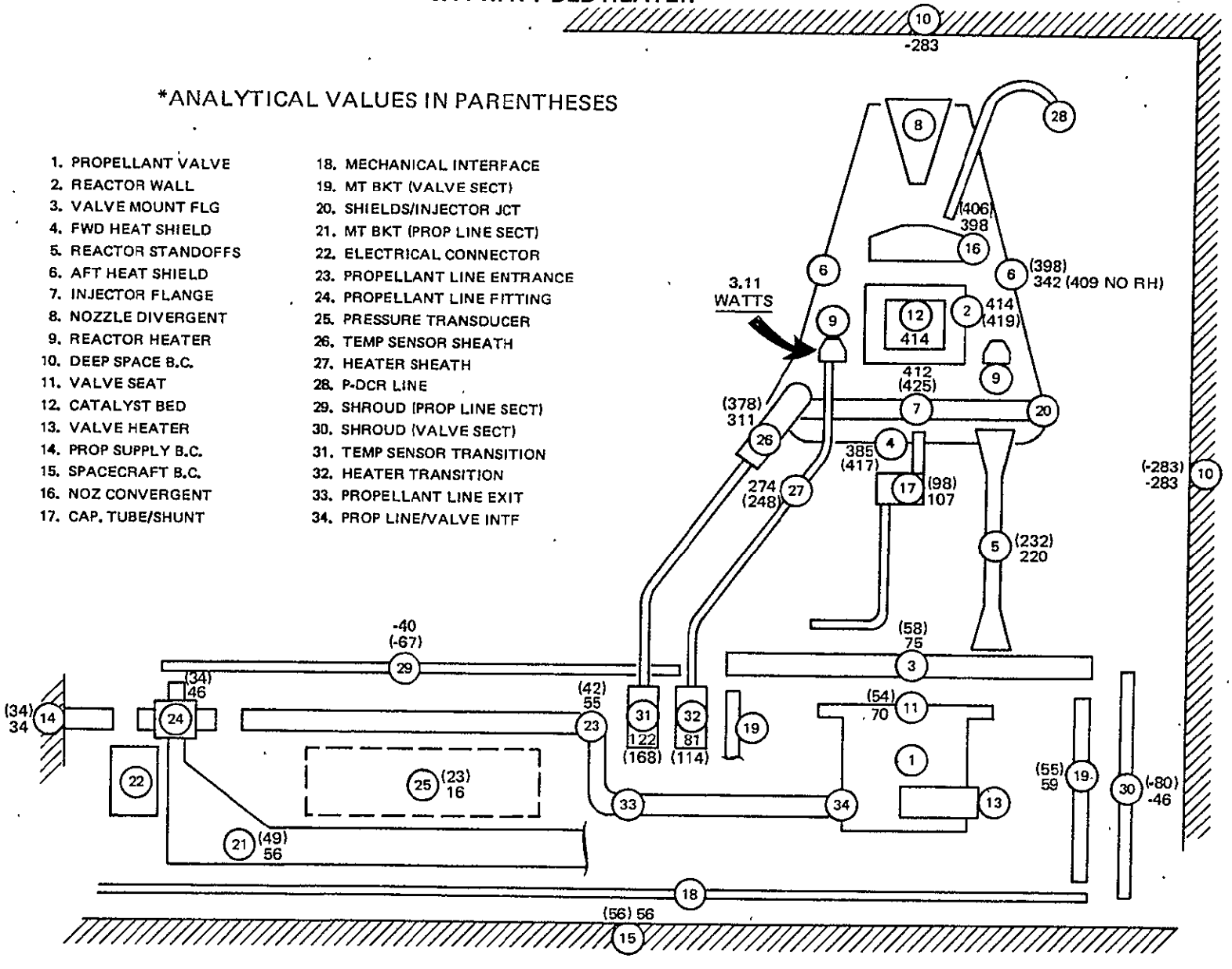

Figure 6-25

OPERATIONAL MODE FINAL FLIGHT PREDICTIONS
MJS 0.2-lbf T/VA CATALYST BED
TEMPERATURE CHARACTERISTICS

- EFFECTS OF SPACECRAFT MOUNT TEMPERATURE VARIATIONS
- PROPELLANT LINE VARIED 40 TO 48°F BUT HAD NO EFFECT ON BED TEMPERATURE

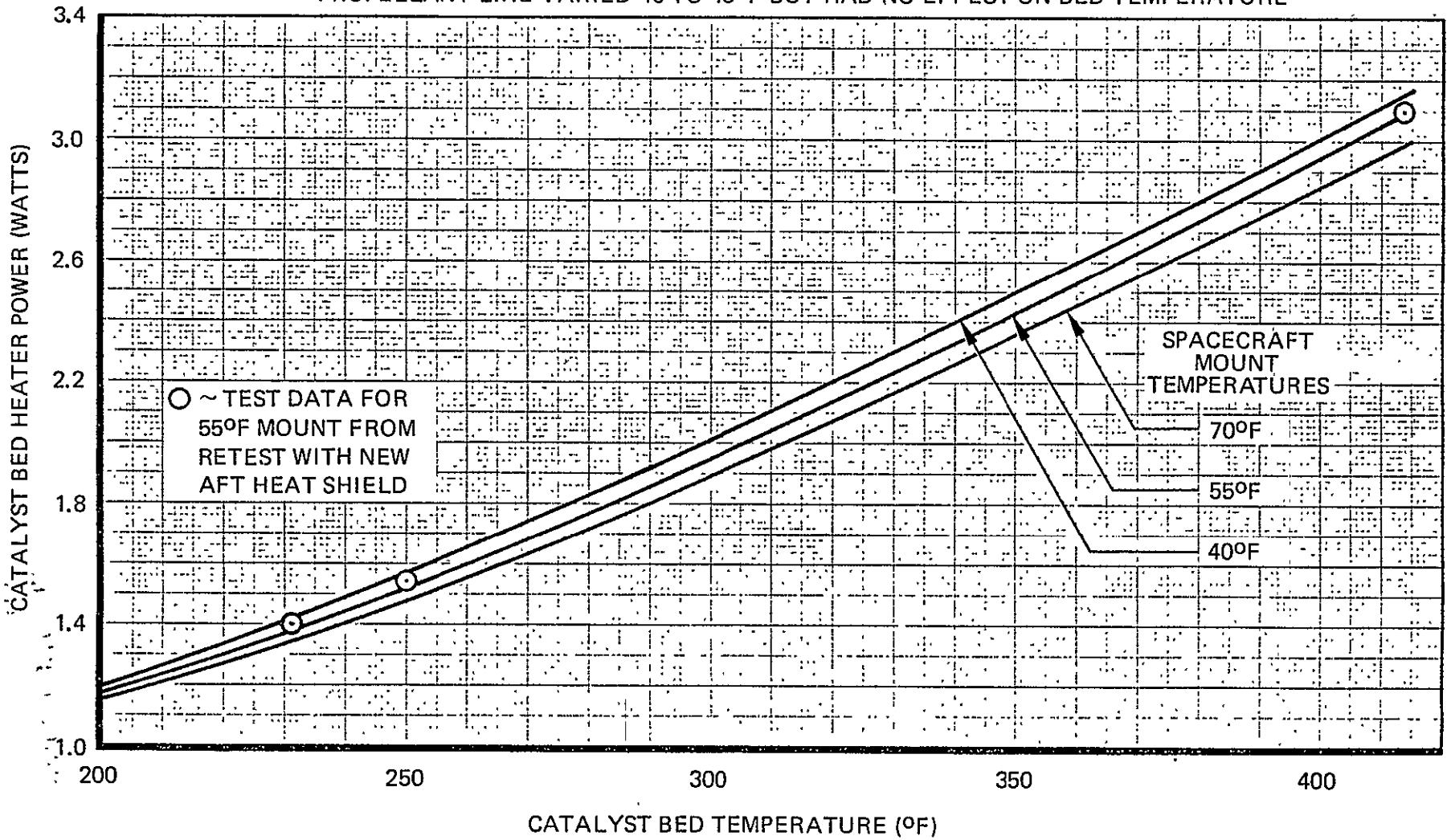

Figure 6-26

Figures 6-27 and 6-28 show limitations relative to Figure 6-26 with respect to hydrazine freezing in shrouded components. Figure 6-27 shows that no freezing will occur for minimum JPL specified spacecraft mount temperature of 46°F. Figure 6-28 shows that this mount temperature could be lowered to 40°F before incipient freezing. Furthermore, the data of Figures 6-27 and 6-28 are conservative since they are based on the thermal model unadjusted for experiment as correlated in Figure 6-23. In Figure 6-23, all predicted critical propellant line and valve temperatures are below test by as much as 5 to 7°F.

6.2.2 Thermal Model for Test Correlation

The method of test correlation consisted of putting the test boundary condition temperatures into the thermal model networks and checking resulting agreement. Furthermore, network components described in reference 74-R-448, as based on worst-case cold bias material property variations, were used. The primary worst-case cold network components were those based on minimum thermal standoff conductive resistance and maximum heat shield surface emittance (i.e., 0.05).

Justification for using the thermal model network components, based on worst-case cold orbit material property assumptions, stems from pretest shield emittance and standoff cross-sectional measurements discussed in the previous section. Also, as previously discussed, the "CONSERVATIVE" thermal model was used instead of the "REALISTIC" model.

The only difference between the "CONSERVATIVE" and the "REALISTIC" thermal model is the method of representing the radiation enclosure between the injector and the mount flange of the T/VA. Emittance assumptions for both models are the same. In the "CONSERVATIVE" thermal model, only one enclosure is considered which is a combination of the two assumed in the "REALISTIC" model. The corresponding combined enclosure and view factor conservation equations are presented in Table 6-9. Revised network components are compared in Table 6-10. Note in Table 6-10 that the new RAD No. 32 is 0.498 compared to the value of 2.95 that was previously presented.

Note in Figures 6-23, 6-24, and 6-25 that there is a rather large difference between predicted and measured temperatures at node 26, the temperature sensor. This difference is due to the thermocouple not being located exactly on the calculated node and does not represent a discrepancy in the thermal model. Better correlation could be obtained by increasing the conductive resistance of the sensor and injector attach joints; however, the net effect on thermal model predictions with and without the sensor would be about the same. Thus, no model changes in the sensor/injector area are recommended.

6.2.3 Standby Prefiring and Firing

Margin testing previously accomplished related to starting the T/VA from an unpowered standby condition, with the propellant line and the spacecraft simulated surface at respective temperatures of 40 and 50°F, failed at the start. The first test was a 10-second steady state at 70 psia feed pressure; however, flow stopped after 2 seconds firing with the valve still open.

MJS 0.2-lbf T/VA PREDICTED OPERATIONAL LIMIT WITH 1.4-WATT BED HEATER

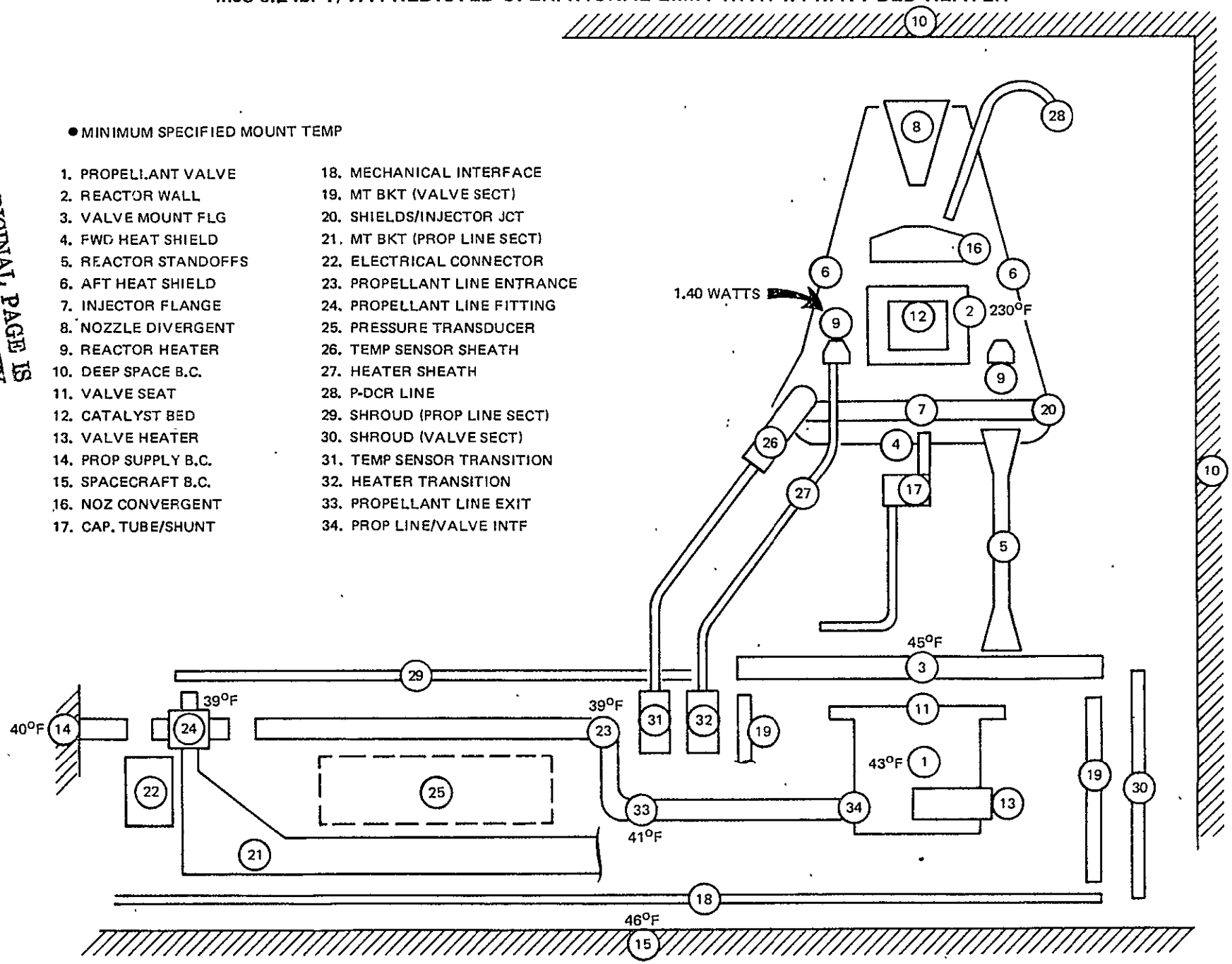

Figure 6-27

MJS 0.2-lbf T/VA PREDICTED OPERATIONAL LIMIT WITH 1.4-WATT BED HEATER

Figure 6-28

Table 6-9

REVISED RADIATION ANALYSIS OF FORWARD SHIELD INTERNAL/EXTERNAL ENCLOSURES

COMBINED ENCLOSURES

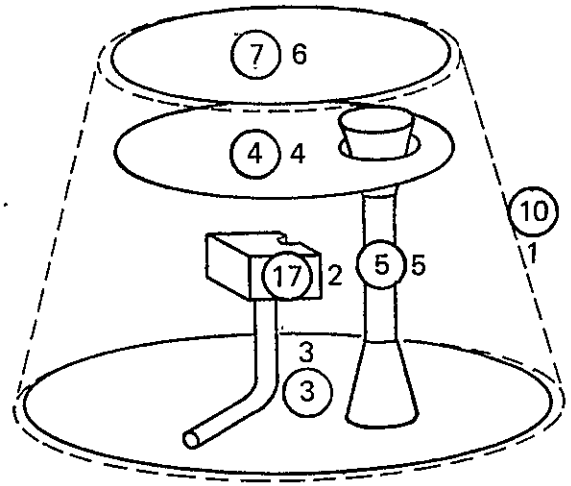

NODE NO	REFERENCE	DESCRIPTION
10	1	Space
17	2	Cap Tube/Shunt
3	3	Mt Flange
4	4	Fwd Shield
5	5	Standoffs
7	6	Injector

GEOMETRIC VIEW FACTOR CONSERVATION EQUATIONS

.243 F_{11}	.051 F_{12}	.391 F_{13}	.123 F_{14}	.186 F_{15}	.002 $F_{16}=1$
.692 F_{21}	0 F_{22}	.124 F_{23}	.083 F_{24}	.101 F_{25}	.0 $F_{26}=1$
.765 F_{31}	.018 F_{32}	0 F_{33}	.115 F_{34}	.085 F_{35}	.017 $F_{36}=1$
.297 F_{41}	.015 F_{42}	.141 F_{43}	0 F_{44}	.047 F_{45}	.500 $F_{46}=1$
.683 F_{51}	.028 F_{52}	.159 F_{53}	.071 F_{54}	.059 F_{55}	0 $F_{56}=1$
.046 F_{61}	0 F_{62}	.038 F_{63}	.916 F_{64}	0 F_{65}	0 $F_{66}=1$

Table 6-10
SUMMARY OF RADIATION TERMS CHANGED IN THERMAL MODEL

Rad No.	Values		Connection			
			Old		New	
	Old (E-4)	New (E-4)	From	To	From	To
19	6.18	5.97	3	10	Same	
20	3.41	1.81	4	7		
21	0.285	0.265	3	5		
22	0.064	0.055	4	3		
23	0.157	0.212	5	10		
24	26.6	25.4	4	10		
25	3.84	3.20	17	3		
26	0.147	0.118	4	5		
27	0.740	0.763	17	5		
28	0.156	0.106	17	4		
29	14.2	13.7	17	10		
30	6.34	6.34	26	10		
31	8.23	8.23	27	10		
32	0.498	0.498	28	10		
33	2.04	2.04	7	10		
34	5.85	16.8	7	10		
35	0.325	0.536	10	4	17	7
36	0.297	0.297	7	3	Same	
37	Not in Mod	1.70	Not in Mod		7	5

Subsequent pulse-mode firings were successful, which would lead one to believe counter to intuition that pulsed starts were more easily accomplished than steady-state firings. Thus, the 10-second steady-state firing was repeated.

Results of the previous and repeated testing are summarized in Figure 6-29. Note in Figure 6-29 that the spacecraft/T/VA propellant line simulated interface temperature was 36°F, not 40°F as it should have been. Furthermore, the propellant line temperature drops 2 to 3°F between the valve and this interface, as had been previously predicted in 74-R-448. With a 36°F interface and a corresponding 35 to 36°F freezing point of hydrazine, it is obvious that a slug of frozen hydrazine blocked the flow from the source in the first test. The 2 seconds of firing that were achieved probably resulted from 70 psia blowdown of the propellant trapped in the valve and that between the frozen blockage and the valve.

STANDBY FIRING FLOW STOPPAGE PHENOMENON

FIRST TWO STANDBY TESTS WITH DEGRADED AFT HEAT SHIELD

RESULTS

TEMPERATURES IN PARENTHESES CORRESPOND TO A REPEATED ATTEMPT 2 HOURS LATER

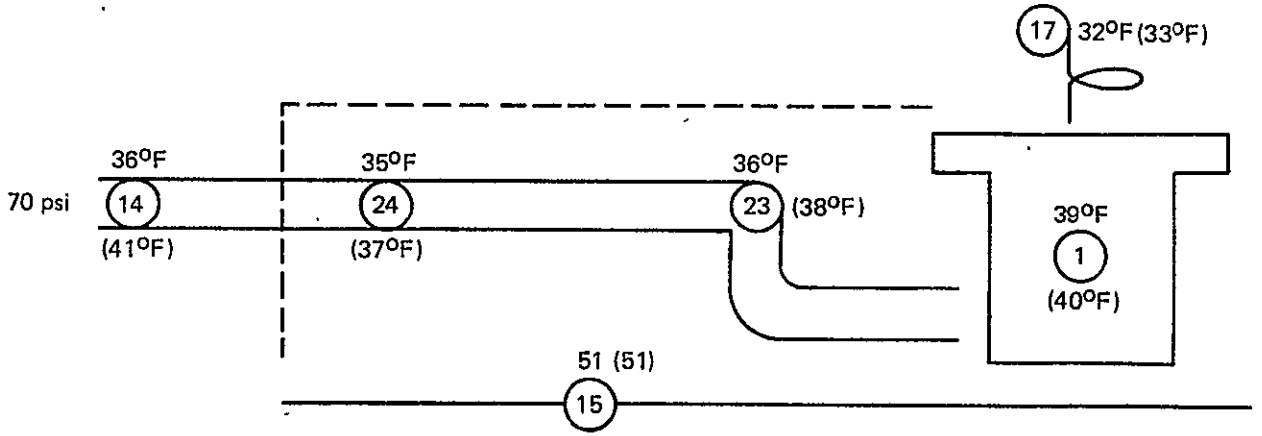

FLOW STOPPAGE AFTER 2 SEC

SECOND STANDBY TEST WITH NEW AFT HEAT SHIELD

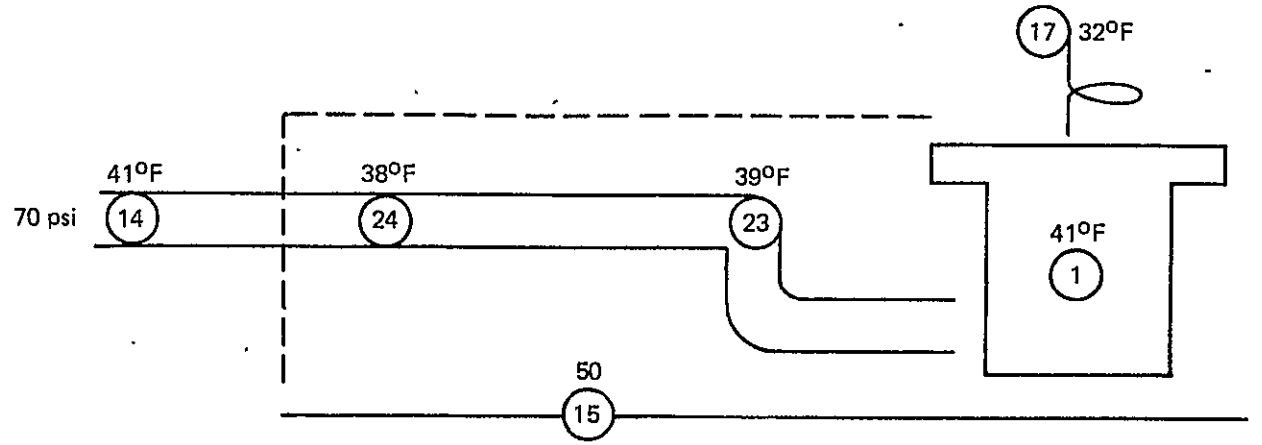

NO FLOW STOPPAGE SMOOTH 10 sec SS FIRING

Figure 6-29

Thus, a second attempt was tried 2 hours later after warming the propellant line/spacecraft interface, node 14, from 36 to 41°F. Again, only 2 seconds of a planned 10-second steady-state firing were accomplished. The corresponding critical temeprature distribution is also depicted in Figure 6-29. This last test was repeated a month later with a new aft heat shield. The 10-second steady-state firing was accomplished satisfactorily. The corresponding temperature distribution is shown in Figure 6-29.

From the test results shown in Figure 6-29, it is concluded that the hydrazine wetted components under the T/VA shroud should be maintained at or above 37°F for satisfactory standby mode starts. This limit represents an average between 36 and 38°F measured propellant line temperatures from the respective flow failure and success testing described in Figure 6-29. Using the 37°F limit, a study was made to determine the boundary condition of the spacecraft mount (node 15) and propellant line interface (node 14) required to achieve successful engine starts from the standby mode. All standby data consisting of four test cases were utilized. The two extreme cases with correlations are presented in Figure 6-30 and 6-31. The thermal model was then utilized to make flight predictions of 40 to 50°F propellant line interface temperatures and 46 to 55°F spacecraft mount temperatures.

Critical hydrazine wetted component temperature variations are presented in Figure 6-32. The data scatter bands are based upon the correlations of Figures 6-30 and 6-31. For instance, the calculated propellant valve temperature, node 1, for 55°F mount and 50°F propellant line interfaces was 49°F. However, Figures 6-30 and 6-31 show that valve temperatures, node 1, calculated by the thermal model are 3 to 6°F too optimistic. Based upon these test and analysis extremes, a variation of 43 to 46°F is plotted in Figure 6-32. Internal shroud emittance variations were found to be negligible (difference between 0.03 and 0.05 gold tape).

Figure 6-31 represents the preconditioned, standby mode, test equilibrium temperature distribution for an attempt to fire the T/VA pulsed mode. The targeted boundary conditions were 46°F mount and 40°F propellant line interfaces. However, for this condition, note that the propellant line, node 23, fell to 33°F and the valve, node 1, to 34°F, both below 35 to 36°F hydrazine freezing range. Since both values were well below previous test conditions where start attempts failed (see Figure 6-29), no attempt was made to fire the engine. Instead, boundary conditions were adjusted up to the values in Figure 6-29. The three limit cycle pulses were successfully completed with no sign of propellant freezing.

These pulses were of 10-millisecond duration. Off time between pulses was determined by letting T/VA component temperatures decrease back to equilibrium values prior to the 10-millisecond pulse. Additionally, the T/VA successfully completed the 10-millisecond on and 1.0-second off duty cycle starting in the standby mode without propellant freezing. The reaction wall was warmed to 350°F within 146 pulses and reached an equilibrium temperature of 1,270°F. Table 6-11 lists interface boundary and shrouded component temperatures prior to each pulse. The data of Figure 6-32 apply for steady-state as well as pulsed firings.

MJS 0.2-lbf T/VA DEVELOPMENT TEST RESULTS
STANDBY TEST WITH NEW AFT HEAT SHIELD

*ANALYTICAL VALUES IN PARENTHESES

1. PROPELLANT VALVE
2. REACTOR WALL
3. VALVE MOUNT FLG
4. FWD HEAT SHIELD
5. REACTOR STANDOFFS
6. AFT HEAT SHIELD
7. INJECTOR FLANGE
8. NOZZLE DIVERGENT
9. REACTOR HEATER
10. DEEP SPACE B.C.
11. VALVE SEAT
12. CATALYST BED
13. VALVE HEATER
14. PROP SUPPLY B.C.
15. SPACECRAFT B.C.
16. NOZ CONVERGENT
17. CAP. TUBE/SHUNT
18. MECHANICAL INTERFACE
19. MT BKT (VALVE SECT)
20. SHIELDS/INJECTOR JCT
21. MT BKT (PROP LINE SECT)
22. ELECTRICAL CONNECTOR
23. PROPELLANT LINE ENTRANCE
24. PROPELLANT LINE FITTING
25. PRESSURE TRANSDUCER
26. TEMP SENSOR SHEATH
27. HEATER SHEATH
28. P-DCR LINE
29. SHROUD (PROP LINE SECT)
30. SHROUD (VALVE SECT)
31. TEMP SENSOR TRANSITION
32. HEATER TRANSITION
33. PROPELLANT LINE EXIT
34. PROP LINE/VALVE INTF

STANDBY
PRIOR TO FIRING

MJS 0.2-lbf T/VA DEVELOPMENT TEST RESULTS
STANDBY TEST WITH 46°F MOUNT

*ANALYTICAL VALUES IN PARENTHESES

1. PROPELLANT VALVE
2. REACTOR WALL
3. VALVE MOUNT FLG
4. FWD HEAT SHIELD
5. REACTOR STANDOFFS
6. AFT HEAT SHIELD
7. INJECTOR FLANGE
8. NOZZLE DIVERGENT
9. REACTOR HEATER
10. DEEP SPACE B.C.
11. VALVE SEAT
12. CATALYST BED
13. VALVE HEATER
14. PROP SUPPLY B.C.
15. SPACECRAFT B.C.
16. NOZ CONVERGENT
17. CAP. TUBE/SHUNT
18. MECHANICAL INTERFACE
19. MT BKT (VALVE SECT)
20. SHIELDS/INJECTOR JCT
21. MT BKT (PROP LINE SECT)
22. ELECTRICAL CONNECTOR
23. PROPELLANT LINE ENTRANCE
24. PROPELLANT LINE FITTING
25. PRESSURE TRANSDUCER
26. TEMP SENSOR SHEATH
27. HEATER SHEATH
28. P-DCR LINE
29. SHROUD (PROP LINE SECT)
30. SHROUD (VALVE SECT)
31. TEMP SENSOR TRANSITION
32. HEATER TRANSITION
33. PROPELLANT LINE EXIT
34. PROP LINE/VALVE INTF

STANDBY
PRIOR TO FIRING

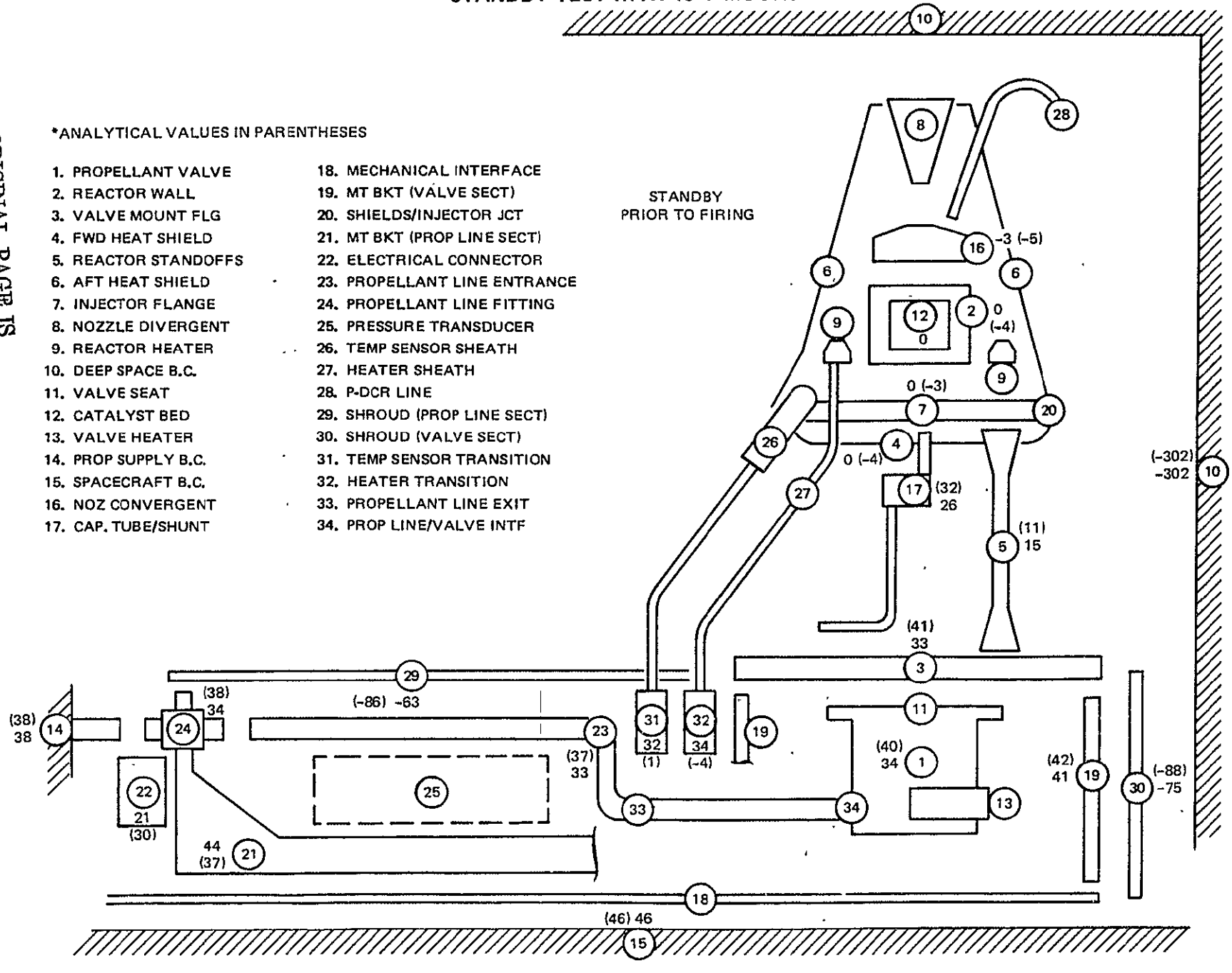

Figure 6-31

STANDBY MODE FINAL FLIGHT PREDICTIONS
MJS 0.2-lbf T/VA SHROUDED COMPONENT
TEMPERATURE CHARACTERISTICS

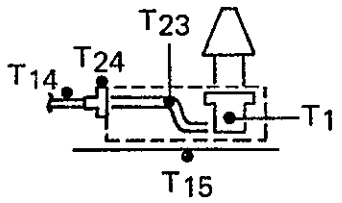

- RESULTS BASED ON THERMAL MODEL ADJUSTED FOR DEVELOPMENT TEST DATA

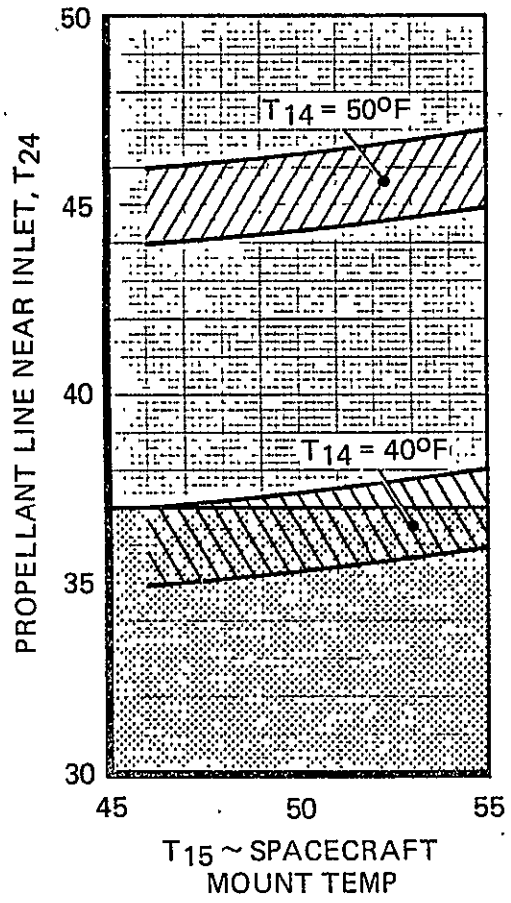

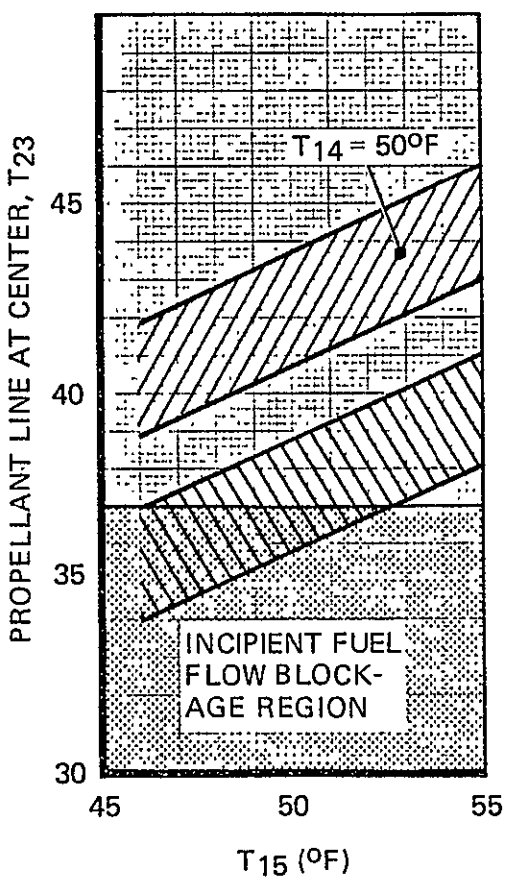

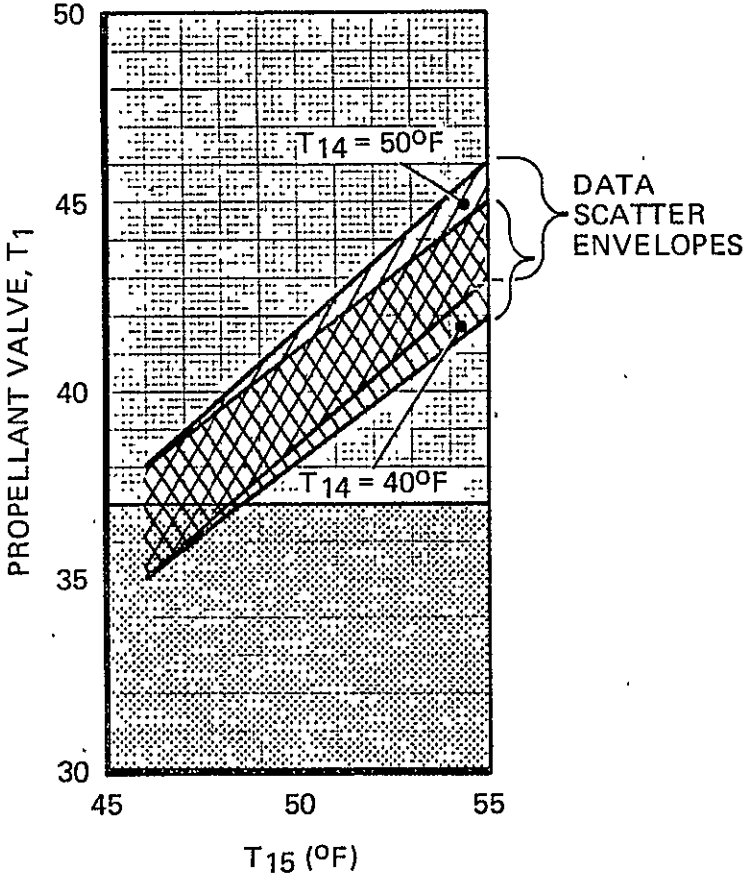

Figure 6-32

Table 6-11
INTERFACE BOUNDARY AND SHROUDED
COMPONENT TEMPERATURES
PRIOR TO PULSED FIRINGS

Pulse No.	T_{14} (°F)	T_{15} (°F)	T_1 (°F)	T_{23} (°F)	T_{24} (°F)
1	40	52	40	37	38
2	40	52	40	37	38
3	40	52	41	38	38

6.2.4 Degradation of Gold Plating on T/VA Heat Shields

It was originally reported in reference 74-R-448 that gold plating deterioration, namely emittance increases to 0.07, were probably due to handling problems. Subsequent testing summarized in Table 6-12 shows the above to be only parially the case. Tests on clean gold plated samples at 800 and 1,100°F at ambient pressure levels, similar to those in RRC vacuum tank test cells with diffusion pumps off, showed significant emittance degradation.

Table 6-12 shows emittance degradations as high as 0.03 to 0.14. Such values were determined from measurements made with a device still under development; however, results from this device compare well with results obtained from the well-known Gier Dunkel D8-100. Such comparisons are also listed in Table 6-12.

The gold shield emittance degradations mentioned above are ambient pressure phenomenon and will not occur to an unsatisfactory degree in space. This was found in tests at 1,100°F on similar gold plated samples in a vacuum greater than 10^{-4} to 10^{-5} torr, the usual range between continuum and free molecular or hard vacuum where ambient effects should be minimum. As shown in Table 6-12, no change could be detected with the RRC emissometer, and the change detected by the Gier Dunkle reflectometer was within the accuracy of the instrument. The change that was measured, 0.04 to 0.05, does not exceed the cold bias material property assumption to 0.05 in the thermal model.

6.3 C_f MAPPING TEST RESULTS

As a part of the LCSSE/MJS TVA development program, C_f mapping tests were conducted for both steady-state and pulse-mode operation. The RRC microthrust pendulum balance was employed for the measurement of thrust and impulse bit. This section presents the results of this testing, and for a complete description of the test setup and the balance fundamentals, the reader is referred to Sections 4.0 and 5.0, respectively.

The primary goal of steady-state and C_f mapping tests was to map the equilibrium C_f for the T/VA operational feed pressures of 420 to 70 psia. This was successfully accomplished by completion of

Table 6-12
SUMMARY OF TESTS TO STUDY
HEAT DEGRADATION OF GOLD PLATE

Gold Plated Couponno	24 Hours at Temperature	In Vacuum Of	Emittance Before (1)	Emmittance After (1)
SPL 1	800°F	$>10^{-2}$ torr	0.03	0.07
Skipped	950°F	Skipped	Skipped	
SPL 6	1,100°F	$<10^{-2}$ torr	0.04	0.14
SPL 2	1,100°F	$>10^{-6}$ torr	0.04	NC
SPL 2	Tested by Lockheed Research Labs Gier Dunkle DB-100, compared with DB-HC-300		0.04	0.05

(1) Measured by RRC Emissometer which is similar in principle to Gier Dunkle DB-100 Reflectometer accuracy ±0.01

the preplanned test sequences consisting of five 300-second steady-state tests at each of the following feed pressures: 420, 350, 150, and 70 psia. The results of the tests are shown in Figure 6-33, which is a correlation of the vacuum thrust coefficient as a function of chamber pressure. The data was subjected to the RRC least-squares curve fit computer program, and the resultant correlation between C_f and P_c is shown as a solid line and given by the equation in Figure 6-33. The value of chi-squared, which is equal to 0.0011, is a measure of the correlation between the curve fit and each of the individual data points and is considered to be very good. The chi-squared value of 0 corresponds to an exact fit between the data and the equation or curve drawn through the data. This equation for C_f as a function of P_c was used to reduce steady-state thrust data from the performance mapping, steady-state life margin, and momentum wheel desaturation tests. Figure 6-34 presents a correlation between chamber wall, nozzle throat, injector, and temperature sensor temperature measurements as a function of feed pressure. The correlations of nozzle throat and injector temperatures turned out to be the best available through the entire development test program, as these thermocouples detached later on in the testing sequences during performance mapping.

During the steady-state mapping tests the feed pressure transducer failed. The transducer mounted on the gas side of the propellant tank (PH) was substituted; refer to Section 4.0 for a schematic of the setup.

The T/VA roughness level during the steady-state tests exceeded the specification of 30 percent peak-to-peak. This presented a problem in reading the strip chart, as the frequency of the engine

0.2-lbf LCSSE T/VA STEADY-STATE PERFORMANCE
VACUUM THRUST COEFFICIENT
AS A FUNCTION OF CHAMBER PRESSURE

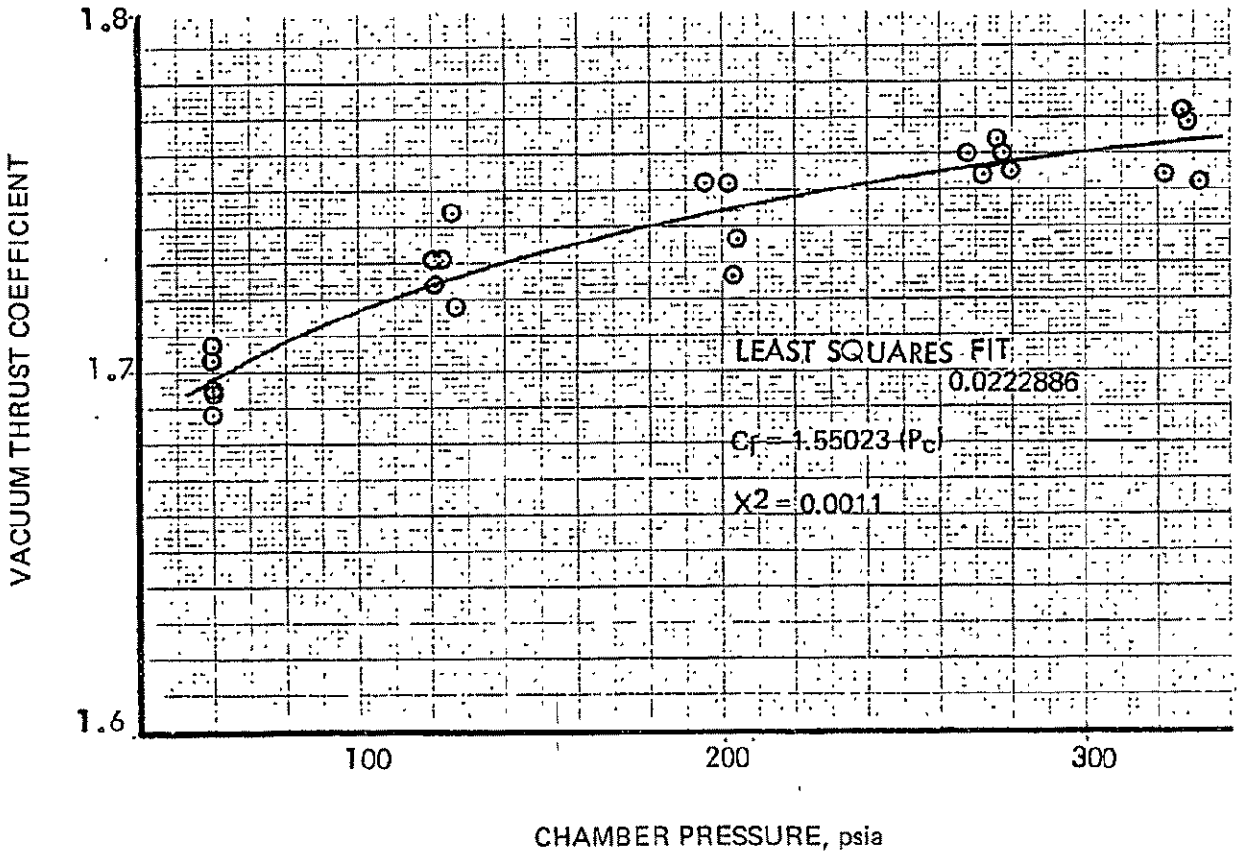

Figure 6-33

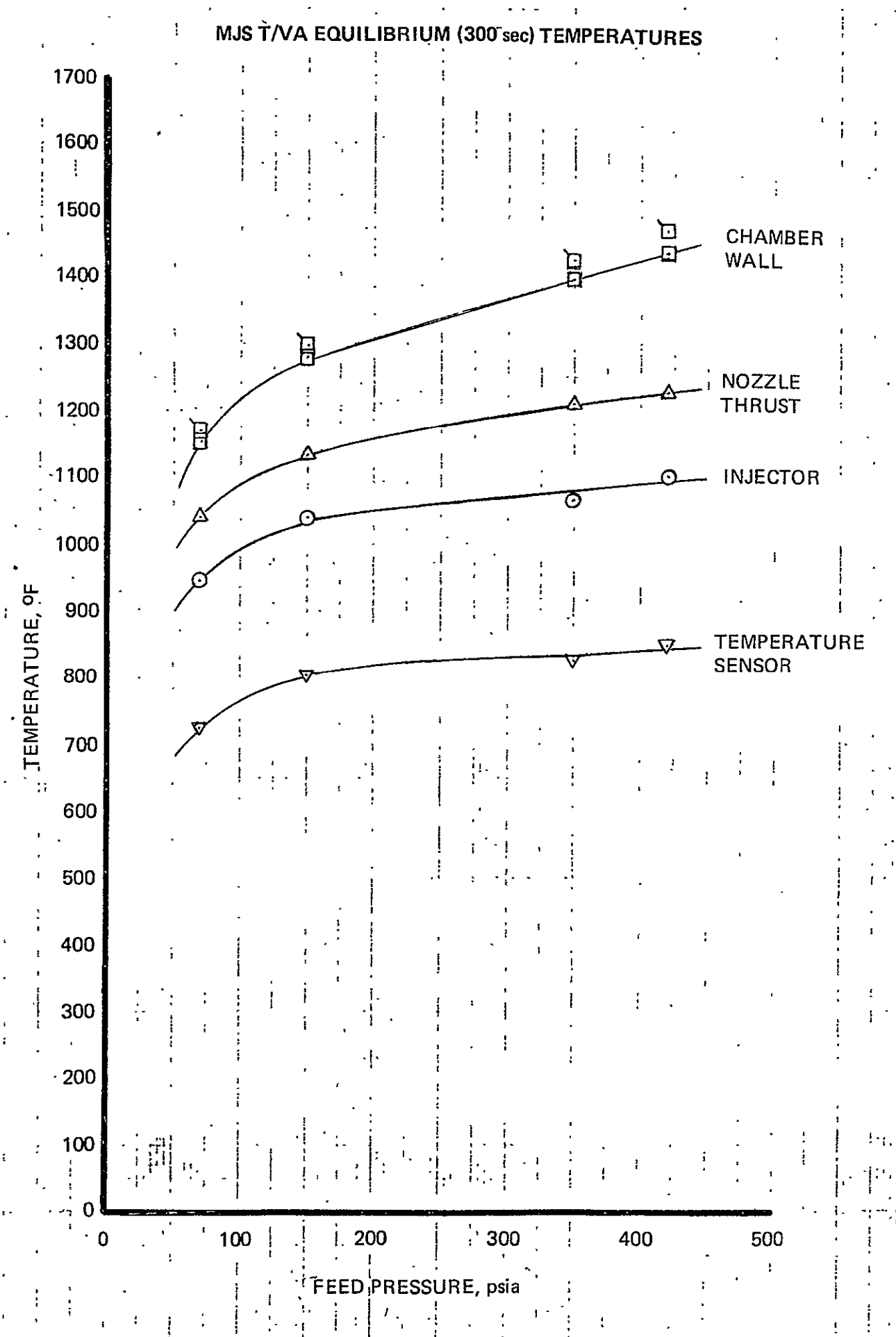
MJS T/VA EQUILIBRIUM (300 sec) TEMPERATURES
1700
1600
1500
1400
1300
1200
1100
1000
900
800
700
600
500
400
300
200
100
0
TEMPERATURE, °F
CHAMBER WALL
NOZZLE THRUST
INJECTOR
TEMPERATURE SENSOR
0
100
200
300
400
500
FEED PRESSURE, psia

Figure 6-34

roughness was faster than the response of the strip chart. The data reduction problem was solved by calculating the average chamber pressure using a planimeter off of oscillograph data. The method was repeatable and the C_f results indicate good correlation with JPL test data.

Pulse-mode C_f mapping tests were also completed in order to completely characterize the pulse-mode C_f for all duty cycles, feed pressures, and pulse widths. Additional goals were to perform a multiple correlation of all possible data, measure impulse bits with pulse widths of 8 milliseconds, and determine if differences exist between purified and Amendment I hydrazine. In order to achieve these goals the test sequences shown in Table 6-13 were constructed. The X's denote which tests were completed, and an X, which has been circled, indicates that the test was repeated using purified hydrazine. Those columns which do not have X's in them were not tested. Notice that no specific duty cycle was tested. Instead, pulses were fired at different reactor chamber wall temperatures. This was done in order to obtain a map which would completely characterize all pulse-mode duty cycles. The procedure used to conduct pulse-mode tests at the variable wall temperature conditions was to fire a short duration steady-state test which would heat the reactor up to its hottest temperature, then to stabilize the microthrust balance and fire pulses at the specific pulse widths as the reactor cooled down. The original test plan included temperatures of 1,200 and 1,400°F. These temperatures could not be tested as the thrust balance could not be stabilized after the steady-state warmup, within a time period which allowed testing at these higher temperatures. This was also the reason that the maximum temperature tested at the smaller pulse widths was limited to 800°F.

- Measurements of impulse bits at the smaller pulse widths was successfully completed. A multiple correlation of the C_f data was conducted with the following parameters: feed pressure, injector temperature, chamber wall temperature, peak chamber pressure, flight temperature sensor, throat temperature, integral of chamber pressure, impulse bit, and pulse width. Results of this correlation indicated that the best fit was obtained with both chamber pressure integral and chamber wall temperature. Figure 6-35 presents a plot of this correlation. The data has been plotted as a function of pressure integral at each chamber temperature and is presented in Figures 6-36 through 6-40. It is apparent from the correlations presented that rather high C_f values were measured at the lower impulse bits. This trend is also consistent with previous programs, such as the ATS 0.1-lbf thruster. It is generally felt that this is caused by a decrease in ammonia dissociation at the lower pulse widths and lower temperatures due to the fact that a smaller amount of heat is available to dissociate the ammonia. However, the maximum C_f value that can be expected, assuming 0 percent ammonia dissociation for a 100 to 1 expansion ratio (T/VA nozzle design), is equal to 2.03. C_f values greater than this were measured as indicated in the corresponding figures. A possible explanation for this is that the available low pressure chamber pressure integral during the tailoff portions of the pulse could not be accurately measured. This would result in a lower than actual chamber pressure integral and a higher than actual C_f calculation. However, since the method for calculating pressure integral will be the same, the high C_f values will then give us the true value of impulse bit for future tests where impulse bit is not measured.

Table 6-13
PULSE MODE C_f MAPPING
TEST SEQUENCES

PULSE WIDTH	FEED PRESSURE, psia				CHAMBER WALL TEMPERATURE, °F				
	420	350	150	70	250	400	600	800	1000
0.008	X	(X)	(X)		(X)	(X)	(X)	(X)	
0.020	X	(X)	(X)	X	(X)	(X)	(X)	(X)*	
0.040	X	(X)	(X)	(X)	(X)	(X)	(X)	(X)	
0.060		X	X		X	X	X	X	
0.100		X	X		X	X	X	X	X
0.200	X	X	X	X	X	X	X	X	X
0.500			X		X	X	X	X	X

* Could not obtain data at the feed pressure of 70 psia

(X) Circled X indicates repeating tests with purified fuel

NOTE: Original test plan included temperatures of 1200°F and 1400°F. These temperatures could not be tested as the thrust balance could not be stabilized in time.

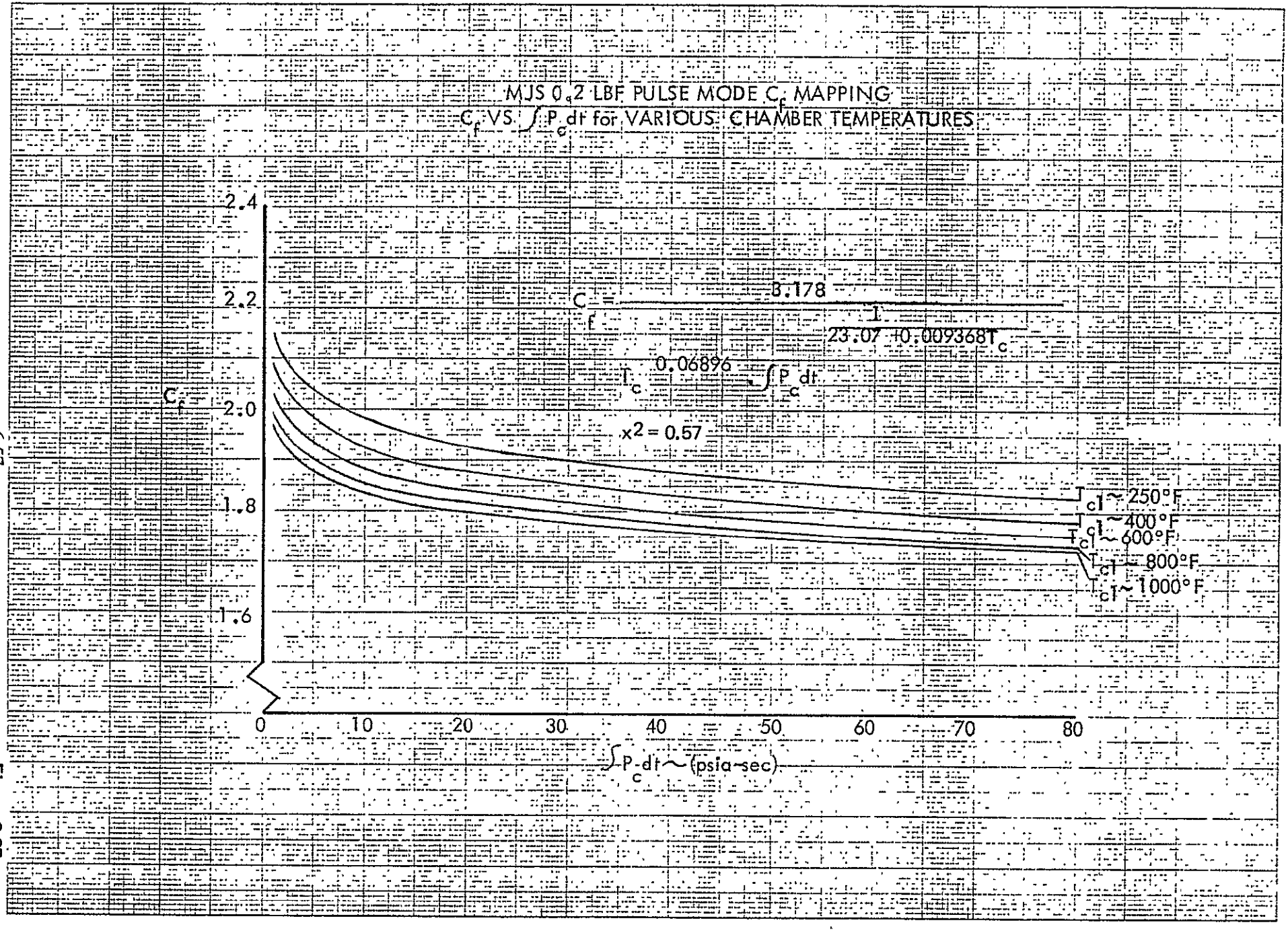

6-57

Figure 6-35

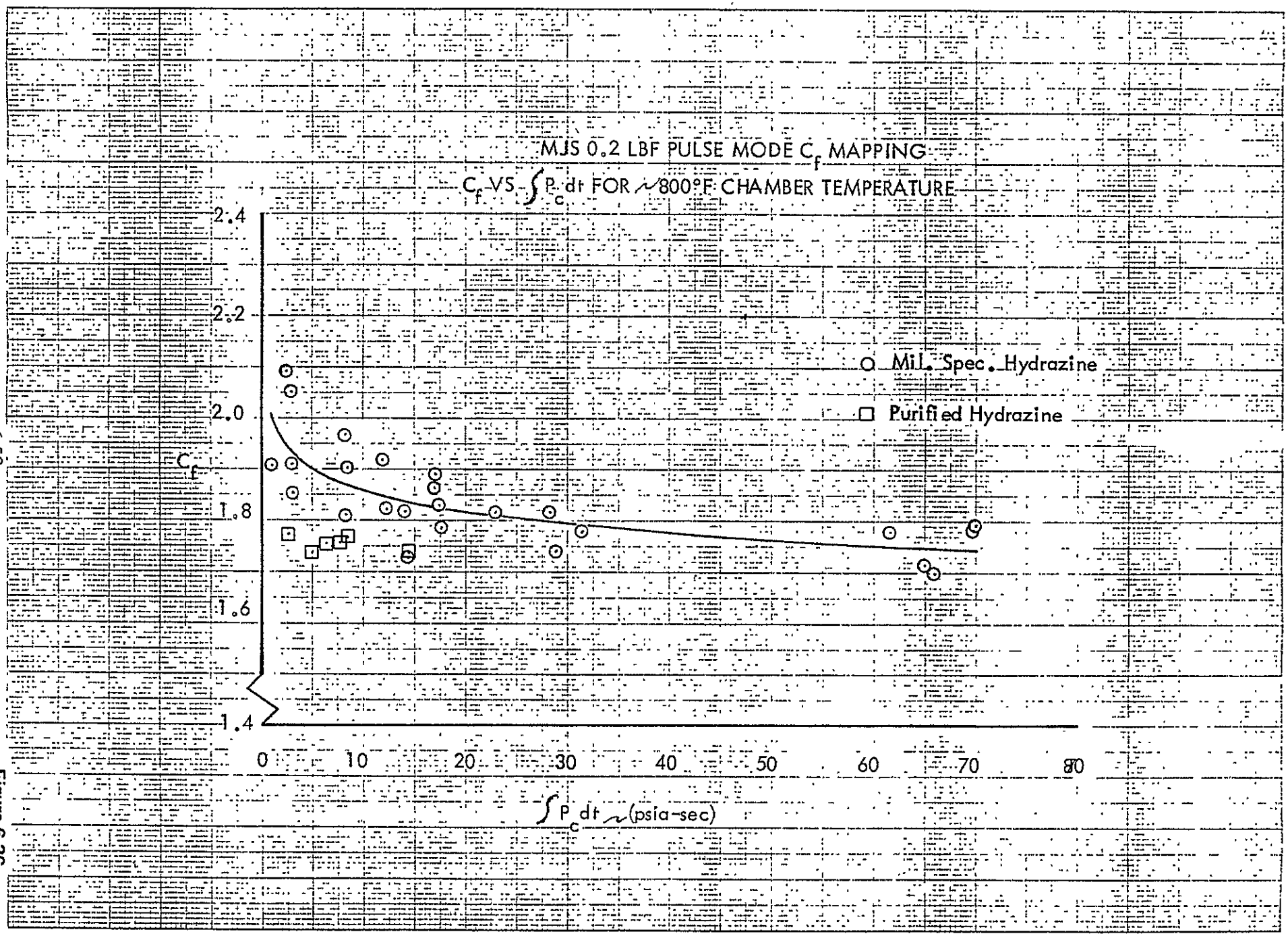
MJS 0.2 LBF PULSE MODE C_f MAPPING
C_f VS $\int P_c\,dt$ FOR ~800°F CHAMBER TEMPERATURE
2.4
2.2
2.0
1.8
1.6
1.4
C_f
MIL. Spec. Hydrazine
Purified Hydrazine
0
10
20
30
40
50
60
70
80
$\int P_c\,dt$ ~(psia-sec)

Figure 6-36

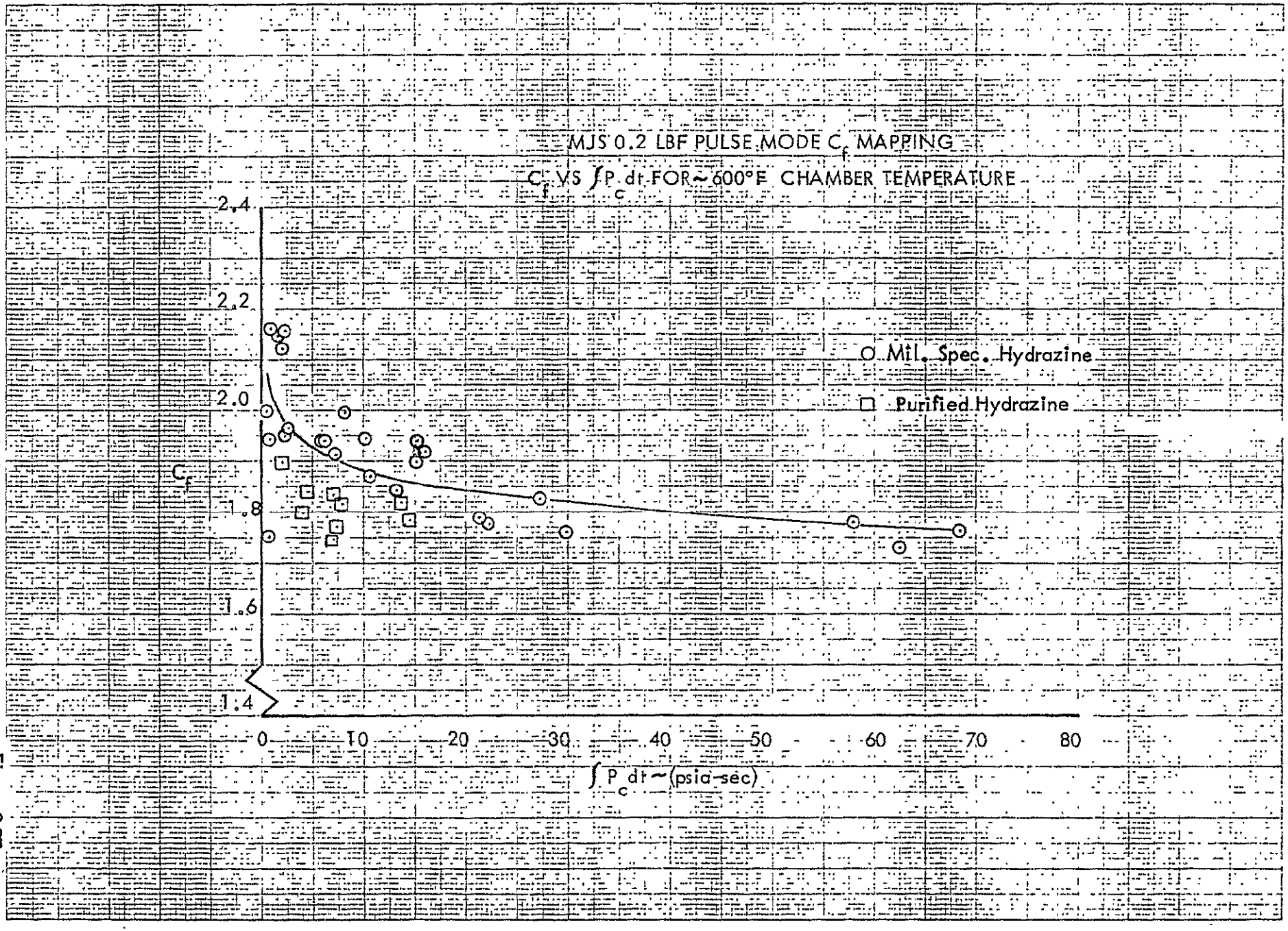
MJS 0.2 LBF PULSE MODE C_f MAPPING
C_f VS $\int P_c\,dt$ FOR ~600°F CHAMBER TEMPERATURE
O Mil. Spec. Hydrazine
□ Purified Hydrazine
C_f
2.4
2.2
2.0
1.8
1.6
1.4
0
10
20
30
40
50
60
70
80
$\int P_c\,dt$ ~ (psia-sec)

Figure 6-37

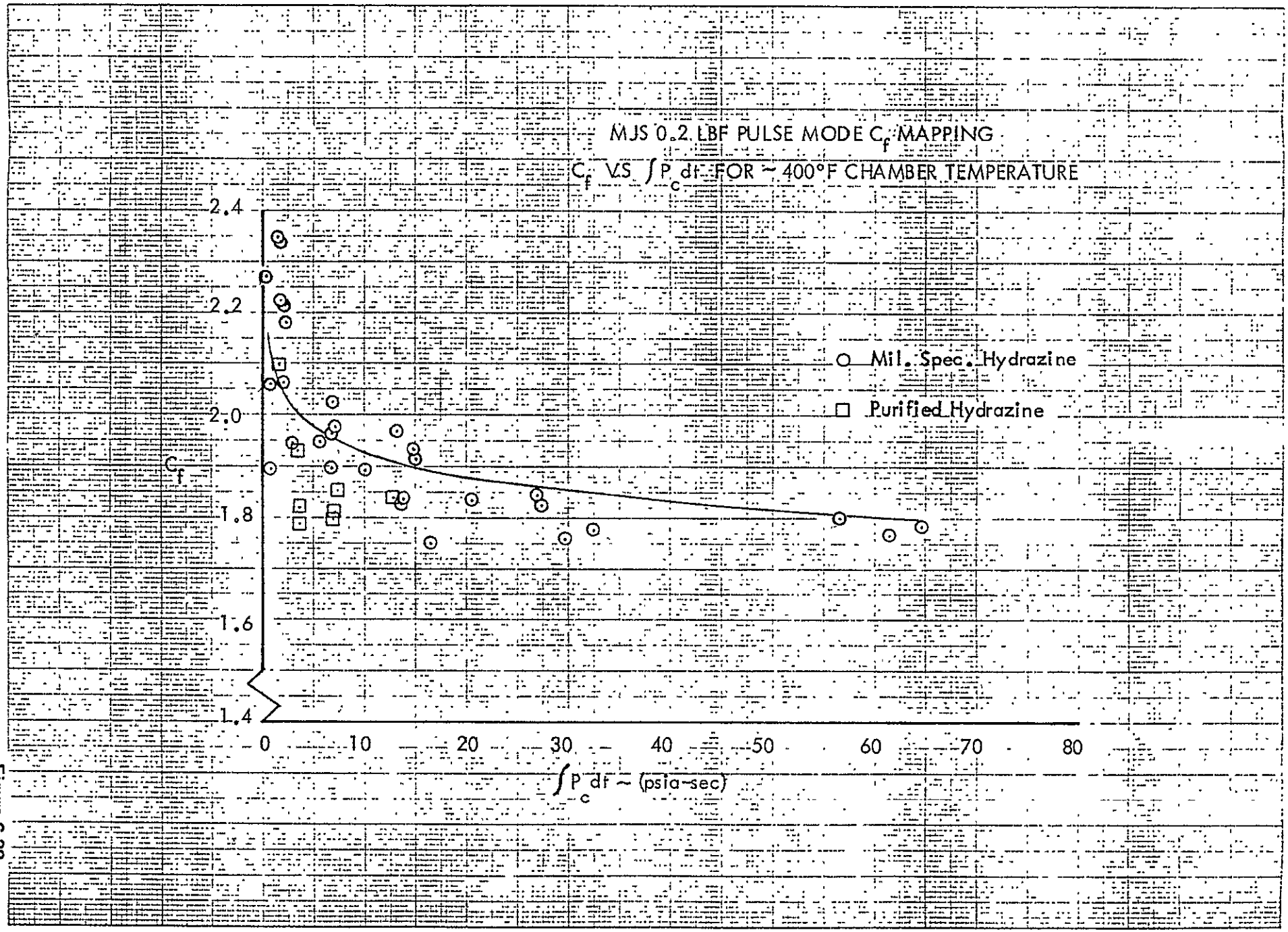
MJS 0.2 LBF PULSE MODE C_f MAPPING
C_f VS $\int P_c\,dt$ FOR ~ 400°F CHAMBER TEMPERATURE
Mil. Spec. Hydrazine
Purified Hydrazine
C_f
2.4
2.2
2.0
1.8
1.6
1.4
0
10
20
30
40
50
60
70
80
$\int P_c\,dt$ ~ (psia-sec)

Figure 6-38

MJS 0.2 LBF PULSE MODE C_f MAPPING
C_f VS $\int P_c\,dt$ FOR ~ 250°F CHAMBER TEMPERATURE
○ Mil. Spec. Hydrazine
□ Purified Hydrazine
C_f
2.4
2.2
2.0
1.8
1.6
1.4
0
10
20
30
40
50
60
70
80
$\int P_c\,dt$ ~ (psia-sec)

Figure 6-39

MJS 0.2 LBF PULSE MODE C_f MAPPING
C_f VS $\int P_c\,dt$ for ≈ 1000°F CHAMBER TEMPERATURES
2.4
2.2
2.0
C_f
1.8
1.6
1.4
0
10
20
30
40
50
60
70
80
$\int P_c\,dt$ ≈ (psia-sec)

Figure 6-40

In Figures 6-36 through 6-40, there is a noticeable trend toward lower C_f values using purified hydrazine. A review of the data indicated no consistent trends toward either lower impulse bits or higher pressure integrals existed. Comparing both propellants on a pulse-to-pulse basis, reasonably close impulse bits and chamber pressure integrals were obtained. Therefore it is assumed that this lower bias is attributed to data scatter.

Additional C_f correlations were obtained and studied during the multiple correlation analysis. These correlations are presented below along with the index of determination. The index of determination is a statistical measurement similar to the chi-squared value and is based upon the calculated and measured values in reference to their respective average values. An index of determination equal to 1 represents a perfect fit.

	Index of Determination
C_f VS FEED PRESSURE (P_h) $C_f = 1.905 + \frac{2.316}{P_h}$	0.003
C_f VS INJECTOR TEMPERATURE (T_i) $C_f = T_i / (-12.5 + 0.5563\ T_{inj})$	0.115
C_f VS CHAMBER WALL TEMPERATURE (T_c) $C_f = T_c / (-14.59 + 0.5570\ T_c)$	0.157
C_f VS PEAK CHAMBER PRESSURE (P_{cf}) $C_f = 2.316\ P_{cf}^{-0.04346}$	0.351
C_f VS FLIGHT TEMPERATURE SENSOR (R_t) $C_f = 1.0/(0.4784 + 0.0001134\ R_t)$	0.166
C_f VS THROAT TEMPERATURE (T_t) $C_f = 1.0/(0.4836 + 0.00007295\ T_t)$	0.230
C_f VS CHAMBER PRESSURE INTEGRAL ($\int Pcdt$) $C_f = 2.122\left[\int Pcdt\right]^{-0.045}$	0.555
C_f VS IMPULSE BIT ($\int Fdt$) $C_f = 1.548\left[\int Fdt\right]^{-0.04391}$	0.478

	Index of Determination
C_f VS PULSE WIDTH (P.W.)	
$C_f = 2.248\ (P.W.)^{-0.03986}$	0.458
C_f VS PEAK P_C (P_{Cf}) and PULSE WIDTH (P.W.)	0.447
$C_f = 2.2335\ (P_C)^{0.001745}\ (P.W.)^{-0.04015}$	

The equations with generally larger index of determinations may be used to estimate the value of C_f in cases where either chamber wall temperature or the chamber pressure integral are not available. For example, if peak chamber pressure only can be derived from the reduced data or data transmitted back from the spacecraft, the value of C_f can be calculated, and if the reactor wall temperature can be estimated, the value for the chamber pressure integral can be derived using the primary C_f correlations shown in Figure 6-35. This then allows calculation of impulse bit.

6.4 PERFORMANCE MAPPING

An extensive performance mapping test was conducted during the LCSSE/MJS development test program using T/VA D01. The goals of the program were as follows:

1. Expand the performance map generated during the preproposal test program to include the effects of propellant temperature, valve voltage, and flight pressure transducer volume.
2. Map pulse widths of 0.008 seconds to steady state with inlet pressures of 70 to 40 psia, propellant temperatures of 40 to 140°F, and valve voltages of 24 to 34 vdc.
3. Provide both transient and equilibrium performance data for steady-state and pulse-mode operation.
4. Incorporate the results into the LCSSE/MJS performance model.

In order to achieve these goals, the duty cycle shown in Table 6-14 was composed. As shown, the entire feed pressure, propellant temperature, and pulse width ranges were tested. The valve voltage changes were tested only at the pulse width of 0.008 and 0.04 second at a constant propellant temperature of 70°F.

All of the test duty cycles, feed pressures, and propellant temperatures were completed as a part of this development test program. The total pulses accumulated for the performance mapping tests equaled 323,007 pulses. The data was recorded and reduced using the digital acquisition system. Approximately 4,000 pulses were reduced and the results correlated to provide the necesssary data to completely characterize the performance of the T/VA for the computer performance model:

Table 6-14
PERFORMANCE MAPPING TEST MATRIX

Test Sequence	Propellant Temp. °F	Feed Pressure psia	Duty Cycle Code
1–23	40	420	A
24–46	40	350	A
47–69	40	150	A
70–92	40	70	A
93–111	70	420	B
112–134	70	350	C
135–157	70	150	C
158–176	70	70	B
177–199	140	420	A
200–222	140	350	A
223–245	140	150	A
246–268	140	70	A

DUTY CYCLE A (VALVE VOLTAGE = 28 v)

Pulse Width (sec)	Duty Cycle %				
	Limit 350°F	1	5	15	100
0.008	X	X	X	X	
0.020	X*	X*	X*	X*	
0.040	X	X	X	X	
0.100		X	X	X	
0.500		X	X	X	
1.00					X
3.00					X
10.00					X
30.00					X
300.00					X

*These tests deleted for Duty Cycle B

DUTY CYCLE C

Pulse Width (sec)	Valve Voltage (volts)	Duty Cycle %				
		Limit 350°F	1	5	15	100
0.008	24	X				
	28	X	X	X	X	
	32	X				
0.040	24	X				
	28	X	X	X	X	
	32	X				
0.100	28		X	X	X	
0.500	28		X	X	X	
1.00	28					X
3.00	28					X
10.00	28					X
30.00	28					X
300.00	28					X

Several problems did occur during the test program. Initially, a test setup problem with the valve suppression circuit was identified during sequence 1 and corrected. The first test setup resulted in a 1 volt clipping at the valve close signal, and therefore the actual seat closure was 10 to 20 milliseconds longer than desired. Fortunately this occurred during the first sequence when the duty cycle called for a 0.008-second pulse, and the additional valve open time of 10 to 20 milliseconds was very apparent. After the test setup problem was fixed, sequence 1 was repeated, and the first firing was deleted from the data analysis.

At the lowest tested feed pressure equal to 70 psia and a propellant temperature of 40°F, the T/V-A failed to produce chamber pressure at limit cycle operation. The problem corrected itself by changing to the 1 percent duty cycle. This problem did not exist at the 70°F temperature. This failure is directly attributed to the aniline in the Amendment I hydrazine used for this test program. This problem was identified early in the LCSSE/MJS contract with a third development thruster which was initiated prior to contract go-ahead and is used completely for limit cycle operation. The corrective action is to use purified hydrazine where the aniline content is required to be less than 80 ppm.

During pulse mode, performance mapping at a feed pressure of 420 psia, a propellant temperature of 70°F, and a pulse width of 40 milliseconds and greater, a decay in peak chamber pressure was observed. The following additional observations were made:

1. The valve temperature was above 110°F.
2. The problem did not occur at lower feed pressures.
3. The valve current signature changed during the anomaly.
4. At a pulse width of 500 milliseconds, feed pressures of 420 psi and a duty cycle of 15 percent, no P_C or propellant flow rate was recorded.
5. The propellant valve was cooled to less than 100°F, and all tests with pulse widths of 40 milliseconds or greater were repeated successfully.

With the above observations made, the TCV seat expansion became the primary suspect for the problem. This problem had been identified previously in a development test program at the TCV vendor, Moog, Incorporated. Moog identified the problem as a flaw in the TCV seat design. The problem was corrected by changing the seat design to incorporate vent holes on the backside of the seat and additional area for thermal expansion of the seat material, AF411. Two other potential failure modes were considered: blockage due to propellant boiling in the cap tube and permanent blockage from contamination. Blockage due to propellant boiling in the cap tube was eliminated because the problem stopped at lower feed pressures. A boiling problem occurs first at low feed pressures where the velocity in the capillary tube is low and the associated heat transfer rate is high. Permanent blockage from contamination was also eliminated, and a successful steady-state operation was obtained.

A conflict with the JPL specification ES 509778 was identified with small pulse width specific impulse. The specification requires the pulse-mode specific impulse to be greater than or equal to 100 lbf-sec/lbm. Values as low as 50 lbf-sec/lbm were recorded at the 0.008-second pulse widths. It

is felt that the primary cause of this is insufficient measurement of the tailoff impulse. This hypothesis is in agreement with tests conducted at JPL which indicates substantial impulse in the tailoff portion from 600 milliseconds to 6 seconds after the pulse termination. JPL test data indicates that approximately double the impulse is available if the tailoff impulse is considered. The results would therefore double the I_{sp} measurement. In order to generate additional data to update the performance model, RRC will incorporate a low range pressure transducer during the qualification tests.

The following test sequences were not retrieved on the digital acquisition system: 31, 37, 52 to 57, 98, 99, 101 to 104, 105, and 160. This data was deleted as it was not needed to generate the performance model.

The results of the steady-state mapping are presented in Figures 6-41 through 6-43 and Table 6-15. Figure 6-41 shows that all of the thrust measurements for the variety of propellant temperatures measured were within the required ±5 percent range at 350 psia inlet pressure and ±7 percent range at the 150-psia inlet pressure. Figure 6-42 presents the steady-state equilibrium specific impulse data. Also shown is the performance model output at the three different propellant temperatures. The steady-state equilibrium roughness values are presented in Table 6-15. Values greater than the requirements of JPL specification ES 509778 were measured. The specification allows 30 percent peak-to-peak which is equal to ±15 percent. Rocket Research Corporation has alerted JPL of this problem during the performance presentation at the critical design review. Rocket Research Corporation recommends increasing this tolerance to ±50 percent. Figure 6-43 presents the steady-state response data measured during performance mapping and shows the correlations with the performance model. The pulse-mode performance results are presented in Figures 6-44 through 6-68. Correlations with the performance model are presented for propellant temperatures of 70°F. Figure 6-68 presents a plot of normalized impulse bit as a function of valve voltage. It is apparent that there is a large effect in impulse bit at the small pulse widths and low feed pressures, and as the feed pressure and pulse width is increased, the effect becomes smaller. Normalized impulse bit was derived by dividing the actual impulse measured by the square-wave impulse based on steady-state thrust levels. Presented in Figures 6-69 through 6-76 are typical pulse shapes measured during performance mapping.

Tables 6-16 through 6-20 present the worst-case impulse bit repeatability measured during the performance mapping tests. The ES 509778 requirement of ±15 percent at feed pressures ranging from 350 to 150 psia has been demonstrated with considerable margin. Based on this data, it is recommended that the ±15 percent tolerance also be applied for feed pressures of 420 to 350 psia and 150 to 70 psia. Table 6-19 presents the overall impulse bit measurements which include the variation of propellant temperature. The data verifies that the ±25 percent JPL requirement is also met with good margin. The 8-millisecond pulses were not included in the data because of the large effect of aniline poisoning as a function of propellant temperature during the limit cycle case. Review of data at the 1 percent duty cycle (8-millisecond pulse width) indicates considerable margin over the ±25 percent requirement.

Table 6-20 presents a summary of the centroid repeatability data. As shown, the T/VA design demonstrates excessive margin over the requirement stipulated by ES 509778. The data presented also includes the centroid value of the first pulses, which is not required by JPL. It is therefore recommended that Table II be deleted and an overall repeatability requirement of ±15 percent be adopted for a given pulse train with a pulse width $\geq$40 milliseconds and a minimum off time of 400 milliseconds.

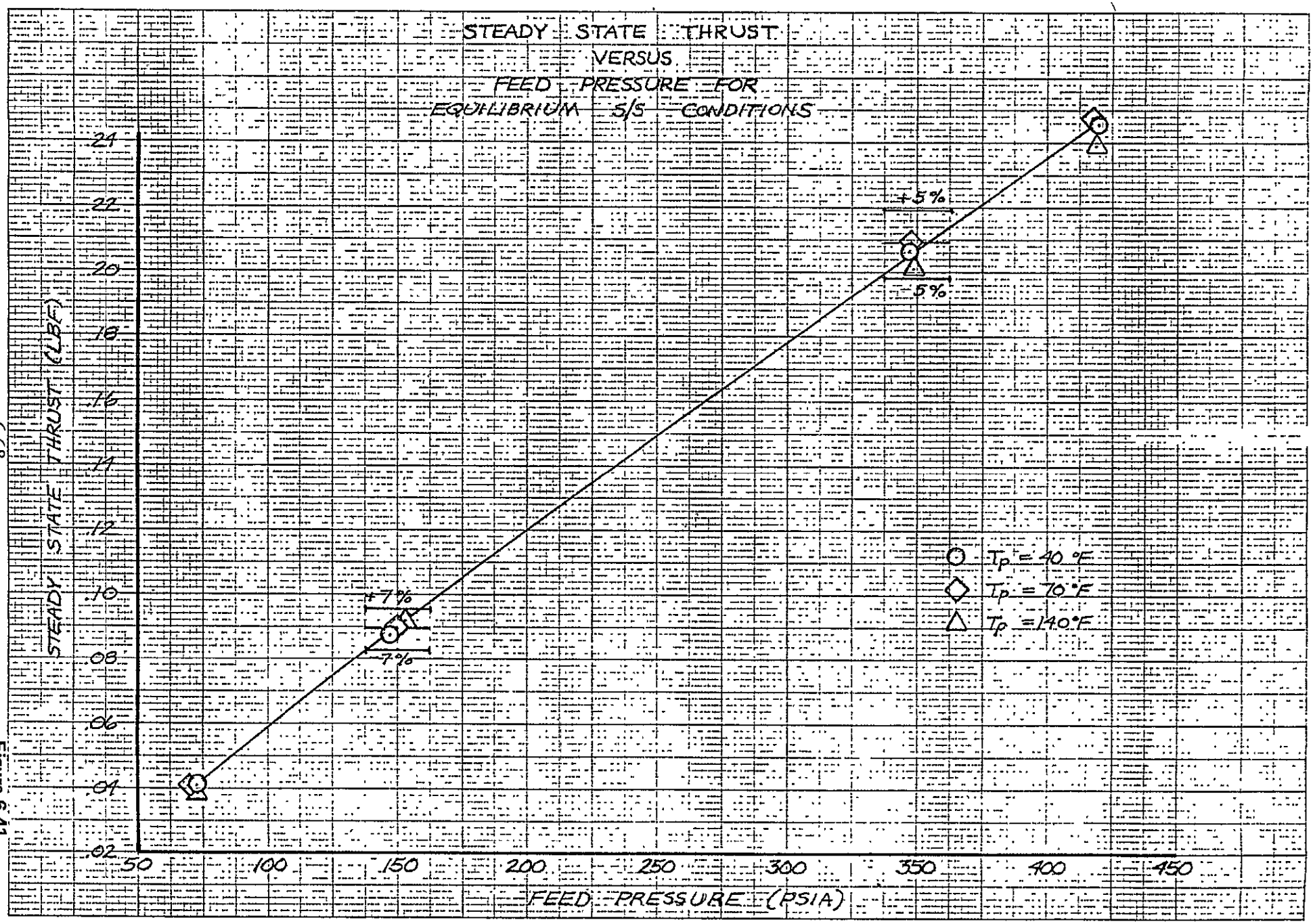
STEADY STATE THRUST
VERSUS
FEED PRESSURE FOR
EQUILIBRIUM S/S CONDITIONS
STEADY STATE THRUST (LBF)
.24
.22
.20
.18
.16
.14
.12
.10
.08
.06
.04
.02
+5%
-5%
+7%
-7%
T_p = 40 °F
T_p = 70 °F
T_p = 140 °F
50
100
150
200
250
300
350
400
450
FEED PRESSURE (PSIA)

Figure 6-41

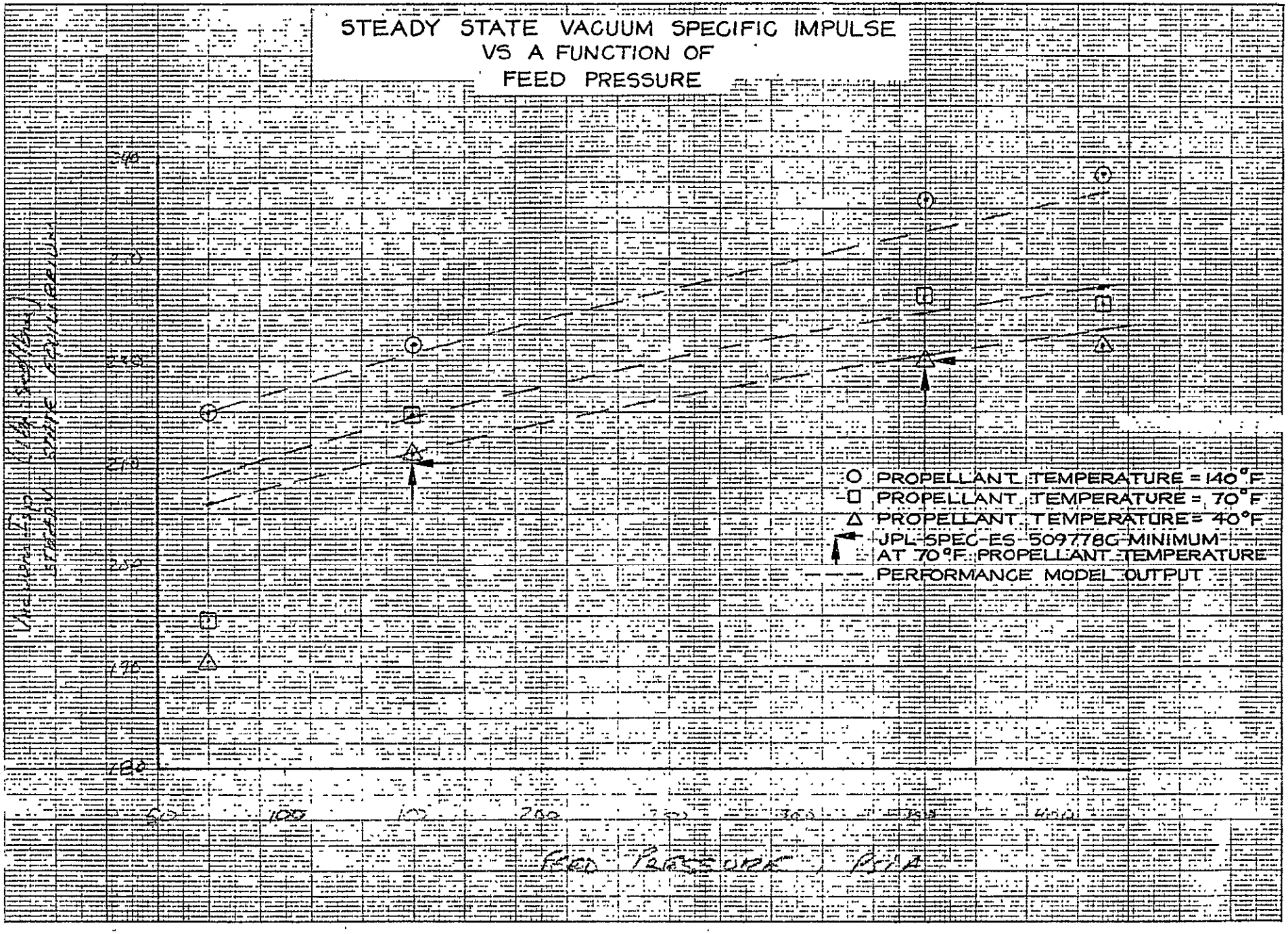
STEADY STATE VACUUM SPECIFIC IMPULSE
VS A FUNCTION OF
FEED PRESSURE
PROPELLANT TEMPERATURE = 140°F
PROPELLANT TEMPERATURE = 70°F
PROPELLANT TEMPERATURE = 40°F
JPL-SPEC-ES-509778G MINIMUM
AT 70°F PROPELLANT TEMPERATURE
PERFORMANCE MODEL OUTPUT
100
200
300
400
FEED PRESSURE, PSIA

Figure 6-42

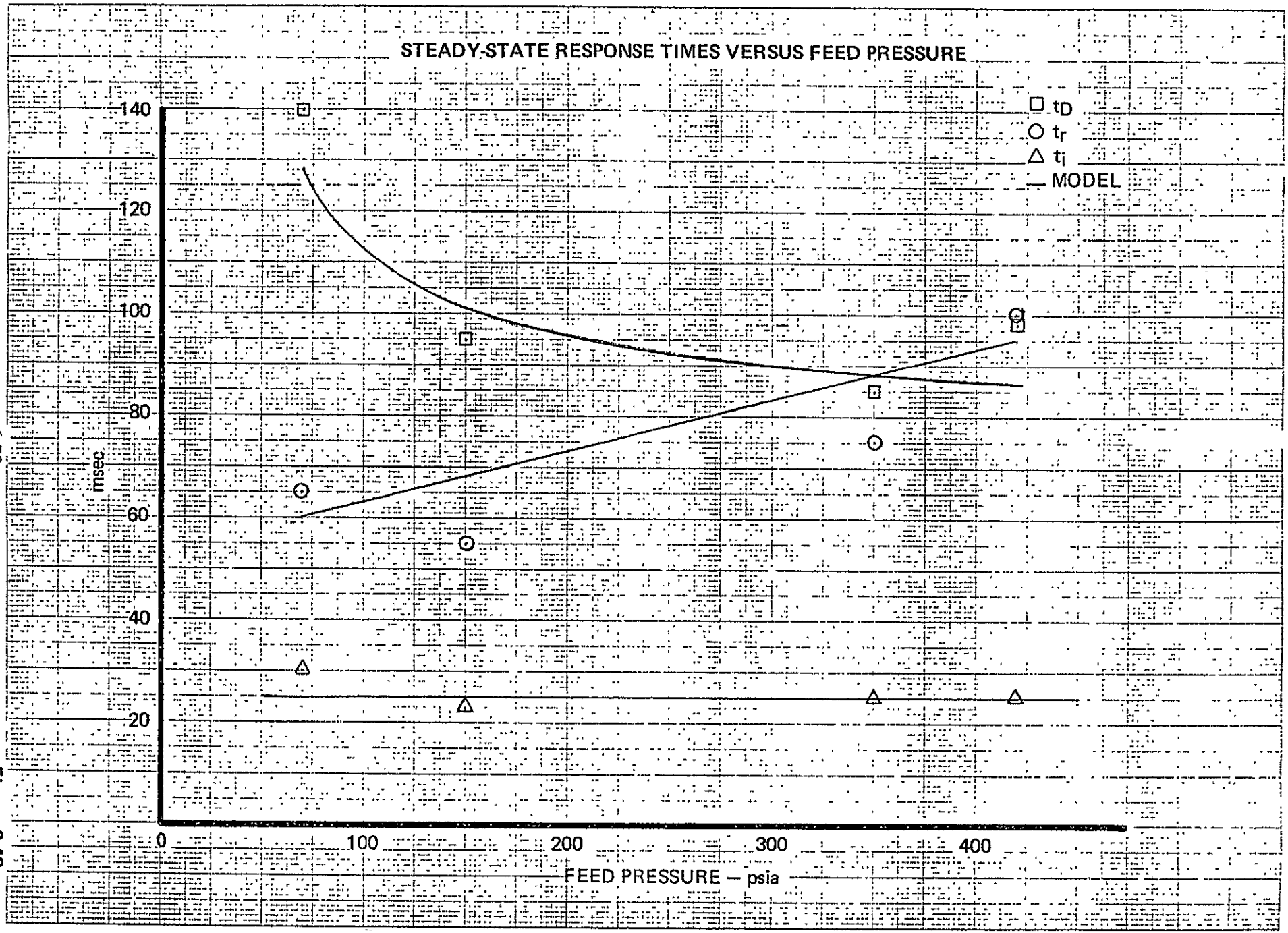
STEADY-STATE RESPONSE TIMES VERSUS FEED PRESSURE
tD
tr
ti
MODEL
msec
140
120
100
80
60
40
20
0
100
200
300
400
FEED PRESSURE — psia

Figure 6-43

Table 6-15
MJS 0.2-lbf REA
STEADY-STATE ROUGHNESS
AT EQUILIBRIUM

Sequence	P_f (psia)	Roughness ± Percent	
		Max-Min	Sigma
23	419.3	16.7	4.1
111	417.7	18.5	4.8
199	419.0	34.7	7.1
46	346.9	16.2	4.2
134	347.4	22.2	5.4
222	348.3	41.7	8.7
69	146.5	24.7	9.5
157	149.2	37.0	12.5
245	152.7	53.4	12.9
92	72.9	11.2	3.0
176	70.5	48.9	9.7
268	72.2	27.4	6.5

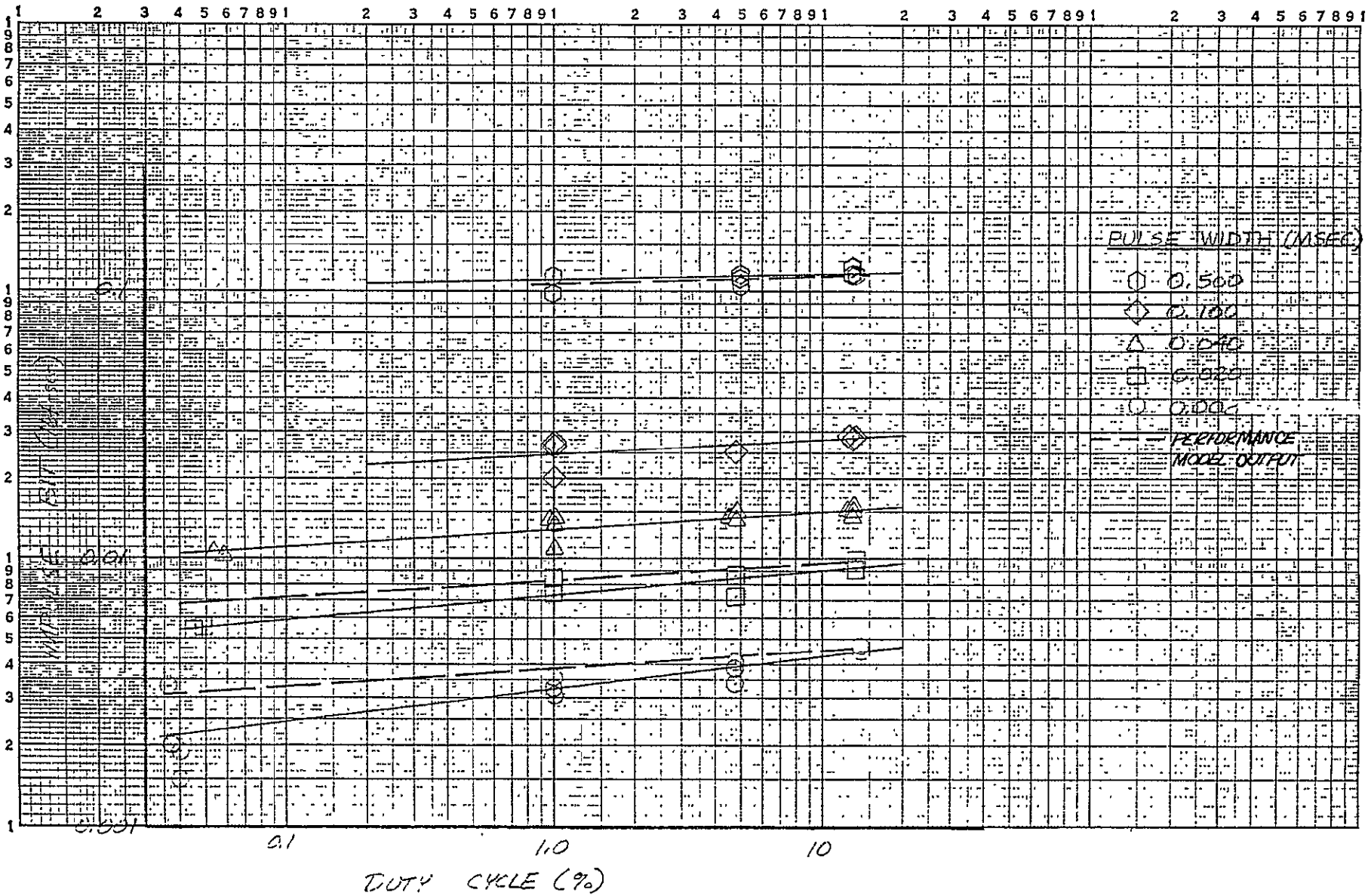
0.2 lbf TIVA Equilibrium I_{BIT} Characteristics (P_f = 420 psia)
PULSE WIDTH (MSEC)
0.500
0.100
0.040
0.020
0.004
PERFORMANCE MODEL OUTPUT
0.1
1.0
10
DUTY CYCLE (%)

Figure 6-44

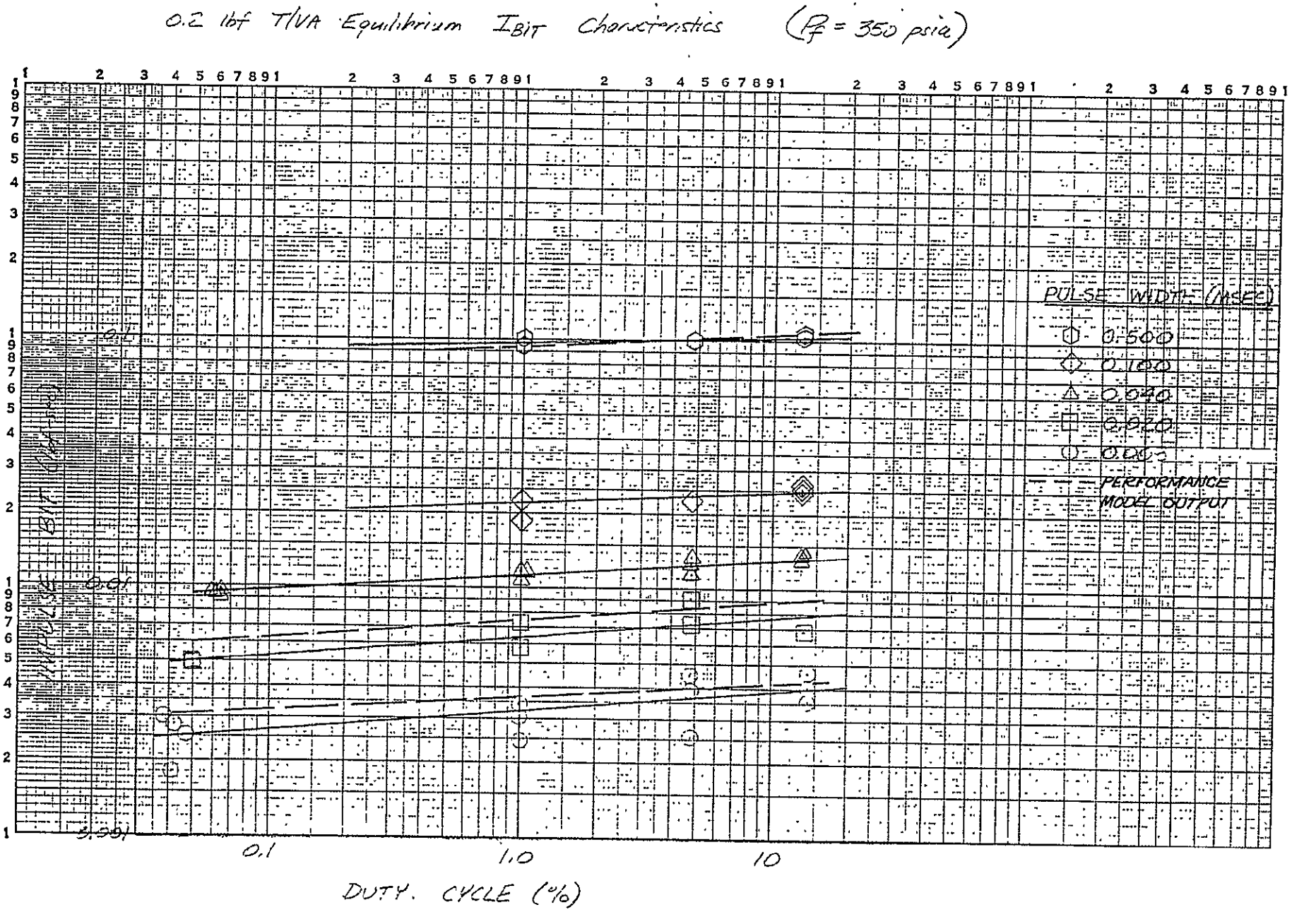
0.2 lbf T/VA Equilibrium I_{BIT} Characteristics (P_f = 350 psia)
PULSE WIDTH (MSEC)
0.500
0.100
0.040
0.020
0.000
PERFORMANCE MODEL OUTPUT
0.1
1.0
10
DUTY CYCLE (%)

Figure 6-45

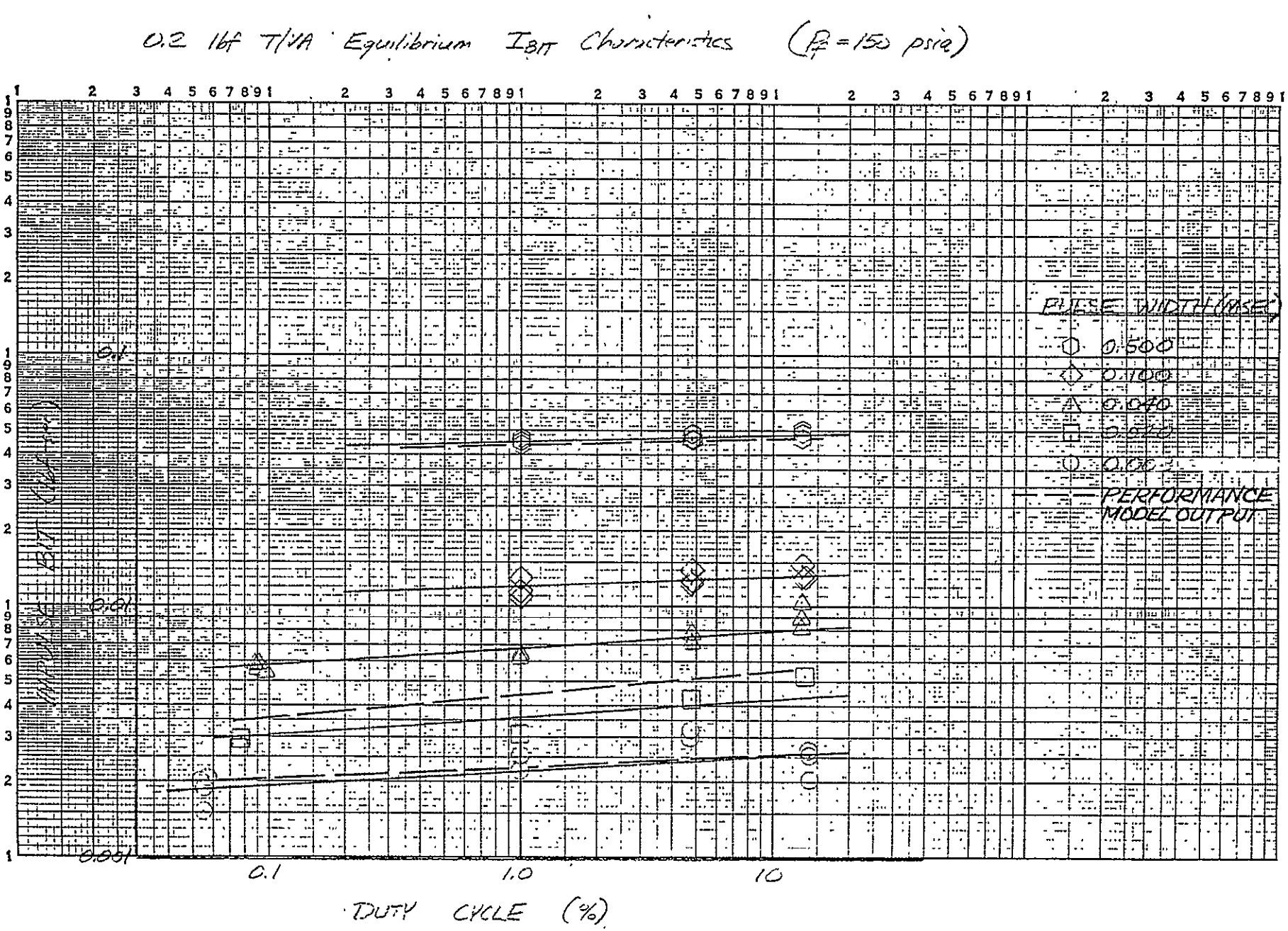
0.2 lbf T/VA Equilibrium I_{BT} Characteristics (P_F = 150 psia)
PULSE WIDTH (MSEC)
0.500
0.100
0.040
0.020
0.010
PERFORMANCE MODEL OUTPUT
0.99
0.9
0.1
0.01
0.001
0.1
1.0
10
DUTY CYCLE (%)

Figure 6-46

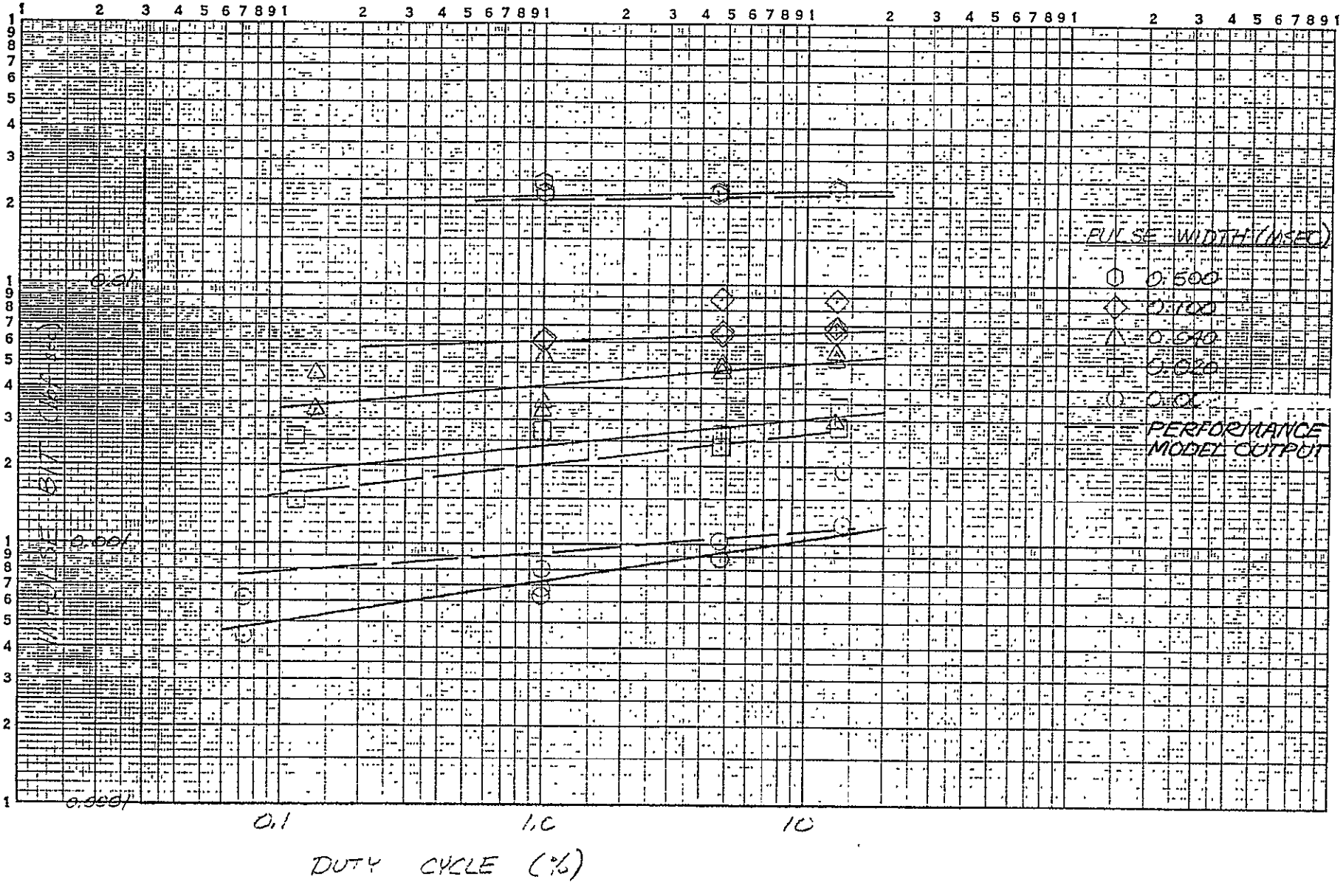
2.2 lbf T/VA Equilibrium I_{BIT} Characteristics (P_f = 70 psia)
PULSE WIDTH (MSEC)
0.500
0.100
0.040
0.020
0.010
PERFORMANCE MODEL OUTPUT
0.1
1.0
10
DUTY CYCLE (%)

Figure 6-47

O2 LH2 T/VA
EQUILIBRIUM VACUUM SPECIFIC IMPULSE
Tp = 70°F
Pc = 420 (psia)
DUTY CYCLE
1 %
4.76 %
13.00 %
13.33 %
13.79 %
PERFORMANCE
MODEL OUTPUT
15% DUTY CYCLE
1% DUTY CYCLE
LIMIT CYCLE (350 °F)
VACUUM SPECIFIC IMPULSE (LBF-SEC/LBM)
240
200
160
120
80
40
10
100
1000
PULSE WIDTH (MSEC)

Figure 6-48

O/F = 2.6 F-1/A-50
EQUILIBRIUM VACUUM SPECIFIC IMPULSE
T_{ch} = 40 °F
P_c = 420 (psia)
DUTY CYCLE
1 %
1.76 %
13.00 %
13.33 %
13.79 %
240
200
160
120
80
40
1
10
100
1000
PULSE WIDTH (msec)

Figure 6-49

O/F 16F TVA
EQUILIBRIUM VACUUM SPECIFIC IMPULSE
Tp = 140 °F
Pc = 420 psia
DUTY CYCLE
1 %
4.76 %
13.00 %
13.33 %
13.78 %
240
200
160
120
80
40
VACUUM SPECIFIC IMPULSE (lbf-sec/lbm)
1
10
100
1000
PULSE WIDTH (MSEC)

Figure 6-50

O/F LBF TLVA
EQUILIBRIUM VACUUM SPECIFIC IMPULSE
Tp = 70 °F
Pc = 350 (psia)
DUTY CYCLE
1 %
4.76 %
13.00 %
13.33 %
13.79 %
PERFORMANCE MODEL OUTPUT
15 % DUTY CYCLE
1% DUTY CYCLE
LIMIT CYCLE (350 °F)
VACUUM SPECIFIC IMPULSE (lbf-sec/lbm)
240
200
160
120
80
40
10
100
1000
PULSE WIDTH (MSEC)

Figure 6-51

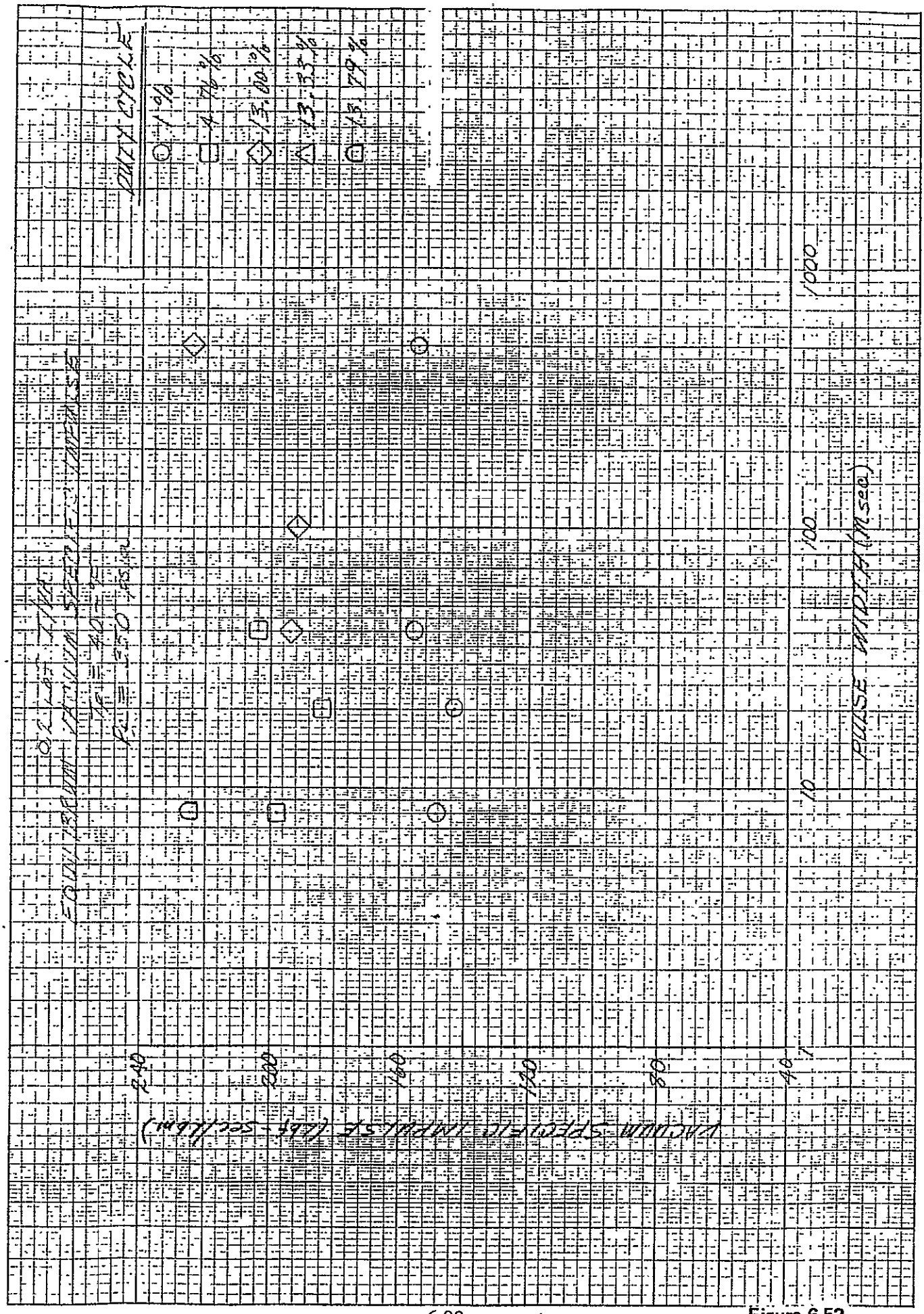

Figure 6-52

C-2 16f T/VA
EQUILIBRIUM VACUUM SPECIFIC IMPULSE
P_f = 350 psia
TP - 140°F
DUTY CYCLE
1.0%
1.16%
3.00%
3.33%
3.75%
240
200
160
120
80
40
VACUUM SPECIFIC IMPULSE (lbf-sec/lbm)
1
10
100
1000
PULSE WIDTH (msec)

Figure 6-53

9.2 Lbf T/VA
EQUILIBRIUM VACUUM SPECIFIC IMPULSE
T_F = 70 °F
P_F = 150 (psia)
DUTY CYCLE
1 %
4.76 %
13.00 %
13.33 %
15.79 %
PERFORMANCE MODEL OUTPUT
15% DUTY CYCLE
1% DUTY CYCLE
LIMIT CYCLE (350 °F)
VACUUM SPECIFIC IMPULSE (LBF-SEC/LBM)
240
200
160
120
80
40
10
100
1000
PULSE WIDTH (m sec)

Figure 6-54

O/F 1.67 T/VA
EQUILIBRIUM VACUUM SPECIFIC IMPULSE
T_P = 40°F
P_F = 150 psia
DUTY CYCLE
1%
4.76%
13.00%
13.33%
15.79%
240
200
160
120
80
40
1
10
100
1000
PULSE WIDTH (MSEC)
VACUUM SPECIFIC IMPULSE (LBF-SEC/LBM)

Figure 6-55

0.2 lbf TIVA
EQUILIBRIUM VACUUM SPECIFIC IMPULSE
Pf = 150 psia
Tp = 140 °F
DUTY CYCLE
1%
4 7% %
3.00 %
3 3 %
5 7 8 %
240
200
160
120
80
40
SPECIFIC IMPULSE (lbf-sec/lbm)
10
PULSE WIDTH (msec)
100
1000

Figure 6-56

0.2 Lbf. T/VA
EQUILIBRIUM VACUUM SPECIFIC IMPULSE
TP = 70 °F
PF = 70 (psia)
DUTY CYCLE
1 %
4.76 %
13.00 %
15.33 %
15.79 %
PERFORM-ANCE-MODEL OUTPUT
15% DUTY CYCLE
1% DUTY CYCLE
LIMIT CYCLE (350°F)
VACUUM SPECIFIC IMPULSE (lbf-sec/lbm)
240
200
160
120
80
40
10
100
1000
PULSE WIDTH (M sec.)

Figure 6-57

O/F
EQUILIBRIUM VACUUM SPECIFIC IMPULSE
T_A = 40 °F
P_c = 70 PSIA
DUTY CYCLE
1 %
4.76 %
13.00 %
13.33 %
13.79 %
VACUUM SPECIFIC IMPULSE (LBF-SEC/LBM)
240
200
160
120
80
40
1
10
100
1000
PULSE WIDTH (MSEC)

Figure 6-58

EQUILIBRIUM
VACUUM
SPECIFIC IMPULSE
DUTY CYCLE
1.%
4.76%
3.00%
3.33%
3.79%
PULSE WIDTH (MSEC)
VACUUM SPECIFIC IMPULSE (lbf-sec/lbm)

Figure 6-59

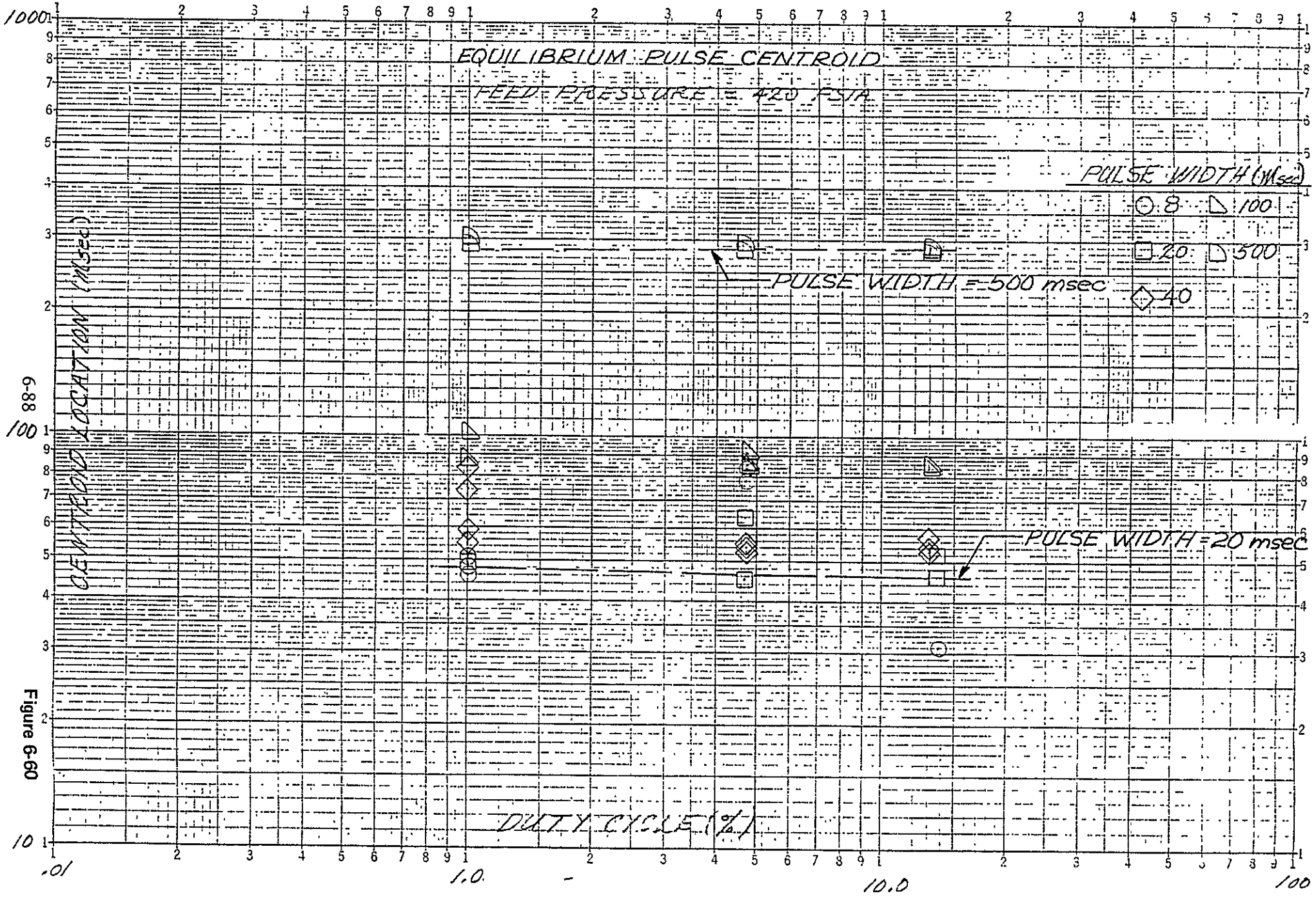
EQUILIBRIUM PULSE CENTROID
FEED PRESSURE = 420 PSIA
PULSE WIDTH (msec)
8
20
40
100
500
PULSE WIDTH = 500 msec
PULSE WIDTH = 20 msec
CENTRIFUGE ROTATION (msec)
DUTY CYCLE (%)
1000
100
10
1
.01
1.0
10.0
100
6-88

Figure 6-60

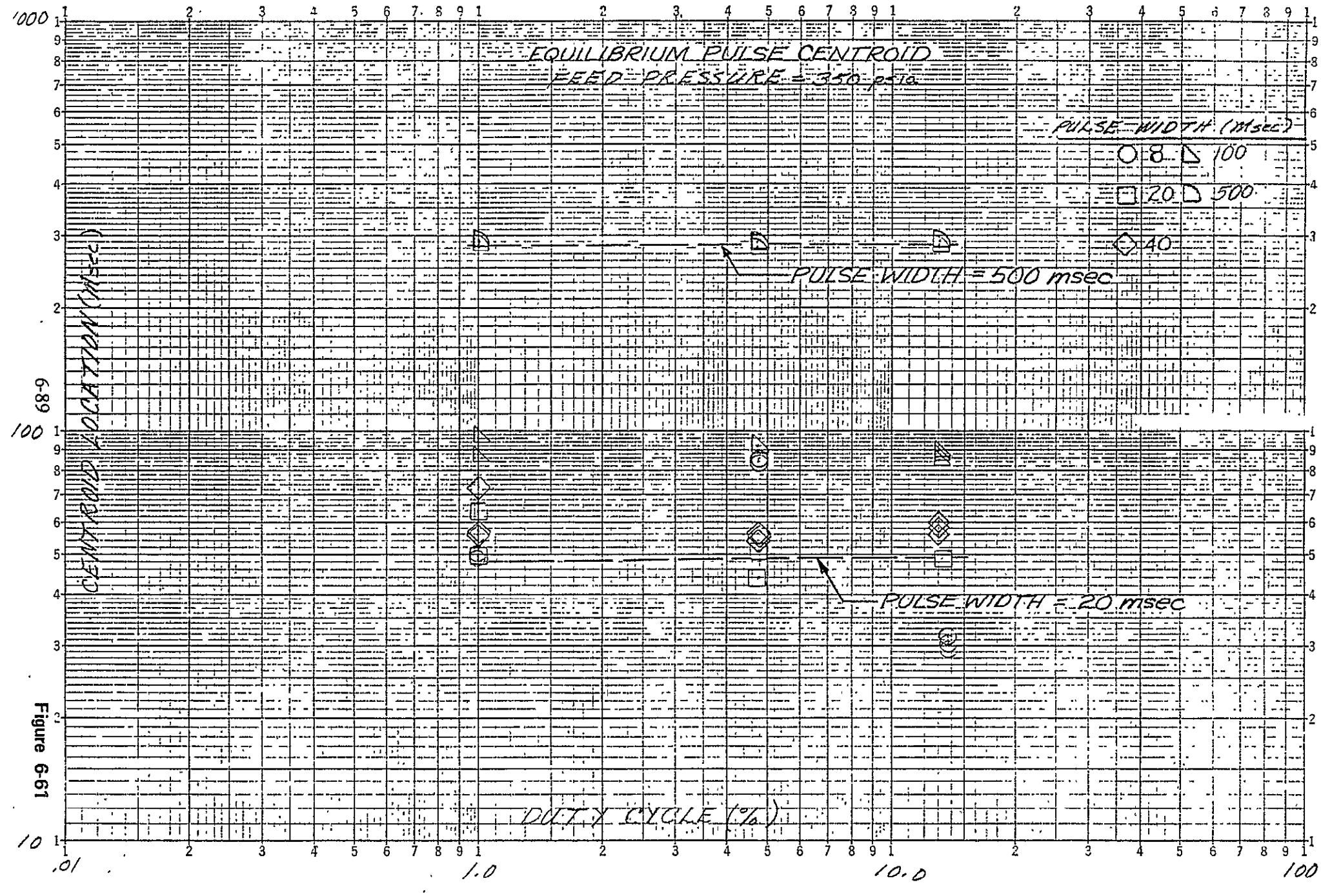
EQUILIBRIUM PULSE CENTROID
FEED PRESSURE = 350 psia
PULSE WIDTH (msec)
8
100
20
500
40
PULSE WIDTH = 500 msec
PULSE WIDTH = 20 msec
EQUILIBRIUM PULSE CENTROID (psia)
DUTY CYCLE (%)
1000
100
10
.01
1.0
10.0
100

Figure 6-61

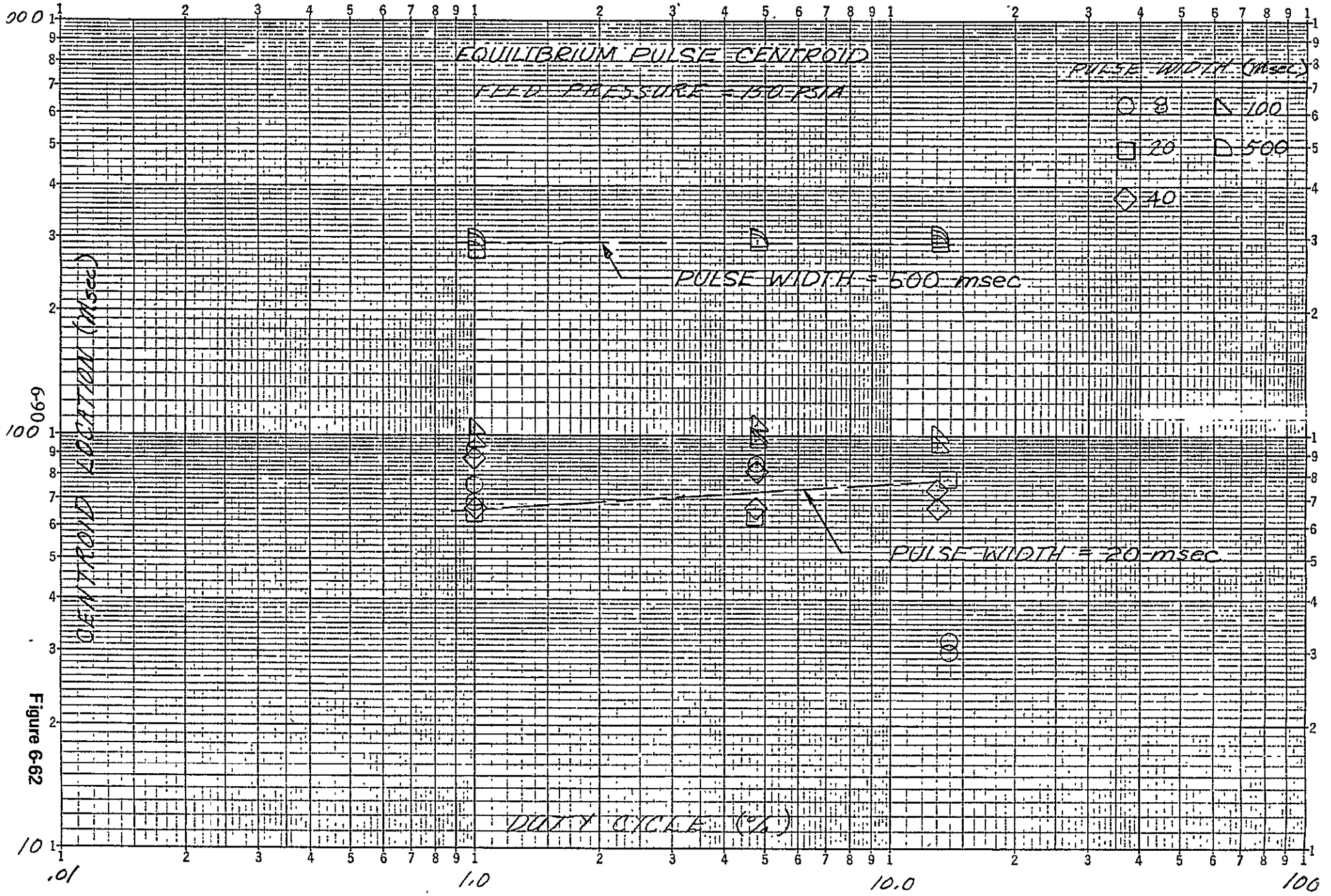
EQUILIBRIUM PULSE CENTROID
FEED PRESSURE = 150 PSIA
PULSE WIDTH (msec.)
3
10
20
50
40
PULSE WIDTH = 500 msec
PULSE WIDTH = 20 msec
EQUILIBRIUM CENTROID (MSEC)
DUTY CYCLE (%)
.01
1.0
10.0
100
6-90

Figure 6-62

Figure 6-63

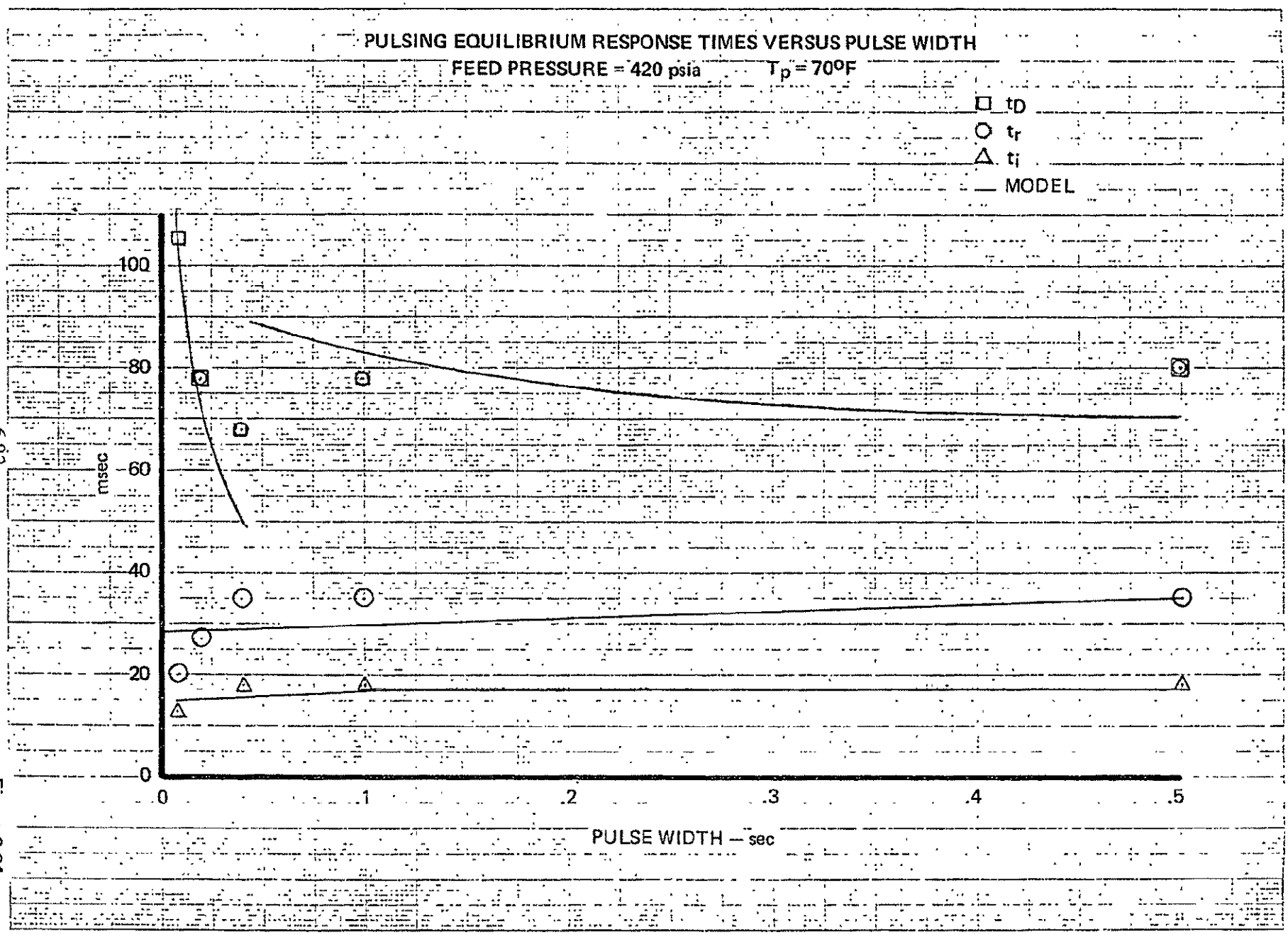
PULSING EQUILIBRIUM RESPONSE TIMES VERSUS PULSE WIDTH
FEED PRESSURE = 420 psia
T_p = 70°F
t_D
t_r
t_i
MODEL
100
80
60
40
20
0
msec
0
.1
.2
.3
.4
.5
PULSE WIDTH — sec

Figure 6-64

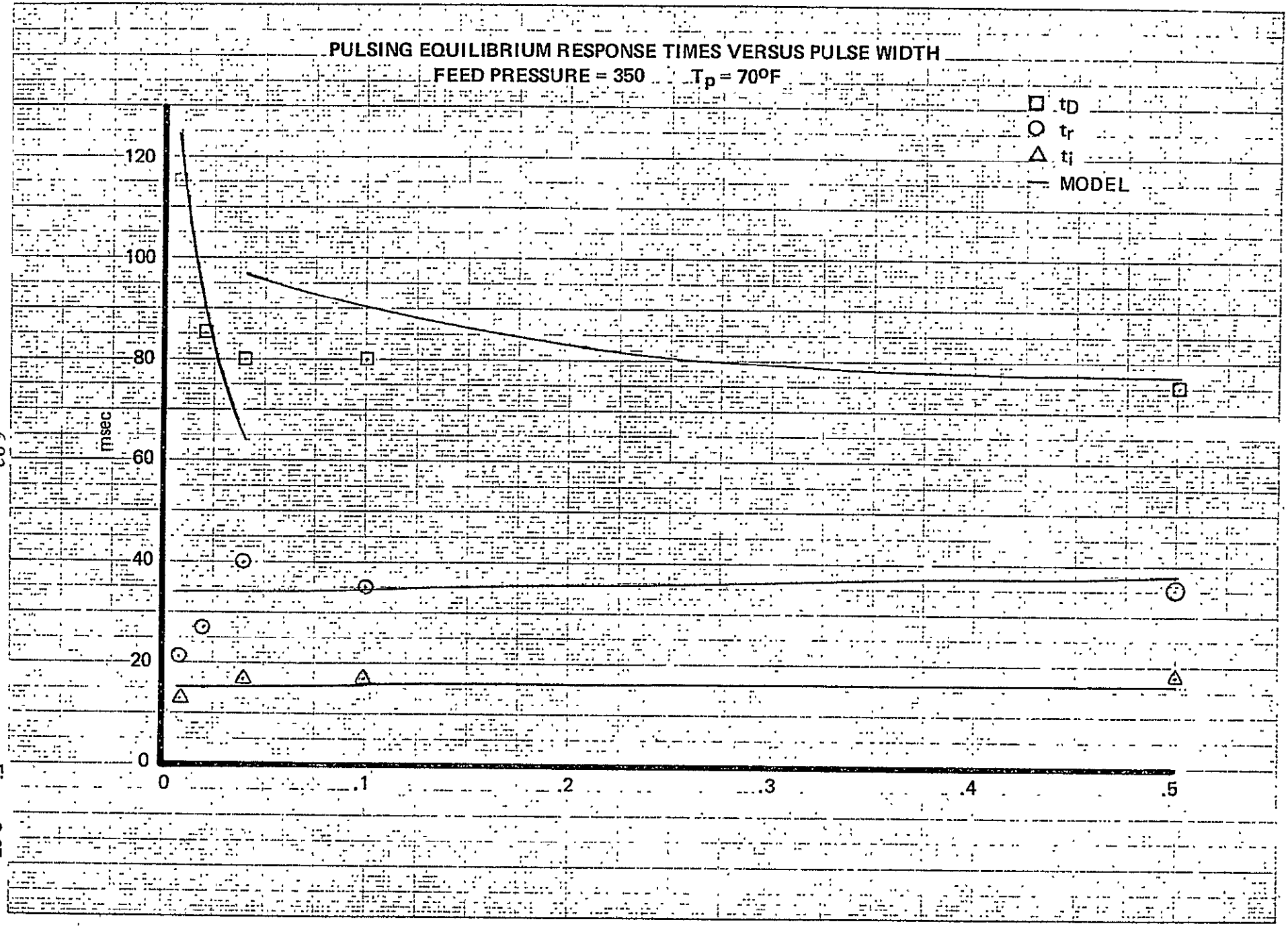

6-93

Figure 6-65

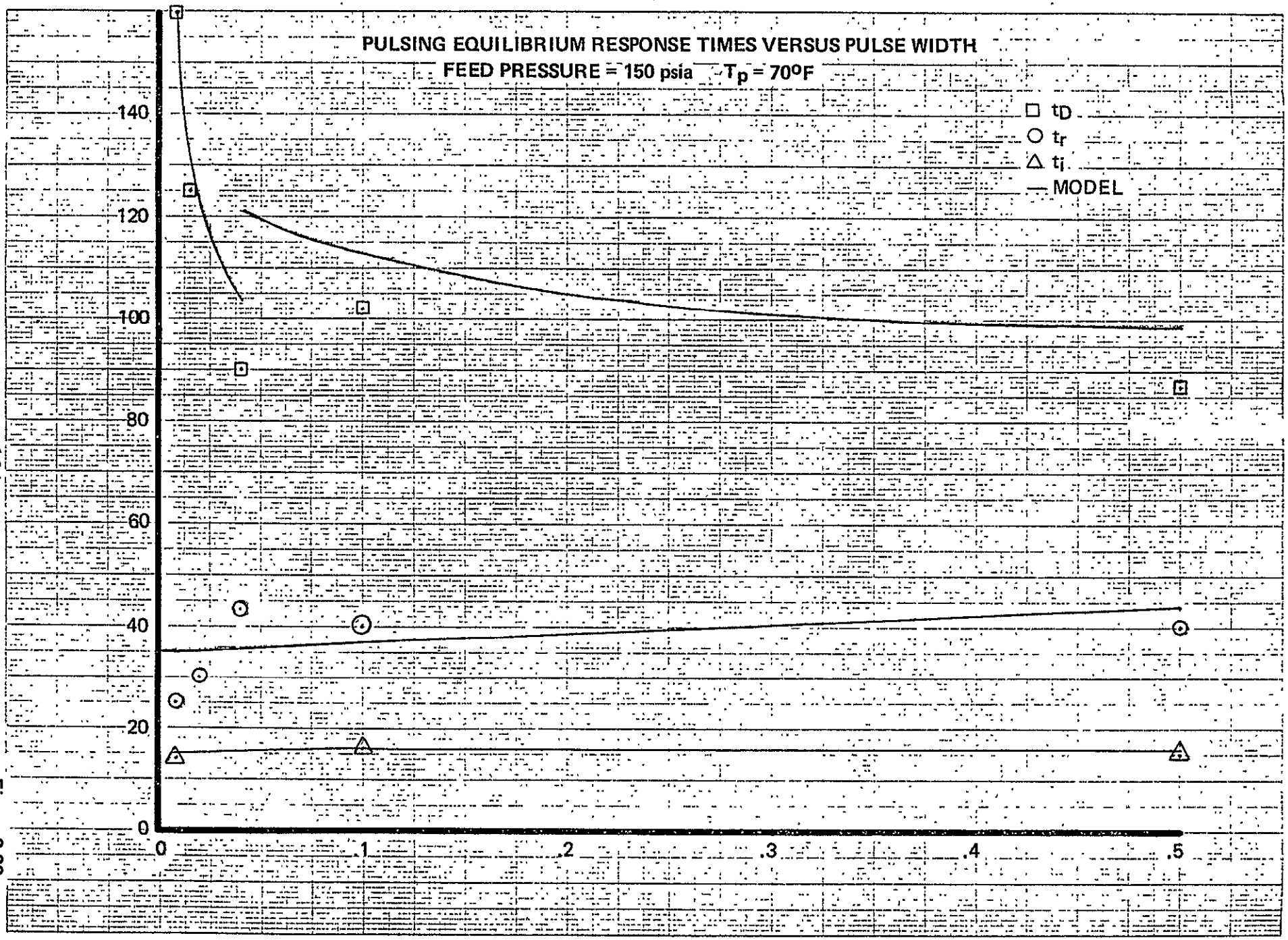
PULSING EQUILIBRIUM RESPONSE TIMES VERSUS PULSE WIDTH
FEED PRESSURE = 150 psia T_p = 70°F
t_D
t_r
t_i
MODEL
140
120
100
80
60
40
20
0
0
.1
.2
.3
.4
.5

Figure 6-66

PULSING EQUILIBRIUM RESPONSE TIMES VERSUS PULSE WIDTH
FEED PRESSURE = 70 psia Tp = 70°F
tD
tr
ti
MODEL
msec
140
120
100
80
60
40
20
0
0
.1
.2
.3
.4
.5

Figure 6-97

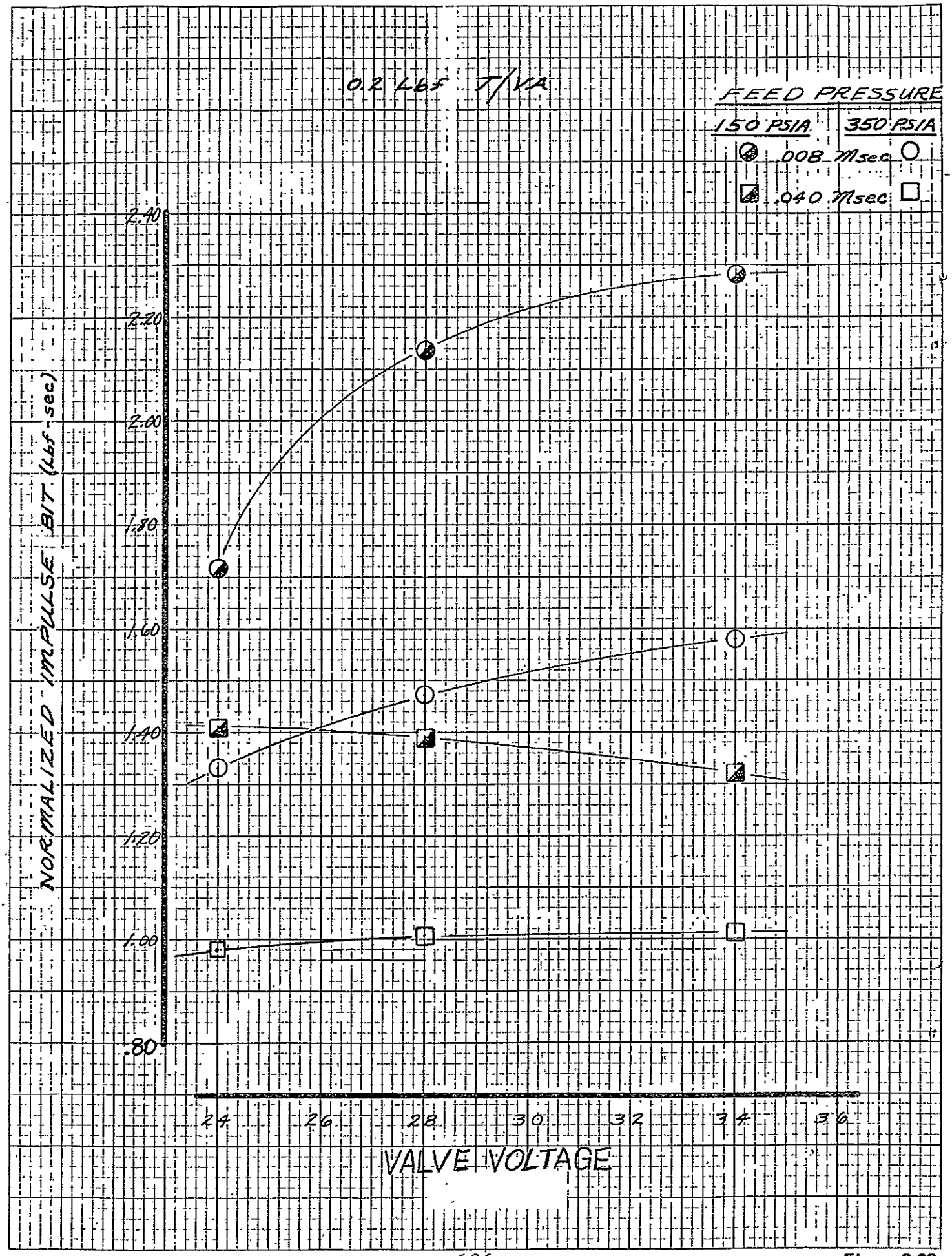
0.2 LBF T/VA
FEED PRESSURE
150 PSIA
350 PSIA
.008 Msec
.040 Msec
NORMALIZED IMPULSE BIT (LBF-sec)
2.40
2.20
2.00
1.80
1.60
1.40
1.20
1.00
.80
24
26
28
30
32
34
36
VALVE VOLTAGE

Figure 6-68

TYPICAL PERFORMANCE MAPPING
PULSE SHAPES

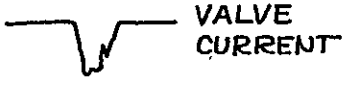

SEQ 5

P_f = 420 psia

T_p = 40 °F

P.W. = .020 sec

D.C. = LIMIT

Figure 6-69

TYPICAL PERFORMANCE MAPPING PULSE SHAPES

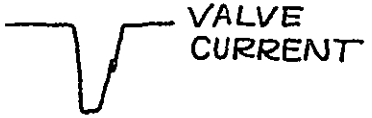

SEQ 181

P_f = 420
T_P = 140
D.W. = .020
D.C. = LIMIT

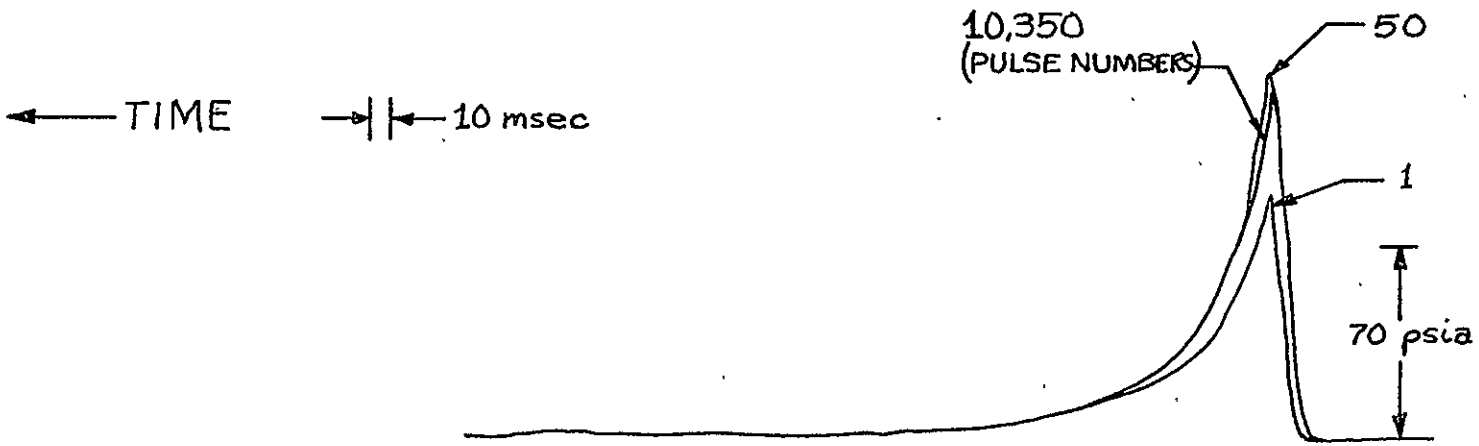

Figure 6-70

TYPICAL PERFORMANCE MAPPING
PULSE SHAPES

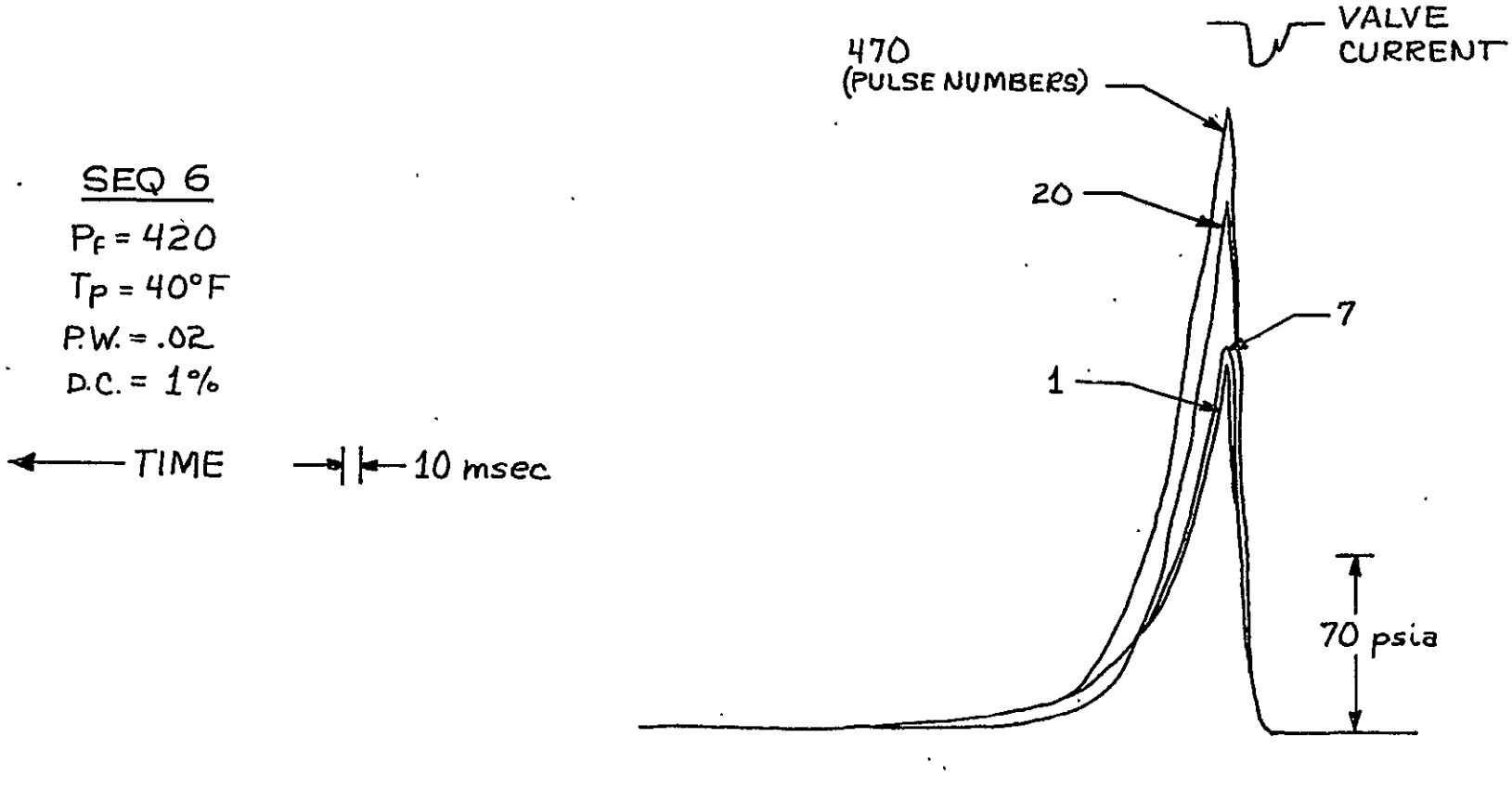

Figure 6-71

TYPICAL PERFORMANCE MAPPING
PULSE SHAPES

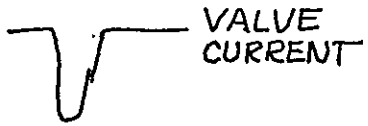

SEQ 183

P_f = 420

T_p = 140

D.W. = .020

D.C. = 1%

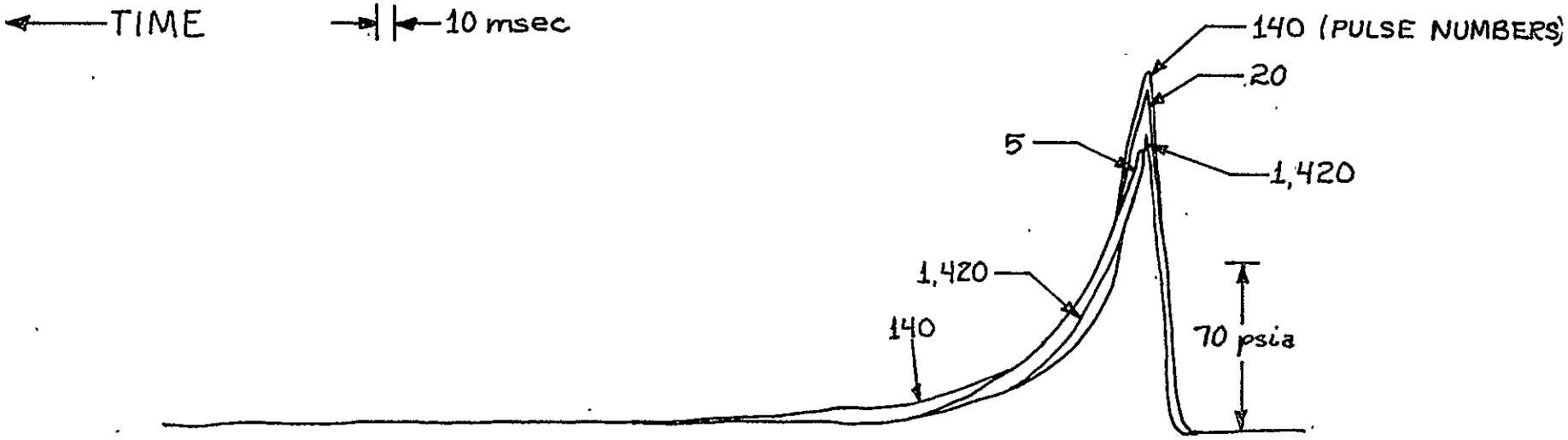

Figure 6-72

TYPICAL PERFORMANCE MAPPING
PULSE SHAPES

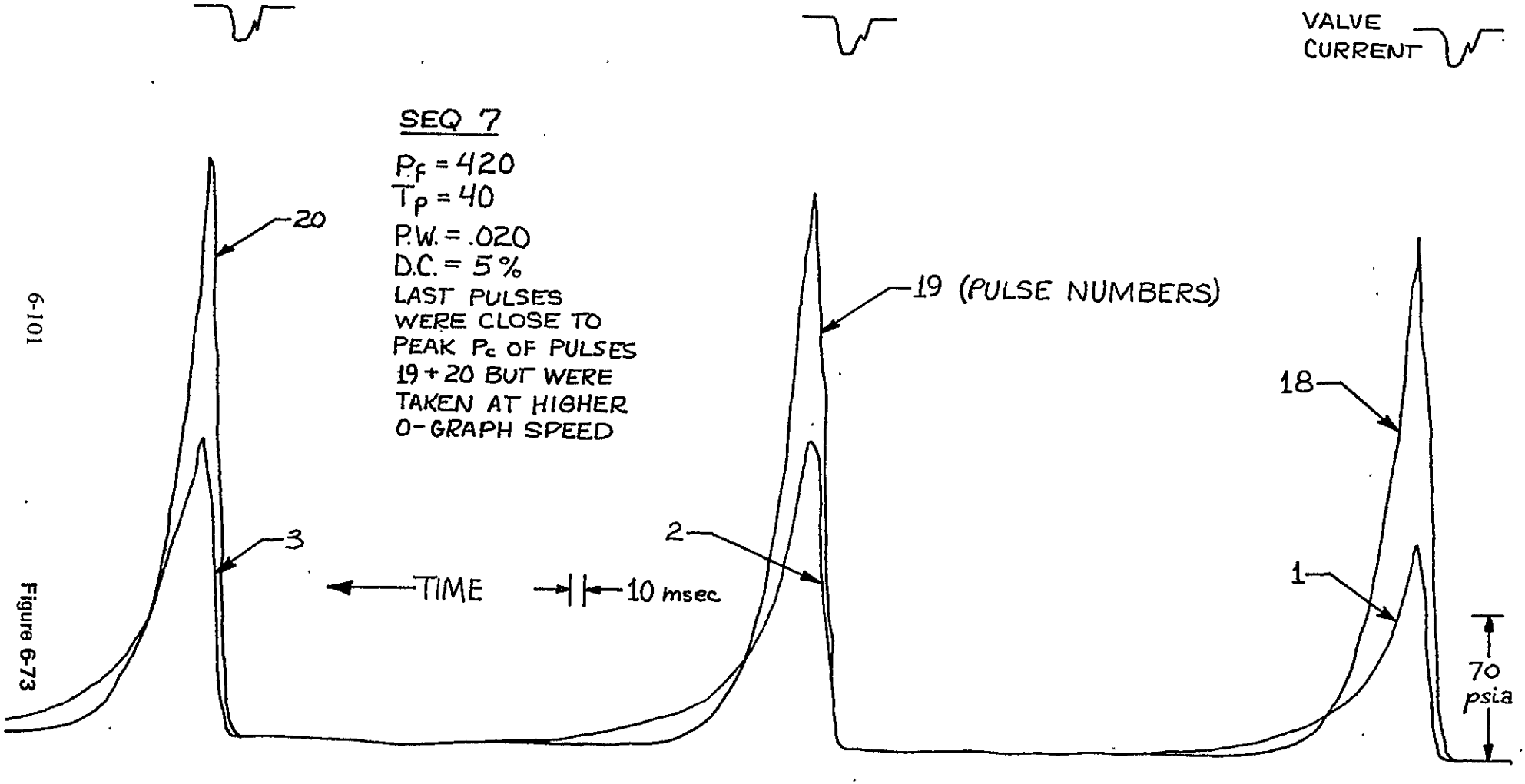

Figure 6-73

TYPICAL PERFORMANCE MAPPING
PULSE SHAPES

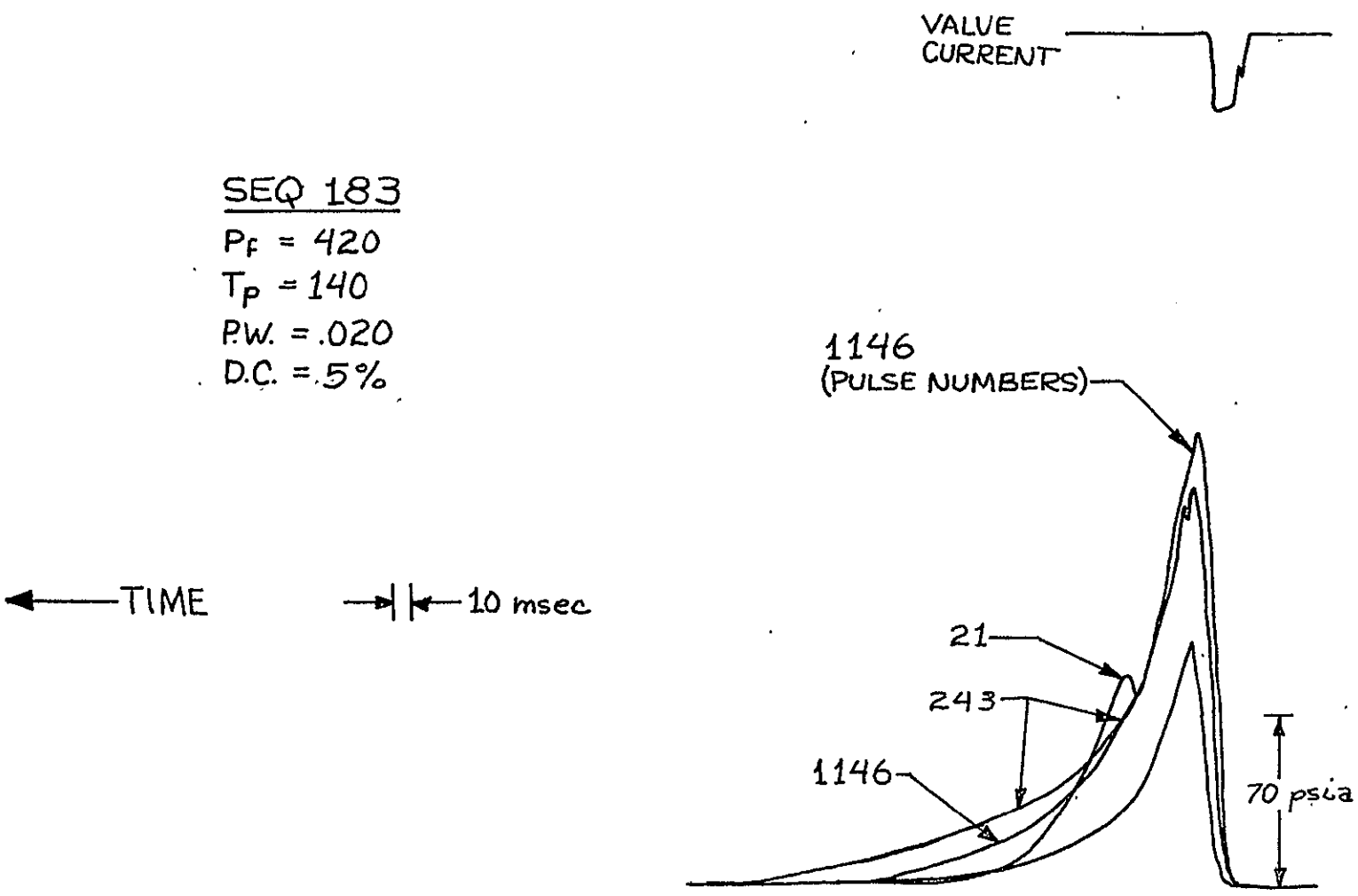

Figure 6-74

TYPICAL PERFORMANCE MAPPING PULSE SHAPES

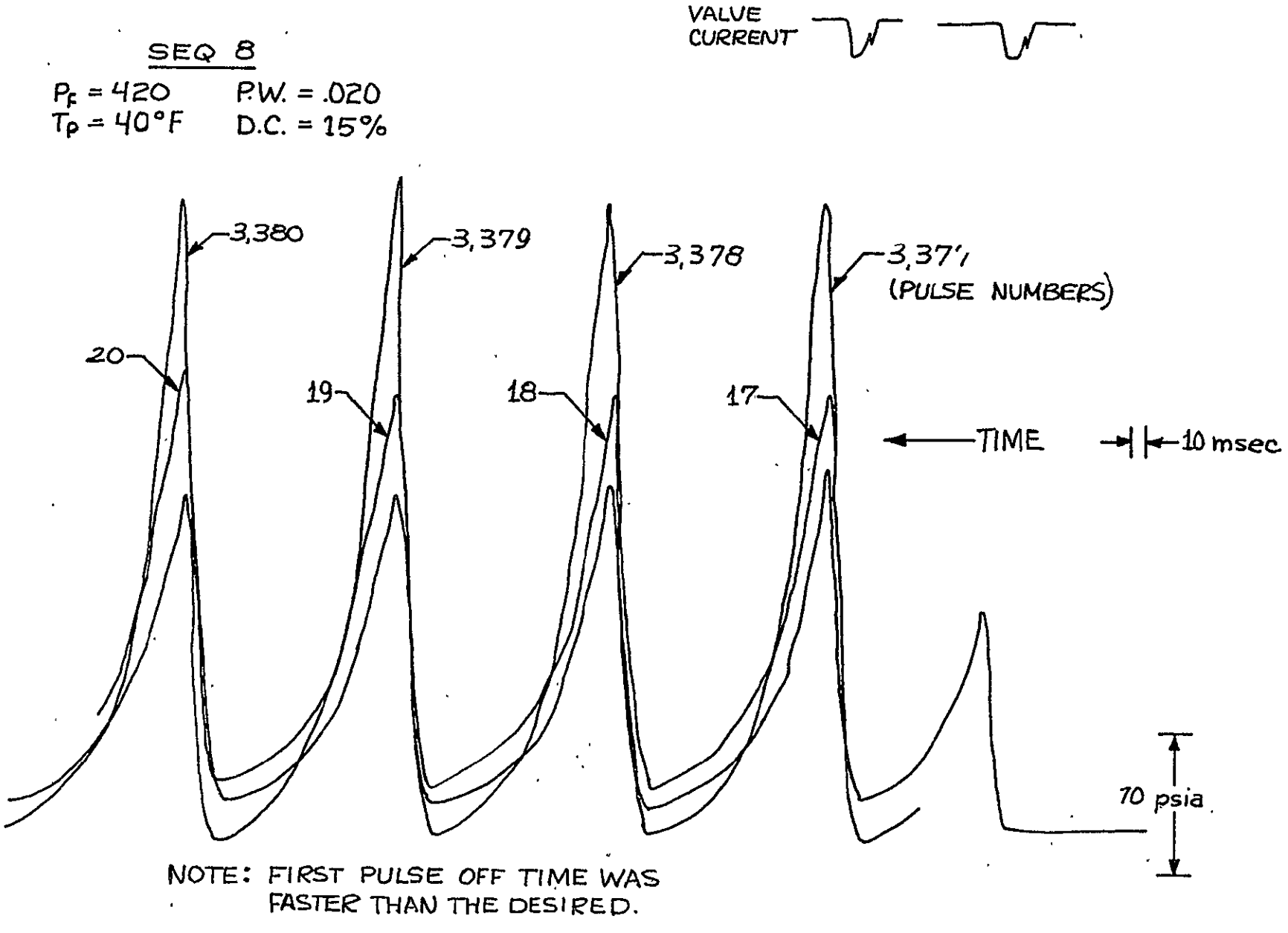

NOTE: FIRST PULSE OFF TIME WAS FASTER THAN THE DESIRED.

Figure 6-75

TYPICAL PERFORMANCE MAPPING
PULSE SHAPES

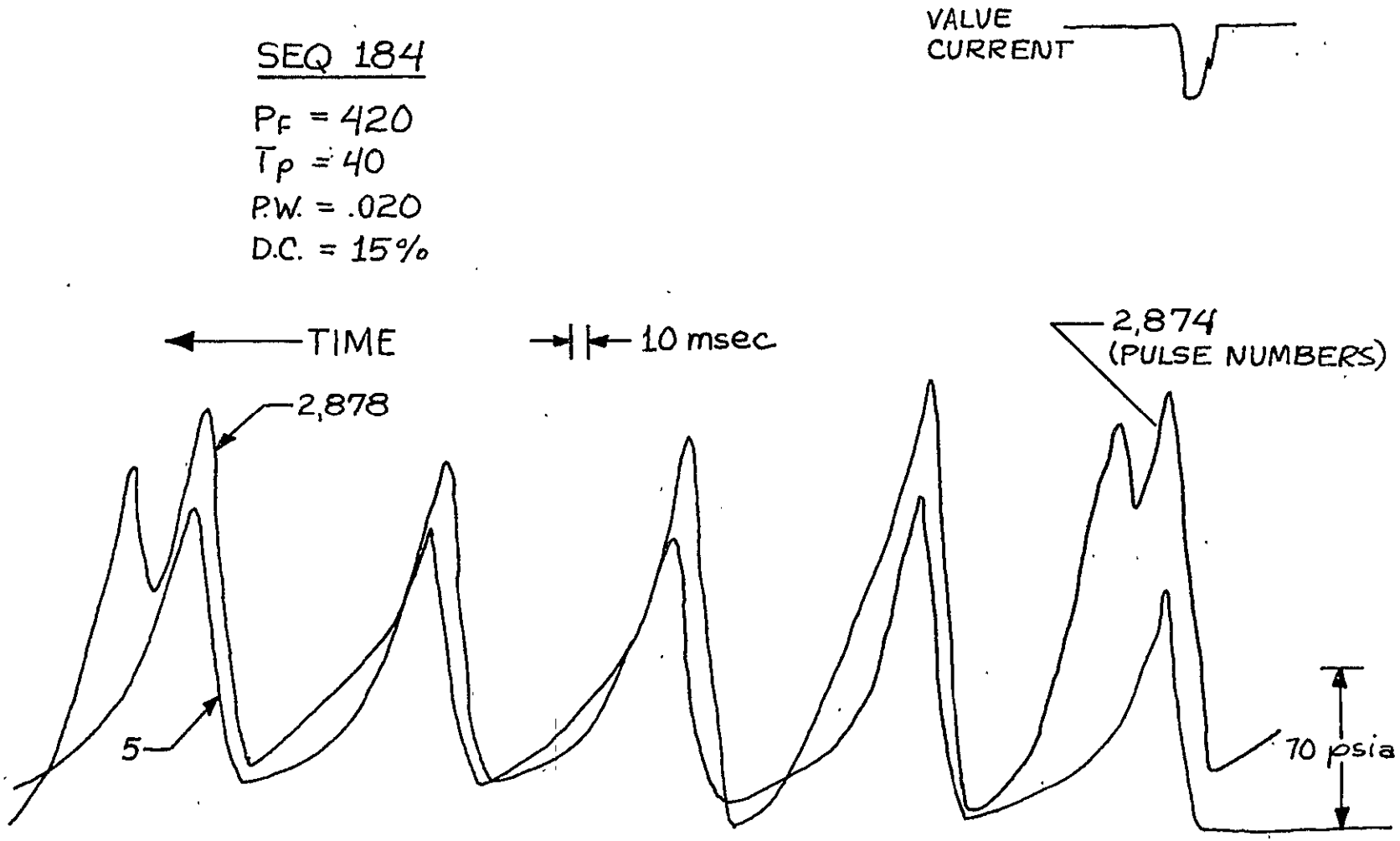

Figure 6-76

Table 6-16
IMPULSE BIT REPEATABILITY
Propellant Temp. = 40°F

Pulse Width (msec) ↓	Pulse-to-Pulse Repeatability ↓			
Feed Pressure (psia) → (ES 509778 Required) →	420 (TBD)	350 (±15%)	150 (±15%)	70 (TBD)
8*	6.5	6.1	2.5	****
20*	7.3	3.8	2.8	5.3
40*	2.5	1.8	***	4.8
100**	2.8	3.1	5.2	3.4
500**	0.27	1.1	0.5	0.5

*Duty cycle = Limit
**Duty cycle = 1%
***No reduction of data due to loss of computer
****Data not available due to aniline poisoning

Table 6-17
IMPULSE BIT REPEATABILITY
Propellant Temp. = 70°F

Pulse Width (msec) ↓	Pulse-to-Pulse Repeatability ↓			
Feed Pressure (psia) → (ES 509778 Required) →	420 (TBD)	350 (±15%)	150 (±15%)	70 (TBD)
8*	5.9	3.1	6.7	5.7
40*	2.1	2.2	5.0	4.4
100**	1.9	4.3	0.7	2.0
500**	0.35	0.80	0.2	1.7

*Duty cycle = Limit
**Duty cycle = 1%

Table 6-18
IMPULSE BIT REPEATABILITY
Propellant Temp. = 140°F

Pulse Width (msec) ↓	Pulse-to-Pulse Repeatability (±%) ↓			
Feed Pressure (psia) → (ES 509778 Required) →	420 (TBD)	350 (±15%)	150 (±15%)	70 (TBD)
8*	3.3	0.2	4.3	7.0
20*	6.2	2.6	1.7	1.9
40*	3.2	1.9	4.8	3.3
100**	6.0	0.99	2.8	5.0
500**	0.7	1.5	0.5	0.4

*Duty cycle = Limit **Duty cycle = 1%

Table 6-19
OVERALL IMPULSE BIT REPEATABILITY*
JPL ES 509778 Requirement = ±25%

Pulse Width (msec) ↓	Pulse-to-Pulse Repeatability (±%) ↓			
Feed Pressure (psia) →	420	350	150	70
20	5.3	3.8	3.8	**
40	1.0	1.6	1.8	18.2
100	7.0	8.4	0.3	7.5
500	6.3	3.3	2.5	5.9

*All pulse widths cover valve temperatures from +40 to +140°F. Maximum predicted valve temperature equal to +260°F will be tested during qualification thermal design verification.

**Data was deleted because of the analine poisoning effect.

Table 6-20
CENTROID REPEATABILITY
Pulse Width = 40 msec
Feed Pressure = 350 psia

% Duty Cycle ↓	Repeatability ±%*		
Propellant Temperature °F →	40	70	140
1%	4.2	1.7	5.0
5%	5.1	4.3	9.7

*Repeatability was calculated by comparing the first pulse at T_{bed} = 380°F to the final pulse at equilibrium. Data shows considerable margin over the requirements of ES 509778. Recommend changing specification to ±15% for a given pulse train.

6.5 STEADY-STATE LIFE MARGIN TEST

The steady-state life margin test program was designed to demonstrate a total of 40 hours of accumulated steady-state operation along with an additional 20 hours to demonstrate life margin. A further goal was to demonstrate the JPL requirement of specification ES 509778 for the T/VA capability of a continuous burn equal to 6 hours. To demonstrate the above, the test plan called for 20 hours of accumulated steady-state operation at each propellant temperature of 40, 70, and 140°F. Feed pressures of 420, 350, 150, and 70 psi were to be fired at each of the propellant temperatures. An additional goal of the test was to determine the T/VA capability to sustain life without degradation due to rough operation (that is, chamber pressure oscillations in excess of 30 percent peak-to-peak).

A total of 60.33 hours of steady-state operation was accumulated. A summary of the test duty cycles conducted and their associated burn times is presented in Table 6-21. Five individual tests were conducted with continuous burn times in excess of 6 hours, and a total throughput of hydrazine equal to 156.85 lbm was demonstrated.

As shown on Table 6-21, the accumulated burn time at a propellant temperature of 140°F was limited to 2.16 hours. This was a result of the valve seat expansion problem discussed in paragraph 6.4 above. In order to demonstrate the total 60 hours, additional tests at 70°F propellant temperature and 40°F propellant temperature were incorporated. Also the 70 psi feed pressure tests at both 40 and 70°F propellant temperatures were deleted because of the valve seat expansion problem. As a result of the increased burn time at the lower propellant temperatures, the last 27.6 hours of steady-state operation was demonstrated with a propellant temperature of 40°F. This achievement represents a considerable demonstration of the margin in the catalyst bed design. Steady-state operation with cold propellant presents the worst-case condition for engine washout. Engine washout can occur in hydrazine reactor designs if loss of catalyst activity with life occurs and, coupled with the cold propellant, the flame front of the reaction moves down the bed until it is completely quenched, and total loss of chamber pressure is a result. Since this demonstration was conducted at the end of life, considerable margin has been demonstrated.

An additional problem occurred during the steady-state life margin test. Both chamber pressure and flow rate decayed as a function of burn time. Figure 6-77 presents a plot of normalized chamber pressure as a function of burn time. The normalized chamber pressure is defined as the measured chamber pressure divided by the predicted chamber pressure. There was no performance dropoff as a function of burn time, and it was therefore hypothesized that the thrust degradation was caused by an increase in T/VA pressure drop. Originally, it was felt that this pressure drop increase was in the valve and was related to the valve seat expansion. However, as presented in Section 7.0 of this report, it was later found during disassembly that the injector cap tube outlet and the injector's screens had large deposits of iron which caused blockage in flow. Also shown on Figure 6-77 is an extra data point which was taken during the thermal design verification tests. This test was done after the steady-state life margin and at T/VA decontamination. After the thermal design verification test, the T/VA was again decontaminated, and upon disassembly, it was shown that the

Table 6-21

STEADY STATE LIFE MARGIN

DUTY CYCLE SUMMARY

Sequence No.	P_{Fuel} psia	T_{Fuel} °F	T_{Mount} °F	Total Time (sec)	REMARKS
1	420	140	70	7,781	Valve Closed Up
5	420	70	70	21,699	
6	350	70	70	14,486	
7	150	70	70	14,494	
8	70	70	70	250	Valve Closed Up
			70	230	
			70	310	
5A	420	70	70	21,745	
6A	350	70	70	14,438	
7A	150	70	70	5,499	Valve Closed Up
6B	350	70	70	16,987	
9	420	40	70/40	21,643	Change T_{mount} during Run
10	350	40	40	14,558	
11	150	40	40	14,280	
12	70	40	40	540	Valve Closed Up
11A	150	40	40	21,600	
10A	350	40	40	26,635	

Total 217,175 seconds = 60.33 hours

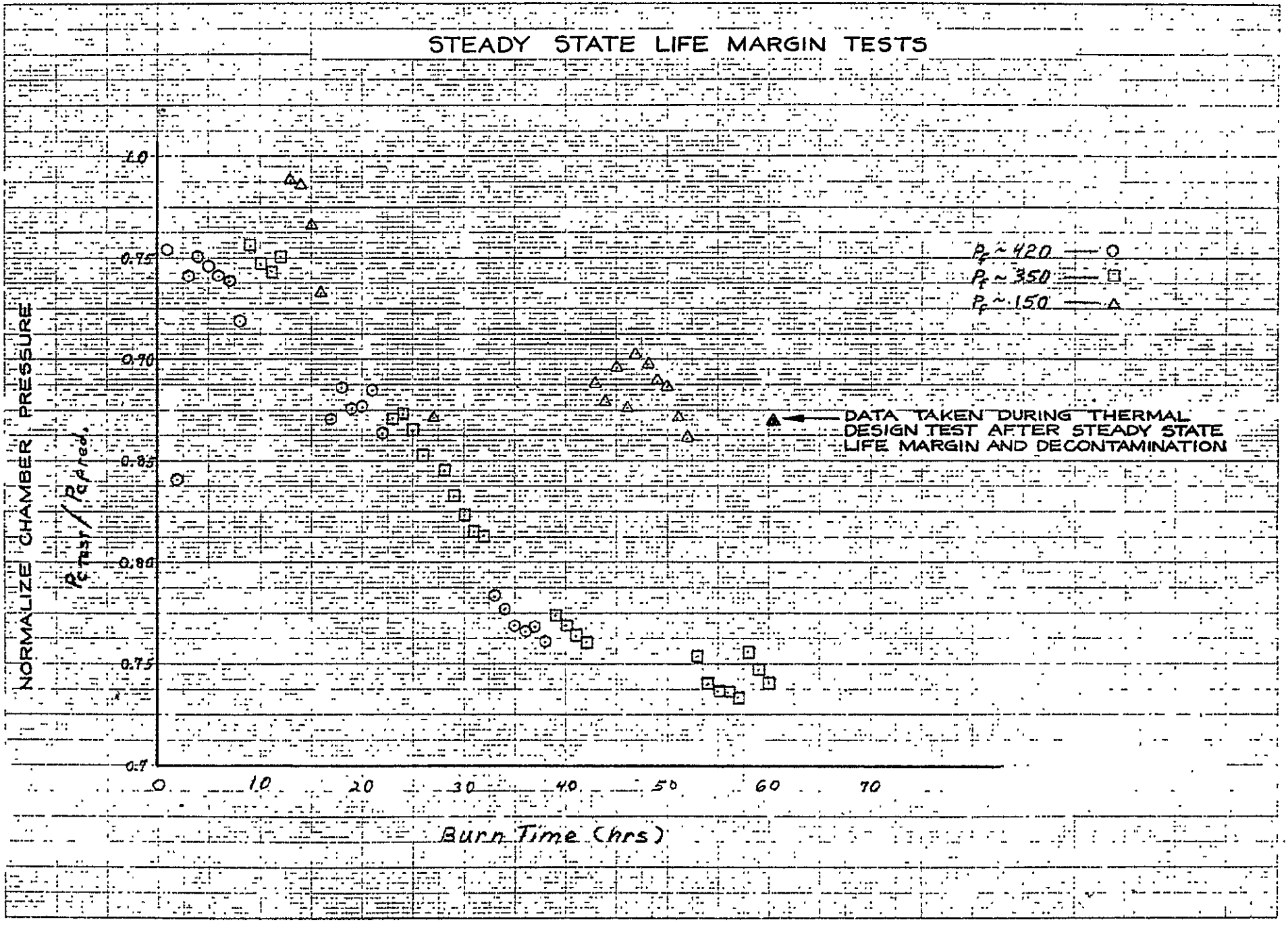
STEADY STATE LIFE MARGIN TESTS
NORMALIZE CHAMBER PRESSURE
$P_{c\ Test} / P_{c\ Pred.}$
1.0
0.95
0.90
0.85
0.80
0.75
0.7
0
10
20
30
40
50
60
70
Burn Time (hrs)
$P_f \sim 420$
$P_f \sim 350$
$P_f \sim 150$
DATA TAKEN DURING THERMAL DESIGN TEST AFTER STEADY STATE LIFE MARGIN AND DECONTAMINATION

Figure 6-77

valve exhibited no increase in pressure drop as a function of flow rate. This supports the fact that the pressure drop increase causing the thrust degradation during the steady-state life margin tests was caused by contamination buildup and not due to the valve. However, as mentioned earlier, the operation of the T/VA was completely terminated at the low feed pressure tests. This failure is caused by the expansion of the valve seat material.

Figure 6-78 presents a plot of the specific impulse as a function of flow rate for the steady-state life margin tests. Specific impulse was correlated as a function of flow rate because of the thrust degradation problem, and it shows that there was no performance drop as a result the thrust degradation. The minimum 3σ curve was calculated by grouping the data points and then plotting the worst-case 3σ. The data points grouped around the flow rate of 0.0015 lbm/sec were excluded from this 3σ calculation. These data points were measured during sequence 5 which occurs very early in the life test. The data is out of the population measured for the remainder portion of the test, and addition does not represent this specific impulse measured during the performance mapping test. A new sightglass control circuitry was installed for this test, and observations made of the raw data indicate that the flow rate was incorrectly measured during this portion of the test.

Figure 6-79 presents a graph of the steady-state roughness (± percent) as a function of chamber pressure. As shown, the worst-case roughness measured throughout the test program was ±20 percent. Because of the thrust degradation, the hardness ratio of the T/VA was increased, and therefore the roughness was decreased. The hardness ratio is defined as the injector pressure drop divided by the chamber pressure. As the hardness ratio is increased, it dampens any instability in the catalyst bed and limits the feed system from amplifying the instability. Since the roughness level measured during the steady-state life margin test was considerably lower than that measured during the performance mapping and in the early life portions, it is considered that the goal to demonstrate the life capability under rough operation was not demonstrated by this test.

During the test setup for the steady-state life margin test, a facility Statham pressure transducer was reinstalled on the T/VA. This had been removed during the performance mapping tests in order to minimize the holdup volume of the pressure measurement system. The steady-state life margin test then represents the first time that a check on the flight pressure transducer had been accomplished since the steady-state C_f mapping tests. Figure 6-80 presents a plot of the ratio of flight pressure transducer measurement divided by the test pressure transducer measurement. As shown, the RSS error for the entire test is equal to 1.013 percent. This is considered to be very good correlation and demonstrates the capability of the flight pressure transducer to accurately measure chamber pressure.

6.6 SURGE FLOW TEST

A surge flow test (water hammer simulation test) was conducted during the LCSSE/MJS development test program immediately after the thermal design verification test. The purpose of the test was to simulate the in-flight filling of the propellant feed system. Figure 6-81 presents a schematic of the approximate fuel line layout in vacuum chamber No. 1. The test was conducted by purging the hydrazine from the enable valve to the T/VA and then evacuating the line by opening

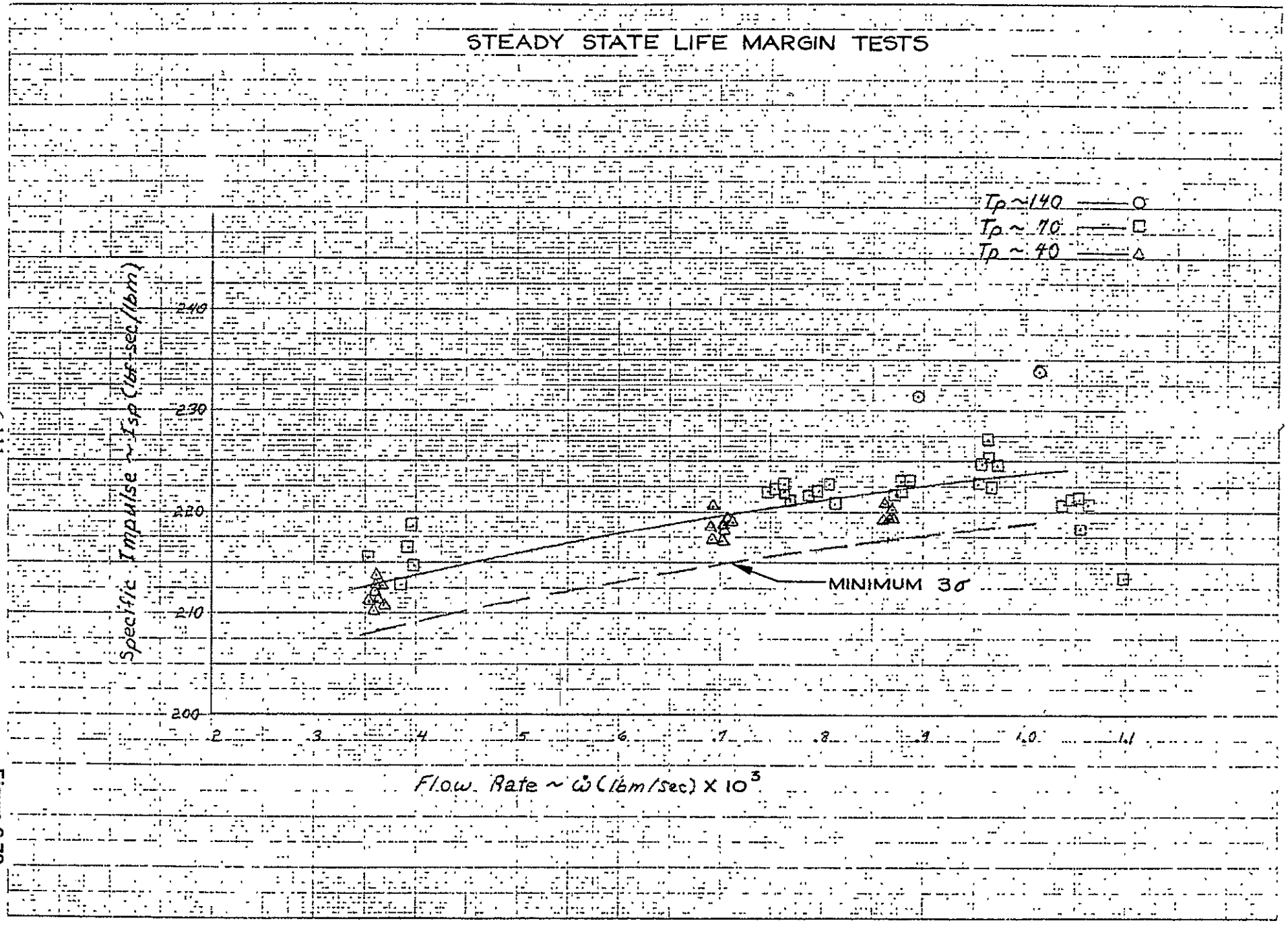
STEADY STATE LIFE MARGIN TESTS
Tp ~ 140
Tp ~ 70
Tp ~ 40
MINIMUM 3σ
Specific Impulse ~ Isp (lbf-sec/lbm)
240
230
220
210
200
2
3
4
5
6
7
8
9
1.0
1.1
Flow Rate ~ ẇ (lbm/sec) X 10^3

Figure 6-78

STEADY STATE LIFE MARGIN
Roughness (Ra)
20
15
10
5
0
0
50
100
150
200
250
300
350
Chamber Pressure ~ Test (Psia)

Figure 6-79

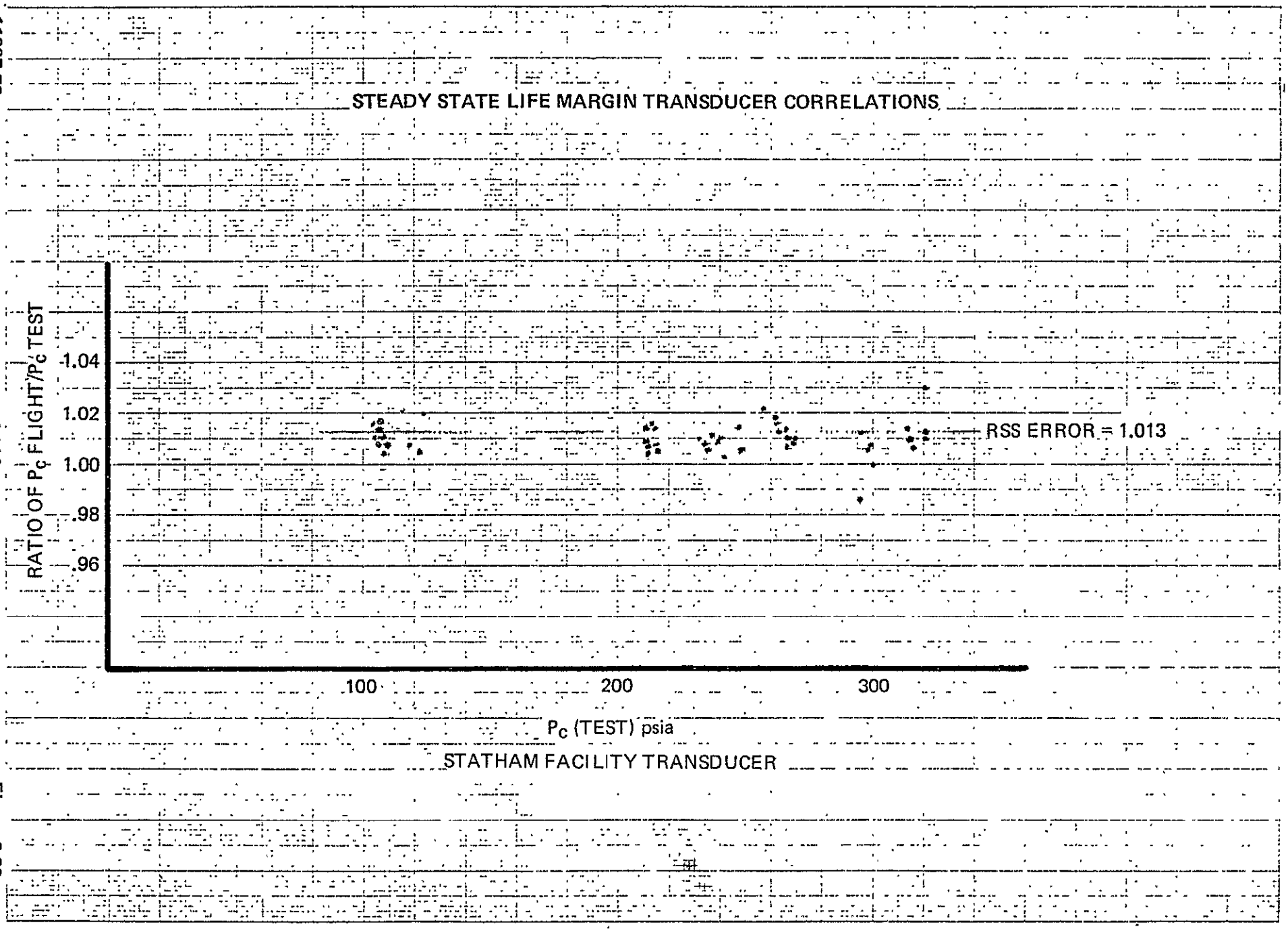
STEADY STATE LIFE MARGIN TRANSDUCER CORRELATIONS
RATIO OF P_c FLIGHT/P_c TEST
1.04
1.02
1.00
.98
.96
RSS ERROR = 1.013
100
200
300
P_c (TEST) psia
STATHAM FACILITY TRANSDUCER

Figure 6-80

APPROXIMATE FUEL LINE LAYOUT

VACUUM CHAMBER NO. 1

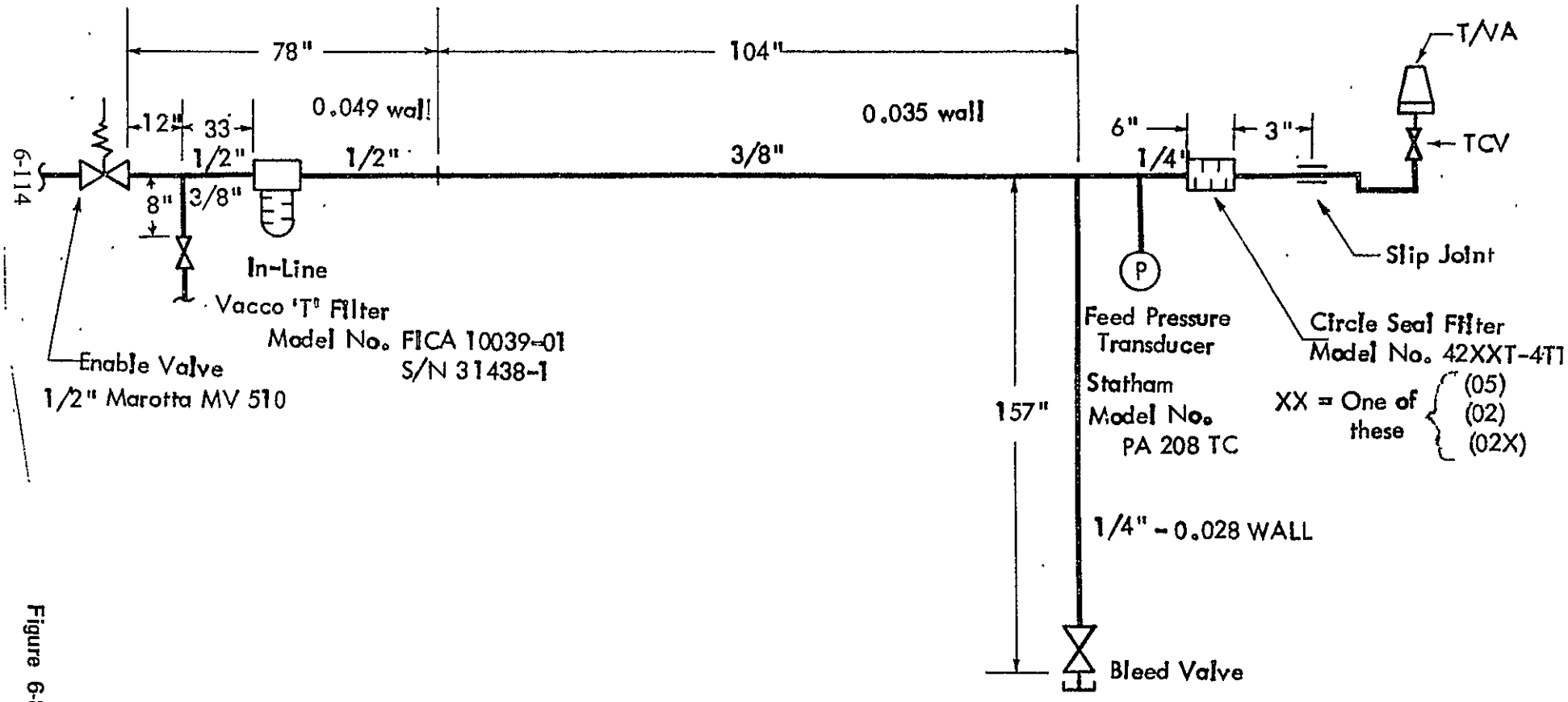

Figure 6-81

the T/VA to the vacuum environment. The T/VA valve was then closed, and the propellant cart was pressurized to 405 psig. The enable valve was then opened, and the feed pressure recorded near the inlet filter for the T/VA was monitored using the oscillograph. Figure 6-82 presents the results of the tests and shows the feed pressure oscillograph trace. The first initial rise in feed pressure occurred 750 milliseconds after the enable valve was opened. The maximum pressure could not be measured due to the limitations of the galvanometer; however, it is felt that it exceeded the desired 1,100 psi. The system was leak checked following the test, and there were no evidences of leakage. As discussed in Section 7.0 of this report, disassembly of the valve indicated that there was no damage to the valve inlet filter. The test was completely successful and demonstrates the T/VA design capability to withstand surge flows which could be expected during in-flight propellant feed system bleed-in.

6.7 MOMENTUM WHEEL DESATURATION TESTS

Momentum wheel desaturation test duty cycles were conducted with T/VA D02 for the LCSSE/MJS development test program. The goals of the test program were to establish life and life margin with the T/VA operating in the momentum wheel desaturation mode and to accumulate a total of 100 cold starts with a catalyst bed at a temperature of 40°F.

Table 6-22 presents a summary of the duty cycles for the momentum wheel desaturation mode, along with the feed pressures to be tested. The numbers shown in the columns directly under feed pressure refer to the test sequence number. Only test sequences which were tested are shown. The remaining test sequences, which are not shown, were not tested as a result of a failure mode which will be described in the following section. Approximately 42% of the life test was completed with an accumulation of 46 cold starts.

All the test duty cycles for the momentum wheel desaturation test were conducted in the automated mode. A general description of the procedure is presented in Section 4.0 of this report. The test sequences were manually controlled during the times when data was gathered, and propellant flow rate was measured. A failure was induced into the T/VA operation during Sequence 34 as a result of the sightglass valve being inadvertently left open and the tank valve left closed when switching from the manual mode back into the automated mode. As a result, after approximately 18 pulse trains, the propellant in the feed system was depleted. Approximately 2,000 1-second on/1-second off pulses were accumulated thereafter with a mixture of GN_2 and hydrazine. After discovery of the failure, the propellant feed system was rehardened and the tank valve opened and the duty cycle reinstituted. However, the pulse length and bed temperature reached at the end of each pulse train were considerably lower than the initial pulse train fired prior to the above failure. The test cell was returned to sea-level pressure, and inspection of the T/VA revealed that a catalyst particle was lodged in the nozzle throat. Review of the data indicated that this failure had also occurred concurrently with the above failure. The particle was removed from the throat using a small wire, and the T/VA was returned back into testing.

Sequences 26, 31, 30, and 21 were then tested after the first failure. A second failure occurred on July 28, 1975, when excessive roughness (±73%) and increased valve pressure drop caused the

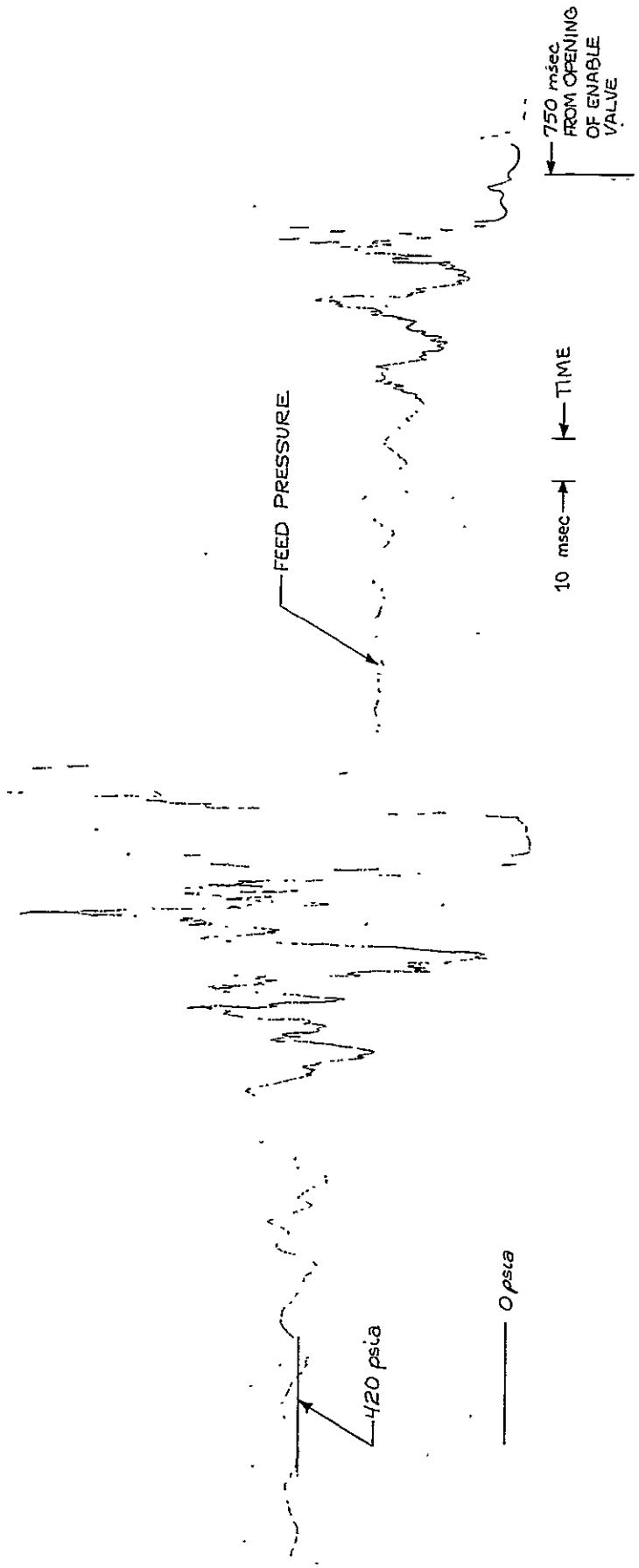

ORIGINAL PAGE IS
OF POOR QUALITY

Figure 6-82

Table 6-22

MOMENTUM WHEEL DESATURATION

TEST SUMMARY

DUTY CYCLE ON/OFF	FEED PRESSURE, Psia 420	350	280	210	140	70
1.0/10.0	1	12	23	34	45	___
0.02/10.0	2	13*(11)	24	___	___	___
0.05/2.0	3	14*	___	___	___	___
0.05/15	4	15*	26	___	___	___
0.075/0.525	5	16*	___	___	___	___
0.12/1.08	6	17*	___	___	___	___
0.50/0.55	7	18*	___	___	___	___
0.40/1.16	8 (8)	19*(12)	30*(15)	___	___	___
0.125/12.375	9	20*	31	___	___	___
1200/*	10	21	___	___	___	___
8.0/*	11*	22*	___	___	___	___

% Complete = $\frac{28}{66}$ = 42%

* No DDS Data taken

( ) Numbers in parenthesis indicate the total cold starts accumulated

NOTE: The sequences were conducted in the following order: 1,2,3,4,5,6,7,10,12,8, 23,9,11,20,16,17,13, 15,18,14,19,13,22,24,34, 34R, 26, 31, 30, 21

operation of the T/VA to "turn itself off". A flow check was made by monitoring the sightglass after the Pc had dropped to zero; and in fact no flow was present, indicating that engine washout was not the problem.

Analysis of the test data indicates the following results. Figure 6-83 presents a plot of the accumulated chamber pressure integral as a function of feed pressure for the momentum wheel duty cycle of 1 second on/10 seconds off. As shown, the T/VA was operating in a normal manner up through and including the first pulse train, Sequence 34. After the failure occurred in Sequence 34, accumulated impulse of each test duty cycle decayed from that expected. Figure 6-84 presents a plot of the chamber pressure integral as a function of pulse number for the first pulse train in Sequence 34 and for pulse train 247. Pulse train 247 occurred after the failure and after the propellant feed system was rehardened. Flow rate was also reduced for pulse train 247, as well as the chamber pressure integral. Pulse-mode c* remains the same at approximately 3,500 feet/sec, indicating that the lowered impulse was a result of an increased T/VA pressure drop rather than a shift in performance. Figure 6-85 presents an oscillograph trace of the pulses conducted during Sequence 26, which immediately followed Sequence 34. As shown, the pulses degraded from the first pulse train to the 55th pulse train, indicating that the pressure drop in the T/VA was continually increasing. Figure 6-86 presents a copy of the oscillograph trace for Sequence 45. During Sequence 45, the pulses did not degrade; however, they were significantly lower than the level expected as shown on the trace. Figures 6-87 and 6-88 present traces of the last sequence conducted with T/VA D01, Sequence 21. As shown, excessive roughness was occurring at this point in time; and at the termination of Pc, the T/VA was operating in a completely degraded mode. As stated earlier, the sightglass was monitored after the termination, and there was no indication of any propellant flowing through the T/VA while the thruster valve remained open.

Section 7.0 of this report presents a summary of the disassembly of this T/VA, and the primary conclusions drawn from the disassembly were that excessive voids existed, and the catalyst bedplate was completely blocked with catalyst particles. The following summary of the failure mode is drawn from the observations made during disassembly and the results of the reduced test data.

1. The operation of the T/VA with GN_2 during Sequence 34 initiated a void in the catalyst bed.
2. Further operation of the T/VA increased the void and caused blockage in the bedplate.
3. The blockage in the bedplate significantly altered the flow characteristics of the catalyst bed and, in turn, amplified the roughness problem.
4. The T/VA performance continued to drop after the initial failure in Sequence 34.
5. Excessive roughness during the last steady-state test, Sequence 21, caused the blockage in the catalyst bedplate to increase to such a level that the flow rate was lowered extensively. Additionally, the excessive roughness allowed backflow through the valve and subsequently caused the valve seat to expand thermally and therefore caused the no-flow condition exhibited at the end of the test.

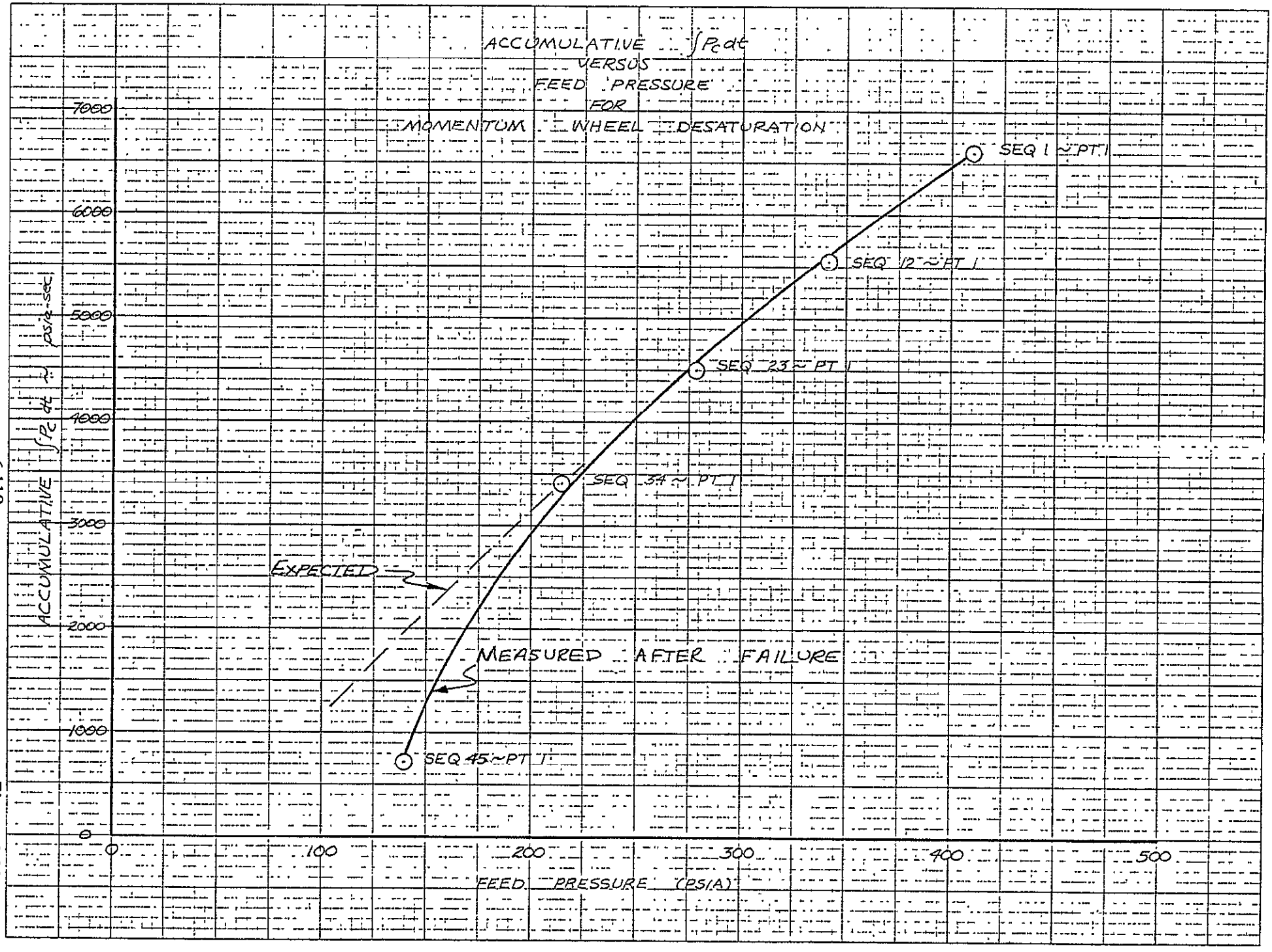
ACCUMULATIVE $\int P_c dt$
VERSUS
FEED PRESSURE
FOR
MOMENTUM WHEEL DESATURATION
SEQ 1 ~ PT 1
SEQ 12 ~ PT 1
SEQ 23 ~ PT 1
SEQ 34 ~ PT 1
SEQ 45 ~ PT 1
EXPECTED
MEASURED AFTER FAILURE
ACCUMULATIVE $\int P_c dt$ ~ psia-sec
7000
6000
5000
4000
3000
2000
1000
0
0
100
200
300
400
500
FEED PRESSURE (PSIA)

Figure 6-83

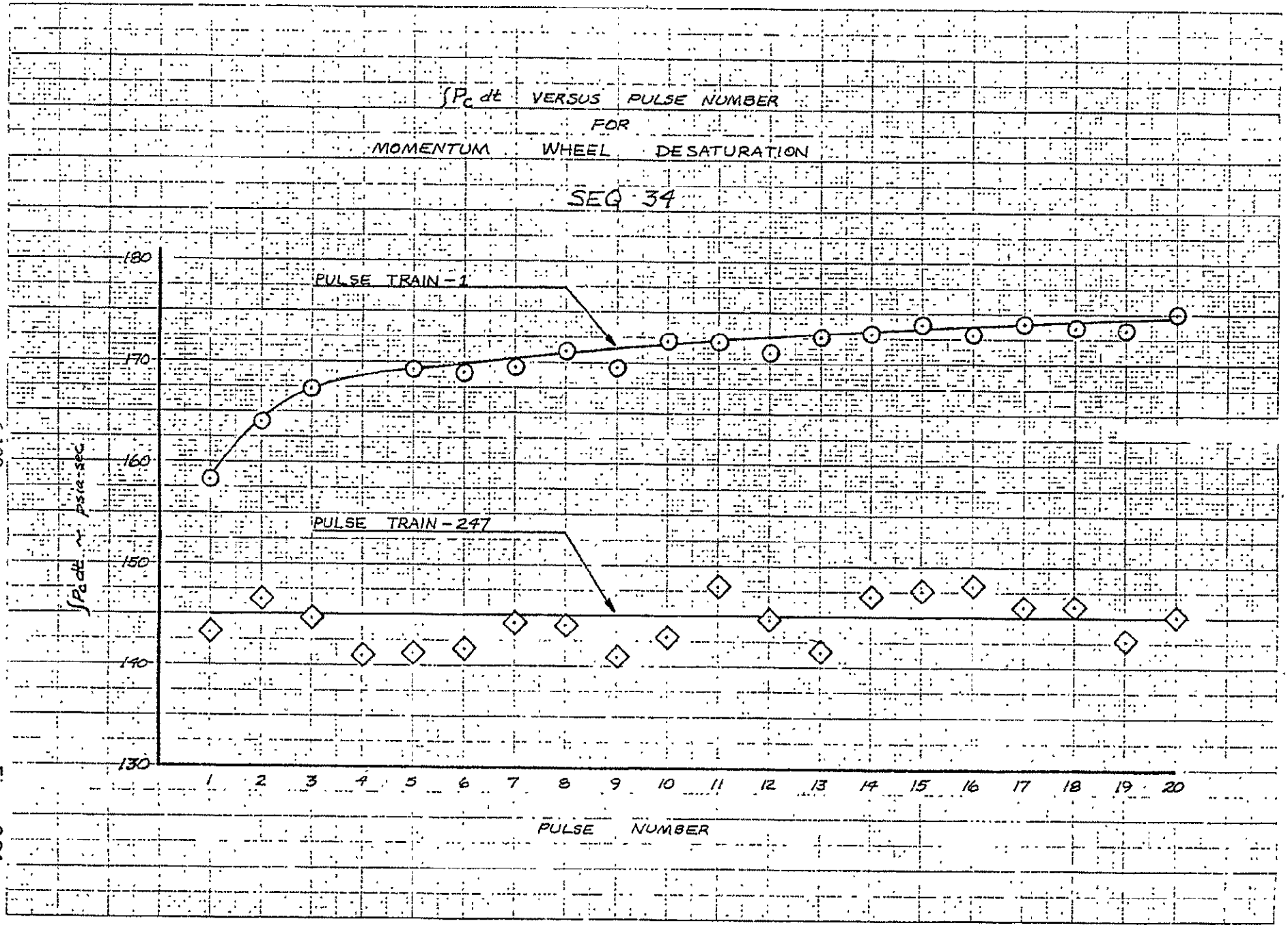
$\int P_c\,dt$ VERSUS PULSE NUMBER
FOR
MOMENTUM WHEEL DESATURATION
SEQ 34
PULSE TRAIN – 1
PULSE TRAIN – 247
$\int P_c\,dt \sim$ psia-sec
180
170
160
150
140
130
1 2 3 4 5 6 7 8 9 10 11 12 13 14 15 16 17 18 19 20
PULSE NUMBER

Figure 6-84

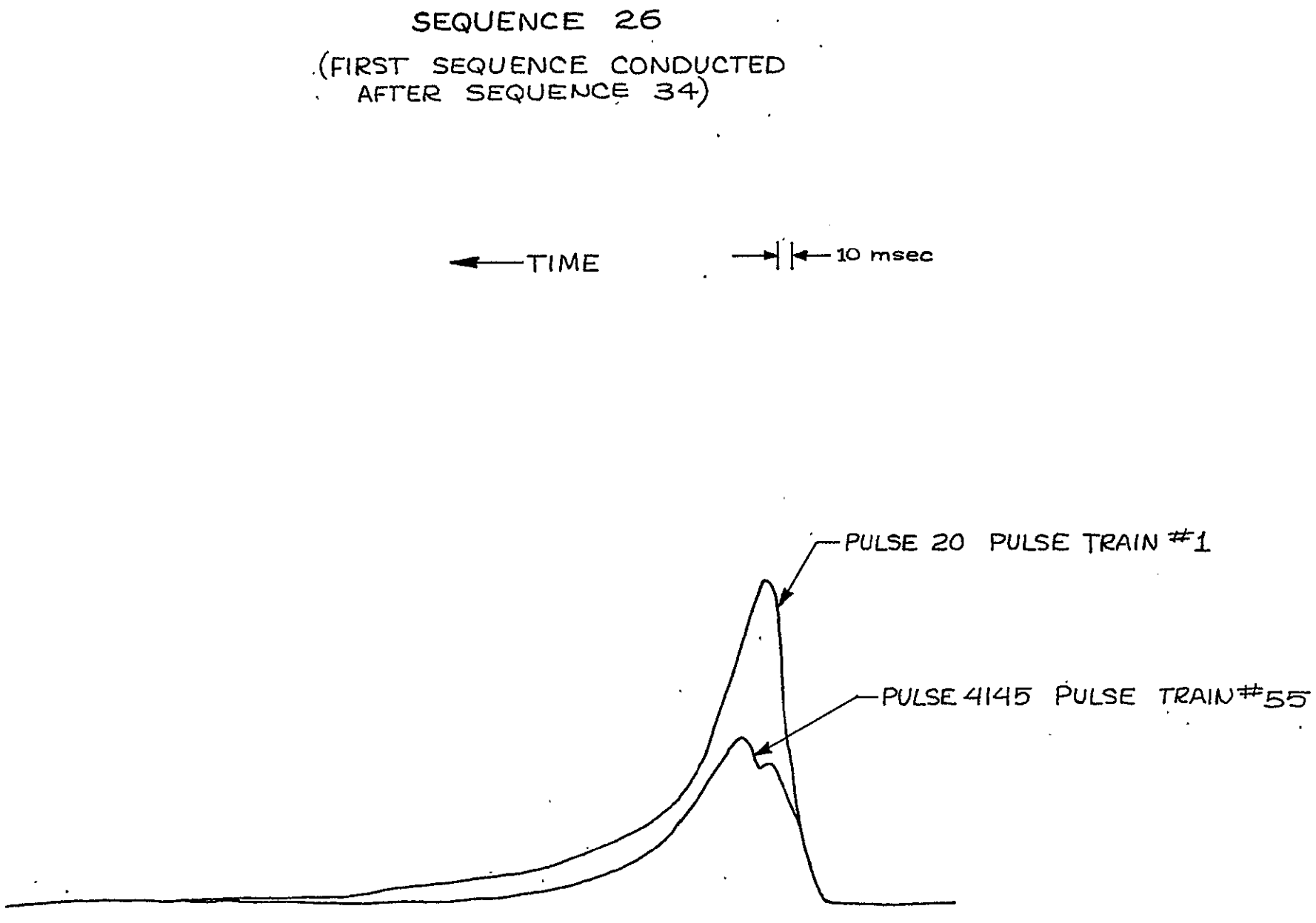
SEQUENCE 26
(FIRST SEQUENCE CONDUCTED
AFTER SEQUENCE 34)
TIME
10 msec
PULSE 20 PULSE TRAIN #1
PULSE 4145 PULSE TRAIN #55

Figure 6-8

SEQUENCE 45
PULSE 6/60
PULSE TRAIN 309

Figure 6-86

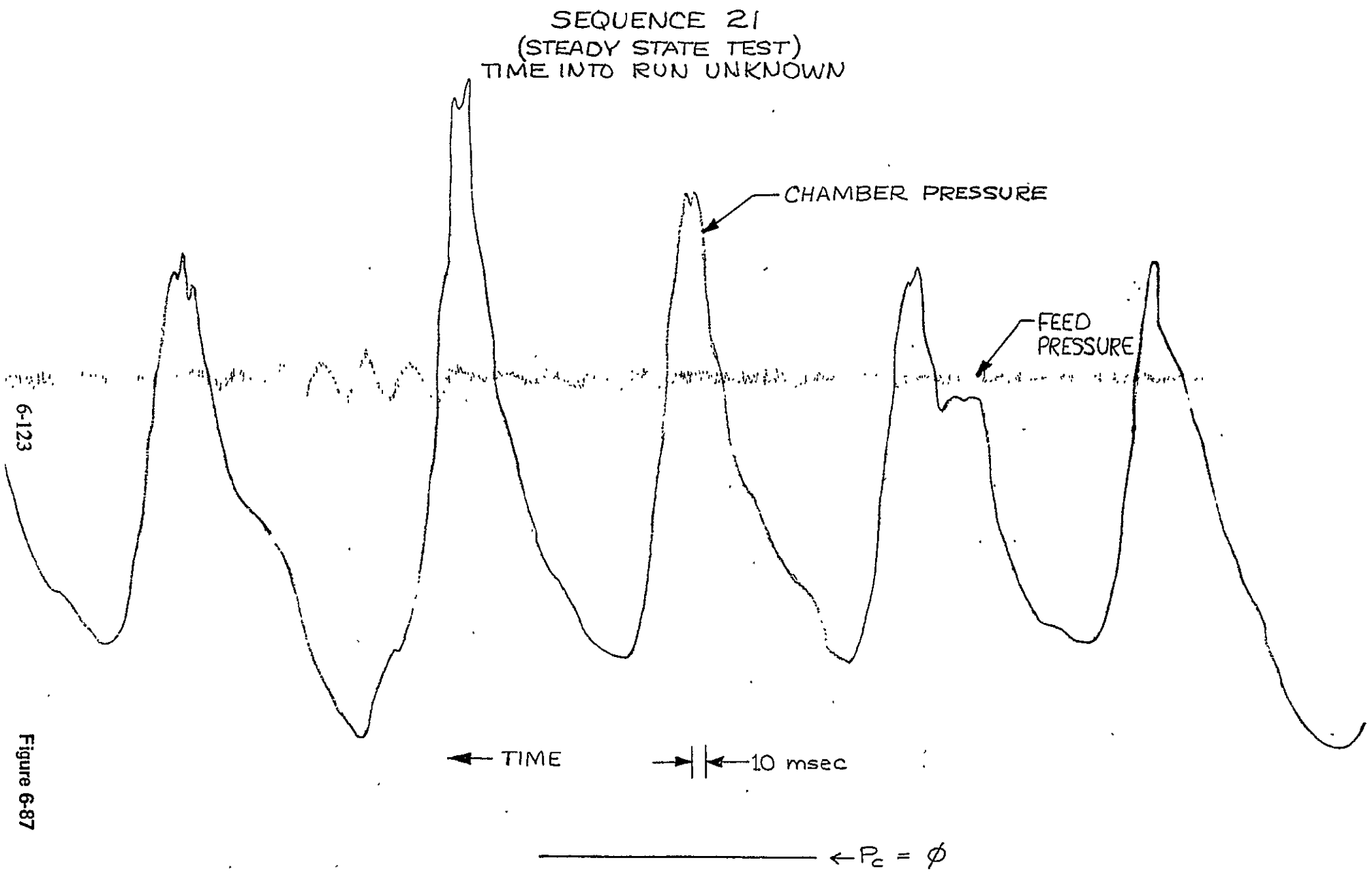
SEQUENCE 21
(STEADY STATE TEST)
TIME INTO RUN UNKNOWN
CHAMBER PRESSURE
FEED PRESSURE
TIME
10 msec
$P_c = \phi$

Figure 6-87

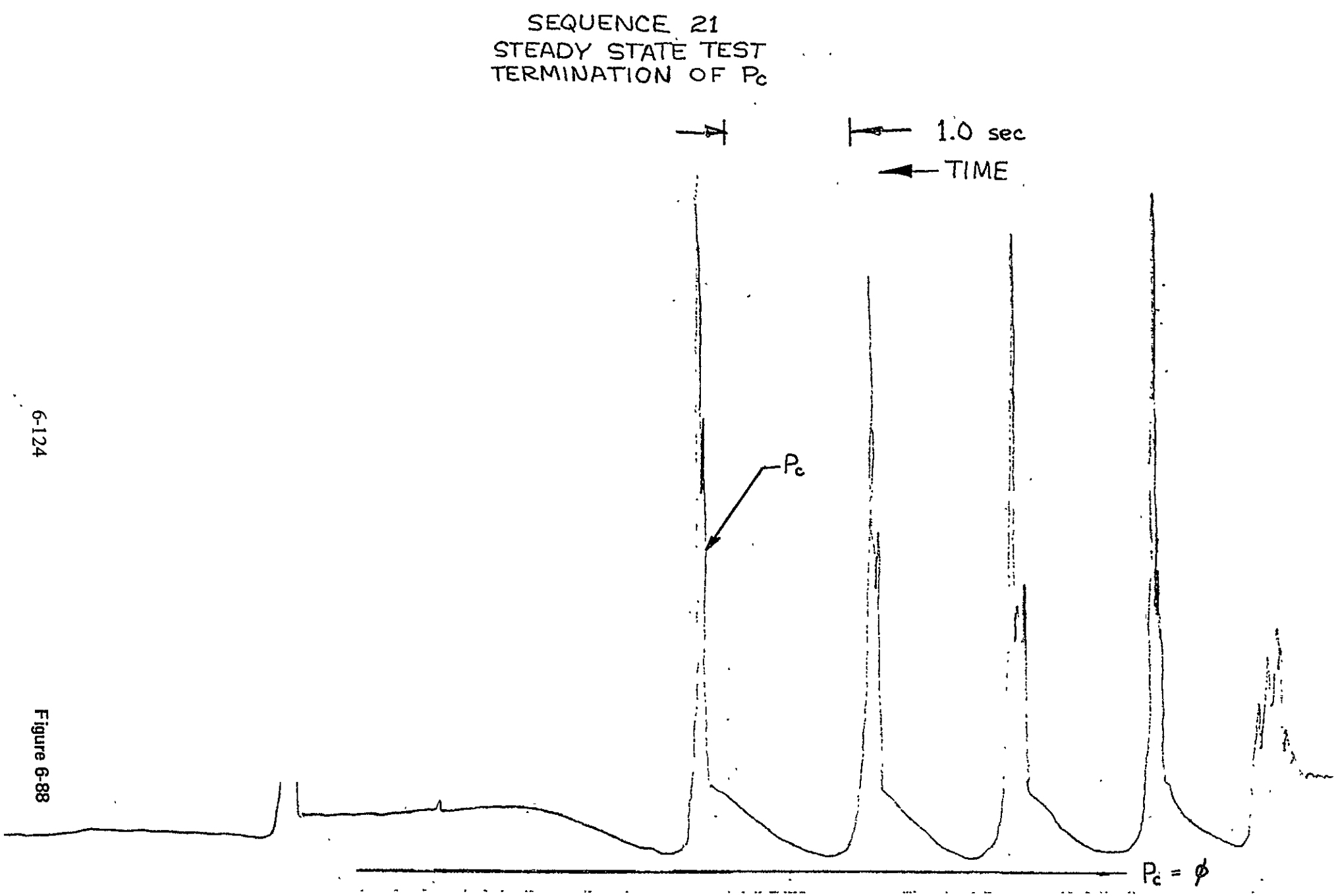
SEQUENCE 21
STEADY STATE TEST
TERMINATION OF Pc
1.0 sec
TIME
Pc
Pc = ϕ

Figure 6-88

6.8 FUNCTIONAL CHECKOUTS

Functional checkout tests with the T/VA components were conducted periodically throughout the development test program to ensure that the T/VA and components survived the environmental testing. A description of these tests and their locations is presented in the test flow diagram for both T/VA's D01 and D02 in Section 2.0 of this report.

All components successfully passed the environmental tests, and the results are presented in Tables 6-23 through 6-29. A problem was encountered with the final GN_2 flow resistance check conducted on both T/VA's D01 and D02. As indicated for D01, there was no flow; and the flow was degraded for D02. The measurement was conducted on T/VA D01 after vibration margin testing was completed and after the entire development firing test program had been completed. The results of the disassembly indicated that the injector was blocked. It is believed that this blockage is caused by catalyst fines which migrated into the injector during the vibration margin test. The low flow measured on T/VA D02 was also caused by an increase in reactor pressure drop. It is believed that the increase in the T/VA resistance was caused largely by the blockage in the catalyst bed retaining plate. The reader is referred to Section 7.0 of this report for a complete description of the disassembly.

Table 6-23

FUNCTIONAL CHECKOUT SUMMARY

Continuity Valve Pull-In And Drop-Out

And

Pressure Transducer Checkout

	T/VA D01			T/VA D02		
	ATP		Development	ATP		Development
	Pre-Fire	Post-Fire	App. G	Pre-Fire	Post-Fire	App. G
Continuity to GR (ohms)						
Connector J - 1	0.093	0.098	0.148	0.096	0.096	0.104
Connector J - 2	0.199	0.198	0.253	0.193	0.198	0.213
Valve Pull-In (vdc)	--	9.3	9.5	--	11.3	11.7
Valve Drop-Out (vdc)	--	2.65	2.9	--	4.4	4.7
Pressure Transducer Checkout			(App. E)			(App. E)
Output (vdc) at 0 psig	--	0.22	0.228	--	0.18	0.18
Output (vdc) at 335 psig	--	2.96	2.963	--	2.90	2.90
Power Consumption (milliwatts)	--	331.8	321.0	--	278.7	272.0

Table 6-24
FUNCTIONAL CHECKOUT SUMMARY

	T/VA D01			T/VA D02		
	ATP		Development	ATP		Development
	Pre-Fire	Post-Fire		Pre-Fire	Post-Fire	
Internal Leakage			(App. E)			(App. E)
50 psig	0	0.12	0	0	0	0
420 psig	0	0	0.6	0	0	0
($\leq$1 scc/hr)						
External Leakage			(App. F)			(App. F)
($\leq 5 \times 10^{-5}$ scc/hr of He)	0	9×10^{-9}	0	0	4.2×10^{-8}	3.97×10^{-7}

Table 6-25

FUNCTIONAL CHECKOUT SUMMARY

GN_2 FLOW RESISTANCE

	T/VA D01		T/VA D02	
	5 psig	10 psig	5 psig	10 psig
BUILD				
F&A-0174	63	-	61	-
ATP PRE FIRE	63	95	62	94
POST FIRE	63	94	59	93
DEVELOPMENT (AppE)				
After structural tests (Prior to firing Cf)	100	92	66	97
DISASSEMBLY	0	0	17	28

Table 6-26

FUNCTIONAL CHECKOUT SUMMARY

Component Electrical Resistance, Ohms

T/VA D01

COMPONENT	BUILD F&A 174	ATP		DEVELOPMENT APP. G
		Pre-Fire	Post-Fire	
Valve				
Pins C - P	207.3	207.1	207.8	206.6
D - R	207.2	207.1	207.8	206.6
Temperature Sensor				
Pins H - J	547.8	547.0	550.0	547.6
M - L	547.6	547.0	550.0	548.5
Thruster Heaters				
Pins U - K	566.9	567.0	576.0	576.8
V - N	569.7	570.0	579.0	579.3
Valve Heaters				
Pins S - F	5266.0	5260.0	5280.0	5259.0
T - G	5274.0	5270.0	5290.0	5268.0
Temperature	69°F	69°F	71°F	74°F

Table 6-27

FUNCTIONAL CHECKOUT SUMMARY

Component Electrical Resistance, Ohms

T/VA D02

COMPONENT	BUILD F&A 174	ATP		DEVELOPMENT App. G
		Pre-Fire	Post-Fire	
Valve				
Pins C - P	206	207.1	206.2	206.3
D - R	206	207.1	206.2	206.3
Temperature Sensor				
Pins H - J	548	547.0	549.0	550.0
M - L	547	547.0	549.0	550.0
Thruster Heaters				
Pins U - K	565	567.0	575.0	575.9
V - N	563	570.0	573.0	573.4
Valve Heaters				
Pins S - F	5310	5260.0	5320.0	5335.0
T - G	5310	5276.0	5320.0	5333.0
Temperature	70°F	69°F	71°F	76°F

Table 6-28
FUNCTIONAL CHECKOUT SUMMARY

INSULATION RESISTANCE (>100 MEGOHMS)

T/VA D01

Component and/or Circuit to Circuit		ATP Post Fire	Development Appendix G (Pre-Fire)
Valve to G_R @ 500 vdc		20K	30K
Temperature Sensor to G_R @ 50 vdc		19K	100K
Valve Heater to G_R @ 50 vdc		15K	150K
Thruster Heater to G_R @ 50 vdc		15K	2.5K
Pressure Transducer to G_R @ 50 vdc		60K	100K
Pins	to Pins @ 50 vdc		
P, R, C, D	H, M, J, L	400K	20K
P, R, C, D	S, F	300K	22K
P, R, C, D	T, G	300K	24K
P, R, R, D	U, K	350K	21K
P, R, C, D	V, N	250K	20K
H, M, J, L	S, F	250K	50K
H, M, J, L	T, G	90K	20K
H, M, J, L	U, K	150K	20K
H, M, J, L	V, N	150K	22K
S, F	T, G	190K	100K
S, F	U, K	260K	150K
S, F	V, N	190K	200K
T, G	U, K	120K	160K
T, G	V, N	120K	110K
U, K	V, N	160K	7K

Table 6-29

FUNCTIONAL CHECKOUT SUMMARY

INSULATION RESISTANCE (>100 MEGOHMS)

T/VA D02

Component and/or Circuit to Circuit	ATP Post Fire	Development Appendix G (Pre-Fire)
Valve to G_R @ 500 vdc	15K	22K
Temperature Sensor to G_R @ 50 vdc	15K	40K
Valve Heater to G_R @ 50 vdc	15K	40K
Thruster Heater to G_R @ 50 vdc	800K	20K
Pressure Transducer to G_R @ 50 vdc	700K	200K
Pins to Pins @ 50 vdc		
P, R, C, D — H, M, J, L	400K	80K
P, R, C, D — S, F	300K	75K
P, R, C, D — T, G	300K	85K
P, R, R, D — U, K	350K	50K
P, R, C, D — V, N	250K	55K
H, M, J, L — S, F	250K	60K
H, M, J, L — T, G	90K	48K
H, M, J, L — U, K	150K	50K
H, M, J, L — V, N	150K	50K
S, F — T, G	190K	100K
S, F — U, K	260K	100K
S, F — V, N	190K	110K
T, G — U, K	120K	65K
T, G — V, N	120K	70K
U, K — V, N	160K	90K

7.0 DISASSEMBLY RESULTS

This section presents the disassembly results for the LCSSE/MJS development program. The section is subdivided to discusss the two T/VA's, D01 and D02.

7.1 DISASSEMBLY OF T/VA D01

T/VA D01 was completely disassembled; however, prior to this disassembly, the unit was examined, and there was no apparent exterior damage to any of the parts. Also a gaseous nitrogen flow resistance check was conducted, and there was no indication of flow at either 5 or 10 psig. Upon disassembly of the valve and injector interface, it was observed that the inner O-ring was extruded between the injector and the valve surfaces. There was no damage to the outer O-ring. Figures 7-1 and 7-2 present photographs of the injector interface and the valve interface, respectively. The dark circular ring around the injector inlet screen, shown in Figure 7-1, represents extruded rubber which was pinched between the two interfaces. In Figure 7-2, the extrusion of the O-ring is easily seen at the outer perimeter of the inner O-ring. Measurement of the valve and injector interfaces indicated that metal-to-metal contact existed between the valve outlet and the injector inlet, providing minimum holdup volume. This area of contact is inside the inner O-ring; and in Figure 7-2, two pieces of wire from the injector inlet screen remained attached to the valve interface.

Approximately 1.78 grams of catalyst were removed from the catalyst bed. This represents an 8% loss over the amount packed during T/VA buildup. However, the nozzle popped off during the disassembly in the lathe, allowing catalyst to fall out. Therefore, it is not necessarily representative of the true loss in catalyst caused by the extensive development testing. The bedplate was observed to have catalyst trapped in the slots, and the approximate blockage of flow area was equal to 40%.

As stated earlier, the GN_2 flow resistance check indicated no flow. The injector cap tube was then checked after disassembly of the valve and removal of the catalyst, and it had to be unplugged using high pressure nitrogen and inserting a 0.007-diameter wire into the outlet. The injector was then subjected to a waterflow calibration, and the results are presented in Figure 7-3. An increase in pressure drop of 19 psid was observed at a flow rate of 0.00095 lbm/sec. This flow rate corresponds to the design thrust level of 0.2 lbf. The increase in pressure drop would cause an approximate drop in chamber pressure equal to 9 psi, which represents a 3% loss in thrust. The T/VA valve was also flow calibrated using water, and the results are presented in Figure 7-4. An increase in pressure drop equal to 0.5 psid was observed at the design flow rate of 0.00095 lbm/sec. This increase in valve pressure drop is considered insignificant and would not affect the overall operational thrust level. The throat diameter of the nozzle was measured upon disassembly and was equal to 0.0228 inch, which repeats precisely the value measured during assembly.

After removal of the catalyst, the injector screens were observed to have large deposits of fine material causing blockage of the flow area. A photograph of the injector outlet is presented in Figure 7-5. The screens were removed and sent to the University of Washington to be analyzed using

T/VA D01 INJECTOR INLET

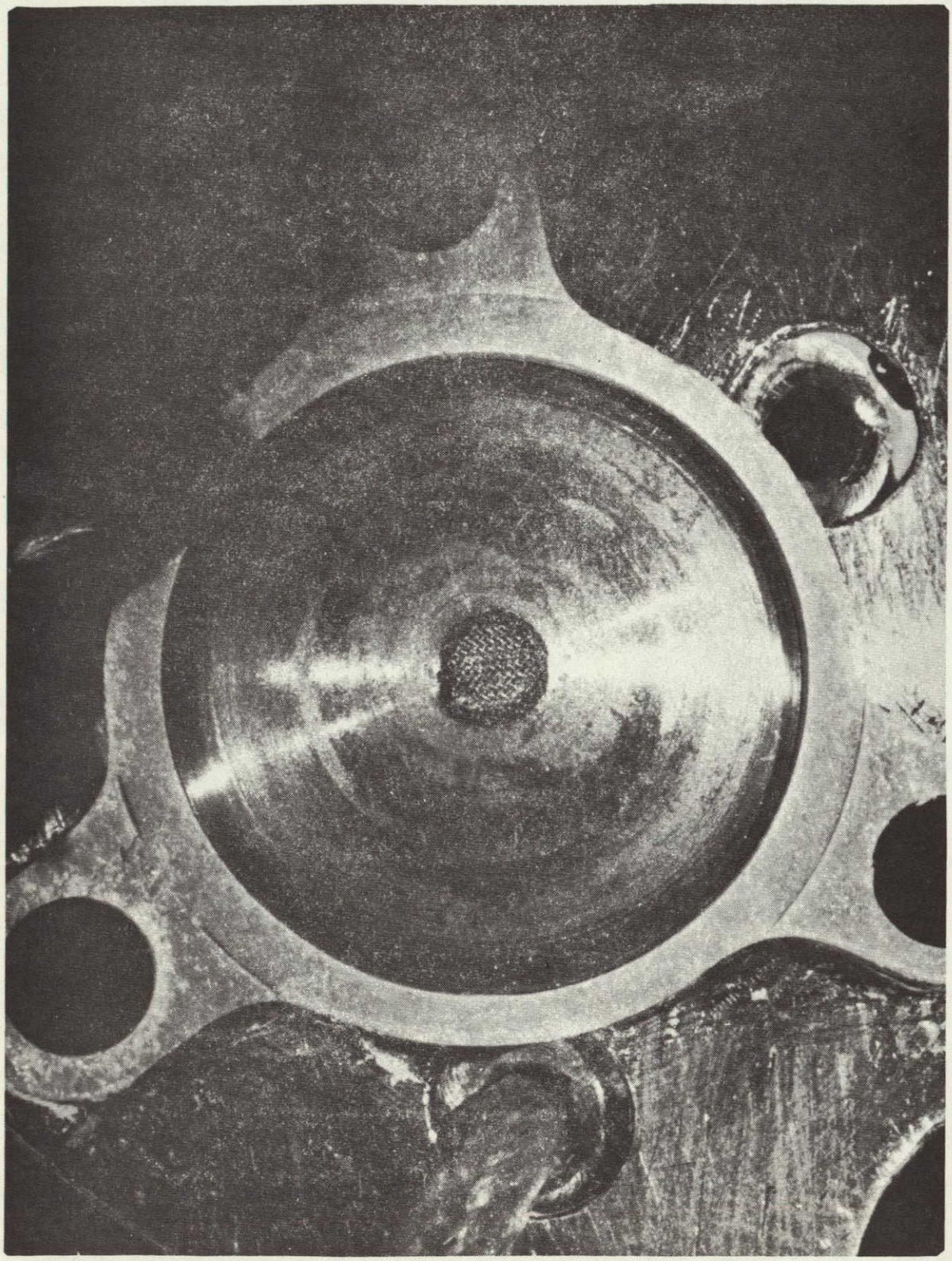

T/VA D01 VALVE OUTLET

Figure 7-2

MTS/LCSSE 0.2 1/4 T/UM DO1 (S/N002)
WATER FLOW CALIBRATION

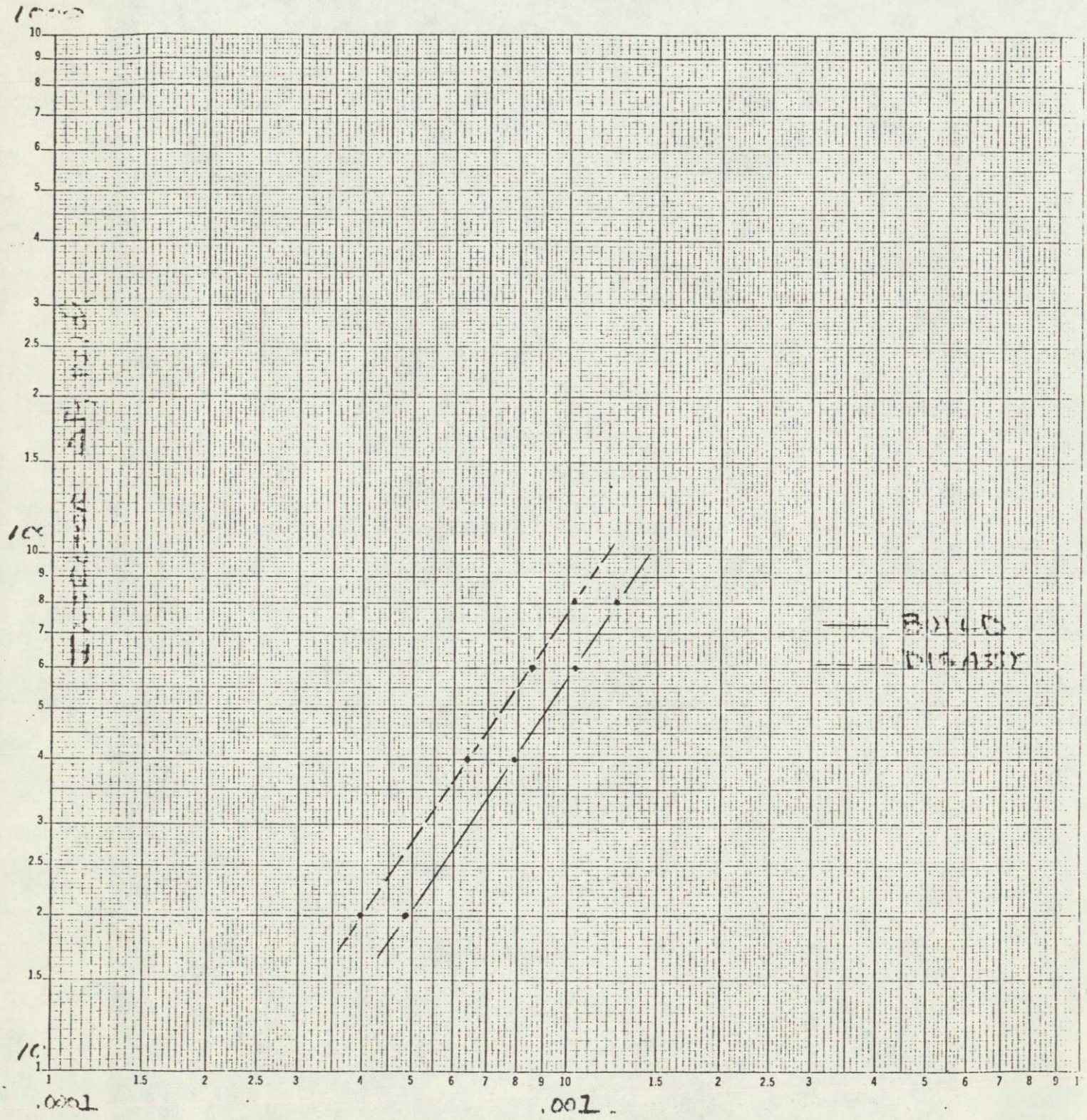

Figure 7-3

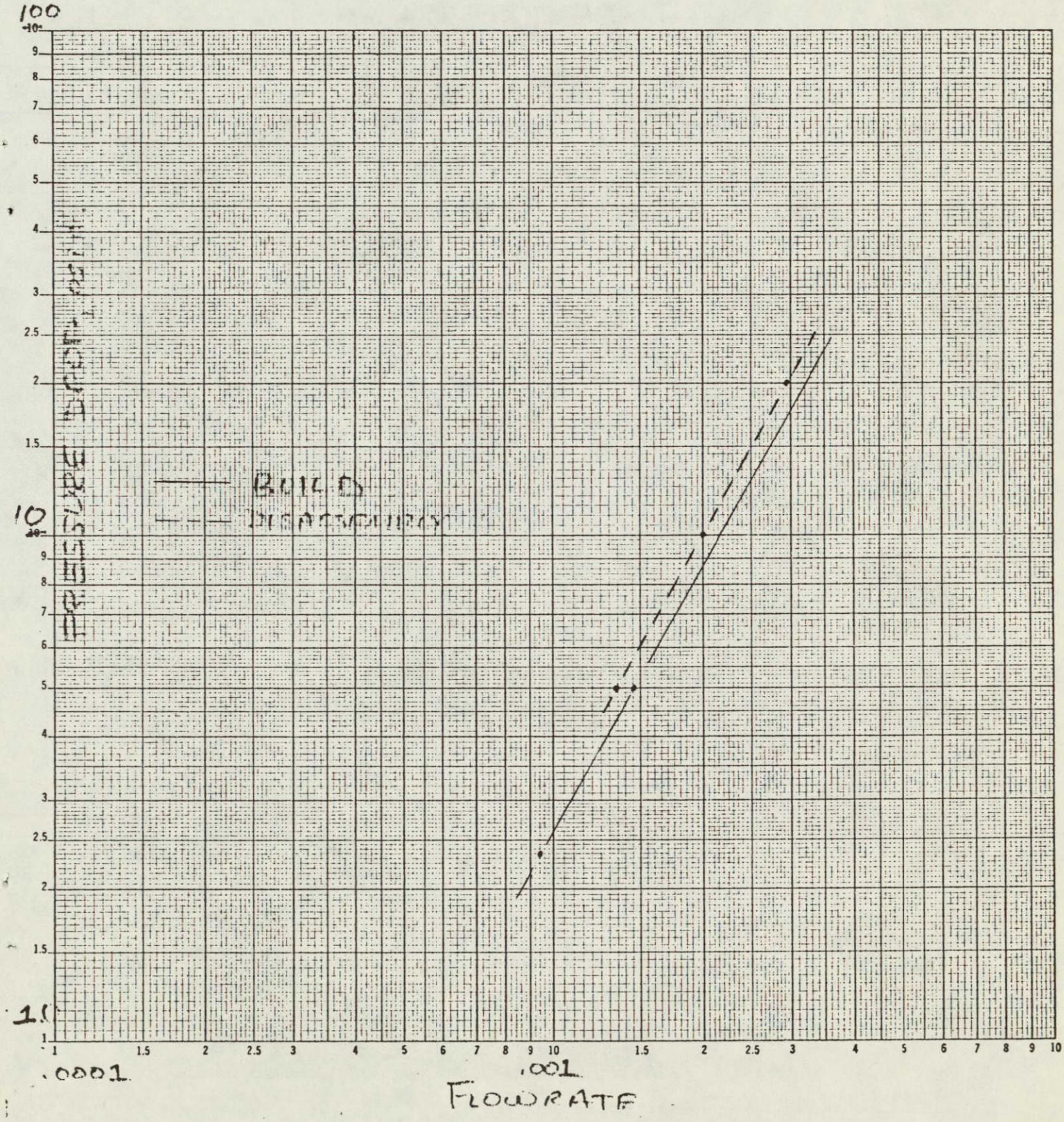
MSS/LCSSF 0.2 1/4 T/NA D07
VALVE WATER FLOW CALIBRATION
100
10
1.0
.0001
.001
FLOWRATE

Figure 7-4

T/VA D01 INJECTOR OUTLET SCREENS

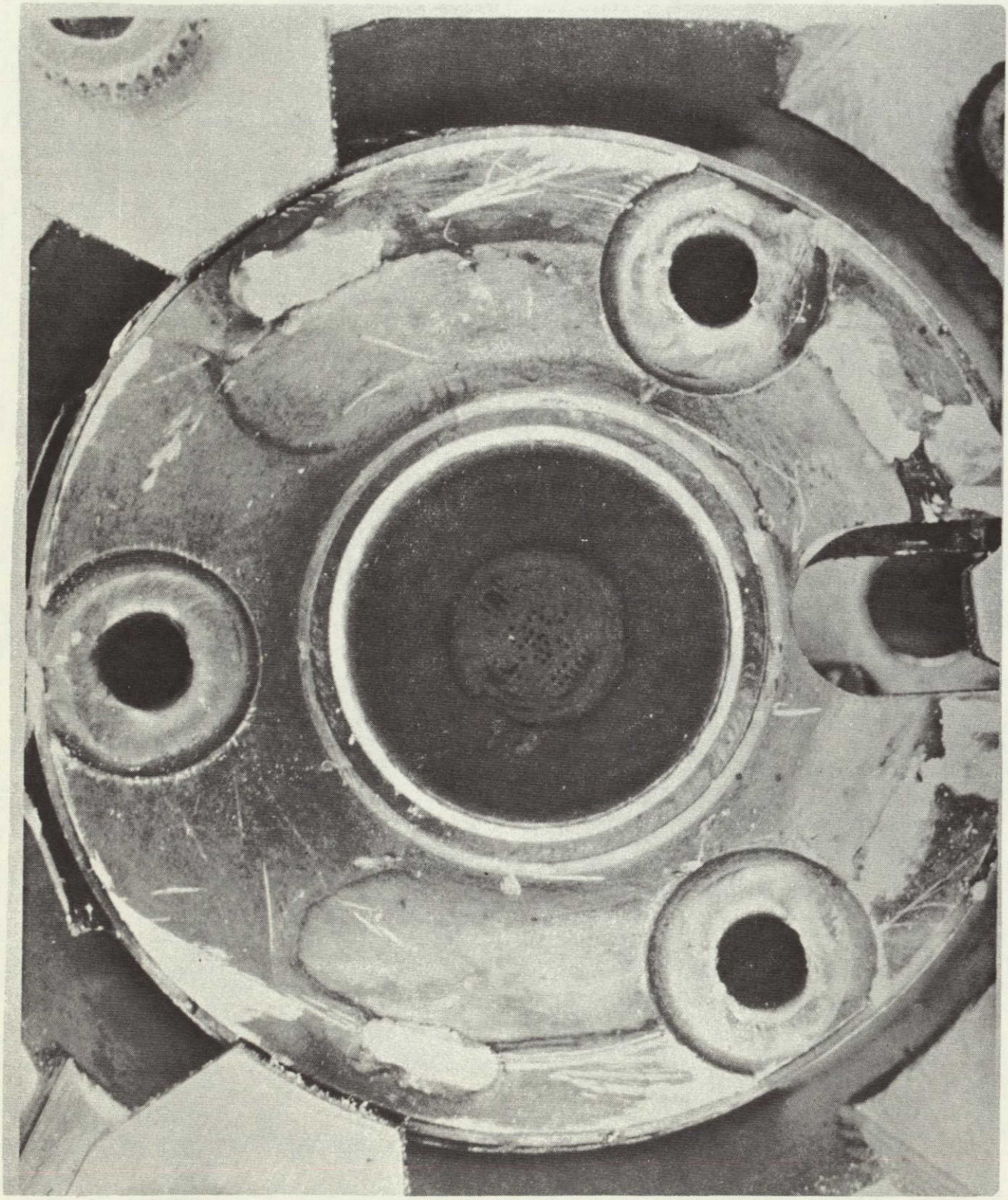

the SEM/EDAX machine. Two screens are assembled into the injector during buildup, and both screens were removed during the disassembly. The upstream screen, that is, the screen closest to the injector outlet, was studied using the EDAX equipment. Figure 7-6 presents a photograph of the upstream side of this screen, and Figure 7-7 presents a photograph of the downstream side. Preliminary investigation of this material that is shown deposited on the screens indicated that it was mainly catalyst; however, this analysis was conducted in one of the smoother areas, shown in Figure 7-7. Further analysis was directed and was localized in the rougher portions of the deposit shown in Figure 7-6. This analysis yielded a very high concentration of iron. Figure 7-8 presents a photograph of the EDAX output and shows that the ratio of iron is a great deal higher than the apparent screen material, which is Haynes 25. It was concluded that the reason the initial investigation showed nothing but catalyst was that the area was coated with fines caused by the vibration margin tests, which were completed after all of the performance testing during the development program. It is further postulated that these fines also caused the plugging of the cap tube which was noted prior to disassembly; however, the large amounts of iron shown on both the upstream and downstream screens, combined with the increased ΔP measured during disassembly, indicate that iron is depositing in that local area and can potentially cause a large thrust degradation to occur in T/VA's with large amounts of propellant throughput. As stated in Section 6.0, a total of 156 pounds of propellant was used during the steady-state life margin development test. The propellant that was used for this test was analyzed, and the results are shown in Figure 7-9. As noted, the iron content is less than 0.1 ppm using the atomic absorption technique. This is well within the requirement of 20 ppm and indicates that further controls are necessary for the iron content for use with the LCSSE/MJS T/VA. This confinement is necessary only if large throughputs of hydrazine will be placed through an individual thruster. For most spacecraft usage, the effects would be negligible.

The D01 T/VA valve was also disassembled completely. Prior to this disassembly, the stroke was measured and was equal to 0.0068 to 0.0070. Additionally, the pull-in and drop-out voltage were measured prior to cut-apart, and the results are presented in Figure 7-10. A cross section of the valve is presented in Figure 7-11 for reference.

During the removal of the end cap, difficulty occurred as a result of binding in the threads. As a result, some metallic particles were generated. Observations made of the valve seat material indicated that there was contamination present; however, there was a good nozzle impression. Areas with blackish stains on the end cap and mating spacer were observed, along with stains on the armature spacer and housing. One spherical metallic particle was noted on the housing face. There was some EDM material in the slots on the back side of the armature; however, the material was securely attached to the armature. It must be noted that the armature on the production units does not have an EDM surface finish. The body face revealed evidences of pounding by the armature EDM'd surface.

Removal of the thruster valve filter indicated excellent appearance. As noted earlier in Section 6.0, this was the filter that was subjected to the surge flow test. No signs of filter collapse were apparent.

UPSTREAM VIEW OF THE UPPER INJECTOR SCREEN

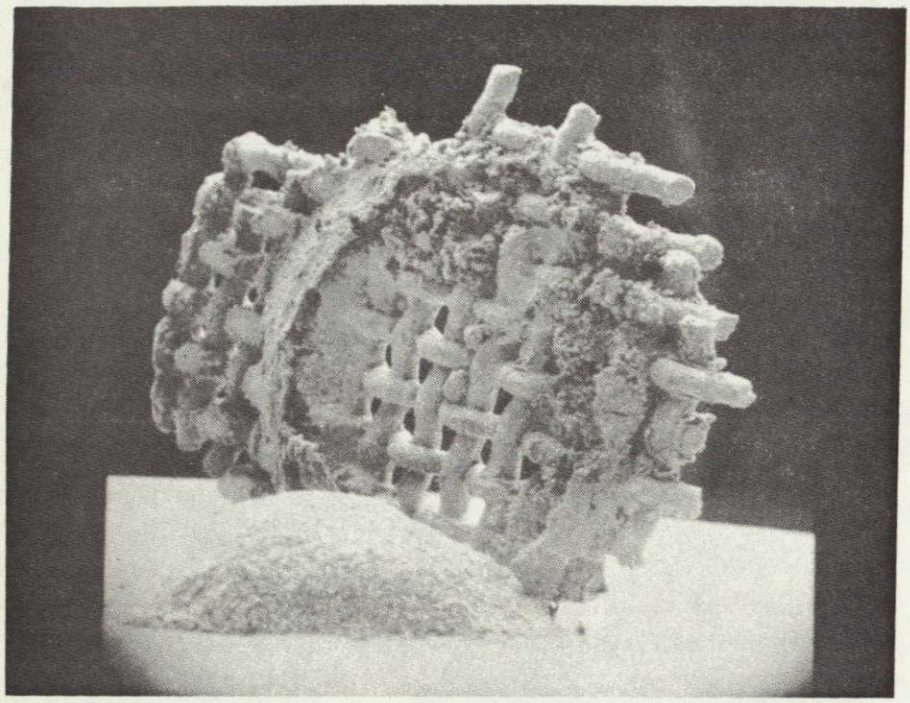

Figure 7-6

DOWNSTREAM VIEW OF THE UPPER INJECTOR SCREEN

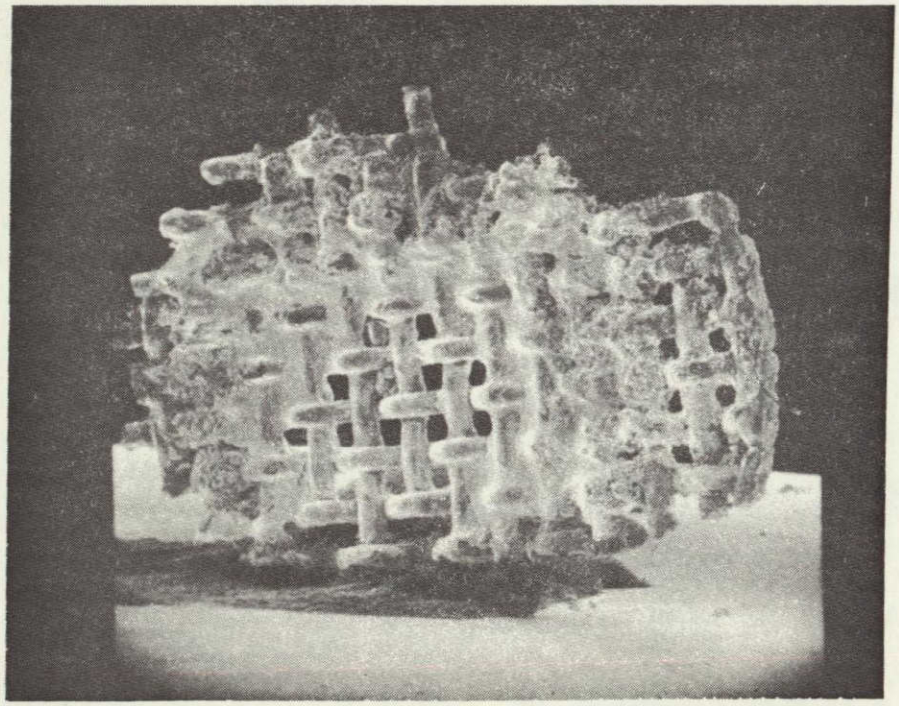

Figure 7-7

SEM/EDAX ANALYSIS RESULTS FOR THE MATERIAL
DEPOSITED ON THE INJECTOR SCREENS

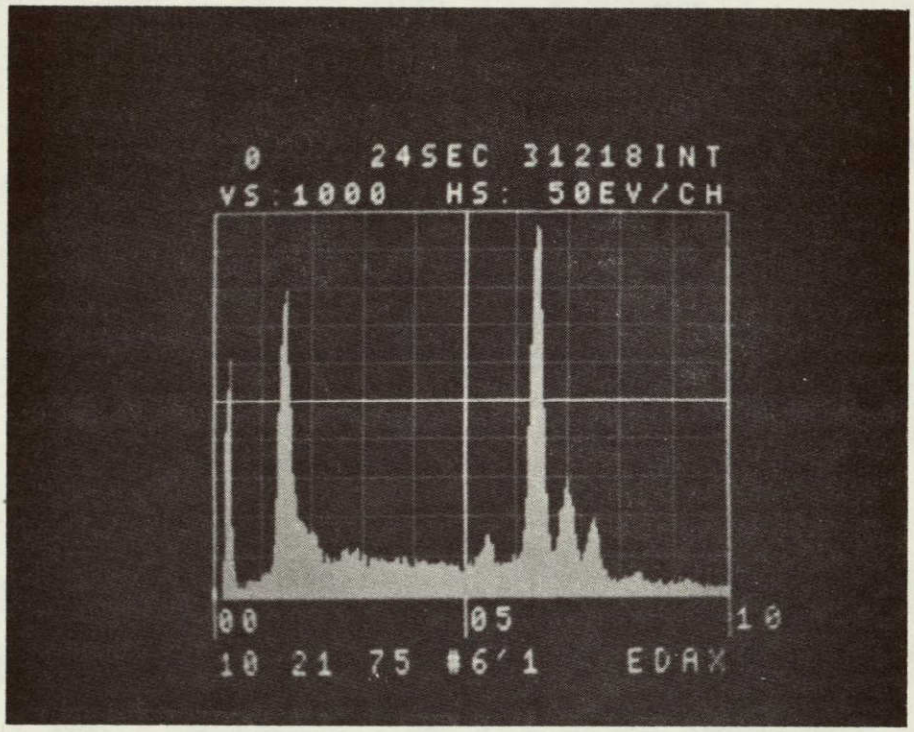

PROPELLANT ANALYSIS USED DURING STEADY-STATE LIFE MARGIN TESTS

HYDRAZINE ANALYTICAL FORM
FOR HYDRAZINE MEETING MIL-P-26536, AMENDMENT 1

AF-38

TEST	RESULTS	METHOD	DATE	ANALYST
a. N_2H_4	98.79 %	Gas Chromatograph	6/24/75	J.C.
b. NH_3	0.10 %	Gas Chromatograph	6/24/75	J.C.
c. H_2O	0.74 %	Gas Chromatograph	6/24/75	J.C.
d. Trace Organics	Toluene 12 ppm	Gas Chromatograph—FID	6/24/75	J.C.
e. Aniline	0.35 %	U.V. Spectrophotometer	6/24/75	J.U.
f. Non-Volatiles	0.0002 %	Rotavapor Evaporator	6/24/75	J.C.
g. Particulate	0 mg/l	Millipore Filter	6/24/75	J.C.
h. Corrosivity	0.5 ppm Fe	Vis. Spectrophotometer	6/24/75	J.E.M.
i. Chloride	2.8 ppm	Vis. Spectrophotometer	6/24/75	J.C.
j. Iron	<0.1 ppm	Atomic Absorption	6/24/75	J.C.
k. CO_2	<2.0 ppm	Gas Chromatograph	6/24/75	J.C.
l. Silicon (optional)	ppm	Atomic Absorption		

ANALYSIS COMPLETED AND REVIEWED:

DATE: 6/25/75

SIGNATURE: J. Mars

Figure 7-9

0.2-lbf LCSSE VALVE RUN NO. 2

P/N 26958-501-11 S/N 002

Figure 7-10

CROSS SECTIONAL VIEW OF THE T/VA VALVE

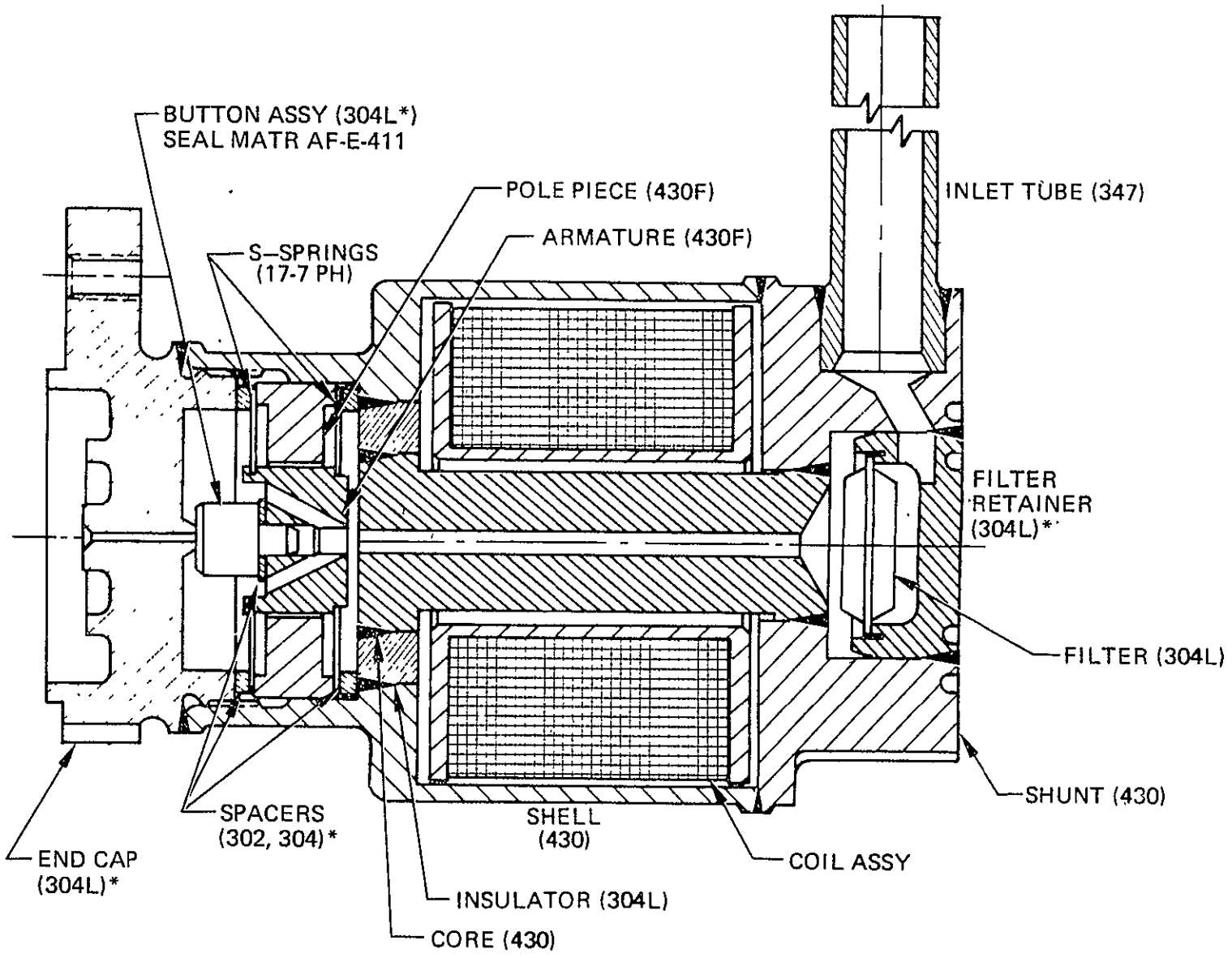

Figure 7-11

7.2 T/VA D02 DISASSEMBLY

Examination of T/VA D02 prior to disassembly indicated no apparent physical exterior damage. However, it was observed that severe degradation of the aft and forward heat shield gold plating had occurred. A GN_2 resistance check was conducted, and the results indicated that the flow was degraded at T/VA inlet pressures of 5 and 10 psig. Upon disassembly of the valve and injector interface, it was noted that there was no damage to the O-rings. Also, measurement of the valve and injector interfaces was conducted, and they indicated that a gap of 0.0015 inch existed between the valve outlet and the injector inlet.

The amount of catalyst that was retrieved from the disassembly was equal to 1.668 grams. This represents a 15% loss of catalyst as the amount loaded during assembly was equal to 1.92 grams. Just prior to removal of the catalyst, the injector assembly was mounted back into the T/VA packing fixture. The tamping tool was then placed into the bed, and the chamber wall was tapped in a similar manner as used for packing. As a result, an effective void length of 0.08 inch was measured. It must be noted, however, that this operation plugged the injector with catalyst fines.

The T/VA reactor piece parts were examined, and it was noted that no damage had occurred to either the injector inlet or outlet screens. The injector was subjected to a waterflow calibration, and the results are shown in Figure 7-12. An increase in injector pressure drop equal to 6 psid is observed at a flow rate equal to 0.00095 lbm/sec. The catalyst bed retaining plate was observed to be completely plugged with catalyst particles and fines. A photograph of the upstream face of the bedplate is shown in Figure 7-13, and the downstream side is shown in Figure 7-14. In the first slot in the upper left-hand corner, it can be observed that there are no catalyst fines in the initial portion of the slot. However, this was completely filled with catalyst fines, but they were jarred loose during disassembly. The only apparent flow area available was the outer perimeter of the bedplate slots, where the bedplate is in contact with the chamber wall. The nozzle throat diameter was measured after disassembly and was equal to 0.0229. This compares to the initial build measurement of 0.0228.

LCSSE 0.2 lb_f T/VA DO2 (SIW004)

WATER FLOW CALIBRATION

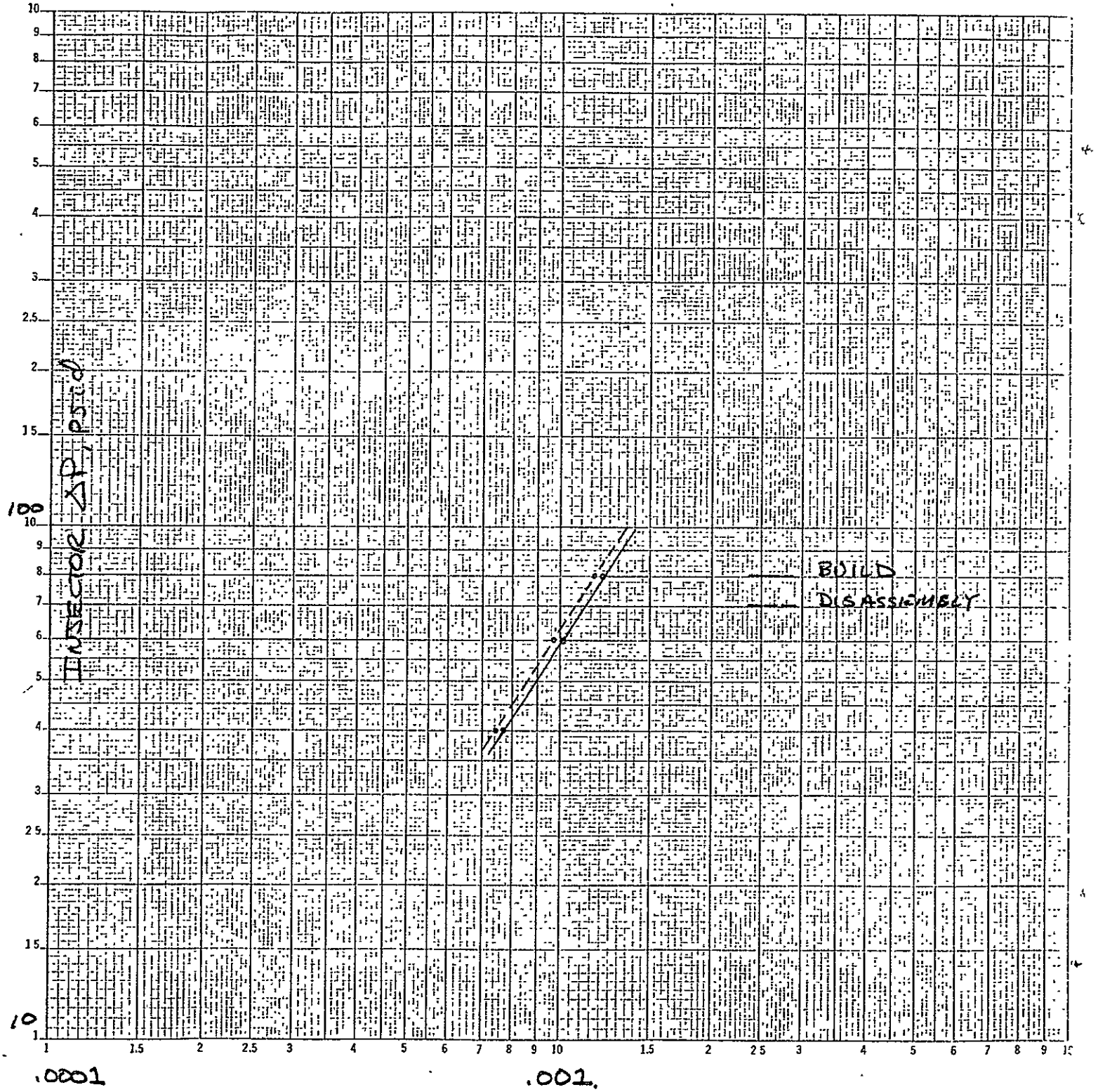

Figure 7-12

T/V-A D02 CATALYST BEDPLATE: UPSTREAM VIEW

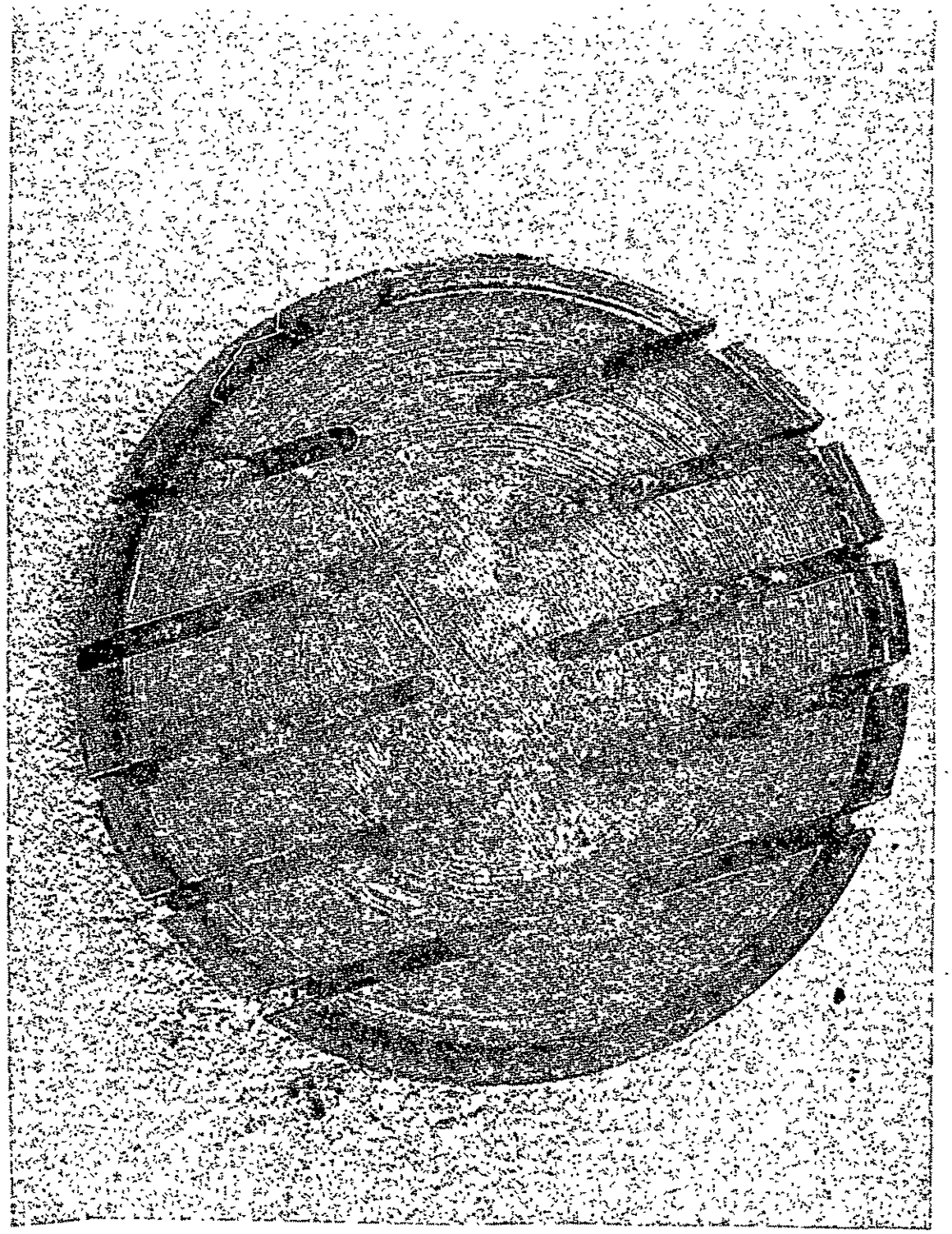

T/VA D02 CATALYST BEDPLATE: DOWNSTREAM VIEW

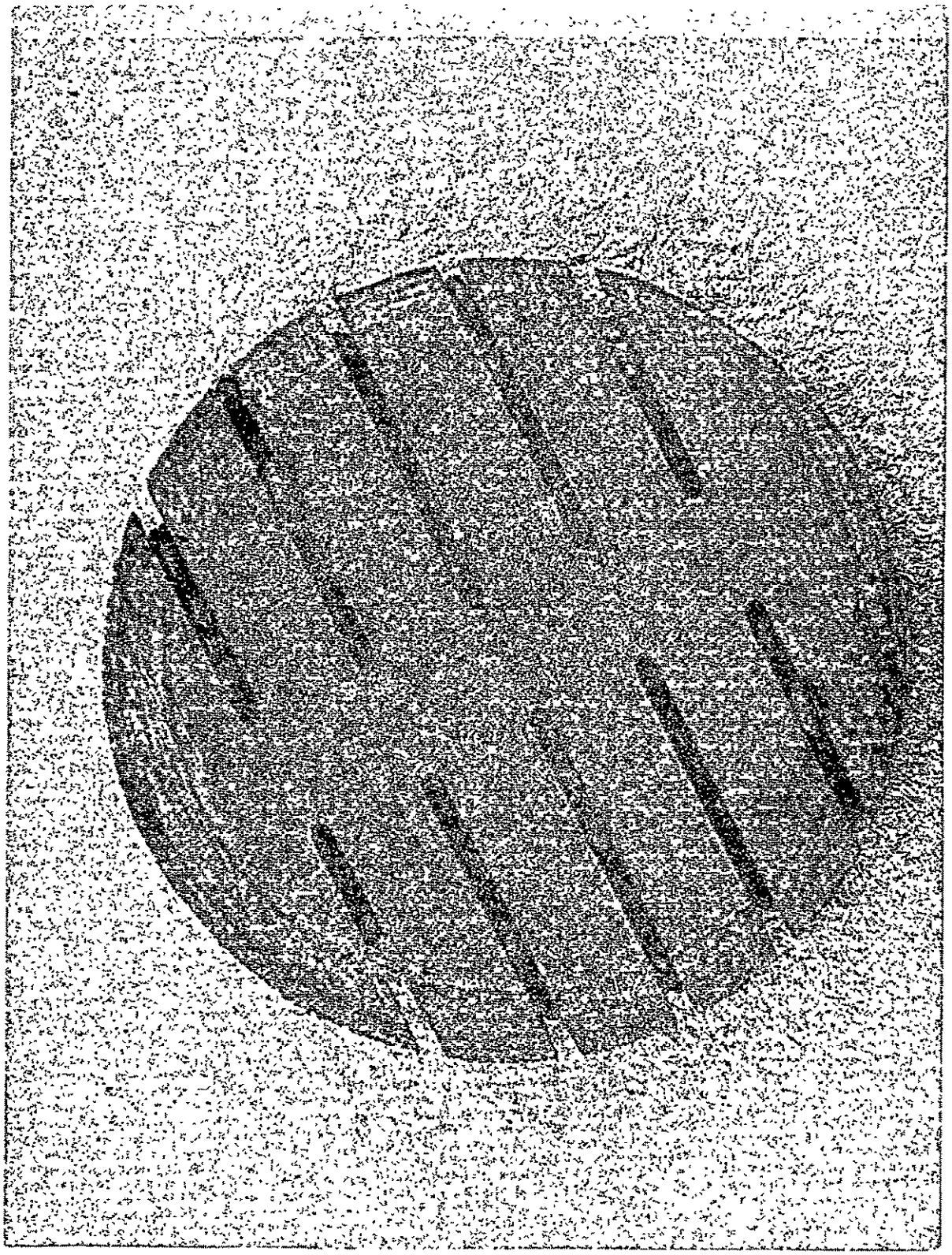

8.0 CONCLUSIONS

The results of the LCSSE/MJS 0.2-lbf T/VA development program demonstrate the T/VA is capable of operation over large duty cycles and with pulse widths of 0.008 and larger. Tests were successfully conducted to ensure that the T/VA will operate with a feed pressure range of 480 to 70 psia and propellant temperatures ranging from 40 to 140°F.

The T/VA design has successfully passed the qualification level vibration and simulated pyrotechnic shock environments. In addition, the unit was subjected to low-level sine vibration and acceptance level random vibrations. After completion of the environmental testing, observations made indicated no structural damage, and analysis of the test data and the strain gauges indicates that no large deformations were observed. Environmental test results were compared with the predicted values, and the results indicate that the analysis was generally on the conservative side for critical structural numbers. Since the mathematical model primarily represented the worst-case condition, a 1-to-1 correlation of the test and analysis was not possible.

The results of the thermal design verification tests indicate that for the MJS duty cycles, a 225°F catalyst bed minimum temperature is adequate and will be achieved with the T/VA-designed 1.4-watt bed heater. However, for the LCSSE application, a 1.4-watt bed heater may not maintain the bed above 225°F. The results of the test program also pointed out that the original conservative thermal model predicts catalyst bed heater power adequately and gives satisfactory representation of the T/VA nodal temperature distributions. A further accomplishment of the thermal design verification tests indicates that for the MJS mission, satisfactory engine starts can be expected with no propellant freezing for the standby condition with bed heaters off if the spacecraft mount and propellant line interface temperatures are maintained at or above 47°F and 41°F, respectively.

Thrust coefficient mapping tests were successfully completed with both steady-state and pulse-mode correlations obtained. The results of this testing will be used during the LCSSE MJS qualification test program, for all flight T/VA acceptance testing, and for all future users of the 0.2-lbf T/VA.

Results of the performance mapping and steady-state life margin tests indicate that the T/VA is capable of accumulating over 300,000 pulses over the design feed pressure and propellant ranges, and in addition accumulate a total of 60 hours of steady-state firing. A total throughput in excess of 156 pounds of propellant has been demonstrated with T/VA D01. Extensive data was reduced and provided the basis of the computerized performance model formulation. A concern for the quality of propellant (over and above the Amendment I criteria) used for long-duration burns was identified during this test program. Inspection of the T/VA with 60 hours of steady state accumulated indicated large quantities of iron had plated out in the injector, cap tube, and injector outlet screens. The propellant used was acceptable for Amendment I hydrazine. The total quantity of all metals must be limited in applications where long-duration firing will occur with one thruster.

Demonstration of the momentum wheel desaturation duty cycles was accomplished at feed pressures of 420 and 350 psia. The test was terminated as a result of an operator error, causing the sightglass valve to be left open and the tank valve closed during the automated test mode. This error allowed gaseous nitrogen to be ingested into the T/VA, causing a void; further operation of the tests caused excessive roughness, and finally test termination. As a result of the large number of pulses accumulated and throughput accumulated during the testing of the first development thruster, T/VA D01, combined with the fact that T/VA D02 successfully completed all of the duty cycles at the two highest feed pressures during the momentum wheel desaturation test, it is concluded that the T/VA design could successfully be qualified for the momentum wheel desaturation duty cycles.

The T/VA design has successfully demonstrated the capability to pass high surge flows without damage to the thruster valve or thruster inlet filter. This test was conducted to simulate worse case in-flight bleed-in of the propellant when the propellant feed system lines between existing latch valves and the T/VA are evacuated.

Analysis of the test results indicates the conclusions presented in Table 8-1 in regard to the JPL T/VA Specification ES 509778. The T/VA meets all of the requirements with the exception of the steady-state roughness and steady-state response criteria. This noncompliance was also verified during development and breadboard ATP testing and announced at the 0.2-lbf T/VA CDR in May 1975. As a corrective action to the roughness problem, RRC revised the catalyst packing procedure and increased the amount of overpack. Rocket Research Corporation recommends increasing the roughness critiera if necessary, pending the results of TA. Rocket Research Corporation recommends increasing the steady-state (10%) rise response from 20 milliseconds to 70 milliseconds (this represents a larger increase than stated at CDR and indicates the effects of 40°F propellant temperature), the steady-state (90%) rise response from 80 milliseconds to 175 milliseconds (presented at CDR), and the steady-state decay response from 120 milliseconds to 350 milliseconds (presented at CDR). The T/VA design showed excessive margins over the requirements of ES 509778 for pulse-mode impulse bit and centroid repeatability. Based on the results of the development tests, RRC recommends ±15 percent impulse bit repeatability for the extended feed pressure ranges of 420 and 70 psia. For the centroid repeatability requirement, RRC recommends a value of ±15 percent be substituted for Table II for pulse numbers of 2 to the equilibrium value reached for the particular duty cycle tested.

Table 8-1
0.2-lbf T/VA
SPECIFICATION ES509778 FUNCTIONAL COMPLIANCE STATUS
RESULTING FROM DEVELOPMENT TESTS

Item	Requirement	Design Capability	Remarks
T/VA			
JPL Dwg. 10071189	Provide pulse mode and steady-state thrust over feed pressure ranges of 70 to 420 psia and propellant temperatures of 40 to 140°F	Complies	
Propellant	MIL-P-26536C Amendment 1 or STM-N020	Partial compliance complies	250 to 350°F limit cycle pulse shape degradation. No pulse shape degradation with STM-N020.. Also the amount of metal content must be limited for long duration burns on a single T/VA
Steady State Performance			
Thrust	0.18- to 0.22-lbf at 350 psia, 28 vdc, 70°F, and vacuum	Complies	Nominal breadboard and development thrust = 0.212 lbf
Thrust reproducibility	3σ = ±5% at 350 psia and ±7% at 150 psia, 28 vdc, 70°F, and vacuum	Complies	Measured ±3.2% at 350 psia, ±1.8 at 150 psia
Specific impulse	220-lbf-sec/lbm min. @ 350 210-lbf-sec/lbm min. @ 150	Complies	Measured minimum = 226 lbf-sec/lbm Measured minimum = 215 lbf-sec/lbm
Total impulse predictability	±5% for total impulse and specific impulse in excess of 2 seconds	Complies	
Roughness	3σ = ±30% from 150 psia to 350 psia, period = 5 sec	Noncompliance	Measured maximum = 53%. Recommend increasing requirement.
Response	30 msec to 10% P_c @ 500 msec 80 msec to 90% P_c @ 500 msec 120 msec to 10% P_c (tailoff)	Noncompliance	Measured maximums: 60 msec to 10% (rise), 150 msec to 90% (rise) at 40°F propellant temp., and 259 msec to 10% (decay) during breadboard ATP's. Recommend increasing requirements.

Table 8-1
SPECIFICATION ES509778 FUNCTIONAL COMPLIANCE STATUS
RESULTING FROM DEVELOPMENT TESTS (Concluded)

Item	Requirement	Design Capability	Remarks
Pulse Mode Performance			
Minimum pulse width	T/VA operational for 0.008 sec on-times	Complies	Verified during proposal development testing
Minimum off time	T/VA capable of operating with 0.012 sec off times	Complies	Verified during proposal tests; to be verified during TA testing
Minimum impulse bit	Minimum impulse bit = 0.003 lbf-sec at 350 psia pulse width = 0.008	Complies	Verified during proposal and development tests; to be verified during TA testing
Impulse bit repeatability	±15% from 150 to 350 psia TBD from 70 to 150 psia and 350 to 400 psia	Complies	Verified during development. Recommend ±15% for the TBD
	±25% for variable temperature environment	Complies	Verified during development
Centroid repeatability Pulse width ⩾40 msec pulse off time ⩾400 msec	Table II	Complies	Verified during development. Recommend substitution of ±15% in lieu of Table II for pulse numbers of 2 to ∝
Response	30 msec to 10% P_c 80 msec to 90% P_c TBD msec to 10% P_c (tailoff) Pressure ranges of 150 to 380 psia	Complies	Verified during development. Recommend establishing tailoff limit with limit cycle development and TA data.
Minimum specific impulse	100-lbf-sec/lbm Pulse widths ⩾10 msec	Predicted compliance	To be verified during TA tests with extended range, transducer, and development
Vacuum duty cycle	Meet the requirements of specification when performing any combination of duty cycles as typified by the two mission sequences of Table III.	Predicted compliance	Verified during extensive proposal and development testing (60 hrs steady state, >300,000 pulses). To be verified during TA testing for mission Sequence I
Hot restarts	T/VA operational under worse case heat soak back	Complies	Verified during proposal testing Mount temp. = 170°F, Prop. temp Initial = 180°F To be verified during TA testing.